Ex Vivo Bone Culture: A Novel Method For Investigating Mechanical Loading Response And Osteocytes In Situ In Trabecular Bone

KAMARUL ARIFFIN KHALID

A thesis submitted to The University of Adelaide in fulfilment of the requirements for the degree of

DOCTOR OF PHILOSOPHY IN MEDICINE

(ORTHOPAEDICS AND TRAUMA)

Discipline of Orthopaedics and Trauma
Adelaide Medical School
Faculty of Health and Medical Sciences
The University of Adelaide
South Australia

August 2019

Table of Contents

Thesis Abstract

Osteocytes plays an important role in controlling and determining the function of the other cell types in bone, especially in response to mechanical loading and biochemical changes. The available data are still incomplete and much information derives from models that do not emulate the three dimensional structure of living bone. The use of the second generation Zetos™ system that enables long-term culture of trabecular bone *ex vivo*, together with the more traditional *in vitro* and *in vivo* models, will enable us to answer some of these knowledge gaps. A better understanding of osteocyte function specifically, and bone response to mechanical loading in general, can be obtained.

In the first study, the second generation Zetos™ system was optimised and its software beta-tested in a series of trial experiments. The methodology and workflow used to prepare twenty four (24) *ex vivo* trabecular bone cores from a single bovine sternum, the maximum for each experiment, was described in great detail. Half of these bone cores had their marrow removed in the described experiment. Three (3) groups of four (4) bone cores, both with and without marrow, were loaded dynamically, with a load of 2,000 μstrain at 1 Hz, either for 100 cycles three times a day (100x3) or 300 cycles once a day (300x1) or not loaded (UL) respectively for 10 consecutive days. The bone cores without marrow showed significantly better increase in stiffness and response of their μCT histomorphometric parameters to loading over time, while their media have a consistently higher pH and lower ionic calcium (Ca^{2+}) levels than that of the bone cores with marrow. Taken together, they indicated that removal of marrow in the bone cores was beneficial to the study of osteocytes in their native bone matrix environment using this Zetos™ system. This was possibly due to the improved fluid flow within the culture chambers when bone marrow was removed.

In the second study, the use of the second generation Zetos™ system to investigate the application of a nano-engineered implant for local drug delivery in trabecular bone was

described. The results demonstrated a consistent gradual release of a model drug, with a characteristic 3-dimensional distribution pattern, from the implant into the surrounding bone, over a 5-day period. The parameters that significantly affect the drug distribution were the flow rate of the bone culture medium, trabecular bone microarchitecture and mechanical loading of the bone core samples. This study demonstrated the usefulness of this system for drug release studies in *ex vivo* bone, which can be used to assist in the design of new drug delivery systems, and the optimisation of specific therapy delivery, in bone.

The third study described the effect of exogenous human recombinant sclerostin (rhSCL) on the osteocytes of trabecular bone that were mechanically loaded *ex vivo* using this system. Bovine trabecular bone cores without marrow were subjected to daily episodes of dynamic loading and compared to unloaded bone cores or with the addition of exogenous rhSCL. Loaded bone showed an increase in apparent stiffness, calcein uptake (as a surrogate for Ca^{2+} influx), the Ca^{2+} and COOH-terminal telopeptide of type I collagen (β-CTX) levels in the perfusate, the mean osteocyte lacunar size (indicative of osteocytic osteolysis), and the expression of catabolic genes. These results indicated the direct contribution of osteocytes to bone mineral accretion and mechanical properties of trabecular bone, and support the concept that sclerostin acts directly on osteocytes to inhibit these effects via modulation of the osteocytic osteolysis process.

In conclusion, the work done in this thesis was able to optimise the use of the second generation Zetos™ system for relevant bone and osteocyte-related research. This includes the investigation of drug delivery implants in large animal trabecular bone and as an additional tool for studying the osteocyte within its native lacuno-canalicular network. Further work using this system can assist in filling up important knowledge gaps on osteocytes mechanobiology and its role in the various metabolic functions of bone.

Declaration

I, **Kamarul Ariffin Khalid**, certify that this work contains no material which has been accepted for the award of any other degree or diploma in my name in any university or other tertiary institution and, to the best of my knowledge and belief, contains no material previously published or written by another person, except where due reference has been made in the text. In addition, I certify that no part of this work will, in the future, be used in a submission in my name for any other degree or diploma in any university or other tertiary institution without the prior approval of the University of Adelaide and where applicable, any partner institution responsible for the joint award of this degree.

I acknowledge that copyright of published works contained within this thesis resides with the copyright holder(s) of those works.

I also give permission for the digital version of my thesis to be made available on the web, via the University's digital research repository, the Library Search and also through web search engines, unless permission has been granted by the University to restrict access for a period of time.

I certify that I have NO affiliations with or involvement in any organisation or entity with any financial interest (such as honoraria; educational grants; participation in speakers' bureaus; membership, employment, consultancies, stock ownership, or other equity interest; and expert testimony or patent-licensing arrangements), or non-financial interest (such as personal or professional relationships, affiliations, knowledge or beliefs) in the Zetos™ system discussed in this thesis.

K

Date: 31 July 2019

Acknowledgements

First of all I would like to express my greatest appreciation to my supervisors, **Professor Gerald J. Atkins** and **Professor David M. Findlay** who gave me the opportunity to join their team at the Centre for Orthopaedics & Trauma Research, Faculty of Health and Medical Sciences, The University of Adelaide. Both have been very patient with me and had provided me with the support to enable me to go into research from my clinical career. The guidance given by Gerald for my research work, scientific communications and writing has been invaluable and allowed me to grow in a new direction for my career in orthopaedics. The wisdom and advice provided by David for my work also helped me to develop further in the field of orthopaedic research..

I would also like to express my heartfelt thanks to colleagues and friends at the Centre for Orthopaedics & Trauma Research and the Bone Cell Biology Group in the Institute of Medical and Veterinary Sciences; such as, **Masakazu Kogawa, Agatha Labrinidis, Asiri Wijenayaka, Renee Ormsby, Lim Hui Ping, Shelley Hay, Katie Welldon, Vasilios Liapis,** and **Irene Zinonos**, to name but a few, for their help and support on getting acquainted with laboratory and research work as part of my learning throughout my time at The University of Adelaide.

I would like to give my gratitude to my employee, the **International Islamic University Malaysia**, and the **Ministry of Education, Government of Malaysia**, for allowing me to pursue this degree and sponsoring it in full.

Last, but definitely not the least, my thanks and eternal gratitude to my beloved wife, **Assoc. Prof. Dr. Hazrina Ab Hadi**, who encouraged me to finish the writing of this thesis and for her ultimate support and sacrifices to ensure that I am able to do so in the last a few months. Without her this thesis would not see the light of day and all of my effort would have gone to waste.

Published Abstracts (Reviewed)

Kogawa, M., Khalid, K. A., Wijenayaka, A. R., Ormsby, R. T., Evdokiou, A., Anderson, P. H., Findlay, D. M., Atkins, G. J. (2018). Recombinant sclerostin antagonizes effects of ex vivo mechanical loading in trabecular bone and increases osteocyte lacunar size. American Journal of Physiology: Cell Physiology, 314(1), C53-c61. doi:10.1152/ajpcell.00175.2017

Aw, M. S., **Khalid, K. A.**, Gulati, K., Atkins, G. J., Pivonka, P., Findlay, D. M., & Losic, D. (2012). Characterization of drug-release kinetics in trabecular bone from titania nanotube implants. Int J Nanomedicine, 7, 4883-4892. doi:10.2147/ijn.s33655

Mokhtarzadeh, H. O. S. S. E. I. N., Aw, M. S., **Khalid, K. A**., Gulati, K., Atkins, G. J., Findlay, D. M., & Pivonka, P. (2014). Computational and experimental model of nano-engineered drug delivery system for trabecular bone. In *Proceedings of 11th World Congress on Computational Mechanics, (WCCM XI)* (pp. 868-879). International Center for Numerical Methods in Engineering (CIMNE).

KA Khalid, RT Ormsby, KJ Welldon, HP Lim, S Syazwani, S Fatin Nabilah, GJ Atkins, DM Findlay. Response to loading in *ex vivo* bovine bone. Proceedings of the IOF Regionals 2nd Asia-Pacific Osteoporosis and Bone Meeting and ANZBMS Annual Scientific Meeting with JBSMR, Gold Coast, Australia. 4th – 8th September 2011, *Osteoporosis International*. September 2011, Vol. 22 Suppl 4: pp S570

Scientific Communications

Masakazu Kogawa, **Kamarul A Khalid**, Asiri R Wijenayaka, Renee T Ormsby, David M Findlay, Gerald J Atkins. *Sclerostin Antagonises The Mechanical Loading Response By A Mechanism Involving Osteocytic Osteolysis*. Australian & New Zealand Orthopaedic Research Society 2013 Conference, The Darlington Centre, University of Sydney, Australia. 4th – 5th September 2013

Khalid KA and Kogawa M, Wijenayaka AR, Findlay DM and Atkins GJ. *Mechanical Loading Response In Trabecular Bone Is Abrogated By Sclerostin – A Direct Demonstration.* 6th Australian Health and Medical Research Congress 2012, Adelaide Convention Centre, Adelaide, South Australia, Australia. 25th – 28th November 2012

KA Khalid, M. Kogawa, DM Findlay, GJ Atkins. *Direct effect of sclerostin on the mechanical loading response in bovine bone.* 1st Asia-Pacific Bone and Mineral Research Meeting and 22nd ANZBMS Annual Scientific Meeting, Pan Pacific Hotel, Perth, Australia. 2nd – 5th September, 2012

KA Khalid, M. Kogawa, DM Findlay, GJ Atkins. *Sclerostin Attenuates the Mechanical Loading Response in Trabecular Bone.* 2012 Postgraduate Research Conference, Faculty of Health Sciences, University of Adelaide, National Wine Centre, Adelaide, South Australia. 31st August 2012

KA Khalid, M. Kogawa, DM Findlay, GJ Atkins. *Sclerostin attenuates the mechanical loading response in trabecular bone.* Presented at the Australian Orthopaedic Association South Australian Branch Annual Scientific Meeting 2012, Flinders Medical Centre, South Australia, Australia. 10th August 2012

KA Khalid, DM Findlay, GJ Atkins. *The Osteocyte – Directing Bone Remodelling, Mineralisation and Phosphate-Calcium Homeostasis Behind the Scenes.* Presented at the 42nd Malaysian Orthopaedic Association Annual Scientific Meeting, Sultan Ahmad Shah International Convention Centre, Kuantan, Pahang. 14th – 17th June 2012

KA Khalid, M. Kogawa, DM Findlay, GJ Atkins. *Effect of Sclerostin on Response of Bovine Bone to Mechanical Loading.* Presented at the 42nd Malaysian Orthopaedic Association Annual

Scientific Meeting, Sultan Ahmad Shah International Convention Centre, Kuantan, Pahang. 14th – 17th June 2012

MS Aw, **KA Khalid**, K Gulati, GJ Atkins, DM Findlay, D Losic. *Drug-eluting implants with titania nanotube arrays for local drug delivery in bone: Ex vivo study using 3-d bone reactor*. Presented at the Australasian Pharmaceutical Science Association Annual Conference 2011, University of South Australia, Adelaide, South Australia, Australia. 11th – 14th December 2011

KA Khalid, RT Ormsby, KJ Welldon, HP Lim, S Syazwani, S Fatin Nabilah, GJ Atkins, DM Findlay. *Response to loading in ex vivo bone*. Presented at IOF Regionals 2nd Asia-Pacific Osteoporosis and Bone Meeting and ANZBMS Annual Scientific Meeting with JBSMR, Gold Coast Convention Centre, Queensland, Australia. 4th – 8th September 2011

KA Khalid, GJ Atkins, Findlay DM. *Role of Osteocytes in Bone Response to Mechanical Loading*. Presented at The Sixth Clare Valley Bone Meeting, Clare Country Club, Clare, South Australia , Australia. 26th – 30th March 2010

Awards and Achievements

Travelling Grant, 1st Asia-Pacific Bone and Mineral Research Meeting and 22nd ANZBMS Annual Scientific Meeting, Pan Pacific Hotel, Perth, Australia. 2nd – 5th September, 2012

Best Basic Science Poster winner, 42nd Malaysian Orthopaedic Association Annual Scientific Meeting, Sultan Ahmad Shah International Convention Centre, Kuantan, Pahang. 14th – 17th June 2012

Travelling Grant, IOF Regionals 2nd Asia-Pacific Osteoporosis and Bone Meeting and ANZBMS Annual Scientific Meeting with JBSMR, Gold Coast, Australia. 4th – 8th September 2011

Abbreviations

3D	three dimensional
5-HT	serotonin
ACP5	acid phosphatase 5, tartrate resistant
ADHR	autosomal dominant hypophosphataemic rickets
AFM	atomic force microscopy
ANOVA	analysis of variance
ARHR	autosomal recessive hypophosphataemic rickets
ASARM	acidic serine aspartate-rich MEPE-associated motif
ATP	adenosine triphosphate
BCP	biphasic calcium phosphate
BMC	bone mineral content
BMD	bone mineral density
BMP	one morphogenetic protein
BRC	bone remodelling compartment
BS	bone surface area
BS/BV	bone surface/volume ratio
BS/TV	bone surface density
BV	bone volume
BV/TV	percent bone volume

CA2	carbonic anhydrase 2
CapG	macrophage-capping protein
cAMP	cyclic adenosine monophosphate
CKD	chronic kidney disease
CKD-MBD	mineral and bone disorder of chronic kidney disease
CO_2	carbon dioxide
CPTHR	carboxyl-terminal parathyroid hormone receptor
CT-1	cardiotropin-1
CTHRC1	collagen triple helix repeat containing 1
CTSK	cathepsin K
Cx43	connexin 43
Dkk1	Dickkopf-1
DMEM	Dulbecco’s modified Eagle medium
DMP1	dentin matrix protein 1
E11	podoplanin
ECF	extracellular fluid
EFNB2	ephrinB2
eNOS	endothelial nitric oxide synthase
ER	oestrogen receptor
FCS	foetal calf serum

FGF23	fibroblast growth factor 23
FGFR	fibroblast growth factor receptor
FRAP	fluorescence recovery after photobleaching
GHz	gigaHerz
GPCR	G-protein coupled receptors
GUI	graphical user interface
HA	hydroxyapatite
HB-GAM	heparin-binding growth associated molecule
HEPES	4-(2-Hydroxyethyl)-1-piperazineethanesulfonic acid
HHH	hereditary hypophosphataemia and hyperparathyroidism
HIFα	hypoxia-inducing factor alpha
Hz	Hertz
IFN-β	interferon β
IGF-1	insulin-like growth factor-1
IL-1	interleukin-1
iS	intersection surface
LRP	low density lipoprotein receptor
M-CSF	macrophage colony-stimulating factor
MEPE	matrix extracellular phosphoglycoprotein
MLO-Y4	murine long-bone osteocyte Y4

MMP-2	matrix metalloproteinase-2
MMP-9	matrix metalloproteinase-9
MPa	megapascal
MT1-MMP	membrane type-1 matrix metalloproteinase
N	Newton
NO	nitric oxide
OCN	osteocalcin
OPG	osteoprotegerin
ORP150	oxygen-regulated protein 150
OSF-1	osteoblast stimulating factor-1
PBS	phosphate buffered saline
PC1	polycystin-1
PDMS	polydimethylsiloxane
PGE_2	prostaglandin E_2
PHEX	phosphate-regulating gene with homologies to endopeptidases on the X chromosome
PPARγ	peroxisome proliferator-activated receptor γ
PTH	parathyroid hormone
PTHR1	parathyroid hormone receptor 1
PTHrP	parathyroid hormone-related peptide

R^2	coefficient of determination
RAM	random access memory
RANK	receptor activator of nuclear factor κB
RANKL	receptor activator of nuclear factor κB ligand
rhSCL	human recombinant sclerostin
RUNX2	runt-related transcription factor 2
S1P	sphingosine 1-phosphate
SCL	sclerostin
SD	standard deviation
SEM	scanning electron microscopy
SEMA4D	semaphorin 4D
SIBLING	small integrin-binding ligand N-linked glycoprotein
SMI	structure model index
SOST	sclerostin gene
SPHK1	sphingosine kinase 1
Tb.N	trabecular number
Tb.Pf	trabecular pattern factor
Tb.Sp	Trabecular separation
Tb.Th	trabecular thickness
TEM	Transmission electron microscopy

TGF-β	transforming growth factor-beta
TIFF	tagged image file format
TNFα	tumour necrosis factor alpha
TV	tissue volume
TWEAK	TNF-related weak inducer of apoptosis
USB	universal serial bus
VDR	vitamin D receptor
VEGF	vascular endothelial growth factor
Wnt	Wingless integration
XLH	X- linked hypophosphataemia
β-CTX	COOH-terminal telopeptide of type I collagen
β-TCP	β-tricalcium phosphate
μCT	micro-computed tomography

List of Figures

List of Tables

CHAPTER 1. Literature Review and Objectives

1.1 Introduction

Bone has been well demonstrated to respond to loads applied to it, whether in terms of maintenance or increase in mass. Conversely, unloading of the skeleton results in loss of bone mass. These relationships have been described by Wolff's Law [1] and, more recently, by Frost according to his 'mechanostat' mechanism [2]. Although much has been learned about the mechanism for these responses [3, 4], the complexity of whole animal physiology has made it difficult to obtain a full understanding. Important questions remain regarding what component of bone response to loading is direct, intrinsic to bone, and to what extent circulating factors and neural inputs might contribute.

To address some of these issues, at least in trabecular bone, the work described in this thesis took advantage of a novel approach to maintaining and loading bone *ex vivo*. This system enabled a focus on the effect of direct loading of bone, devoid of extrinsic influences. The Zetos™ system, originally developed by Dr David Jones at Marburg University, Germany and Dr Everett Smith at the University of Wisconsin [5], was designed to enable long-term cultures of bone explants, to which physiologically relevant mechanical loading could be applied (Fig. 1.1). The system has the ability to apply specific and measurable compressive strain to a cylinder of trabecular bone, delivered in various configurations, and also to measure the resultant deformation in the cylinders with the application of specific forces onto it; the latter allowing measurement of the elastic modulus of the bone. The first generation Zetos™ system has been described [5], tested [6-8] and validated against other *in vitro* and *in vivo* models [9-11]. Other authors have also reported its use on tissue engineering constructs [12], testing of implants for local drug delivery [13] and biomaterials biocompatibility testing [14].

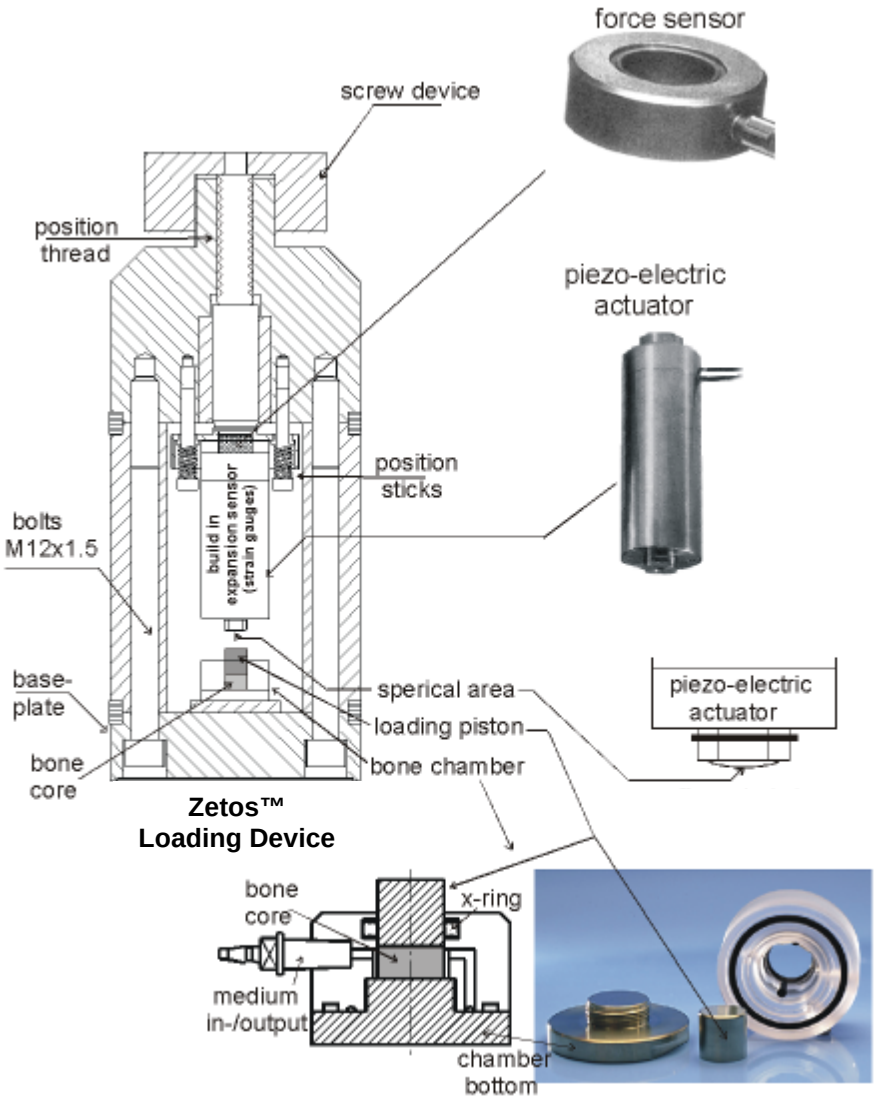

Figure 1.1 – 1st Generation Zetos™ System
Schematic diagram and pictures of the components for the first generation Zetos™ system. (Adapted from Jones 2003 [5])

There have been several other appliances developed by other investigators to perform similar investigative procedures on bone explants [15-17]. However, they appear to have important limitations compared with the Zetos system and, in general, have not been as extensively tested, validated and reported. For example, Meyer and colleagues designed a bioreactor system that allows for the long-term culture of bovine chondral explants or tissue engineered constructs with the application of defined strains of different magnitudes to the samples being studied [15]. This bioreactor allows for four samples to be mechanically loaded at the same time (Fig. 1.2) but it was not able to measure the stiffness of the samples.

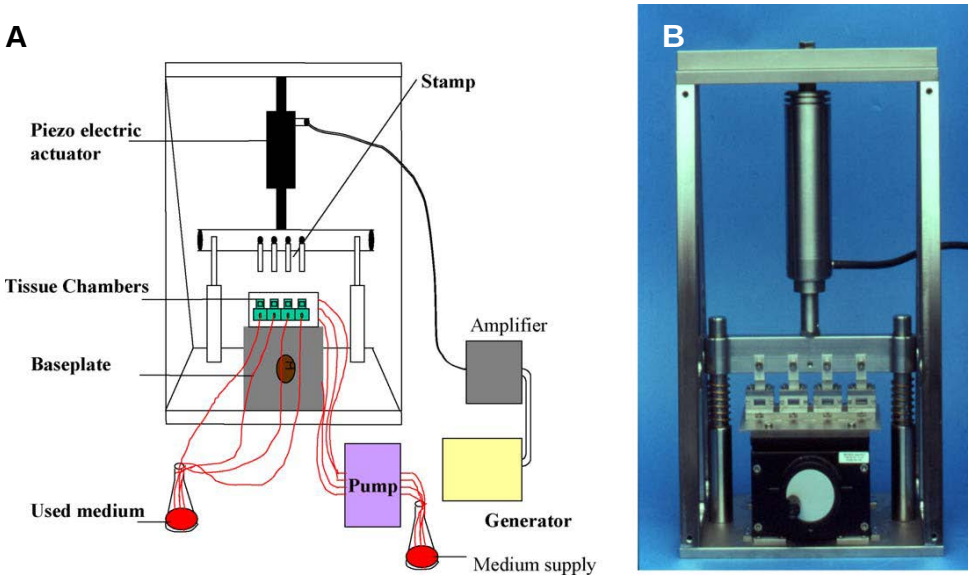

Figure 1.2 –Loadable Bioreactor System by Meyer et al.
The diagram **(A)** and picture **(B)** of the bioreactor system used by Meyer and colleagues [15]. The system enables the mechanical loading of tissue samples while placed in a CO_2 incubator. (Adapted from Meyer 2006)

A device that can be used to culture trabecular bone cores, with the marrow removed, in a loadable perfusion chamber (Fig. 1.3) was first reported by El Haj and colleagues in 1990 [16]. Short-term culture of the bone cores for 24 hours only were performed using this device. There was no detailed description of the device in the report, which does not seem able to measure the stiffness of the bone cores used in the study.

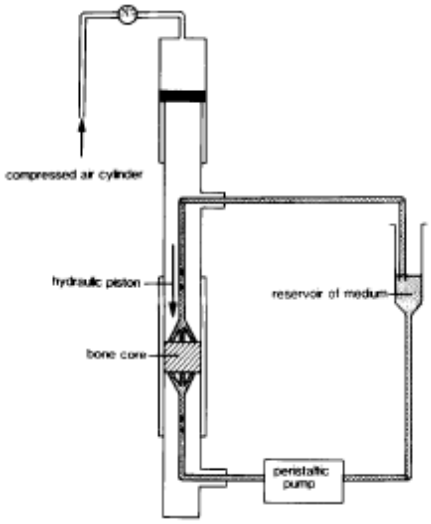

Figure 1.3 –Loadable Culture System by El Haj et al.
Diagram of the device used for the short term culture (24 hours) of bone cores without marrow as reported by El Haj [16] A mechanical load of 5,000 μstrain (0.005 bulk strain or 0.5% deformation) at 1Hz was applied for 15 minutes to the bone core. (Adapted from El Haj 1990)

The method by El Haj et al. was modified by Takai and colleagues for the application of a mechanical load to trabecular bone cores seeded with osteoblasts [17]. A custom bioreactor with feedback-control, first developed by Mauck et al. for applying load onto tissue engineered cartilage constructs [18], was used to investigate the effect of dynamic hydrostatic pressure loading on osteocyte and osteoblast interactions in long-term culture. However, in the report, the bone cores were sealed in a plastic bag filled with culture medium and loaded indirectly (Fig. 1.4). Bone core stiffness cannot be measured using this device.

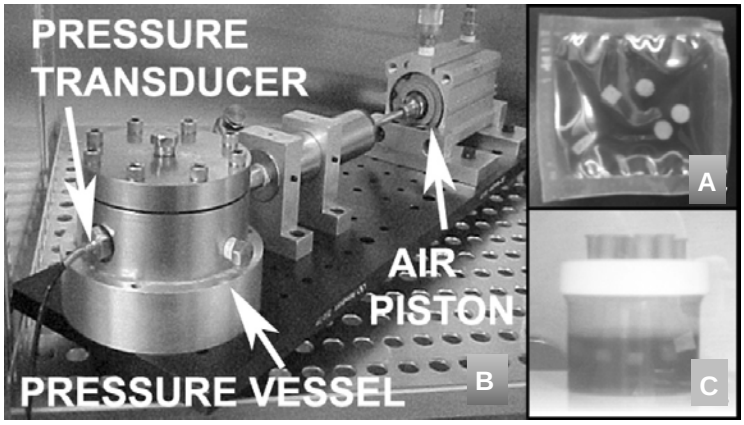

Figure 1.4 –Loadable Custom Bioreactor by Takai et al.
Bone cores without marrow, seeded with primary osteoblasts, were sealed in a sterile plastic bag with culture medium **(A)** before being placed in the pressure vessel **(B)** filled with distilled water. A peak load of 3 megapascals (MPa) at 0.33Hz, as measured by the built-in pressure transducer, was applied by the air piston. Osteoblast seeding of the bone cores was performed using a custom-made cell seeder **(C)**. (Adapted from Takai 2004 [17])

A detailed description on the method for harvesting trabecular bone cores from bovine fetlock joints of 6-week-old calves was described recently by Marino and colleagues [19]. A perfusion bioreactor, coupled to a mechanical testing device was illustrated in this technical report (Fig. 1.5). It enabled the application of a dynamic and deformational load to individual bone cores that were seeded with osteoblasts. This device was able to measure the stiffness of the bone cores. It can only load or test one bone core at a time, similar to the Zetos™ system. However, there was no mention on how the bone cores were kept at 37°C during the loading sessions as opposed to the protocol for the Zetos™ system [5]. Interestingly, Chan et al. had used the Zetos™ system on a similar bovine trabecular bone osteocyte-osteoblast co-culture model to

investigate the functional bone adaption to dynamic deformational loading, gap junction intercellular communication and prostaglandin E_2 (PGE_2) production [20].

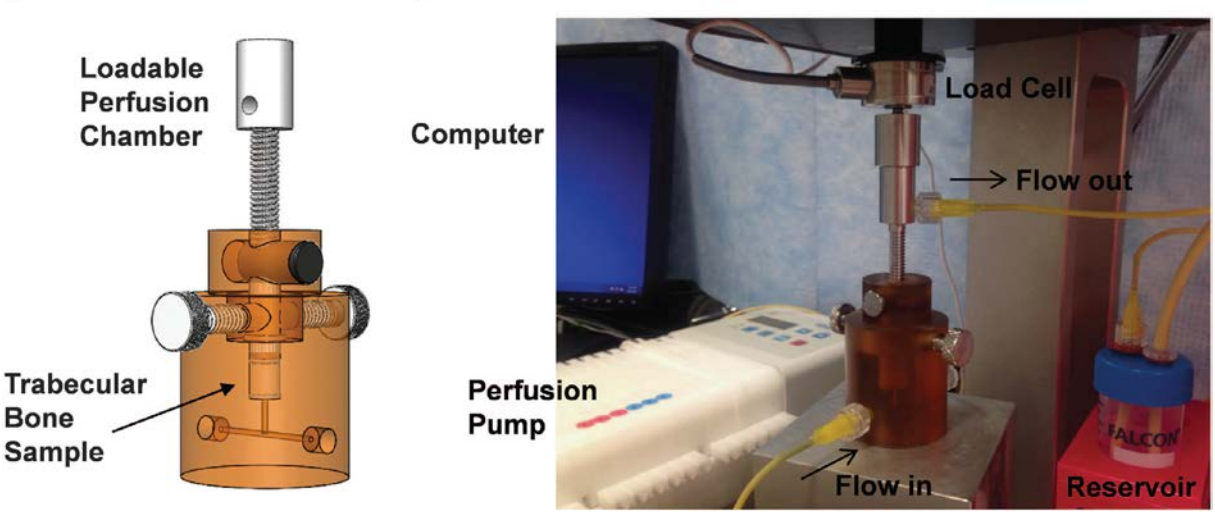

Figure 1.5 – Perfusion Bioreactor by Marino et al.
A device that can be coupled to a mechanical testing device and with similar functionality to the Zetos™ system was illustrated in a paper describing various *ex vivo* bone explant cultures [19] (Adapted from Marino 2016)

New methods for culturing osteoblast lineage cells that resembled osteocytes phenotypically had also been described. Boukhechba et al. used biphasic calcium phosphate (BCP) ceramic particles, composed of 60% hydroxyapatite [$Ca_{10}(PO_4)_6(OH)_2$] (HA) and 40% of β-tricalcium phosphate [$Ca_3(PO_4)_2$] (β-TCP), as a 3D scaffold for the culture of human primary osteoblasts [21]. It was demonstrated that the osteoblasts differentiated into osteocytes after one week of culture (Fig. 1.6). Gu et al. [22] and Sun et al. [23] reported using BCP microbeads, made up of 68% HA and 38% β-TCP, seeded with murine early osteocytes (MLO-A5) cells to biomimetically construct a 3D cellular network of primary murine osteocytes (Fig. 1.7). When seeded with primary human osteoblasts, the same method was shown to be able to produce a human primary 3D-networked osteocytes bone tissue model [24]. However, no reports on the use of these methods for the investigation of mechanosensation and mechanotransduction in osteocytes was found to date. Future work utilising these osteocyte bone constructs in a bone loading and testing system like Zetos™ may be a feasible option.

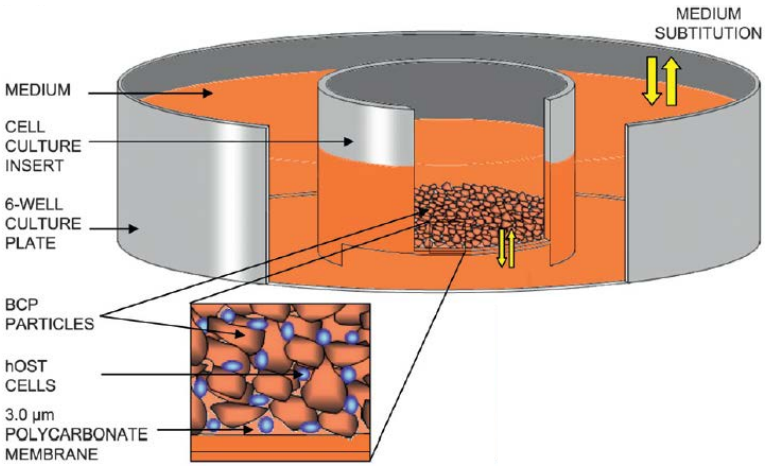

Figure 1.6 – Osteocyte Culture System by Boukhechba et al.

Human primary osteoblasts (hOSTs) differentiates into osteocytes after 1 week of culture, when seeded within BCP particles in culture inserts with a polycarbonate membrane of 3-mm pore size and placed in 6-well tissue culture plates. (Adapted from Boukhechba 2009 [21])

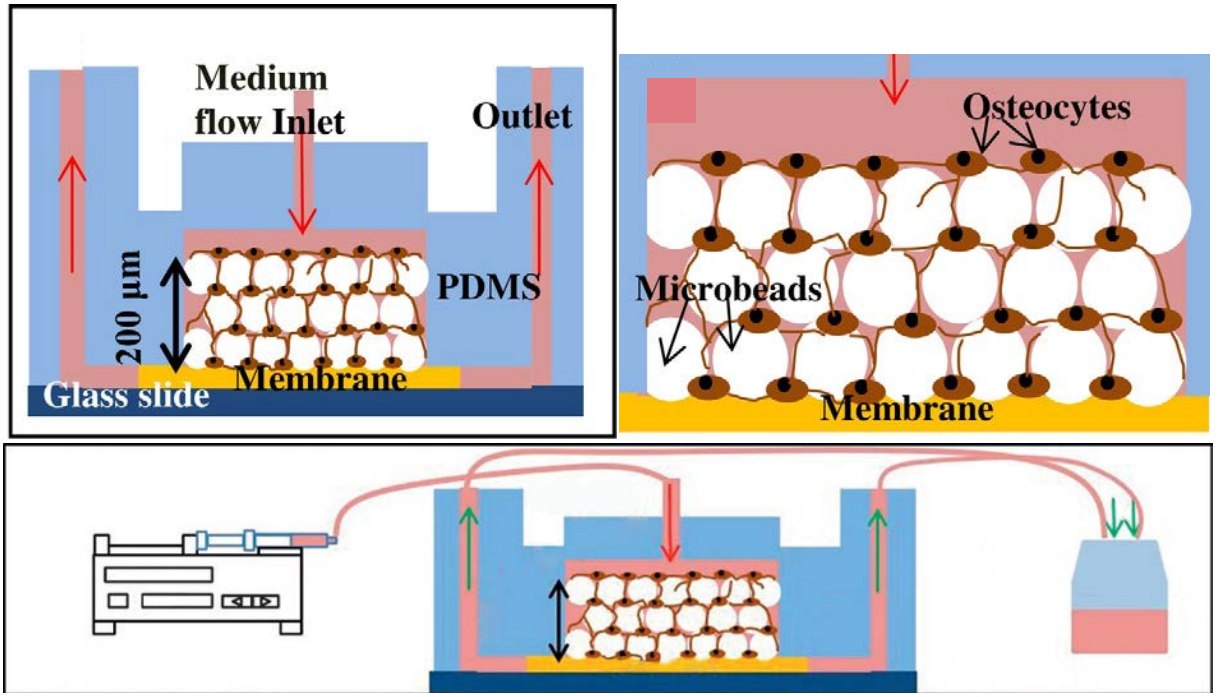

Figure 1.7 – Osteocyte Culture System by Sun et al.

Cross-section of the polydimethylsiloxane (PDMS) microfluidic culture device **(top left)** and its setup **(bottom)**, used to biomimetic construction of a 3D-osteocyte network bone tissue model using BCP microbeads **(top right)**. (Adapted from Sun 2015 [23] & 2017 [24])

The new Zetos system described in this thesis was a second generation version, representing a major upgrade, with a complete change in software configuration. As a beta-testing site for this machine, there was much work to be done in order to use the Zetos for experimental purposes. Therefore, much of the initial work in this PhD was directed to validating and optimising the

new improved Zetos system for use with trabecular bone explants. Following this validation work, the Zetos was used to perform a number of experiments. The way that these experiments were conducted, with removal of bone marrow and osteoclasts and osteoblasts from the bone surface, implicated osteocytes, residing within the bone matrix, in the observed responses. To explain the experimental results obtained, a detailed understanding of the biology of osteocytes was required, and will be discussed further below.

Other cells types that were known to respond to mechanical stimuli include mesenchymal stem cells [25], fibroblasts, chondrocytes, cardiomyocytes, endothelial cells, rhabdomyocytes and also osteoblasts [26]. Although osteoblasts are known to be the active bone-forming cells in bone remodelling [27] and it was initially thought to be the mechanosensors of bone [28], work in recent years have identified osteocytes as the most likely candidate to respond to the mechanical stimulation of bone [29]. Uda et al. recently reviewed the body of evidence on the ability of osteocytes to sense mechanical stimuli and transduce it to modulate the biological activity of both osteoblasts and osteoclasts [30]. Hence the focus on osteocytes in this thesis.

1.2 The Osteocyte

Osteocytes are the most abundant cells in bone (approximately 95% of bone cells) but the least investigated of the bone cells. This is principally due to two factors. Firstly, osteocytes were previously thought to be a rather inert cell that does little to contribute to the myriad functions of bone [31, 32]. This has been proven wrong in recent years [33]. Secondly, and probably more importantly, is the technical difficulty of extracting osteocytes from their lacunae in bone or to study them *in situ* [34]. However, in the last few decades there has been much renewed interest in osteocytes and their function, as more and more evidence shows that osteocytes may be the key cells in regulating bone remodelling *via* mechanotransduction [35], and also for the homeostasis of calcium and phosphate, the elements that make up HA mineral in bone [36-38]. The development of osteocyte-like cell lines [39-43], animal models with cell specific gene

mutations [44], various ways to load animal bones *in vivo* [45], together with the evolution of new and better techniques for isolating and culturing osteocytes and characterising them, has helped in fuelling the sudden wealth of new knowledge on osteocyte biology [46, 47].

Osteocytes had long been documented as being the non-proliferative, terminally differentiated osteoblasts that became embedded in the osteoid matrix being laid down. Only 10-20% of osteoblasts differentiate into osteocytes [48]. The remainder either undergo apoptosis, become bone lining cells, or in specific situations, differentiate into chondrogenic cells, forming cartilage matrix [49]. The exact process of osteoblast differentiation into osteocytes is still not fully elucidated. Suffice to say that the whole process appears to be a continuum that begins with the identification of which osteoblasts will differentiate, their embedding in the developing osteoid matrix and the mineralisation of the osteoid. Up to six different stages have been identified during the transition of a preosteoblast to an osteocyte [48], with three distinct preosteocyte types described [50]. The different osteoblast-osteocyte transitional stages are the pre-osteoblast, osteoblast, embedding osteoblast, osteoid-osteocyte, mineralizing osteocyte, and mature osteocytes (Fig. 1.8) [51]. Underlying all this is the change in morphology of the cell and changes to the genes and proteins being expressed by it.

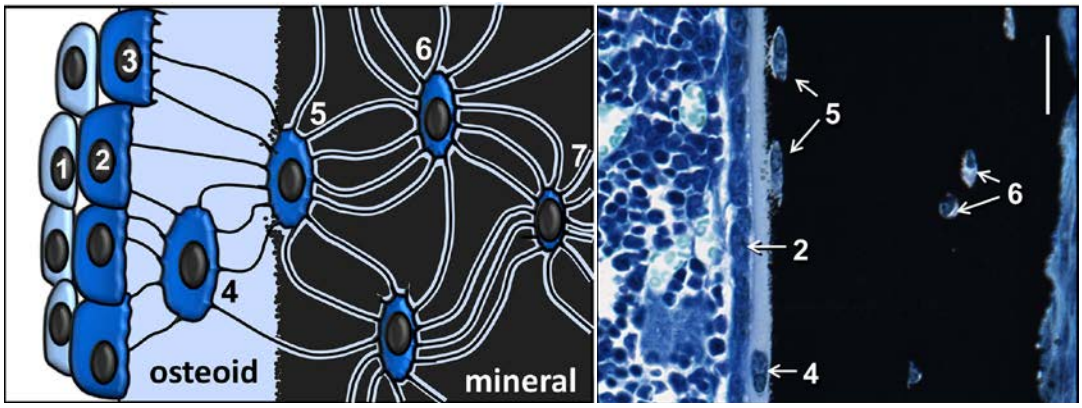

Figure 1.8 – Transition of Osteoblasts to Osteocytes
(Left) Diagram depicting the osteoblast-osteocyte transitional stages. (1 = pre-osteoblast; 2 = osteoblast; 3 = embedding osteoblast; 4 = osteoid-osteocyte; 5 = mineralizing osteocyte; 6 & 7 = mature osteocytes). **(Right)** Tetrachrome stained section of an adult mouse tibia (bar = 25 μm) illustrating some of these transition stages. (Adapted from Dallas 2013 [51])

As an osteoblast differentiates into a mature osteocyte its cell body volume and number of cell organelles decreases as the cell processes are being formed [51]. It was suggested that the osteoid-osteocyte is responsible for the initiation of the osteoid mineralisation [52]. Small calcified spheres were formed along the cell membrane at the mineralisation front as the maturing osteocyte cell processes branched out and becomes thinner with the shrinking down of the cell cytoplasm (Fig. 1.9). These mineralised spheres were associated with the collagen fibres being laid down simultaneously by the cell.

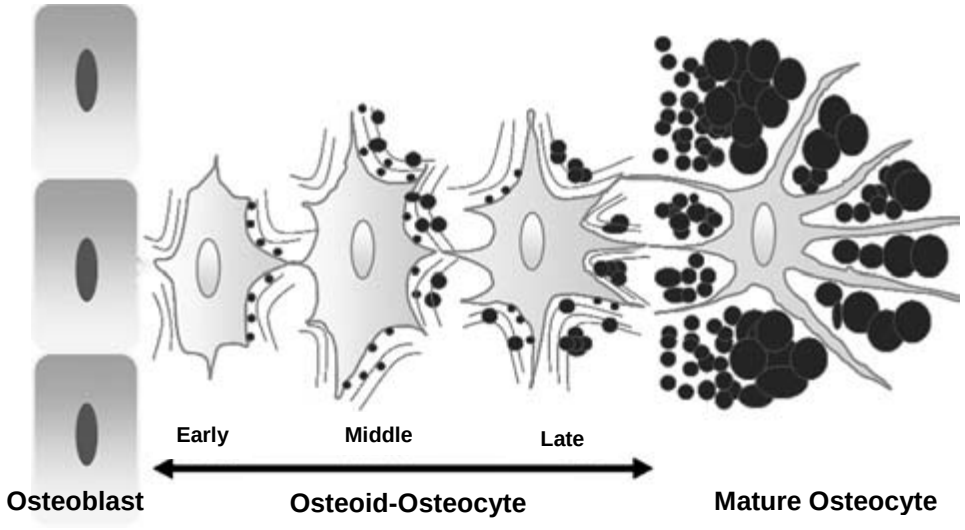

Figure 1.9 – Osteocytic Bone Matrix Mineralisation
Process of mineralisation of the osteoid matrix by the maturing osteocyte via formation of calcified spheres (black circles) toward the mineralising front by the osteoid-osteocyte. The size of the initial mineralised spheres increases as new spheres were formed with the shrinkage of the cell body and elongation the cell processes. (Adapted from Barragan-Adjemian 2006 [52])

It is important to note that the expression of molecular markers during the various stages of osteocytogenesis varies [51] and that it also differs between different sites in the body and different bone ages [48]. Some of these molecular markers will be elaborated on later in this chapter. Table 1.1 lists some of the osteogenic markers that are produced by the various cells during the osteoblast-osteocyte transition process.

Table 1.1 – Osteogenic Molecular Markers During Osteoblast to Osteocyte Transition

Osteogenic Marker	Pre-osteoblast	Osteoblast	Embedding osteoblast	Osteoid osteocyte	Mineralizing osteocyte	Mature osteocytes
RUNX2	+	+				
OCN		+	+	+	+	
E11			+	+	+	
DMP1			+	+	+	+
PHEX			+	+	+	+
MEPE				+	+	+
Sclerostin						+
CapG			+	+	+	+
ORP150						+

(Adapted from Dallas 2013 [51])

Mature osteocytes are stellate-shaped cells found within the lacunae of the bone matrix that have numerous thin cytoplasmic processes running through a canalicular network [53]. During intramembranous bone growth (modelling), two types of osteocytogenesis have been reported, static and dynamic [54], where the arrangement, movement and polarisation of the osteocytes as they become embedded in new bone are different. Dynamic osteocytogenesis is the classically described sequence of events alluded to above, where the osteoblasts undergoing transition to osteocytes are buried in a polarised manner by the bone-forming osteoblasts production of extracellular matrix forming the osteoblastic lamina.

Static osteocytogenesis precedes dynamic osteocytogenesis in intramembranous ossification, such as in the calvaria, sternum, scapula, clavicle bones of the pelvis and during bone modelling (Fig. 1.10), where pluristratified cords of stationary osteoblasts undergo transformation into osteocytes in a non-polarised and irregularly arranged manner [55]. The static bone formation-derived osteocytes are larger and more rounded in shape, located inside confluent lacunae, and with short symmetrical cytoplasmic processes radiating simultaneously from all around their cell bodies. The static osteocytogenesis process is to provide a rigid framework, the primary trabeculae, for the more classical dynamic osteocytogenesis to occur, as the latter requires a rigid mineralised surface, on which to lay osteoid [56]. This appears to be why static

osteocytogenesis does not occur in endochondral ossification [57], such as in the long bones during remodelling.

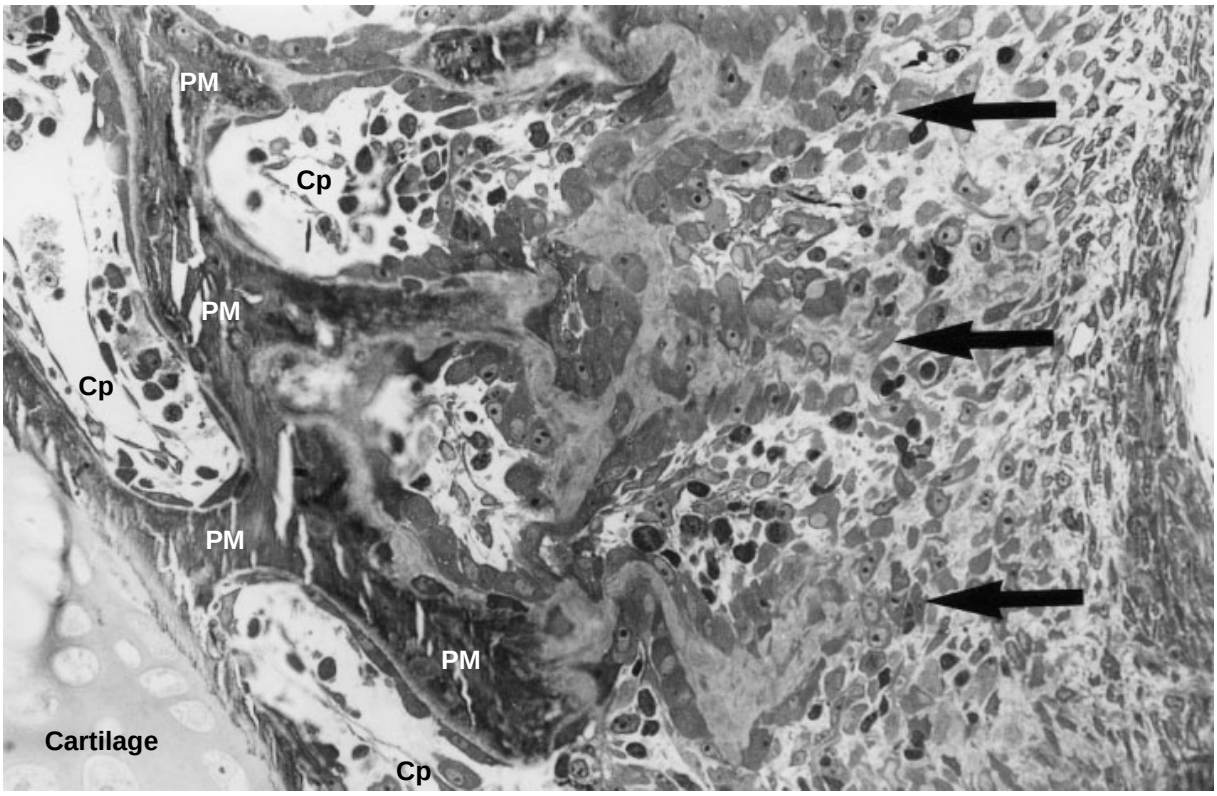

Figure 1.10 – Micrograph of Static Osteocytogenesis
Light microscopy micrograph (x440) of the intramembranous perichondral centre of ossification around the cartilaginous bud of the tibia, at the mid-shaft level, in a 15-day-old chick embryo. Cords of stationary osteoblasts (**arrows**), which will differentiate into osteocytes, can be seen surrounding the pre-osseous matrix (**PM**) and capillaries (**Cp**) in the inner layer of the periosteum. (Adapted from Palumbo 2004 [55] and Ferretti 2002 [54])

The morphology of the osteocyte has long been observed to be different between non-lamellar and lamellar bone [58], where they are either more rounded or more elongated in appearance, respectively. The morphology also differs in disease states that change the bone mineral density (BMD) [59]. Bone with low BMD has relatively large and round osteocytes, while in high BMD bone they tend to be smaller and more discoid shaped. Osteocytes are large and elongated in bone with intermediate BMD (Fig. 1.11). It is likely that the shape of the osteocyte plays a role in its ability respond to mechanical stimuli [60]. However, other factors, such as the osteocyte lacunae and the osteocyte cytoskeleton, are also involved and this will be further elaborated on later in this chapter.

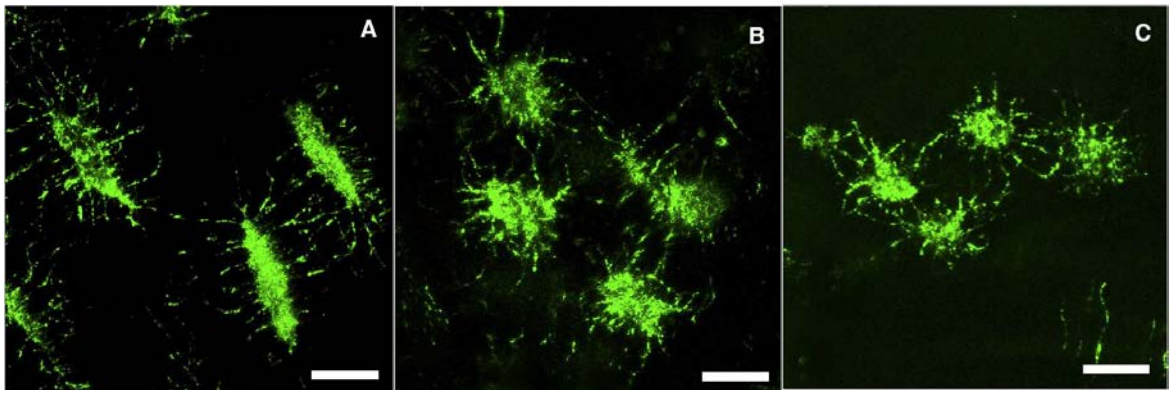

Figure 1.11 – Osteocyte Morphology in Bone with Different BMD

Confocal laser scanning microscopy scans of **(A)** osteoarthritic, **(B)** osteopenic and **(C)** osteopetrotic cortical bone showing the differently shaped osteocytes in each, which are elongated, round, and round but small, respectively. Bar, 15 μm (Adapted from van Hove 2009 [61])

1.3 Osteocyte Density

Previously reported observations have noted that not all lacunae contain an osteocyte, with a range of about 19% to 23% unoccupied lacunae being reported in adults [62]. The percentage of empty lacunae seems to be very much related to age, with only 1% at birth and up to 75% at the age of seventy. Differences are seen also between osteonal (Haversian) and interstitial bone [63].

The osteocyte density between different animal species also differs greatly, with 31,900 cells/mm^3 in domestic cattle, 37,300 cells/mm^3 in Rhesus monkeys, 43,100 cells/mm^3 in domestic pigs, 61,500 cells/mm^3 in New Zealand White rabbits and 93,200 cells/mm^3 in Wistar rats being reported [64]. There was a significant difference of the osteocyte density between species; except between the domestic pigs and Rhesus monkeys for osteocyte nuclei per bone area and between domestic pigs and Rhesus monkeys and between domestic cows and Rhesus monkeys for osteocyte nuclei per bone volume. (Table 1.2). There seemed to be an inversely proportional relationship between the size of the mammal and its metabolic rate with osteocyte density.

Table 1.2 - Osteocyte Density in Trabecular Bone of Five Mammalian Species

Osteocyte Density	Rat (n=6)	Rabbit (n=6)	Monkey (n=7)	Pig (n=6)	Cow (n=5)
Osteocyte nuclei per bone area (mm^{-2})	942.8 ± 49.5	679.2 ± 68.5	400.1 ± 47.9	399.5 ± 65.4	294.8 ± 24.4
Osteocyte nuclei per bone volume (mm^{-3}) x 10^3	93.2 ± 5.4	61.5 ± 6.8	37.3 ± 4.8	43.1 ± 7.6	31.9 ± 2.9

Adapted from Mullender 1996 [64].

In humans the number of osteocytes per volume of bone is reported to range from 10,500 [62] to 80,000 cells/mm^3 [48]. This great variation is probably due to a number of causes such as the bone that was investigated (i.e. iliac crest versus proximal femur), the type of bone investigated (cortical versus cancellous) and also the method of bone preparation and/or analysis performed [65]. Cane and his colleagues [66] have also reported a difference in the density of the lacunae between different parts of the long bones, with the highest being in the metaphyseal cancellous bone and the lowest in the diaphyseal compact bone. Interestingly, they also showed that there is a correlation between the relative number of lacunae and bone turnover rate as both are lowest at the diaphysis, intermediate at the epiphysis and highest at the metaphysis.

An age-related osteocyte decrease seems to occur in deep bone (greater than 45 μm from bone surface), but not in superficial bone (less than 25 μm from bone surface) [67], with a concomitant increase in the percentage of empty lacunae [68]. This suggests that reduced osteocyte number is related to the effective age of the bone (time since remodelling) rather than to the age of the individual. However, with aging there also seems to be a reduction in the size of the osteocyte lacunae, an increase in osteocyte apoptosis and a reduction in canaliculi number per lacuna, which likely affect the ability of aged bone to respond to mechanical loading [69].

There also seems to be ethnic differences, where healthy African American women were found to have a higher lacunae density, osteocyte density and empty lacunae when compared to healthy White American women of the same age [70]. The number of osteocytes per bone area is about 15% more in females, with fewer osteocytes in both males and females with osteoporosis [71]. The iliac cancellous bone osteocyte density of women with non-traumatic fragility fracture of the vertebra was reported 34% lower compared to healthy women in the same age group [68]. A higher osteocyte lacunae density has also been observed in woven bone and plexiform bone when compared to primary lamellar (parallel-fibred) bone [72], with an even lower density seen in secondary lamellar bone [73].

All the above point to the difficulty faced when comparing experiments performed on bone explants, more so when looking specifically at the osteocyte population, as a significant variation of the osteocyte lacunae density can occur, depending on the many various factors mentioned. Unless all of them are kept uniform, it will require an extremely large number of specimens to obtain a statistically significant conclusion. Thus, in the course of this study, it was important to take note of all these possible confounding factors to minimise their occurrence when performing experiments. They also need to be taken into account in the interpretation of the results.

1.4 Osteocyte Processes and the Canaliculi

Observations using transmission electron microscopy (TEM) have demonstrated that the development of the cytoplasmic processes during osteocytogenesis is highly organised and polarised [74]. As an osteoblast starts to differentiate into a Type 1 preosteocyte it begins to extend short, stumpy cytoplasmic processes (mineral processes) from its mineralisation front-facing surface. The processes of the mature osteocytes found deeper in the bone matrix form either invaginated finger-like, side-to-side or end-to-end contacts with the mineral processes or cell bodies of the preosteocytes [50]. Eventually, as the pre-osteocyte cell body detaches from

the osteogenic lamina (Type 3), it begins to radiate long, thin cytoplasmic processes from its vascular-facing surface, aptly named the vascular processes, which maintain connection, in the form of either adherens or gap junctions, with the osteoblasts and other pre-osteocytes at the osteoblastic lamina. Some of the osteocyte cytoplasmic processes have also been reported to extend beyond the vascular-facing surface of the osteoblasts [75], raising the possibility that osteocytes are in communication with some of the bone marrow and haematopoietic cells. Recently, Honma and colleagues [76], using a novel 3D co-culture system, demonstrated that osteocytes directly interact with osteoclast precursors *via* their cytoplasmic processes.

The osteocyte canalicular diameter, measured using scanning electron microscopy (SEM), has been reported to vary from 50 - 1000 nm [77-79]. However, using atomic force microscopy (AFM), it was concluded that the width of the canaliculi is actually between 490 - 600 nm [77]. A highly ordered collagen fibril arrangement is seen on the canaliculi walls, forming ridges that are approximately 100 nm apart. The osteocyte cytoplasmic processes are much smaller with a diameter of 150 - 200 nm and a pericellular space of between 14 - 100 nm. The cytoplasmic processes of osteocytes almost always lie in the centre of the canaliculi, due to regularly spaced transverse elements anchoring them to the canalicular walls [79].

Various reports describe possible methods for visualising the highly complex nature of the osteocyte lacuno-canalicular network [53, 75, 80, 81]. Taking into account the osteocyte density, the lacuno-canalicular network was estimated to have a surface area that is approximately 133 times larger (1,200 m^2) than the total surface area for trabecular bone (9 m^2), and 400 times larger than the total combined area available for the Haversian and Volkmann systems (3 m^2) [32]. Accordingly, the surface area of the osteocyte (1,509 mm^2) is much larger than its cell and cell body volume (394 mm^3 and 257 mm^3 respectively) [53]. This extremely large surface area makes the lacuno-canalicular network and the osteocytes within well-suited to cater for the myriad functions that the osteocytes are now known to have.

1.5 Osteocyte Functions

As previously mentioned, the advent of new and highly sensitive molecular biology techniques in the last few decades has provided evidence for the highly important and central role that osteocytes seem to have with regards to regulating bone remodelling and other functions of bone as a whole [31, 32, 46, 47]. Osteocytes are well suited for this purpose, due to their unique morphology, density, connectivity and longevity within the lacuna and canaliculi network of bone, as detailed above. In addition, the large number of osteocytes means that relatively small changes brought about by the osteocytes on their microenvironment can be amplified to result in significant changes at the organism level [82]. It will be beyond the scope of this work to discuss in detail all of the known osteocyte functions. But, briefly, the various osteocyte functions that have been elucidated and the associated molecules expressed or produced by osteocytes are:

1.5.1 Matrix formation and mineralisation

This function of osteocytes is associated with the expression of dentin matrix protein-1 (DMP-1), matrix extracellular phosphoglycoprotein (MEPE, previously known also as Osteoblast/osteocyte factor 45 (OF45)), osteocalcin, osteopontin, matrix metalloproteinase-2 (MMP-2) and collagen type 1. It was suggested that MMP-2 not only degrades Type 1 collagen in the extracellular matrix but it is also crucial in the formation and maintenance of the osteocyte canaliculi network [83]. Holmbeck and colleagues [84] demonstrated that membrane type-1 matrix metalloproteinase (MT1-MMP) activity is required for the development and maintenance of the osteocyte cytoplasmic processes and canaliculi.

1.5.2 Autocrine and paracrine signalling activity

This function is associated with response to and/or production of insulin-like growth factor-1 (IGF-1) [85] and prostaglandin E_2 (PGE_2) [86], among others. Recent work by other investigators in this laboratory has demonstrated the role of the osteocyte in regulating some of the key functions in both osteoblasts and osteocytes *via* its autocrine and paracrine vitamin D3 metabolism pathways [87].

1.5.3 Osteoclastogenesis and regulation of osteoclast function

This function of osteocytes has been shown to be closely related to their expression of the receptor activator of NF-κB ligand (RANKL) [88], osteoprotegerin (OPG) [89] and macrophage colony-stimulating factor (M-CSF) [90], interferon β (IFN-β) [91], endothelial nitric oxide synthase (eNOS) [92] and nitric oxide (NO) [51, 93]. This pro-catabolic effect of osteocytes was shown to promote RANKL-dependent osteoclast formation and activity via the regulation of the RANKL-OPG axis (Fig. 1.12) [88]. Osteocytes was shown to be the main source of RANKL necessary for osteoclastogenesis in trabecular bone undergoing bone remodelling [94].

1.5.4 Regulation of osteoblast function

Osteoblasts are powerfully regulated by osteocytes by the production of the negative regulator of bone formation, sclerostin [90], Dickkopf-1 (Dkk1), NO, wingless integration (Wnt) signalling molecules and PGE_2 [86]. Sclerostin is emerging as an important osteocytic protein in both normal physiological states and pathological conditions [95]. A review of its biology is deemed necessary for this work and will be dealt with in the following sub-section.

1.5.4.1 Sclerostin

Sclerostin, the product of the SOST gene, is a potent negative modulator of the canonical Wnt/β-catenin pathway [96] and inhibitor of bone formation [82, 97, 98] via the down-regulation of osteoblastogenesis [99, 100]. It does so by binding to the Wnt co-receptors, low density lipoprotein receptor (LRP)-5 and 6 [101]. Its role in the regulation of bone formation was initially identified during work on the hereditary bone sclerosing conditions sclerosteosis, which was found to be due to inactivating mutation of SOST gene [102], and Van Buchem's disease, where a distal enhancer element mutation for the SOST gene results in its under-expression [103]. Sclerostin was found to be expressed by mature, mineral-embedded osteocytes only and was also found along the osteocyte processes in the canaliculi [104].

Mechanical stimulation of bone *in vivo* downregulated osteocyte expression of SOST and, therefore, reduced production of sclerostin, which led to increased bone formation [105, 106]. Conversely, loss of the SOST gene prevented bone loss due to mechanical unloading [106]. Osteocyte sclerostin expression was also found to be induced by the proinflammatory cytokines TNFα and TNF-related weak inducer of apoptosis (TWEAK) [107].

Sclerostin was also identified as the master regulator of late-osteoblast/pre-osteocyte differentiation and bone mineralisation [108]. Figure 1.12 illustrates how anti-anabolic stimuli increase sclerostin expression by mature osteocytes that stimulate (arrow A) the expression of phosphorylated MEPE by nearby late osteoblasts/pre-osteocytes in the osteoid. MEPE is cleaved by cathepsin B into phosphorylated ASARM peptides (ASARM-PO4) that attach to nascent hydroxyapatite-like (HA) crystals and prevent further mineralization of the osteoid. Additionally, sclerostin decreases PHEX expression by osteoblast-linage cells (yellow bar B) to decrease PHEX reversal of the inhibitory effect of MEPE on mineralization The net inhibition of mineralization by sclerostin is accompanied

by inhibition of late osteoblast/pre-osteocyte transition into mature osteocytes (yellow bar C).

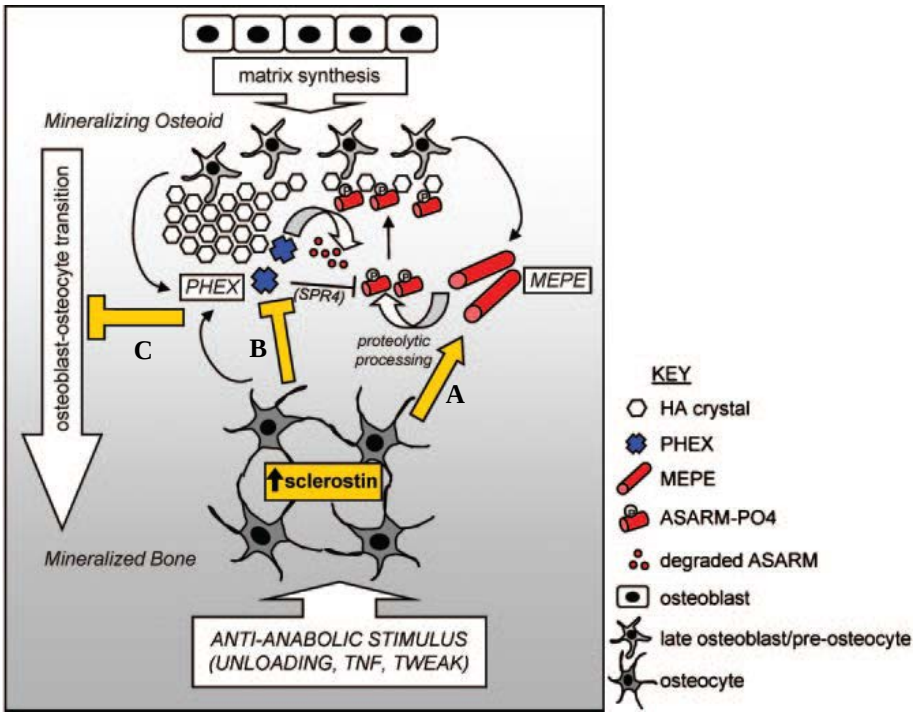

Figure 1.12 – Sclerostin and Bone Mineralisation

Diagrammatic representation on the role of sclerostin in bone mineralisation. Explanation in text above. (Adapted from Atkins 2011 [108])

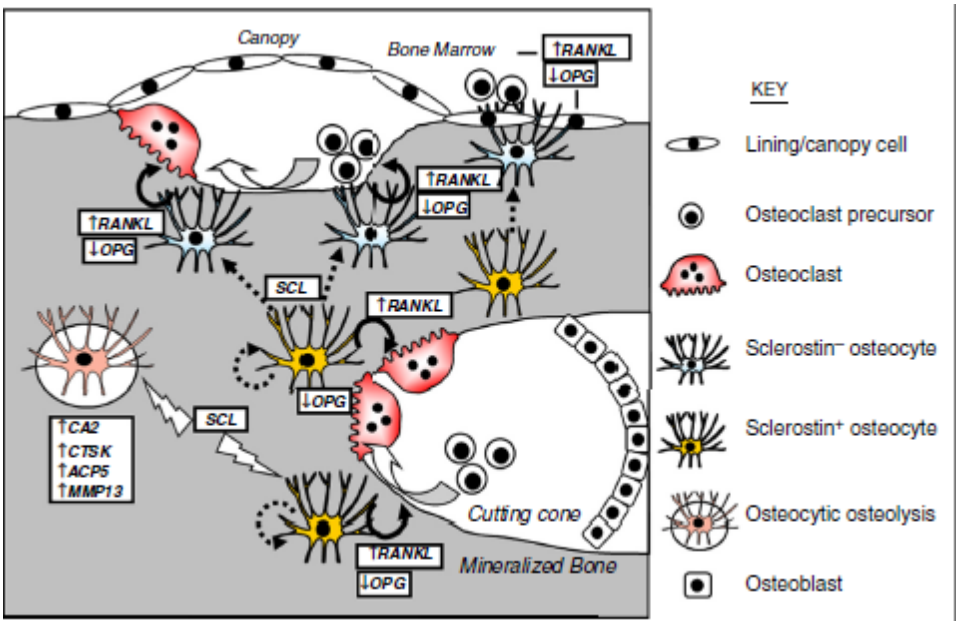

Figure 1.13 – Roles of Sclerostin

Diagrammatic representation on the role of osteocyte-derived sclerostin in regulating osteoclastogenesis, bone mineralisation and perilacunar remodelling. (Adapted from Prideaux 2016 [109])

Sclerostin also plays a role in the regulation of osteoclastogenesis by osteocytes [82], as previously mentioned above (section 1.5.3) and illustrated in Figure 1.13.

Sclerostin was also found to be expressed by other tissues, such as cartilage, kidney, heart, liver, testicular epididymis and vas deferens, stomach pyloric sphincter, carotid arteries and cerebellum [110]. It is also expressed by some of these tissues in pathological conditions that include osteoarthritis, rheumatic joint disease, bone and non-bone neoplasms, and vascular calcifications. However, its exact role in these conditions are not fully elucidated yet.

The role of sclerostin in the response and adaptation of bone to mechanical loading, or the lack of it, is proving to be complex and not fully understood yet [111]. Investigating the changes brought about by sclerostin in *ex vivo* trabecular bone using the Zetos™ will be part of this thesis work.

1.5.5 Neuronal signalling

Osteocytes may play a role in neuronal signalling, as glutamate transporter, nerve growth factor (in response to fracture) and serotonin receptor 5-HT_{2B} are expressed by them. The highest expression of 5-HT_{2B} mRNA was found in osteocytes. [112]

1.5.6 Phosphate homeostasis

This function is known to be associated with DMP1 and PHEX, which regulates fibroblast growth factor-23 (FGF23) production by osteocytes [113]. FGF23, together with its co-receptor the *Klotho* protein, not only plays a role in matrix mineralisation [114] but also decreases phosphate reabsorption and inhibits 25(OH)$vitD_3$ conversion to 1,25$(OH)_2vitD_3$ in the kidneys [36, 115]. Klotho gene deleted mice have a disturbed spatial distribution of

osteocytes and synthesis of bone matrix proteins together with the prematurely-aged appearance of its bone cells [116]. Although Klotho was initially thought of as an aging gene it is now known that Klotho mutant mice die prematurely due to tissue calcification brought about by very high levels of calcium, phosphate, and $1,25(OH)_2D$ [117]. The αKlotho protein is an essential component of the endocrine fibroblast growth factor (FGF) receptor complexes, as it is required for the high- affinity binding of FGF23 to bind to and activate its cognate FGF receptors (FGFRs) in physiologically relevant tissues [118, 119]. Recent reviews have elaborated on the association of osteocyte-derived FGF23 with the mineral and bone disorder of chronic kidney disease (CKD-MBD) [118, 120]; cardiovascular diseases, such as left ventricular hypertrophy, vascular dysfunction and arterio/atherosclerosis [118, 121]; secondary hyperparathyroidism (including hereditary hypophosphataemia and hyperparathyroidism (HHH)); hereditary phosphate- wasting syndromes, which includes autosomal dominant hypophosphataemic rickets (ADHR), X-linked hypophosphataemia (XLH) and autosomal recessive hypophosphataemic rickets (ARHR) [120, 122]; and the $1,25(OH)_2D$ counter-regulatory effects of FGF23 on mineral metabolism, innate immunity and cardiovascular responses [123].

1.5.7 Endocrine signalling

There is strong evidence for this function as various hormone receptors are found on the osteocyte cell surface or in the cytoplasm, such as oestrogen receptor (ER) α and β, glucocorticoid receptor, vitamin D receptor (VDR), and parathyroid hormone (PTH)/parathyroid hormone-related peptide (PTHrP) type 1 receptor (commonly known as PTHR1) [124]. Bone is now recognised as an endocrine organ as osteocytes produce FGF23 that acts on other tissues distantly [51] as mentioned in 1.5.6.

The osteocyte function that is of most interest in this work is related to the ability of bone to sense and respond to mechanical stimulation. Much work has been done on determining the process of mechanosensing and mechanotransduction in bone and the central role of osteocytes in these processes [30]. Mechanotransduction is the mechanism, by which a mechanical load applied to bone is converted to biological signals for maintaining appropriate strength and mechanical integrity of the bone. When loaded, osteocytes have been shown to respond by increasing their production and release of NO, PGE_2 and IGF-1, expressing type I collagen, reducing their expression of glutamate transporter [125], and the activation of ion channels with concomitant increase in intracellular calcium ion (Ca^2) levels. A more detailed review of the current knowledge on this major function of osteocytes is given below.

1.6 Mechanosensing and the Osteocyte Lacunae

The orientation of the osteocyte lacunae was found to be parallel to the collagen fibre orientation in the surrounding matrix in osteons [126] and its shape is also likely to be in response to the mechanical loading that it perceives [60]. Additionally, the perilacunar matrix surrounding the osteocyte behaves differently than the rest of the mineralised bone matrix [127] and osteocytes seem to be able to directly modulate this region in various physiological and pathological circumstances [109]. This 2 to 8 μm wide region has not only a very different collagen fibril orientation but is also usually not as well mineralised and has a lower elastic modulus as more distal bone. Using machine vision photogrammetry, a digital stereoimaging correlation-based technique [128], the osteocyte lacunae was demonstrated to act as a strain concentrator that generates peak levels close to 35,000 μstrain locally from loads that produce only 2,000 μstrain at the tissue level [129]. A decrease in the modulus of the perilacunar matrix seems to increase this strain amplification effect further, while an increase in the modulus lessens the effect [130]. When 1.4 mg/kg/day of prednisolone was continuously administered subcutaneously in Swiss-Webster mice over a 21-day period, an increase in the size of the

osteocyte lacunae, with a reduced perilacunar elastic modulus, was observed [131] and this probably enhanced this strain concentrating effect. The maintenance of the perilacunar matrix stiffness was suggested to be *via* the regulation of dentin matrix protein-1 (DMP1) and matrix extracellular phosphoglycoprotein (MEPE) expression by osteocytes, in response to mechanical loading [132], hence the fact both these molecules are found to be mechanically responsive, as will be further explained below.

Primary cultures of human osteoblast-like cells and cells in bone organ cultures do not seem to respond to physiological levels of strain [133]. Work *in vitro* has shown that a relatively large strain of more than 5,000 μstrain (10,000 μstrain to 100,000 μstrain) is required to elicit a biochemical intracellular response to loading in bone cells [134], where strain is defined as cellular deformation with 10,000 μstrain being equal to 1% deformation of the cell [135]. However, in humans, the tibia will normally experience much smaller strains in the range of only 400 μstrain during walking and 850 μstrain when running [136]. Similar figures are also observed in sheep [137] and other animals. Even during extremely strenuous physical activity, in conditions similar to what an army recruit in training goes through, strain in the tibia is kept below 2,000 μstrain [138]. However, using fluorescence recovery after photobleaching (FRAP) techniques and confocal microscopy, a load of 1.7 Newton applied at 2Hz to the distal epiphysis of a rat femur was shown to enhance molecular transport in the cortical bone by approximately 25% without inducing a significant deformation (<100 μstrain) in the diaphysis [78]. This indicates that localised strain at the microscopic level is not reflected by the strain at the tissue (macroscopic) level.

A new model has been proposed, whereby strain applied to the bone is amplified by a factor of at least 20 to over 200 times at the osteocyte cytoplasmic process cell membrane in the canaliculi, producing strain levels of 3000 μstrain to nearly 50,000 μstrain [139]. This model is able to demonstrate mathematically how fluid drag on the pericellular matrix gets transmitted

to the aforementioned transverse element in the canaliculi and ultimately generate an outward hoop strain on the osteocyte cytoplasmic process cell membrane and cytoskeleton.

Mechanosensing by the osteocyte also seems to involve both stretch-activated and voltage-dependent ion channels found on its cell membrane. The presence of various integrins and their relation to the osteocyte cytoskeleton is also important, as has been mentioned previously. Cytoskeleton mediated response is probably due to the drag forces from fluid flow on the pericellular matrix that are attached to the cytoskeleton by the integrins [79]. The gap junctions and hemichannels on the osteocyte cell membrane are important for propagating an intracellular calcium ion wave and fluid flow-induced release of adenosine triphosphate (ATP) and PGE_2, respectively. Both are formed by connexin 43 (Cx43), a protein known to be highly expressed by osteocytes. Recent reports have demonstrated the presence of primary cilia and the expression of polycystin-1 (PC1) in osteocytes and their possible role in bone triggering anabolic responses in these cells [140, 141]. This structure seems to be necessary for fluid flow-induced PGE_2 release in osteocytes [142, 143].

1.7 Role of Molecular Markers of Osteocytogenesis in Mechanotransduction

One of the questions that has been frequently asked is how a particular osteoblast is chosen to be transformed into an osteocyte. This process of osteocytogenesis and its control is still unclear and is the subject of ongoing investigation [46, 48]. A number of molecules have been found to be expressed during various stages of osteocytogenesis. Previous work at this laboratory has shown that vitamin K and strontium ranelate promote osteocytogenesis [144, 145]. Describing in detail all the molecular markers is beyond the scope of this work. Emphasis will be given to those markers that are known to be associated with the osteocyte cytoplasmic processes and mechanotransduction.

DMP1 is a non-collagenous extracellular bone matrix protein that belongs to the small integrin-binding ligand N-linked glycoprotein (SIBLING) family of proteins. It is specifically expressed by osteocytes [146] and preosteocytes but not osteoblasts [147]. Its expression is stimulated by mechanical loading of bone [148]. DMP1 is localised not only in the osteocytic pericellular matrix but also along the canaliculi walls and the lamina limitans. Its expression in the extracellular matrix has been shown to be critical for osteocyte maturation and, subsequently, osteoid mineralisation [149].

MEPE, also known previously as osteoblast/osteocyte factor-45 (OF45) [150], is another member of the SIBLING family of proteins that has been shown to modulate bone formation and mineralisation [151] and also promote phosphate excretion by the kidneys [152]. MEPE is also expressed by mechanical stimulation of the osteocyte but in a delayed fashion when compared to DMP1 [153]. It is cleaved by cathepsin B to release a highly phosphorylated carboxy-terminal containing the acidic, serine- and aspartate-rich MEPE associated motif (ASARM) peptide that is known to inhibit mineralisation, while MEPE with its ASARM peptide removed is suggested to be the *in vivo* anabolic variant [154]. Post-translational modification of MEPE is proposed to be important for the site-specific activity and different effects each component has on the osteogenic signalling processes [155].

A recent review by Uda and colleagues [30] summarises much that has been written so far. Mechanosensing is *via* integrins, cilia, calcium channels and G-protein coupled receptors (GPCR) [156] of osteocytes that results in the secretion of several factors, such as sclerostin, RANKL, PGE_2, NO, IGF-1 and PTHrP, which are capable of giving rise to the appropriate response to mechanical stimuli in neighbouring bone cells.

1.8 Parathyroid Hormone, Glucocorticoid Administration and the Possible Role of Osteocytic Osteolysis in Mechanotransduction

Early investigators in the last century have noted the enlarged appearance of the lacunae in bone following administration of parathyroid hormone (PTH) extracts over a period of several days and the term 'osteocytic osteolysis' was coined by them for this phenomena [157]. This was reconfirmed by Tazawa and his colleagues when they reported evidence of osteocytic osteolysis in 8-month-old rats that were continuously administered with human PTH for 4 weeks [158]. Parathyroid hormone-related protein (PTHRP) was first isolated from tumours associated with the paraneoplastic syndrome of humoral hypercalcaemia of malignancy [159]. It shares structural and functional homology with PTH [160] and was shown to be integral to bone formation [161]. Both PTH and PTHrP act directly on osteocytes by binding to the PTH/PTHrP type 1 receptor (PTHR1) on its cell membrane. The actions of activated PTH1Rs in osteocytes are multi-fold. Among others, it promotes gap junction-mediated intercellular coupling, potentiates calcium influx via stretch-activated cation channels, increases expression of MMP-9, amplifies the osteogenic response to mechanical loading in vivo, and regulates osteocyte apoptosis [162].

PTH stimulates bone remodelling and may cause bone loss or bone gain depending on the balance between bone resorption and bone formation. In hyperparathyroidism, where there is a chronic excess of PTH, the number of osteoblasts increases and it is associated with bone catabolism. Intermittent elevation of PTH by daily injections, on the other hand, also increases osteoblast number but it is associated with bone anabolism and the attenuation of osteoblast apoptosis, which requires the transcription factor RUNX2. With chronic elevation of PTH osteoblast apoptosis was not affected because it stimulates the proteasomal degradation of RUNX2. The activation of PTHR1 by PTH or PTHrP also results in the greatly reduced expression of the SOST mRNA, resulting in the decrease of sclerostin production by osteocytes, and is partly responsible for the increased osteoblast number [163, 164]. Mice with constitutive

activation of PTHR1 in osteocytes showed an increased in bone mass and remodelling, the skeletal actions of PTH, with decreased expression of the osteocyte-derived Wnt antagonist SOST/sclerostin, similar to PTH administration. It was demonstrated that active PTH receptor signalling in osteocytes increases bone mass through LRP5-dependent mechanisms and the rate of bone remodelling via LRP5-independent mechanisms, involving increased levels of RANKL and M-CSF, in these mice [165, 166]. Activity in the periosteal and endocortical surfaces of cortical bone have a profound effect on bone geometry and its mechanical properties and PTH is known to stimulate cortical periosteal expansion and intracortical bone remodelling. It was reported that PTHR1 activation influences cortical bone by acting on osteocytes, which defines the role of PTHR1 action in Wnt signalling in transgenic mice [167]. Even though SOST downregulation and the consequent Wnt activation is required for the stimulatory effect of PTHR1 activation on periosteal bone formation, the Wnt-independent increase in osteoclastogenesis induced by PTHR1 activation in osteocytes overrides the effect on SOST. PTHR1 signalling was also reported to be able to modulate not only the endocrine but also the autocrine and paracrine functions of osteocytes by regulating FGF23 through cAMP- and Wnt-dependent mechanisms [168]. The periosteal bone formation induced by the activation of PTHR1 in osteocytes depends on Wnt signalling but not on resorption. Endocortical bone formation, on the other hand, is from a combination of Wnt-driven increased osteoblast number and resorption-dependent osteoblast activity. The elevated osteoclasts and intracortical porosity is exacerbated by overexpressing SOST and reversed by blocking resorption. While increased cancellous bone is abolished by Wnt inhibition but further increased by blocking resorption. Therefore, resorption induced by PTHR1 action in osteocytes is critical for full anabolism in cortical bone, but modulates bone gain in cancellous bone [169]. A recent study suggested that the anabolic action on the skeleton induced by short-term administration of PTH is due to the increase in osteoprogenitors cells in cancellous bone and the decrease in mature osteocytes in cortical bone [170]. These studies demonstrated increased osteoblastogenesis with subsequent bone formation and also increased M-CSF expression, RANKL to OPG ratio,

osteoclastogenesis, cortical bone porosity and elevated blood and urine resorption markers due to high bone resorption. The current concept is that PTH utilizes both catabolic (OPG/RANKL/RANK) and anabolic (SOST/sclerostin) pathways in exerting its effect on bone. More recently, PTH signalling in osteocytes was also demonstrated to also have an important role in calcium homeostasis [171]

Conversely, the carboxyl-terminal region of PTH, which comprise the majority of circulating PTH, produces specific actions on bone metabolism and calcium homeostasis via a different osteocyte surface receptor known as the carboxyl-terminal PTH receptor (CPTHR) [42]. Activation of CPTHRs in osteocytes seems to cause increased apoptosis and a rapid increase in intracellular calcium, most likely through the opening of voltage-dependent calcium channels (VDCCs) [172], with rapid modification of the cytoskeleton [173]. Osteocyte apoptosis in itself is associated with a series of events that result in the localised recruitment of osteoclasts and initiation of bone remodelling [174].

Osteocyte apoptosis can also be induced by glucocorticoids [175]. Excess glucocorticoids can also reduce osteoblastogenesis, induce osteoblast apoptosis, impair osteoblast function and increase osteoclastogenesis [176]. This involves the early upregulation of genes involved with both osteoclast activation and function in mice that peaked at day 7; followed by a later peak at day 28 in the expression of genes associated with osteoclast cytoskeleton reorganisation and matrix degradation; decreased expression of genes for osteoblast activation and maturation, increased Wnt antagonist expression, and also expression of osteocytic genes involved with bone mineralisation [177]. There is a significant reduction in the trabecular bone volume and bone strength in glucocorticoid (prednisolone) treated mice [131]. Administration of PTH reverses these effects by increasing bone formation, which subsequently improves bone mass, bone mineralisation and bone strength in glucocorticoid-treated mice [178]. A more detailed discussion on the role of PTH, PTHRP and CPTHR on the osteocytes can be found in some recent reviews [124, 179-181] , which are beyond the scope of this work.

Together with the connection between the osteocyte lacunae, the perilacunar matrix and osteocyte mechanosensing, which was described at some length earlier in this chapter, there is a strong implication that osteocytic osteolysis plays a role in mechanotransduction and the ability of the osteocyte to respond to mechanical loading [182].

1.9 The Relationship between Bone Remodelling and Biomechanics

Bone adapts its form to mechanical demands through a mechanism known as bone modelling, whereby bone resorption by osteoclasts and bone formation by osteoblasts occurs on different surfaces of the skeleton as the bone undergoes reshaping to adapt to the physiological influences or mechanical forces on it. Bone remodelling, on the other hand, is the continuous and spatially coupled, resorption and formation of the skeleton to preserve functional integrity [183]. Frost's mechanostat [2] distinguishes between bone modelling, which is the formation and shaping of bone to adapt to mechanical loading above physiological loading, and remodelling, which is the replacement or renewal of old bone, bone microdamage due to pathological loading or net resorption of bone due to disuse and mineral homeostasis requirements. [184]

Disuse (lack of loading) causes an accelerated bone turnover, where bone resorption is more than bone formation, and this eventually results in rapid bone loss in both human and animal alike [1, 2, 185]. Bone overuse, on the other hand, gives rise to bone microdamage and this stimulates targeted remodelling of the affected area of bone [186-189]. Periosteal bone formation had been shown to increase most with loading. In cancellous bone the trabeculae are aligned in the same direction as the maximum stress that the bone is subjected to normally. This anisotropic behaviour of bone provides for increasing load-carrying capacity without much increase in bone mass. Bone strength is also further improved by the change in the alignment of the collagen fibres during remodelling. In regions of compression, the collagen fibres are aligned in transverse to the long axis of the bone, while in regions that undergo tensile forces the collagen fibres are aligned longitudinally [190].

Previous work in rats showed that loading of bone gives rise to an increase in strength by 64%, the second moment of area by 69% and the energy absorbed before fracture by 94%. [191]. However, these substantial increases of the bone biomechanical properties are followed by a modest 7% increase only of the bone mineral content. This ability of bone to adapt to the changing mechanical stresses that it experiences during modelling and remodelling seems to follow three fundamental rules that were put forward by Turner in 1998 [192], which are:

1.9.1 Bone adaptation to its mechanical environment is driven by dynamic, rather than static, loading.

Loading frequency and strain rate are both important for bone to respond to the mechanical stress applied to it. Rates of loading above 0.5Hz are required to produce bone formation [193, 194]. The bone formation increase to mechanical loading seems to be in a dose-response manner that differs between different sites on the same bone [195]. Above 10Hz the same load will have a similar anabolic effect with no further significant increase in the bone formation rate [196]. However, very low loading levels at higher frequency (90Hz) can reverse disuse bone loss [197, 198].

1.9.2 Only a short duration of mechanical loading is necessary to initiate this bone adaptation response.

Robling and colleagues [199] described a decrease by more than 95% of the mechanosensitivity in bone after loading for 20 consecutive cycles, while the anabolic effect plateaus at 40 cycles. However, a rest of 4 hours in between loading sessions will result in 80% more bone formation [200] and full mechanosensitivity returns with 8 hours of rest between the loading sessions [201]. Loading of bone in a single session (360 cycles x 1) in rats gave rise to significant increases in strength, the second moment

of area and energy absorbed before fracture (64%, 69% and 94%, respectively) but with a very modest increase in bone mineral content (BMC) only (6.9%). However, when the loading sessions were divided into 4 equal sessions (90 cycles x 4) with a 3 hours rest intervals between them, the same parameters increased even more substantially, with 87%, 96% and 165%, respectively for strength, second moment of area and energy absorbed before fracture. The BMC only increased by 11.7% in these animals [191], indicating that only a small change in the bone added is required, when it is added at sites of high strain, to produce these dramatic increases in the bone material properties. A 10 second rest interval amplified the mechanical loading induced response of bone significantly to small increases in strain magnitudes or the cycle numbers within the peri-threshold range [202, 203].

1.9.3 The bone cells accommodate to the mechanical loading environment, causing them to be less responsive to routine loading signals.

In an experiment reported by Saxon and colleagues [204], rats were loaded over a period of 15 weeks in 3 different groups; either for 15 weeks straight, 5 weeks loaded and 10 weeks without, or loaded for 5 weeks in two different sessions with a 5 weeks break in between. They found that long-term loading of bone results in a similar increase of bone mass and bone geometry. However, the bone formation response is maximal only within the first two weeks and the response gradually decreases with continued loading to return to normal levels after 10 weeks has passed. But bone formation rate and resistance to fracture is significantly increased if there is a break from loading in between.

1.10 Long-Term Disuse and Bone Loss

Long-term disuse, such as prolonged bed rest, results in reduced bone formation on periosteal surfaces, with an increase in bone resorption and turnover on endocortical and trabecular surfaces. In growing bones, the bones become thin and spindly, with smaller cross section and a greatly reduced second moment of area [205]. In more mature bones, the bone loss is mainly at the endosteal and trabecular surfaces of the long bones, giving rise to much thinner and more porous cortical bone [206]. In humans, with prolonged bed rest, there is more prominent bone loss in regions normally under the greatest amount of loading on weight bearing [207]. There is more bone loss in the calcaneum, which normally experiences up to 4.2 to 5.4 times the body weight during walking and 7.9 to 11.1 times body weight on running [208], than in the hip, which only experiences less than 3 times the body weight during walking and going up or down the stairs [209] and up to 5.5 times body weight during fast walking and jogging [210]. Conversely, there is an increase in bone density in the skull, which is normally under lower mechanical stress when upright.

An interesting question that has not been addressed in the current literature is the effect of unloading bone from a biochemical and molecular point of view with respect to the increased bone loss, increase osteoclast activity and role of osteocytic osteolysis, such as the production of collagen breakdown products and crosslap among others. Another interesting area, which can be investigated using the Zetos™ system, is the protective effect of certain agents against these effects of mechanical unloading of bone. The application of the results of many of the previously published works are limited by the fact that they use non-human cells, such as the murine long-bone osteocyte Y4 (MLO-Y4) cell line [211], foetal chick cells [212], mouse calvarial cells etc. [47]. Most of these cells are cultured on plastic, giving rise to a very artificial 2-dimensional environment as opposed to the 3-dimensional nature of the bone matrix that osteocytes are normally found in. In cell culture work, more often than not, the cells are grown in isolation without the normal interaction with the other bone cells and also the haemopoietic

bone marrow cells. The reported mechanotransduction studies use many *in vivo* and *in vitro* models in their investigations, including cell culture, organ culture [213], whole organism, cells in bioreactors and cells seeded on 3-dimensional scaffolds, as described earlier in this chapter. However, many investigations were not performed under normal physiological conditions and the mechanical parameters were not able to be measured in real-time. All of these limitations could be addressed, in full or in part, with the Zetos™ system.

1.11 Summary and research gap

The last two decades have seen unprecedented interest in the research community on the osteocyte ability to sense mechanical loading of bone and transduce these signals into biological cues that modulates the response of bone to these forces. A better understanding of Wolff's Law and Frost's mechanostat on bone remodelling is made possible with these findings. New research techniques and modalities have made it possible to unravel the myriad functions of the osteocytes, which was previously almost impossible to do. In spite of this, methods to investigate the function of osteocytes within the environment of its lacuno-canalicular network is still very limited. The Zetos™ system have made it possible to do so to in trabecular bone samples. Significant improvements were made recently to both the hardware and software of the Zetos™ system to further improve its application for bone research. However, optimisation of the second generation Zetos™ system, especially with its software to automate and control the function of the improved hardware, is necessary before it can be reliably used for this or other purpose.

Sclerostin is an important osteocyte-specific protein that has been found to be central to the various facets of osteocyte mechanotransduction. Many of sclerostin functions and effects were inferred indirectly from *in vitro* work on osteoblast lineage cells and *in vivo* work in whole animal studies or whole organ culture. It is now possible to investigate the direct effects of sclerostin on trabecular bone with the Zetos™ system.

1.12 Research objectives

The research described in this thesis is meant to look at the feasibility of using the second generation Zetos™ system for bone research, specifically on osteocytes in trabecular bone. The work is divided into two components, which are, firstly, the optimisation and validation of the second generation Zetos™ system itself, with particular emphasis on the beta-testing of its software; and, secondly, on the use of the second generation Zetos™ system for various forms of bone and osteocyte research.

1.12.1 Hypotheses:

Chapter 2 – The second generation Zetos™ system can be further optimised as a suitable investigation tool for bone and osteocyte research.

Chapter 3 – The drug-release kinetics and drug distribution in *ex vivo* trabecular bone of a novel nano-engineered drug delivery device can be studied using the second generation Zetos™ system.

Chapter 4 – Osteocytes in trabecular bone that are mechanically loaded using the second generation Zetos™ system are effected by exogenous sclerostin

1.12.2 Project Aims:

Chapter 2

- To beta-test the Zetos™ software together with its hardware
- To optimise the second generation Zetos™ system and its methodology
- To investigate the effect of marrow removal on mechanically loaded *ex vivo* trabecular bone cores

Chapter 3

- To monitor the release and transport of a model drug from nanoengineered titanium wires generated with titania nanotube arrays (TNT-Ti) *in vitro*
- To characterise the drug diffusion pattern from the TNT-Ti implant in *ex vivo* trabecular bone
- To determine the effects of culture medium perfusion on the drug diffusion of the TNT-Ti implant
- To investigate the application of the second generation Zetos™ system for studying drug-release kinetics and drug distribution in *ex vivo* trabecular bone

.

Chapter 4

- To examine the effect of exogenous sclerostin on mechanically loaded *ex vivo* trabecular bone samples, using the second generation Zetos™ system.
- To investigate the effect of exogenous sclerostin on ionic calcium uptake in *ex vivo* trabecular bone that are mechanically loaded
- To determine how osteocytic osteolysis is effected by exogenous sclerostin when *ex vivo* trabecular bone is mechanically loaded

Chapter 2 is a detailed description on the methodology for the optimisation and use of the second generation Zetos™ system, including the beta-testing of its software. Chapter 3 is a recently published study in which the application of nano-engineered titanium wires generated with titania nanotube arrays as drug-releasing implants for local drug delivery in trabecular bone were investigated using the second generation Zetos™ system. Chapter 4 is another recently published study that investigated the contribution of osteocytes to bone mineral accretion and the mechanical properties of trabecular bone in response to mechanical loading. The effects of exogenous sclerostin on this response and their potential mechanisms were also investigated.

1.13 References

1. Wolff, J., *The law of bone remodelling*. 1986: Springer-Verlag. 126.

2. Frost, H.M., *Bone "mass" and the "mechanostat": a proposal.* Anatomical Record, 1987. **219**(1): p. 1-9.

3. Hughes, J.M. and M.A. Petit, *Biological underpinnings of Frost's mechanostat thresholds: the important role of osteocytes.* J Musculoskelet Neuronal Interact, 2010. **10**(2): p. 128-35.

4. Chen, J.H., et al., *Boning up on Wolff's Law: mechanical regulation of the cells that make and maintain bone.* J Biomech, 2010. **43**(1): p. 108-18.

5. Jones, D.B., et al., *Development of a mechanical testing and loading system for trabecular bone studies for long term culture.* Eur Cell Mater, 2003. **5**: p. 48-59; discussion 59-60.

6. Davies, C.M., et al., *Mechanically loaded ex vivo bone culture system 'Zetos': systems and culture preparation.* Eur Cell Mater, 2006. **11**: p. 57-75; discussion 75.

7. Stoddart, M.J., et al., *A comparison of non-radioactive methods for assessing viability in ex vivo cultured cancellous bone: technical note.* Eur Cell Mater, 2006. **12**: p. 16-25; discussion 16-25.

8. Mann, V., et al., *The influence of mechanical stimulation on osteocyte apoptosis and bone viability in human trabecular bone.* J Musculoskelet Neuronal Interact, 2006. **6**(4): p. 408-17.

9. David, V., et al., *Ex Vivo bone formation in bovine trabecular bone cultured in a dynamic 3D bioreactor is enhanced by compressive mechanical strain.* Tissue Eng Part A, 2008. **14**(1): p. 117-26.

10. Endres, S., et al., *Zetos: a culture loading system for trabecular bone. Investigation of different loading signal intensities on bovine bone cylinders.* J Musculoskelet Neuronal Interact, 2009. **9**(3): p. 173-83.

11. David, V., et al., *Mechanical loading down-regulates peroxisome proliferator-activated receptor gamma in bone marrow stromal cells and favors osteoblastogenesis at the expense of adipogenesis.* Endocrinology, 2007. **148**(5): p. 2553-62.

12. Dumas, V., et al., *The effect of dual frequency cyclic compression on matrix deposition by osteoblast-like cells grown in 3D scaffolds and on modulation of VEGF variant expression.* Biomaterials, 2009. **30**(19): p. 3279-88.

13. Rahman, S., et al., *Drug diffusion, integration, and stability of nanoengineered drug-releasing implants in bone ex-vivo.* J Biomed Mater Res A, 2016. **104**(3): p. 714-725.

14. Schnieders, J., et al., *Ex vivo human trabecular bone model for biocompatibility evaluation of calcium phosphate composites modified with spray dried biodegradable microspheres.* Adv Healthc Mater, 2013. **2**(10): p. 1361-9.

15. Meyer, U., et al., *Design and performance of a bioreactor system for mechanically promoted three-dimensional tissue engineering.* Br J Oral Maxillofac Surg, 2006. **44**(2): p. 134-40.

16. el Haj, A.J., et al., *Cellular responses to mechanical loading in vitro.* J Bone Miner Res, 1990. **5**(9): p. 923-32.

17. Takai, E., et al., *Osteocyte viability and regulation of osteoblast function in a 3D trabecular bone explant under dynamic hydrostatic pressure.* J Bone Miner Res, 2004. **19**(9): p. 1403-10.

18. Mauck, R.L., et al., *Functional tissue engineering of articular cartilage through dynamic loading of chondrocyte-seeded agarose gels.* J Biomech Eng, 2000. **122**(3): p. 252-60.

19. Marino, S., et al., *Models of ex vivo explant cultures: applications in bone research.* Bonekey Rep, 2016. **5**: p. 818.

20. Chan, M.E., et al., *A Trabecular Bone Explant Model of Osteocyte-Osteoblast Co-Culture for Bone Mechanobiology.* Cell Mol Bioeng, 2009. **2**(3): p. 405-415.

21. Boukhechba, F., et al., *Human primary osteocyte differentiation in a 3D culture system.* J Bone Miner Res, 2009. **24**(11): p. 1927-35.

22. Gu, Y., et al., *Microbeads-Guided Reconstruction of 3D Osteocyte Network during Microfluidic Perfusion Culture.* J Mater Chem B, 2015. **3**(17): p. 3625-3633.

23. Sun, Q., et al., *Ex vivo 3D osteocyte network construction with primary murine bone cells.* Bone Res, 2015. **3**: p. 15026.

24. Sun, Q., et al., *Ex vivo construction of human primary 3D-networked osteocytes.* Bone, 2017. **105**: p. 245-252.

25. Li, Z., et al., *Chondrogenesis of Human Bone Marrow Mesenchymal Stem Cells in Fibrin-Polyurethane Composites is Modulated by Frequency and Amplitude of Dynamic Compression and Shear Stress.* Tissue Eng Part A, 2009.

26. Gusmao, C.V. and W.D. Belangero, *HOW DO BONE CELLS SENSE MECHANICAL LOADING?* Rev Bras Ortop, 2009. **44**(4): p. 299-305.

27. Capulli, M., R. Paone, and N. Rucci, *Osteoblast and osteocyte: games without frontiers.* Arch Biochem Biophys, 2014. **561**: p. 3-12.

28. Buckwalter, J.A., et al., *Bone biology. II: Formation, form, modeling, remodeling, and regulation of cell function.* Instr Course Lect, 1996. **45**: p. 387-99.

29. Rosa, N., et al., *From mechanical stimulus to bone formation: A review.* Med Eng Phys, 2015. **37**(8): p. 719-28.

30. Uda, Y., et al., *Osteocyte Mechanobiology.* Curr Osteoporos Rep, 2017. **15**(4): p. 318-325.

31. Kogianni, G. and B.S. Noble, *The biology of osteocytes.* Curr Osteoporos Rep, 2007. **5**(2): p. 81-6.

32. Noble, B.S., *The osteocyte lineage.* Arch Biochem Biophys, 2008. **473**(2): p. 106-11.

33. Chen, H., T. Senda, and K.Y. Kubo, *The osteocyte plays multiple roles in bone remodeling and mineral homeostasis.* Med Mol Morphol, 2015. **48**(2): p. 61-8.

34. Bonewald, L.F., *Osteocyte messages from a bony tomb.* Cell Metab, 2007. **5**(6): p. 410-1.

35. Klein-Nulend, J., et al., *Sensitivity of osteocytes to biomechanical stress in vitro.* Faseb J, 1995. **9**(5): p. 441-5.

36. Fukumoto, S., *The role of bone in phosphate metabolism.* Mol Cell Endocrinol, 2009. **310**(1-2): p. 63-70.

37. Talmage, D.W. and R.V. Talmage, *Calcium homeostasis: how bone solubility relates to all aspects of bone physiology.* J Musculoskelet Neuronal Interact, 2007. **7**(2): p. 108-12.

38. Talmage, R.V. and D.W. Talmage, *Calcium homeostasis: solving the solubility problem.* J Musculoskelet Neuronal Interact, 2006. **6**(4): p. 402-7.

39. Kato, Y., et al., *Establishment of an osteocyte-like cell line, MLO-Y4.* J Bone Miner Res, 1997. **12**(12): p. 2014-23.

40. Kato, Y., et al., *Establishment of an osteoid preosteocyte-like cell MLO-A5 that spontaneously mineralizes in culture.* J Bone Miner Res, 2001. **16**(9): p. 1622-33.

41. Bodine, P.V., S.K. Vernon, and B.S. Komm, *Establishment and hormonal regulation of a conditionally transformed preosteocytic cell line from adult human bone.* Endocrinology, 1996. **137**(11): p. 4592-604.

42. Divieti, P., et al., *Receptors for the carboxyl-terminal region of pth(1-84) are highly expressed in osteocytic cells.* Endocrinology, 2001. **142**(2): p. 916-25.

43. Woo, S.M., et al., *Cell line IDG-SW3 replicates osteoblast-to-late-osteocyte differentiation in vitro and accelerates bone formation in vivo.* J Bone Miner Res, 2011. **26**(11): p. 2634-46.

44. Imai, Y., et al., *Regulation of bone metabolism by nuclear receptors.* Mol Cell Endocrinol, 2009. **310**(1-2): p. 3-10.

45. Hinton, P.V., S.M. Rackard, and O.D. Kennedy, *In Vivo Osteocyte Mechanotransduction: Recent Developments and Future Directions.* Curr Osteoporos Rep, 2018. **16**(6): p. 746-753.

46. Klein-Nulend, J. and L. Bonewald, *The Osteocyte*, in *Principles of Bone Biology*, J.P. Bilezikian, L.G. Raisz, and T.J. Martin, Editors. 2008, Academic Press: San Diego. p. 153-174.

47. Kalajzic, I., et al., *In vitro and in vivo approaches to study osteocyte biology.* Bone, 2013. **54**(2): p. 296-306.

48. Franz-Odendaal, T.A., B.K. Hall, and P.E. Witten, *Buried alive: how osteoblasts become osteocytes.* Dev Dyn, 2006. **235**(1): p. 176-90.

49. Li, M., et al., *Histochemical evidence of the initial chondrogenesis and osteogenesis in the periosteum of a rib fractured model: implications of osteocyte involvement in periosteal chondrogenesis.* Microsc Res Tech, 2004. **64**(4): p. 330-42.

50. Palumbo, C., S. Palazzini, and G. Marotti, *Morphological study of intercellular junctions during osteocyte differentiation.* Bone, 1990. **11**(6): p. 401-6.

51. Dallas, S.L., M. Prideaux, and L.F. Bonewald, *The osteocyte: an endocrine cell ... and more.* Endocr Rev, 2013. **34**(5): p. 658-90.

52. Barragan-Adjemian, C., et al., *Mechanism by which MLO-A5 late osteoblasts/early osteocytes mineralize in culture: similarities with mineralization of lamellar bone.* Calcif Tissue Int, 2006. **79**(5): p. 340-53.

53. Sugawara, Y., et al., *Three-dimensional reconstruction of chick calvarial osteocytes and their cell processes using confocal microscopy.* Bone, 2005. **36**(5): p. 877-883.

54. Ferretti, M., et al., *Static and dynamic osteogenesis: two different types of bone formation.* Anat Embryol (Berl), 2002. **206**(1-2): p. 21-9.

55. Palumbo, C., M. Ferretti, and G. Marotti, *Osteocyte dendrogenesis in static and dynamic bone formation: an ultrastructural study.* Anat Rec A Discov Mol Cell Evol Biol, 2004. **278**(1): p. 474-80.

56. Palumbo, C., M. Ferretti, and A. De Pol, *Apoptosis during intramembranous ossification.* Journal of Anatomy, 2003. **203**(6): p. 589-98.

57. Ferretti, M., et al., *Does static precede dynamic osteogenesis in endochondral ossification as occurs in intramembranous ossification?* Anat Rec A Discov Mol Cell Evol Biol, 2006. **288**(11): p. 1158-62.

58. Sissons, H.A., G.J. Kelman, and G. Marotti, *Mechanisms of bone resorption in calcium-deficient rats.* Calcif Tissue Int, 1984. **36**(6): p. 711-21.

59. van Hove, R.P., et al., *Osteocyte morphology in human tibiae of different bone pathologies with different bone mineral density -- Is there a role for mechanosensing?* Bone, 2009. **45**(2): p. 321-329.

60. van Oers, R.F., H. Wang, and R.G. Bacabac, *Osteocyte shape and mechanical loading.* Curr Osteoporos Rep, 2015. **13**(2): p. 61-6.

61. van Hove, R.P., et al., *Osteocyte morphology in human tibiae of different bone pathologies with different bone mineral density--is there a role for mechanosensing?* Bone, 2009. **45**(2): p. 321-9.

62. Mullender, M.G., et al., *Osteocyte density changes in aging and osteoporosis.* Bone, 1996. **18**(2): p. 109-13.

63. Frost, H.M., *In vivo osteocyte death.* Journal of Bone and Joint Surgery, 1960. **42-A**: p. 138-43.

64. Mullender, M.G., et al., *Osteocyte density and histomorphometric parameters in cancellous bone of the proximal femur in five mammalian species.* J Orthop Res, 1996. **14**(6): p. 972-9.

65. Sissons, H.A. and P. O'Connor, *Quantitative histology of osteocyte lacunae in normal human cortical bone.* Calcif Tissue Res, 1977. **22 Suppl**: p. 530-3.

66. Cane, V., et al., *Size and density of osteocyte lacunae in different regions of long bones.* Calcif Tissue Int, 1982. **34**(6): p. 558-63.

67. Qiu, S., et al., *Age and distance from the surface but not menopause reduce osteocyte density in human cancellous bone.* Bone, 2002. **31**(2): p. 313-8.

68. Qiu, S., et al., *Reduced iliac cancellous osteocyte density in patients with osteoporotic vertebral fracture.* J Bone Miner Res, 2003. **18**(9): p. 1657-63.

69. Hemmatian, H., et al., *Aging, Osteocytes, and Mechanotransduction.* Curr Osteoporos Rep, 2017. **15**(5): p. 401-411.

70. Qiu, S., et al., *Differences in osteocyte and lacunar density between Black and White American women.* Bone, 2006. **38**(1): p. 130-5.

71. Mullender, M.G., et al., *Differences in osteocyte density and bone histomorphometry between men and women and between healthy and osteoporotic subjects.* Calcif Tissue Int, 2005. **77**(5): p. 291-6.

72. Remaggi, F., et al., *Histomorphometric study on the osteocyte lacuno-canalicular network in animals of different species. I. Woven-fibered and parallel-fibered bones.* Ital J Anat Embryol, 1998. **103**(4): p. 145-55.

73. Ferretti, M., et al., *Histomorphometric study on the osteocyte lacuno-canalicular network in animals of different species. II. Parallel-fibered and lamellar bones.* Ital J Anat Embryol, 1999. **104**(3): p. 121-31.

74. Palumbo, C., *A three-dimensional ultrastructural study of osteoid-osteocytes in the tibia of chick embryos.* Cell Tissue Res, 1986. **246**(1): p. 125-31.

75. Kamioka, H., T. Honjo, and T. Takano-Yamamoto, *A three-dimensional distribution of osteocyte processes revealed by the combination of confocal laser scanning microscopy and differential interference contrast microscopy.* Bone, 2001. **28**(2): p. 145-9.

76. Honma, M., et al., *RANKL subcellular trafficking and regulatory mechanisms in osteocytes.* J Bone Miner Res, 2013. **28**(9): p. 1936-49.

77. Knapp, H.F., et al., *Development of preparation methods for and insights obtained from atomic force microscopy of fluid spaces in cortical bone.* Scanning., 2002. **24**(1): p. 25-33.

78. Su, M., et al., *Knee-loading modality drives molecular transport in mouse femur*. Annals of Biomedical Engineering, 2006. **34**(10): p. 1600-6.

79. You, L.D., et al., *Ultrastructure of the osteocyte process and its pericellular matrix.* Anat Rec A Discov Mol Cell Evol Biol, 2004. **278**(2): p. 505-13.

80. Kubek, D.J., V.H. Gattone, 2nd, and M.R. Allen, *Methodological assessment of acid-etching for visualizing the osteocyte lacunar-canalicular networks using scanning electron microscopy.* Microsc Res Tech, 2009.

81. Ciani, C., S.B. Doty, and S.P. Fritton, *An effective histological staining process to visualize bone interstitial fluid space using confocal microscopy*. Bone, 2009. **44**(5): p. 1015-7.

82. Atkins, G.J. and D.M. Findlay, *Osteocyte regulation of bone mineral: a little give and take.* Osteoporos Int, 2012. **23**(8): p. 2067-79.

83. Inoue, K., et al., *A crucial role for matrix metalloproteinase 2 in osteocytic canalicular formation and bone metabolism.* J Biol Chem, 2006. **281**(44): p. 33814-24.

84. Holmbeck, K., et al., *The metalloproteinase MT1-MMP is required for normal development and maintenance of osteocyte processes in bone.* J Cell Sci, 2005. **118**(Pt 1): p. 147-56.

85. Sheng, M.H., K.H. Lau, and D.J. Baylink, *Role of Osteocyte-derived Insulin-Like Growth Factor I in Developmental Growth, Modeling, Remodeling, and Regeneration of the Bone.* J Bone Metab, 2014. **21**(1): p. 41-54.

86. Bonewald, L.F., *The Role of the Osteocyte in Bone and Nonbone Disease.* Endocrinol Metab Clin North Am, 2017. **46**(1): p. 1-18.

87. Atkins, G.J., et al., *Metabolism of vitamin D3 in human osteoblasts: evidence for autocrine and paracrine activities of 1 alpha,25-dihydroxyvitamin D3.* Bone, 2007. **40**(6): p. 1517-28.

88. Wijenayaka, A.R., et al., *Sclerostin stimulates osteocyte support of osteoclast activity by a RANKL-dependent pathway.* PLoS One, 2011. **6**(10): p. e25900.

89. Honma, M., et al., *Regulatory mechanisms of RANKL presentation to osteoclast precursors.* Curr Osteoporos Rep, 2014. **12**(1): p. 115-20.

90. Han, Y., et al., *Paracrine and endocrine actions of bone-the functions of secretory proteins from osteoblasts, osteocytes, and osteoclasts.* Bone Res, 2018. **6**: p. 16.

91. Hayashida, C., et al., *Osteocytes produce interferon-beta as a negative regulator of osteoclastogenesis.* J Biol Chem, 2014. **289**(16): p. 11545-55.

92. Basso, N. and J.N. Heersche, *Effects of hind limb unloading and reloading on nitric oxide synthase expression and apoptosis of osteocytes and chondrocytes.* Bone, 2006. **39**(4): p. 807-14.

93. Klein-Nulend, J., et al., *Pulsating fluid flow increases nitric oxide (NO) synthesis by osteocytes but not periosteal fibroblasts--correlation with prostaglandin upregulation.* Biochem Biophys Res Commun, 1995. **217**(2): p. 640-8.

94. Xiong, J., et al., *Osteocytes, not Osteoblasts or Lining Cells, are the Main Source of the RANKL Required for Osteoclast Formation in Remodeling Bone.* PLoS One, 2015. **10**(9): p. e0138189.

95. Compton, J.T. and F.Y. Lee, *A review of osteocyte function and the emerging importance of sclerostin.* J Bone Joint Surg Am, 2014. **96**(19): p. 1659-68.

96. Krishnan, V., H.U. Bryant, and O.A. Macdougald, *Regulation of bone mass by Wnt signaling.* J Clin Invest, 2006. **116**(5): p. 1202-9.

97. ten Dijke, P., et al., *Osteocyte-derived sclerostin inhibits bone formation: its role in bone morphogenetic protein and Wnt signaling.* J Bone Joint Surg Am, 2008. **90 Suppl 1**: p. 31-5.

98. van Bezooijen, R.L., et al., *Chapter 7 - SOST/Sclerostin: An Osteocyte-Derived Inhibitor of Bone Formation that Antagonizes Canonical Wnt Signaling*, in *Principles of Bone Biology (Third Edition)*, J.P. Bilezikian, L.G. Raisz, and T.J. Martin, Editors. 2008, Academic Press: San Diego. p. 139-152.

99. Piters, E., E. Boudin, and W. Van Hul, *Wnt signaling: a win for bone.* Arch Biochem Biophys, 2008. **473**(2): p. 112-6.

100. Silverman, S.L., *Sclerostin.* J Osteoporos, 2010. **2010**: p. 941419.

101. Li, X., et al., *Sclerostin binds to LRP5/6 and antagonizes canonical Wnt signaling.* J Biol Chem, 2005. **280**(20): p. 19883-7.

102. Brunkow, M.E., et al., *Bone dysplasia sclerosteosis results from loss of the SOST gene product, a novel cystine knot-containing protein.* Am J Hum Genet, 2001. **68**(3): p. 577-89.

103. Staehling-Hampton, K., et al., *A 52-kb deletion in the SOST-MEOX1 intergenic region on 17q12-q21 is associated with van Buchem disease in the Dutch population.* Am J Med Genet, 2002. **110**(2): p. 144-52.

104. Poole, K.E., et al., *Sclerostin is a delayed secreted product of osteocytes that inhibits bone formation.* Faseb J, 2005. **19**(13): p. 1842-4.

105. Robling, A.G., et al., *Mechanical stimulation of bone in vivo reduces osteocyte expression of Sost/sclerostin.* J Biol Chem, 2008. **283**(9): p. 5866-75.

106. Lin, C., et al., *Sclerostin mediates bone response to mechanical unloading through antagonizing Wnt/beta-catenin signaling.* J Bone Miner Res, 2009. **24**(10): p. 1651-61.

107. Vincent, C., et al., *Pro-inflammatory cytokines TNF-related weak inducer of apoptosis (TWEAK) and TNFalpha induce the mitogen-activated protein kinase (MAPK)-dependent expression of sclerostin in human osteoblasts.* J Bone Miner Res, 2009. **24**(8): p. 1434-49.

108. Atkins, G.J., et al., *Sclerostin is a locally acting regulator of late-osteoblast/preosteocyte differentiation and regulates mineralization through a MEPE-ASARM-dependent mechanism.* J Bone Miner Res, 2011. **26**(7): p. 1425-36.

109. Prideaux, M., D.M. Findlay, and G.J. Atkins, *Osteocytes: The master cells in bone remodelling.* Curr Opin Pharmacol, 2016. **28**: p. 24-30.

110. Weivoda, M.M., S.J. Youssef, and M.J. Oursler, *Sclerostin expression and functions beyond the osteocyte.* Bone, 2017. **96**: p. 45-50.

111. Galea, G.L., L.E. Lanyon, and J.S. Price, *Sclerostin's role in bone's adaptive response to mechanical loading.* Bone, 2017. **96**: p. 38-44.

112. Westbroek, I., et al., *Expression of serotonin receptors in bone.* J Biol Chem, 2001. **276**(31): p. 28961-8.

113. Martin, A., et al., *Bone proteins PHEX and DMP1 regulate fibroblastic growth factor Fgf23 expression in osteocytes through a common pathway involving FGF receptor (FGFR) signaling.* Faseb J, 2011. **25**(8): p. 2551-62.

114. Strewler, G.J., *Untangling klotho's role in calcium homeostasis.* Cell Metab, 2007. **6**(2): p. 93-5.

115. Schiavi, S.C., *Bone talk.* Nat Genet, 2006. **38**(11): p. 1230-1.

116. Suzuki, H., et al., *Histological evidence of the altered distribution of osteocytes and bone matrix synthesis in klotho-deficient mice.* Arch Histol Cytol, 2005. **68**(5): p. 371-81.

117. Tsujikawa, H., et al., *Klotho, a gene related to a syndrome resembling human premature aging, functions in a negative regulatory circuit of vitamin D endocrine system.* Mol Endocrinol, 2003. **17**(12): p. 2393-403.

118. Donate-Correa, J., et al., *FGF23/Klotho axis: phosphorus, mineral metabolism and beyond.* Cytokine Growth Factor Rev, 2012. **23**(1-2): p. 37-46.

119. Kuro, O.M., *The Klotho proteins in health and disease.* Nat Rev Nephrol, 2019. **15**(1): p. 27-44.

120. Kuro, O.M., *The FGF23 and Klotho system beyond mineral metabolism.* Clin Exp Nephrol, 2017. **21**(Suppl 1): p. 64-69.

121. Bonewald, L.F. and M.J. Wacker, *FGF23 production by osteocytes.* Pediatr Nephrol, 2013. **28**(4): p. 563-8.

122. Martin, A., V. David, and L.D. Quarles, *Regulation and function of the FGF23/klotho endocrine pathways.* Physiol Rev, 2012. **92**(1): p. 131-55.

123. Han, X. and L.D. Quarles, *Multiple faces of fibroblast growth factor-23.* Curr Opin Nephrol Hypertens, 2016. **25**(4): p. 333-42.

124. Yavropoulou, M.P., A. Michopoulos, and J.G. Yovos, *PTH and PTHR1 in osteocytes. New insights into old partners.* Hormones (Athens), 2017. **16**(2): p. 150-160.

125. Brakspear, K.S. and D.J. Mason, *Glutamate signaling in bone.* Front Endocrinol (Lausanne), 2012. **3**: p. 97.

126. Kerschnitzki, M., et al., *The organization of the osteocyte network mirrors the extracellular matrix orientation in bone.* J Struct Biol, 2011. **173**(2): p. 303-11.

127. Nicolella, D.P., et al., *Effects of nanomechanical bone tissue properties on bone tissue strain: implications for osteocyte mechanotransduction.* J Musculoskelet Neuronal Interact, 2008. **8**(4): p. 330-1.

128. Nicolella, D.P., et al., *Machine vision photogrammetry: a technique for measurement of microstructural strain in cortical bone.* Journal of Biomechanics, 2001. **34**(1): p. 135-9.

129. Nicolella, D.P., et al., *Osteocyte lacunae tissue strain in cortical bone.* Journal of Biomechanics, 2006. **39**(9): p. 1735-43.

130. Bonivtch, A.R., L.F. Bonewald, and D.P. Nicolella, *Tissue strain amplification at the osteocyte lacuna: a microstructural finite element analysis.* Journal of Biomechanics, 2007. **40**(10): p. 2199-206.

131. Lane, N.E., et al., *Glucocorticoid-treated mice have localized changes in trabecular bone material properties and osteocyte lacunar size that are not observed in placebo-treated or estrogen-deficient mice.* J Bone Miner Res, 2006. **21**(3): p. 466-76.

132. Harris, S.E., et al., *DMP1 and MEPE expression are elevated in osteocytes after mechanical loading in vivo: theoretical role in controlling mineral quality in the perilacunar matrix.* J Musculoskelet Neuronal Interact, 2007. **7**(4): p. 313-5.

133. Brand, R.A., C.M. Stanford, and D.P. Nicolella, *Primary adult human bone cells do not respond to tissue (continuum) level strains.* Journal of Orthopaedic Science, 2001. **6**(3): p. 295-301.

134. You, J., et al., *Substrate deformation levels associated with routine physical activity are less stimulatory to bone cells relative to loading-induced oscillatory fluid flow.* Journal of Biomechanical Engineering, 2000. **122**(4): p. 387-93.

135. Owan, I., et al., *Mechanotransduction in bone: osteoblasts are more responsive to fluid forces than mechanical strain.* Am J Physiol, 1997. **273**(3 Pt 1): p. C810-5.

136. Lanyon, L.E., et al., *Bone deformation recorded in vivo from strain gauges attached to the human tibial shaft.* Acta Orthopaedica Scandinavica, 1975. **46**(2): p. 256-68.

137. Lanyon, L.E. and R.N. Smith, *Bone strain in the tibia during normal quadrupedal locomotion.* Acta Orthopaedica Scandinavica, 1970. **41**(3): p. 238-48.

138. Burr, D.B., et al., *In vivo measurement of human tibial strains during vigorous activity.* Bone, 1996. **18**(5): p. 405-10.

139. You, L., et al., *A model for strain amplification in the actin cytoskeleton of osteocytes due to fluid drag on pericellular matrix.* Journal of Biomechanics, 2001. **34**(11): p. 1375-86.

140. Whitfield, J.F., *The solitary (primary) cilium--a mechanosensory toggle switch in bone and cartilage cells.* Cell Signal, 2008. **20**(6): p. 1019-24.

141. Xiao, Z., et al., *Cilia-like structures and polycystin-1 in osteoblasts/osteocytes and associated abnormalities in skeletogenesis and Runx2 expression.* J Biol Chem, 2006. **281**(41): p. 30884-95.

142. Malone, A.M., et al., *Primary cilia mediate mechanosensing in bone cells by a calcium-independent mechanism.* Proceedings of the National Academy of Sciences of the United States of America, 2007. **104**(33): p. 13325-30.

143. Malone, A.M., et al., *Primary cilia in bone.* J Musculoskelet Neuronal Interact, 2007. **7**(4): p. 301.

144. Atkins, G.J., et al., *Strontium ranelate treatment of human primary osteoblasts promotes an osteocyte-like phenotype while eliciting an osteoprotegerin response.* Osteoporos Int, 2009. **20**(4): p. 653-64.

145. Atkins, G.J., et al., *Vitamin K promotes mineralization, osteoblast-to-osteocyte transition, and an anticatabolic phenotype by {gamma}-carboxylation-dependent and -independent mechanisms.* Am J Physiol Cell Physiol, 2009. **297**(6): p. C1358-67.

146. Butler, W.T., et al., *Extracellular Matrix Proteins and the Dynamics of Dentin Formation.* Connect Tissue Res, 2002. **43**: p. 301-307.

147. Toyosawa, S., et al., *Dentin matrix protein 1 is predominantly expressed in chicken and rat osteocytes but not in osteoblasts.* J Bone Miner Res, 2001. **16**(11): p. 2017-26.

148. Gluhak-Heinrich, J., et al., *Mechanical loading stimulates dentin matrix protein 1 (DMP1) expression in osteocytes in vivo.* J Bone Miner Res, 2003. **18**(5): p. 807-17.

149. Feng, J.Q., et al., *Loss of DMP1 causes rickets and osteomalacia and identifies a role for osteocytes in mineral metabolism.* Nat Genet, 2006. **38**(11): p. 1310-5.

150. Gowen, L.C., et al., *Targeted disruption of the osteoblast/osteocyte factor 45 gene (OF45) results in increased bone formation and bone mass.* J Biol Chem, 2003. **278**(3): p. 1998-2007.

151. David, V., et al., *Matrix extracellular phosphoglycoprotein (MEPE) is a new bone renal hormone and vascularization modulator.* Endocrinology, 2009. **150**(9): p. 4012-23.

152. Rowe, P.S., et al., *MEPE has the properties of an osteoblastic phosphatonin and minhibin.* Bone, 2004. **34**(2): p. 303-19.

153. Gluhak-Heinrich, J., et al., *MEPE expression in osteocytes during orthodontic tooth movement.* Arch Oral Biol, 2007. **52**(7): p. 684-90.

154. Sprowson, A.P., A.W. McCaskie, and M.A. Birch, *ASARM-truncated MEPE and AC-100 enhance osteogenesis by promoting osteoprogenitor adhesion.* Journal of Orthopaedic Research, 2008. **26**(9): p. 1256-62.

155. Boskey, A.L., et al., *MEPE's diverse effects on mineralization.* Calcif Tissue Int, 2010. **86**(1): p. 42-6.

156. Robling, A.G., *The interaction of biological factors with mechanical signals in bone adaptation: recent developments.* Curr Osteoporos Rep, 2012. **10**(2): p. 126-31.

157. Belanger, L.F., *Osteocytic osteolysis.* Calcif Tissue Res, 1969. **4**(1): p. 1-12.

158. Tazawa, K., et al., *Osteocytic osteolysis observed in rats to which parathyroid hormone was continuously administered.* J Bone Miner Metab, 2004. **22**(6): p. 524-9.

159. Strewler, G.J., R.D. Williams, and R.A. Nissenson, *Human renal carcinoma cells produce hypercalcemia in the nude mouse and a novel protein recognized by parathyroid hormone receptors.* J Clin Invest, 1983. **71**(3): p. 769-74.

160. Strewler, G.J., et al., *Parathyroid hormonelike protein from human renal carcinoma cells. Structural and functional homology with parathyroid hormone.* J Clin Invest, 1987. **80**(6): p. 1803-7.

161. Xu, J., et al., *Effects of different dosages of parathyroid hormone-related protein 1-34 on the bone metabolism of the ovariectomized rat model of osteoporosis.* Calcif Tissue Int, 2013. **93**(3): p. 276-87.

162. Bringhurst, F.R., *PTH receptors and apoptosis in osteocytes.* J Musculoskelet Neuronal Interact, 2002. **2**(3): p. 245-51.

163. Bellido, T., et al., *Chronic elevation of parathyroid hormone in mice reduces expression of sclerostin by osteocytes: a novel mechanism for hormonal control of osteoblastogenesis.* Endocrinology, 2005. **146**(11): p. 4577-83.

164. Bellido, T., *Downregulation of SOST/sclerostin by PTH: a novel mechanism of hormonal control of bone formation mediated by osteocytes.* J Musculoskelet Neuronal Interact, 2006. **6**(4): p. 358-9.

165. O'Brien, C.A., et al., *Control of bone mass and remodeling by PTH receptor signaling in osteocytes.* PLoS One, 2008. **3**(8): p. e2942.

166. O'Brien, C.A., T. Nakashima, and H. Takayanagi, *Osteocyte control of osteoclastogenesis.* Bone, 2013. **54**(2): p. 258-63.

167. Rhee, Y., et al., *PTH receptor signaling in osteocytes governs periosteal bone formation and intracortical remodeling.* J Bone Miner Res, 2011. **26**(5): p. 1035-46.

168. Rhee, Y., et al., *Parathyroid hormone receptor signaling in osteocytes increases the expression of fibroblast growth factor-23 in vitro and in vivo.* Bone, 2011. **49**(4): p. 636-43.

169. Rhee, Y., et al., *Resorption controls bone anabolism driven by parathyroid hormone (PTH) receptor signaling in osteocytes.* J Biol Chem, 2013. **288**(41): p. 29809-20.

170. Ogura, K., et al., *Short-term intermittent administration of parathyroid hormone facilitates osteogenesis by different mechanisms in cancellous and cortical bone.* Bone Rep, 2016. **5**: p. 7-14.

171. Powell, W.F., Jr., et al., *Targeted ablation of the PTH/PTHrP receptor in osteocytes impairs bone structure and homeostatic calcemic responses.* J Endocrinol, 2011. **209**(1): p. 21-32.

172. Selim, A.A., et al., *Role of calcium channels in carboxyl-terminal parathyroid hormone receptor signaling.* Am J Physiol Cell Physiol, 2006. **291**(1): p. C114-21.

173. Divieti, P.P., *PTH and osteocytes.* J Musculoskelet Neuronal Interact, 2005. **5**(4): p. 328-30.

174. Jilka, R.L., B. Noble, and R.S. Weinstein, *Osteocyte apoptosis.* Bone, 2013. **54**(2): p. 264-71.

175. Canalis, E., et al., *Glucocorticoid-induced osteoporosis: pathophysiology and therapy.* Osteoporos Int, 2007. **18**(10): p. 1319-28.

176. Mazziotti, G., et al., *Glucocorticoid-induced osteoporosis: clinical and therapeutic aspects.* Arq Bras Endocrinol Metabol, 2007. **51**(8): p. 1404-12.

177. Yao, W., et al., *Glucocorticoid excess in mice results in early activation of osteoclastogenesis and adipogenesis and prolonged suppression of osteogenesis: a longitudinal study of gene expression in bone tissue from glucocorticoid-treated mice.* Arthritis and Rheumatism, 2008. **58**(6): p. 1674-86.

178. Yao, W., et al., *Glucocorticoid-induced bone loss in mice can be reversed by the actions of parathyroid hormone and risedronate on different pathways for bone formation and mineralization.* Arthritis and Rheumatism, 2008. **58**(11): p. 3485-97.

179. Osagie-Clouard, L., et al., *Parathyroid hormone 1-34 and skeletal anabolic action: The use of parathyroid hormone in bone formation.* Bone Joint Res, 2017. **6**(1): p. 14-21.

180. Silva, B.C. and J.P. Bilezikian, *Parathyroid hormone: anabolic and catabolic actions on the skeleton.* Curr Opin Pharmacol, 2015. **22**: p. 41-50.

181. Bellido, T., V. Saini, and P.D. Pajevic, *Effects of PTH on osteocyte function.* Bone, 2013. **54**(2): p. 250-7.

182. Tsourdi, E., et al., *Physiological and pathological osteocytic osteolysis.* J Musculoskelet Neuronal Interact, 2018. **18**(3): p. 292-303.

183. Divieti Pajevic, P., *Recent progress in osteocyte research.* Endocrinol Metab (Seoul), 2013. **28**(4): p. 255-61.

184. Katsimbri, P., *The biology of normal bone remodelling.* Eur J Cancer Care (Engl), 2017. **26**(6).

185. Skerry, T.M., *One mechanostat or many? Modifications of the site-specific response of bone to mechanical loading by nature and nurture.* J Musculoskelet Neuronal Interact, 2006. **6**(2): p. 122-7.

186. Noble, B., *Microdamage and apoptosis.* Eur J Morphol, 2005. **42**(1-2): p. 91-8.

187. Kennedy, O.D., et al., *Activation of resorption in fatigue-loaded bone involves both apoptosis and active pro-osteoclastogenic signaling by distinct osteocyte populations.* Bone, 2012. **50**(5): p. 1115-22.

188. Kennedy, O.D., et al., *Osteocyte apoptosis is required for production of osteoclastogenic signals following bone fatigue in vivo.* Bone, 2014. **64**: p. 132-7.

189. Dittmer, K.E. and E.C. Firth, *Mechanisms of bone response to injury.* J Vet Diagn Invest, 2017. **29**(4): p. 385-395.

190. Takano, Y., et al., *Elastic anisotropy and collagen orientation of osteonal bone are dependent on the mechanical strain distribution.* Journal of Orthopaedic Research, 1999. **17**(1): p. 59-66.

191. Robling, A.G., et al., *Shorter, more frequent mechanical loading sessions enhance bone mass.* Med Sci Sports Exerc, 2002. **34**(2): p. 196-202.

192. Turner, C.H., *Three rules for bone adaptation to mechanical stimuli.* Bone, 1998. **23**(5): p. 399-407.

193. Warden, S.J. and C.H. Turner, *Mechanotransduction in the cortical bone is most efficient at loading frequencies of 5-10 Hz.* Bone, 2004. **34**(2): p. 261-70.

194. Turner, C.H., M.R. Forwood, and M.W. Otter, *Mechanotransduction in bone: do bone cells act as sensors of fluid flow?* Faseb J, 1994. **8**(11): p. 875-8.

195. Hsieh, Y.F., et al., *Mechanical loading of diaphyseal bone in vivo: the strain threshold for an osteogenic response varies with location.* J Bone Miner Res, 2001. **16**(12): p. 2291-7.

196. Warden, S.J., R.K. Fuchs, and C.H. Turner, *Steps for targeting exercise towards the skeleton to increase bone strength.* Eura Medicophys, 2004. **40**(3): p. 223-32.

197. Rubin, C., G. Xu, and S. Judex, *The anabolic activity of bone tissue, suppressed by disuse, is normalized by brief exposure to extremely low-magnitude mechanical stimuli.* Faseb J, 2001. **15**(12): p. 2225-9.

198. Rubin, C.T., et al., *Inhibition of osteopenia by low magnitude, high-frequency mechanical stimuli.* Drug Discovery Today, 2001. **6**(16): p. 848-858.

199. Robling, A.G., A.B. Castillo, and C.H. Turner, *Biomechanical and molecular regulation of bone remodeling.* Annu Rev Biomed Eng, 2006. **8**: p. 455-98.

200. Burr, D.B., A.G. Robling, and C.H. Turner, *Effects of biomechanical stress on bones in animals.* Bone, 2002. **30**(5): p. 781-6.

201. Robling, A.G., D.B. Burr, and C.H. Turner, *Recovery periods restore mechanosensitivity to dynamically loaded bone.* J Exp Biol, 2001. **204**(Pt 19): p. 3389-99.

202. Srinivasan, S., et al., *Rest-inserted loading rapidly amplifies the response of bone to small increases in strain and load cycles.* J Appl Physiol, 2007. **102**(5): p. 1945-52.

203. Srinivasan, S., et al., *Low-magnitude mechanical loading becomes osteogenic when rest is inserted between each load cycle.* J Bone Miner Res, 2002. **17**(9): p. 1613-20.

204. Saxon, L.K., et al., *Mechanosensitivity of the rat skeleton decreases after a long period of loading, but is improved with time off.* Bone, 2005. **36**(3): p. 454-64.

205. Uhthoff, H.K. and Z.F. Jaworski, *Bone loss in response to long-term immobilisation.* Journal of Bone and Joint Surgery. British Volume, 1978. **60-B**(3): p. 420-9.

206. Jaworski, Z.F., M. Liskova-Kiar, and H.K. Uhthoff, *Effect of long-term immobilisation on the pattern of bone loss in older dogs.* Journal of Bone and Joint Surgery. British Volume, 1980. **62-B**(1): p. 104-10.

207. Leblanc, A.D., et al., *Bone mineral loss and recovery after 17 weeks of bed rest.* J Bone Miner Res, 1990. **5**(8): p. 843-50.

208. Giddings, V.L., et al., *Calcaneal loading during walking and running.* Medicine and Science in Sports and Exercise, 2000. **32**(3): p. 627-34.

209. Bergmann, G., et al., *Hip contact forces and gait patterns from routine activities.* Journal of Biomechanics, 2001. **34**(7): p. 859-71.

210. Bergmann, G., F. Graichen, and A. Rohlmann, *Hip joint loading during walking and running, measured in two patients.* Journal of Biomechanics, 1993. **26**(8): p. 969-90.

211. Rosser, J. and L.F. Bonewald, *Studying osteocyte function using the cell lines MLO-Y4 and MLO-A5.* Methods Mol Biol, 2012. **816**: p. 67-81.

212. Kamioka, H., et al., *Primary cultures of chick osteocytes retain functional gap junctions between osteocytes and between osteocytes and osteoblasts.* Microsc Microanal, 2007. **13**(2): p. 108-17.

213. Staines, K.A., G. Brown, and C. Farquharson, *The Ex Vivo Organ Culture of Bone.* Methods Mol Biol, 2019. **1914**: p. 199-215.

CHAPTER 2. Beta-Testing and Optimisation of the Zetos™ System

Abstract

Introduction:

The response of bone *in vivo* to mechanical loading was widely reported in the last quarter of the 20th century. However, elucidating the biological and molecular mechanisms at the cellular and tissue level has been challenging, largely because the *in vitro* models commonly used are very different to the normal environment, in which bone cells are found. In humans, the necessary invasive experiments are obviously not possible. In recent years, it has become increasingly evident that osteocytes play a central role in regulating bone cell activity and function. Extrapolating these findings to the organism level, and especially in humans, can be very difficult. Many of the mechanotransduction studies performed *in vitro* did not measure biomechanical parameters in real-time and were not able to emulate the three dimensional structure of the bone matrix. A novel machine, the Zetos™ system, has the potential to overcome the above limitations, as it enables the long-term culture *ex vivo* of trabecular bone cores and the precise application of loading forces, as well as concurrent measurement of tissue stiffness. However, this second iteration of the Zetos™ system, which was available for the work of this thesis by special arrangement with its designer and builder (Dr. Smith), required beta-testing and substantial optimisation in order to be experimentally useful. Initial work performed will be used to beta-test the Zetos system software together with the software designer company (Simplex Scientific LLC, Wisconsin, USA). This chapter provides a summary of the beta-testing for the custom software and details of the work to optimise the second generation Zetos™ system.

Methodology:

The beta testing of the Zetos™ software was performed prior to the running of this experiment, which involved recommending and testing changes to the software in collaboration with the software designer. This resulted in version 2.0.0.1 of the Zetos™ software being made available for use in this study. Bovine trabecular bone cores approximately 10 mm in diameter and

between 4 to 5 mm thick were prepared from a freshly harvested sternum of a 9-month old steer. Care was taken to maintain sterility and viability of the samples at all times. Half of the 24 bone cores isolated had their marrow removed by washing using a dental water jet device (WP-450A, Water Pik Inc., Colorado, USA). The bone cores were then perfused with culture media, at a rate of 7ml/hr in custom made chambers. The entire apparatus was maintained at 37°C. Treatment groups consisted of eight samples (four with marrow and four without) that were cultured either unloaded (UL) or mechanically loaded using the Zetos™ device according to 2 protocols: 2,000 μstrain, 1 Hz, 300 cycles daily (300x1) or 2,000 μstrain, 1 Hz, 100 cycles thrice daily (100x3). All cores were cultured under these protocols for 10 consecutive days. The stiffness of the samples (Young's Modulus) was measured daily until Day 11. The samples were analysed using a SkyScan 1174 μCT scanner before and after the 10 days of loading to determine structural parameters, such as tissue volume (TV), bone volume (BV), percent bone volume (BV/TV), bone surface area (BS), intersection surface (iS), bone surface / volume ratio (BS/BV), bone surface density (BS/TV), trabecular pattern factor (Tb.Pf), structure model index (SMI), trabecular thickness (Tb.Th), trabecular number (Tb.N) and trabecular separation (Tb.Sp). Media were changed daily and the pH measured.

Results:

Despite using bone cores prepared from the same bone in a single animal, the parameters measured by μCT and their stiffness prior to the experiment varied widely. There was an initial sharp drop in the stiffness of the bone cores followed by an increase in all treatment groups, including the unloaded bone cores. The stiffness of all samples also dropped sharply 24 hours after the last loading session. Loading episodes that were spaced out with a rest of 4 hours in between sessions (100x3) resulted in a persistent and significant increase in stiffness. In general, the samples without bone marrow had a better increase in stiffness, higher uptake of ionic calcium from the culture media, and significant increases in the association of all μCT

histomorphometric parameters with stiffness after 10 days of mechanical loading, especially for the 100x3 group.

Conclusion:

Young bovine bone may not be optimal for mechanotransduction studies since there appears to be a loading-independent growth response *ex vivo*. However, there is still a clear loading-dependent effect, validating the second generation system. Preliminary work suggests that removal of bone marrow may be beneficial in terms of uniformity of effect, possibly due to improved access of culture media to the bone cells, while the canalicular structure of bone may allow effective perfusion of the culture medium to the osteocytes embedded in the bone matrix. Future work will focus on the response of bovine bone to agents that affect bone mass.

2.1 Introduction

Bones are metabolically active organs that undergo modelling during growth and continuous remodelling throughout life [1, 2]. Modelling occurs mainly during growth as the skeleton adapts to the structural needs of the growing skeleton, whereby there is a need for an increase in both the bone length and diameter. Remodelling is the temporal and spatial coupling of bone resorption and regrowth as it adapts in response to various stimuli; such as microdamage, disuse and mineral homeostasis, and this is necessary to maintain the structural integrity of the skeleton [3-5]. A lack of loading, or disuse, causes more bone resorption than bone formation, hence resulting in net bone loss. Within the physiological loading range, the complex process of bone remodelling will be at its lowest [6]. Contrarily, with bone overuse, bone is exposed to more 'microdamage' which will then activate signals for bone resorption and the subsequent formation of new bone [7]. Remodelling rates, however, vary not only between different species but also between different bones, between different regions in the same bone and with age.

Recent evidence indicates that osteocytes play a key role in the regulation of bone remodelling by activating osteoclastogenesis and regulating osteoblastogenesis [8-11]. Osteocytes are also now believed to play a much larger role than previously appreciated in controlling and determining the function of these other cell types in bone, especially in response to mechanical loading and biochemical changes [12-14]. In response to mechanical loading, osteocytes are the mechanosensors and are responsible for mechanotransduction, the mechanism by which a mechanical load applied to bone is converted to biological signals for maintaining appropriate strength and mechanical integrity of the bone [15-17].

The current literature provides information on the effects of loading and unloading of bone from both biochemical and molecular point of views [18, 19]. However, with loading experiments in intact animals, it is difficult to determine the separate contributions of local cells and factors within the bone, compared with systemic and central contributions brought by blood vessels

and nerves. With *in vitro* studies results might be difficult to interpret due to the fact that cell cultures are mostly performed in an artificial 2-dimensional (2D) environment, such as in plastic wells or glass slides, as opposed to the 3-dimensional (3D) nature of the bone matrix where osteocytes are found. Additionally, the usage of non-human cells, for example the murine long-bone-derived osteocyte-Y4 (MLO-Y4) cell line, foetal chick cells, mouse calvarial cells and others will probably have different responses to loading and may not be directly comparable to human bone cells [20]. There are some *in vitro* studies using 3D scaffolds that try to emulate the bone matrix environment [21] and *in vivo* or *ex vivo* studies using bone explants [22]. However, the conditions they were conducted under were non-physiological and real-time measurement of mechanical parameters were not possible in most instances [23-25].

The present study takes advantage of the novel Zetos™ system [26] that has the potential to be a valuable tool to investigate the response of osteocytes, within their natural bone matrix, to mechanical loading in a very precise and reproducible manner. Thus, a better understanding of the osteocyte function specifically can be obtained using this *ex vivo* model. Our laboratory was among the first to acquire a second generation Zetos™ machine. As such, we embarked on an extensive beta-testing exercise, providing direction to the software designer to optimise the operating system and then testing the resultant software updates.

2.2 Literature Review

2.2.1 Bone remodelling

Bone remodelling is important in maintaining bone strength and mineral homeostasis [18]. It is a highly complex cycle, which requires interaction between different cell types and is regulated by a variety of biochemical and mechanical factors. The stages of bone remodelling can be generally divided into five sequential phases that are tightly coupled to one another: activation, resorption, reversal, formation and termination [27].

Activation of the remodelling process begins when local or systemic molecular signals induce osteoclastogenesis by upregulation of receptor activator of nuclear factor κB ligand (RANKL), thought originally to be primarily expressed by osteoblasts and bone lining cells [28]. Factors that are known to do this include parathyroid hormone (PTH), prostaglandin E_2 (PGE_2), dexamethasone, interleukin-1 (IL-1), tumour necrosis factor α (TNFα) and 1,25 dihydroxyvitamin D_3 [29]. In contrast, oestrogen and transforming growth factor-beta (TGF-β) are able to downregulate the expression of RANKL. Local signals are produced by damaged/apoptotic osteocytes in response to (the lack of) mechanical stimulation and/or microdamage [30-32]. The membrane bound form of RANKL interacts with its receptor, RANK, found on both circulating and bone marrow osteoclast precursors, as well as bone resorbing osteoclasts [33]. This RANK/RANKL signalling, together with macrophage-colony stimulating factor/colony stimulating factor-1 (M-CSF/CSF-1) that is also produced by osteoblast and bone lining cells, induces differentiation of the osteoclast precursors into mononuclear preosteoclasts and their fusion into the multinucleated osteoclasts [34, 35]. The osteoclast formed attaches itself to the exposed mineralized bone surface to initiate the resorption phase by secreting hydrogen ions to dissolve hydroxyapatite, and lysosomal enzymes, particularly cathepsin K (CTSK), which can degrade the organic components of bone matrix, including collagen [36]. The irregular scalloped cavities on the trabecular bone surface caused by the resorption process are known as Howship lacunae, while in cortical bone cylindrical Haversian canals are formed [37]. In the resorption process, molecular signals such as transforming growth factor-beta (TGF-β) [38], insulin-like growth factor-1 (IGF-1) [39] and cardiotropin-1 (CT-1) [40] are released from the bone matrix, which in turn appear to activate the subsequent phases.

Once resorption is completed, it is followed by the reversal phase, in which mononuclear cells migrate to the resorbed lacunae surface to remove the remaining undigested demineralised collagen matrix in preparation for bone formation [36, 41]. TGF-β is known to affect osteocytes, osteoblasts and osteoclasts and regulates many of their activities, such as cellular

migration, proliferation, differentiation, matrix synthesis and apoptosis [38]. Nguyen and colleagues have demonstrated that the TGF-β pathway is crucial for the regulation of sclerostin expression and bone formation by mechanical loading *in vivo* [42], indicating that osteocytes may be involved with osteoblastogenesis. Osteocytes was also suggested to be involved in the ensuing osteoblastogenesis due to their expression of heparin-binding growth associated molecule (HB-GAM; also known as pleiotrophin or osteoblast stimulating factor-1 (OSF-1)), which stimulates osteoblast recruitment and differentiation [10, 43].

The subsequent formation phase begins when preosteoblasts are recruited to differentiate into mature and functional osteoblasts. The resorption sites are filled with successive layers of osteoid, which mineralises to become mineralised matrix. Once an osteoblast has completed its matrix synthesis, it can either become a flattened lining cell on the bone surface, be buried in the bone as an osteocyte, or undergo programmed cell death (apoptosis) [37]. When this phase is complete the termination phase begins, which gives rise to a prolonged resting period until a new remodelling cycle is initiated.

Several regulatory systems, both systemic and local, are required to maintain resorption and remodelling in balance, and alterations of these regulatory steps can disturb the balance between these two processes. The major systemic factors include parathyroid hormone, calcitriol, calcitonin, glucocorticoids, thyroid hormones, estrogens and androgens, whereas local regulation of bone remodelling depends on a large number of cytokines and growth factors [36, 44], some of which are mentioned below. (Table 2.1)

Table 2.1 - Local Factors Affecting Bone Remodeling

Local Factors	Source	Role
Monocyte/macrophage colony stimulating factor (M-CSF)	Osteoblast	Critical for osteoclast formation
Receptor activation of NF-κB ligand (RANKL)	Osteoblast, osteocyte	Formation, fusion, activation, and survival of osteoclasts
Osteoprotegerin (OPG)	Osteoblast	Antagonize RANKL and interrupt osteoblasts/osteoclasts crosstalk
Semaphorin 3A (SEMA3A)	Osteoblast	Regulates osteoclast differentiation
Wingless integration (Wnt) gene family 5A (WNT5A)	Osteoblast	Enhance RANKL-induced osteoclastogenesis
Wingless integration (Wnt) gene family 16 (WNT16)	Osteoblast lineage	Reduces osteoclast differentiation and increases osteoblast OPG expression
Sclerostin (SOST)	Osteocyte	Inhibits osteoblast differentiation, stimulate RANKL-dependent osteoclastogenesis, induce the release of bone mineral from bone matrix
Dickkopf-1 (DKK1)	Osteocyte	↓osteoblastogenesis, ↑osteoclastogenesis
Bone morphogenetic protein 6 (BMP6)	Osteoclast	Recruit osteoprogenitors and stimulates bone formation
Collagen triple helix repeat containing 1 (CTHRC1)	Osteoclast	Upregulates osteoblastic bone formation
EphrinB2 (EFNB2) with osteoblast receptor EphB4	Osteoclast	Link suppression of osteoclast differentiation to osteoblastic bone formation
Sphingosine kinase 1 (SPHK1) / Sphingosine 1-phosphate (S1P)	Osteoclast	Increases osteoblastic RANKL expression to upregulate osteoclastogenesis
Wingless integration (Wnt) gene family 10b (WNT10B)	Osteoclast	Enhances osteoclast to osteoblast coupling
Semaphorin 4D (SEMA4D)	Osteoclast	Modulates osteoblast motility and suppresses insulin-like growth factor-1 (IGF-1) signalling to inhibit bone formation
Cardiotrophin-1 (CT-1)	Osteoclast	Essential for normal bone resorption, acts on osteocytes and osteoblasts to stimulate bone formation

Adapted from Han et al. 2018 [44]

2.2.2 Role of osteocytes in bone remodelling

Since the systemic and local regulation of bone remodelling has been widely studied, researchers nowadays are concentrating more on the role of osteocytes in bone remodelling, as they represent the majority of bone cells in bone. Osteocytes are now known to play a crucial role in maintaining bone strength. Mechanical loading of bone is believed to promote fluid flow through the lacuno-canalicular network of bone, and changes in this fluid flow may provide the signal for the osteocytic response to mechanical forces such as impact loading. It is hypothesised that deformation of osteocyte cytoskeletons by fluid flow occurs via tethers between osteocyte membranes and the walls of the lacuno-canalicular system [45].

Osteocytes appear to be the most mechanosensitive cells in bone and they produce factors that transduce mechanical load into a biological response [18, 46, 47]. Mechanical stimulus of osteocytes induce changes to intracellular Ca^{2+} and ATP and also the secretion of NO and PGE_2, which activates a cascade of downstream events culminating in the regulation of several mechanosensitive genes that produces sclerostin, RANKL, OPG, FGF23, DMP1, PHEX, MEPE and osteopontin among others [17].

In support of the idea of osteocytes as mechanosensors, is evidence that unloading of bone causes osteocyte apoptosis and a progressive decrease in bone mineral density and bone strength [47]. In a mouse model, in which osteocytes were ablated, increased intracortical porosity was observed, as was decreased sensitivity to unloading [48]. These data also support the role of osteocytes in the mechanotransduction process.

Osteocyte apoptosis can occur in response to a number of insults on bone, including microdamage of the bone matrix, ischaemia, oestrogen deprivation, immobilisation and pharmacological agents, such as glucocorticoids or chemotherapy. Mechanical overloading has been shown to cause microdamage and microcracks in bone, which in turn disrupts the osteocyte canalicular network and results in reduced availability of nutrients and oxygen. It appears that the dying osteocytes are capable of inducing signalling to recruit osteoclasts at

these sites of fatigue-loaded bone [18, 49, 50] either by the release of apoptotic bodies that express RANKL [51] or by upregulating the expression of RANKL in the neighbouring viable osteocytes [32, 52]. Osteoclastic resorption is always accompanied by new blood vessels, whose growth is likely induced in these areas of microdamage by hypoxia-inducing factor-alpha, HIF-1α, a transcriptional activator. Factors produced by apoptotic osteocytes to initiate bone remodelling include tumour necrosis factor α (TNFα), vascular endothelial growth factor (VEGF), osteopontin, a mediator of environmental stress and a potential chemoattractant for osteoclasts, and, most importantly, RANKL [10, 47].

There is now strong evidence that viable osteocytes also support osteoclastogenesis [53], driven by their expression at least of RANKL and M-CSF [18]. RANKL expression has been detected on dendritic processes of the murine long bone osteocyte (MLO)-Y4 cells [50, 54] and has since been shown to greatly promote osteoclast formation without the induction of apoptosis [55] and in remodelling cancellous bone [56]. This suggests the mechanism of how the osteocytes, which are embedded in the bone matrix, influences osteoclastogenesis by extending osteocytic processes to the bone surface [57] and even beyond into the marrow cavity [58] and the blood vessels within [14]. Honma and colleagues had proposed that direct interaction between the osteocyte processes and osteoclast precursors are required for the provision of RANKL and the regulation of osteoclastogenesis [59, 60]. Deletion of RANKL in DMP1 expressing osteocytes resulted in an osteopetrotic phenotype in adult mice, suggesting that osteocytes are a major regulator of osteoclastic activity in adult bone [55, 61]. Evidence from our group showed that the osteocyte product, sclerostin, induced osteocytic expression of RANKL and stimulated an osteoclastogenic response [62], linking mechanotransduction to this process.

2.2.3 The Zetos™ system

Dr. David Jones at Marburg University, Germany and Dr. Everett Smith at the University of Wisconsin co-developed the original version of the *Zetos*™ system for the loading and testing

of trabecular bone in long-term culture [26]. This system reportedly enables the *ex vivo* culture of viable bone samples for extended periods of up to 3 months. The system is made up of a set of cross flow culture chambers, allowing constant perfusion of bone samples with nutrients and oxygen. Agents of interest can be added to the medium and metabolic products can be measured in the perfusate. The system has a loading device, which can apply physiological strain to the bone samples and at the same time measure their stiffness.

2.2.4 Previous reports using the Zetos™ system

A detailed account of the first generation Zetos™ system and the method for setting up an experiment with it has been published previously [26, 63]. The method described was modified to suit facilities and materials available in the laboratory setup at The University of Adelaide. The calibration protocol for the system has also been reported in detail [64]. However, this is vastly different than the calibration protocol currently in use in this laboratory as both the hardware and software of the second generation Zetos™ system have undergone major changes.

A number of investigators have published the results of their work using the first generation Zetos™ system. David and colleagues were able to reproduce similar osteogenic effects seen *in vivo*, when mechanical strain is applied to bone, in the *ex vivo* bone samples mechanically loaded with the Zetos™ system [65]. Strain is a measure of deformation without dimension in which 1 strain represents a deformation of 100% and 1 μstrain equals to 0.0001% deformation [66]. Endres et al. demonstrated that loading the samples at 2,000 μstrain results in the highest amount of osteoid formation and that there is a positive correlation between osteoid thickness and an apparent increase in stiffness of the trabecular bone [67].

Davies and colleagues reported that the drilling process resulted in a layer of non-viable cells and bone debris up to 1mm deep around the periphery of the prepared bone cores, which may

be due to inadequate irrigation [63]. However, it was unclear if the dead cells are mainly from marrow, intact bone or bone debris itself. They also demonstrated that Procion Red dye particles in culture medium, which are 400 Da in size, penetrate the bone core via diffusion rather than perfusion. Perhaps, removing the bone marrow during preparation of the bone cores may allow for better perfusion of the osteocytes within the bone culture chamber. The difference between bone cores having and not having marrow will be investigated in this chapter.

The first generation Zetos™ system has also been used to validate the effect of mechanical stimuli on the expression of RUNX2 and peroxisome proliferator-activated receptor γ (PPARγ) by bone cells in suitable *in vitro* and *in vivo* models [68]. Dumas and colleagues used the Zetos™ system to investigate the effect of various loading regimens on a 3-dimensional porous hydroxyapatite scaffold seeded with MG 63 human osteoblast-like cells [69].

Stoddard and colleagues reported work on comparing the best method for assessing the viability of the cells, especially the osteocytes within the bone cores, studied using the Zetos™ system [70], and Mann *et al.* demonstrated that mechanical stimulation using this system is able to maintain the viability of the osteocytes within the bone samples [71]. However, the number of viable osteocytes was reduced by almost 50% after 7 days of loading in the bone culture chamber when compared to fresh samples. Simpson and colleagues reported the increased viability of osteocytes within bone cores that had TGF-β administered together with mechanical loading daily when compared with just having either stimulus alone [72]. A study by Vivanco and colleagues demonstrated the ability of this system to produce an apparent increase in the elastic modulus and reduction of osteocyte apoptosis of trabecular bone cores that were loaded with physiological load of 4000 μstrain similar to jumping [73].

The Zetos™ system has been shown to be suitable for the evaluation of devices implanted in the trabecular bone cores for local delivery of drugs [74, 75]. It was also shown to be able to be used to investigate the biocompatibility of biomaterials loaded with pharmacological agents and the effect it has on human trabecular bone [76]. Chan et al. used the Zetos™ system to

apply mechanical loading and measure the apparent elastic modulus to their novel 3D trabecular bone explant co-culture model, which allows live osteocytes in trabecular bone to be interconnected with osteoblasts seeded on the bone surface [77].

2.3 Problem Statement

Bone modelling and remodelling have largely been considered a function of osteoblasts and osteoclasts. It is becoming clear that much of what these cells do in bone is regulated by osteocytes, yet the mechanisms by which osteocytes do so are poorly understood. This is largely due to the lack of an experimental system to study osteocytes in their native state of a 3-dimensional cell syncytium in bone. The Zetos™ system now allows such study of animal or, potentially, human bone and this study describes the set-up and optimisation of the 2nd generation Zetos.

2.4 Research Hypotheses

The hypotheses of this study were that:

1. The mechanical properties of the bovine bone cores are increased after undergoing a period of loading when compared to unloaded bone;
2. There is a parallel increase in the microstructure of the bovine bone cores after undergoing loading;
3. The absence of marrow does not have any significant effect on the loading response of the bovine bone cores.

2.5 Objectives

The objectives of this study were:

1. To determine if there is a significant difference in the stiffness of bovine bone cores between different bone loading regimes;
2. To determine if there is a significant difference in the microstructure and properties of bovine bone cores undergoing different loading regimes;
3. To investigate if the presence of marrow in the bovine bone cores is required for it to respond adequately to loading.

2.6 Beta testing of the Zetos™ software

Prior to this experiment, the software for controlling the Zetos ™ system (Simplex Scientific LLC, Wisconsin, USA) went through several versions based on trial experiments conducted using bone cores with intact bone marrow. In the initial version of the Zetos™ software (version 1.0.0.2), it was not possible to key in the measurements of the individual bone cores into the experiment file on site. The measured diameter and thickness of each bone core and the corresponding culture chamber number had to be sent to the software developer, Simplex Scientific, via email for them to create the experiment file for the samples and to program in the required exercise sessions accordingly. The initial manual provided by the software developer (Appendix I – Zetos Manual v1.0.0.1) showed the availability of a Session Editor in the software. However, it was not possible to be opened or used by the end-user at this point. This is because the experiment portion of the software was still under development and needed further testing at that time. Subsequent versions of the Zetos™ software (versions 1.0.0.3, 1.0.0.5 and 1.0.0.6) was developed in the course of running trial experiments based on the problems that were encountered. A summary of the changes that was made to the software for each new version is shown in Table 2.2.

Table 2.2. Changes Made in Version 1 of the Zetos™

Zetos software version	Changes made
Version 1.0.0.3	Logging of the force calibration data with the samples
Version 1.0.0.5	Solution to problems with the barcode scanner and with samples that does not require any loading regime: - Pressing the Calibrate button on the remote controller will make the system assume the correct barcode has been entered. - Pressing the Enter button on the remote controller will make the system skip that sample and go to the next sample in the experiment file.
Version 1.0.0.6	Able to run several sessions together. In the case of two sessions with the same name, the first one will be used. Clicking the Stop Testing button on the software user interface works better as it will not interrupt when a session is running, but it should not start any more after that. Pressing the Enter button on the remote controller should skip additional sessions for a sample. Software runs noticeably faster as it does not release time to other processes as much as in the previous versions

In the latest version of the Zetos™ software (version 2.0.0.1), the end-user is able to create an experiment file by inputting the individual barcode and the respective diameter and height for each bone core. The Sessions Editor can now be used by the end-user to create the loading sessions to be performed on each bone core. The sessions can be either an exercise regime to stimulate the bone cores or a calculation of the Young's modulus of the respective bone cores. The procedure for creating the experiment file and loading sessions are as shown in the user manual supplied by the software developer (Appendix II – Zetos Manual v2.0.0.1).

It was also noted that there was a 'drift' on the force being measured by the Zetos ™system during use, which was attributed to the response of the piezo actuator after it was energised or deenergised. The developer of the second generation Zetos™ system was notified of this matter, resulting in a further upgrade and refinement to both the hardware and software of the system.

2.7 Optimisation of the Zetos™ system

2.7.1 Procurement of fresh viable bone

Trabecular bone cores were prepared from the freshly procured sternum of a 9-months old healthy steer (young male cow) from an abattoir in Hahndorf, Adelaide Hills, South Australia (Fig. 2.1). The procured bone was kept moist in a plastic bag filled with cold sterile saline (0.85%) and transported in a cool box containing ice packs.

Figure 2.1 – Procurement of Fresh Bovine Sternum
Taking the sternum from a freshly slaughtered steer.

2.7.2 Cleaning and cutting the sternum

Preparation of the bone samples was completed within 12 hours after removal. Care was taken to maintain sterility as much as possible during the handling of the bone with the liberal use of 70% ethanol and an industrial strength disinfectant spray (Oust®, S.C. Johnson & Son Inc., Wisconsin) on all surfaces and instruments and the use of sterile surgical gloves and sterile draping. All soft tissues and cartilage, including the ventral ends of the ribs that make up the sternocostochondral joints, were removed from the sternum (Fig. 2.2).

The bone was then cut into 1-1.5 cm thick sections along the sagittal plane using a sterile hand-held hacksaw. The orientation of the bovine sternum and cut sections was maintained the same throughout this process to ensure that the bone cores produced at the end will all be orientated in the same plane. A large vice of an appropriate size was used to hold the sternum during the cutting process. The vice and workbench were covered with a large sterile disposable surgical drape during this process (Fig. 2.3). The long sections of bone were reduced in size by cutting through the cartilage between each bone segments. Prepared sections were kept immersed for at least 1 hour in a pre-prepared prewash media consisting of high glucose Dulbecco's Modified Eagle Medium (DMEM)(Invitrogen Corporation, California) with 20mM 4-(2-Hydroxyethyl)-1-piperazineethanesulfonic acid (HEPES), 2.4 mg/mL benzyl-penicillin, 3.2 mg/mL gentamicin sulphate and 4 µg/mL Amphotericin B (Fig. 2.4).

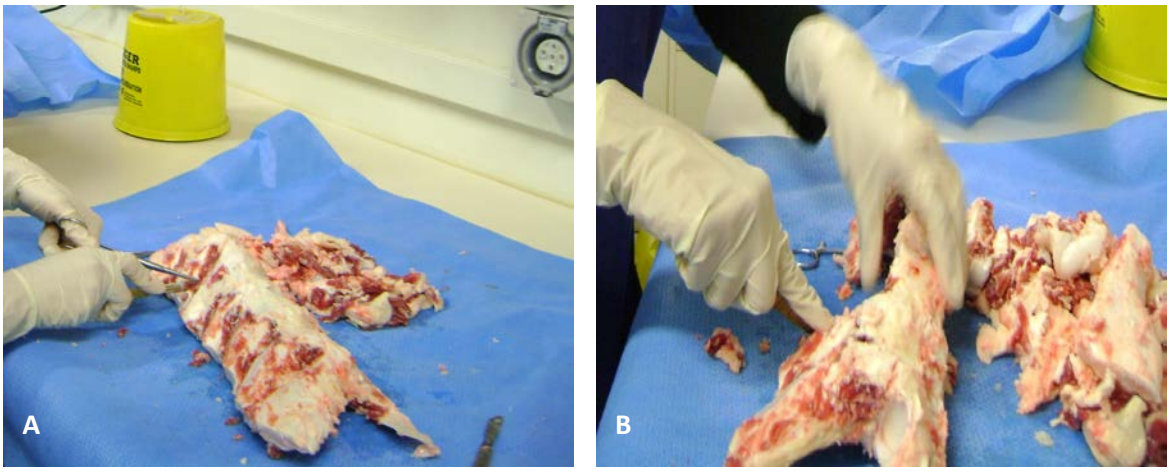

Figure 2.2 – Cleaning the Procured Sternum

A) The soft tissues were removed using a size 22 scalpel blade with suitable forceps and tweezers. **B)** The attached ends of the ribs were removed by cutting through each of the sternocostochondral joints.

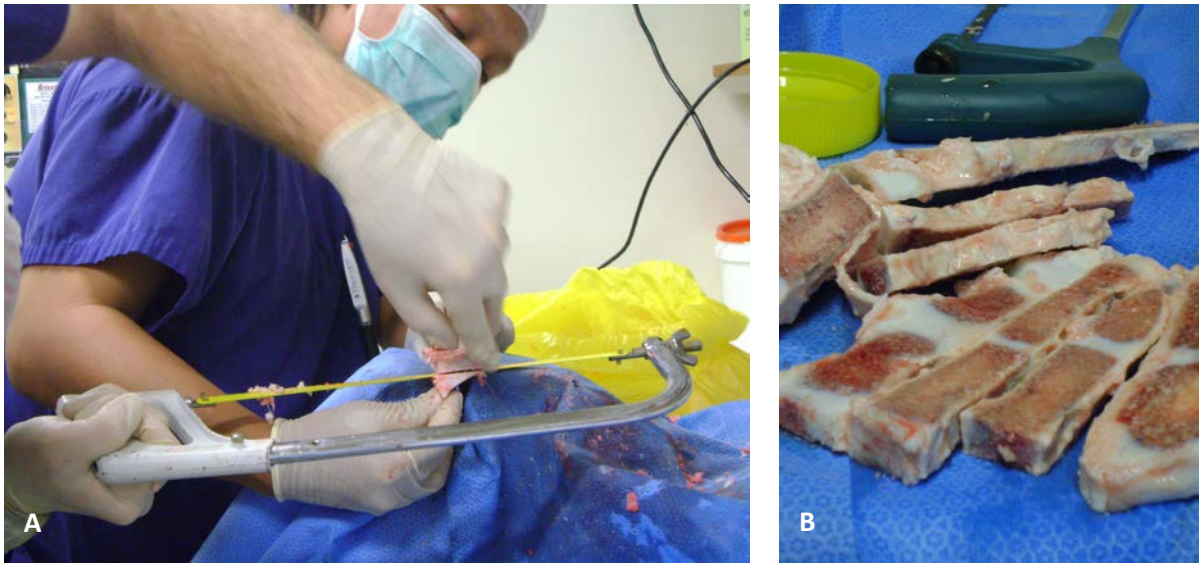

Figure 2.3 – Cutting the Procured Sternum

A) The cleaned sternum was cut into slices using a sterile hacksaw. **B)** Sterility was maintained with the use of disposable sterile surgical drapes covering the work area.

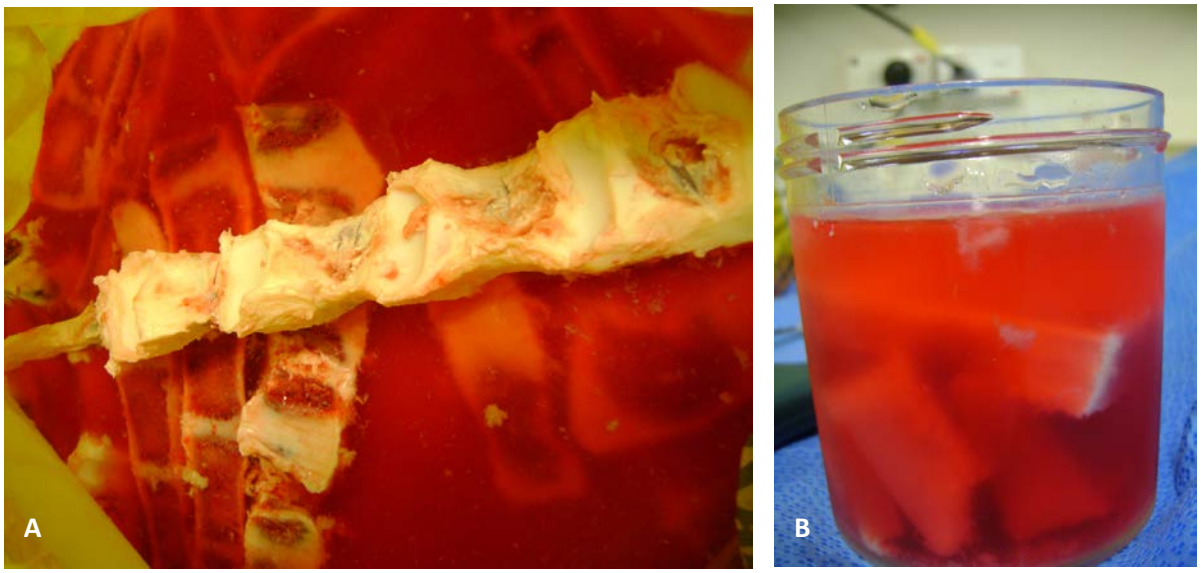

Figure 2.4 – Soaking in Prewash Media

A)The cut slices of bone were kept moist at all times to prevent desiccation of the tissues before being cut into smaller pieces by cutting through the cartilage between the bone segments. **B)** The smaller bone pieces were kept soaked in antibiotic containing media before the drilling and milling process is performed.

2.7.3 Drilling process

Next, cylindrical shaped bone cores 10 mm in diameter were cored out from the prepared bone sections using a custom made diamond coated coring drill bit on an industrial milling machine (Grizzly Industrial® Inc., USA). All bone cores produced will be from the same plane (sagittal)

in the bone, with the flat ends orientated towards the left and right side of the animal. Throughout the drilling process, the bone pieces were immersed in cold (4°C) sterile saline (0.85%) or phosphate buffered saline (PBS) on a custom made polyoxymethylene drilling jig to avoid thermal-necrosis of the tissues (Fig. 2.5). Prepared bone cores were put back in the prewash media before going to the next processing step. A total of 52 bone cores were able to be produced from the single bovine sternum used.

2.7.4 Milling process

The prepared bone cores were then fitted on a milling plate eight (8) at a time, which was then fitted onto a custom made milling platform. The milling plate enables the bone cores to be milled down to about 5mm thickness with a 1cm diameter tungsten carbide milling bit on another milling machine. The bone pieces were kept immersed in either cold (4°C) sterile saline (0.85%) or phosphate buffered saline (PBS) in the milling platform to prevent desiccation and/or thermal necrosis (Fig. 2.6). Only 24 out of the 52 bone cores drilled out were milled. The final bone cores should consist of trabecular bone only and not have any visible cartilage within it. The bone cores were kept overnight at 4°C in a refrigerator.

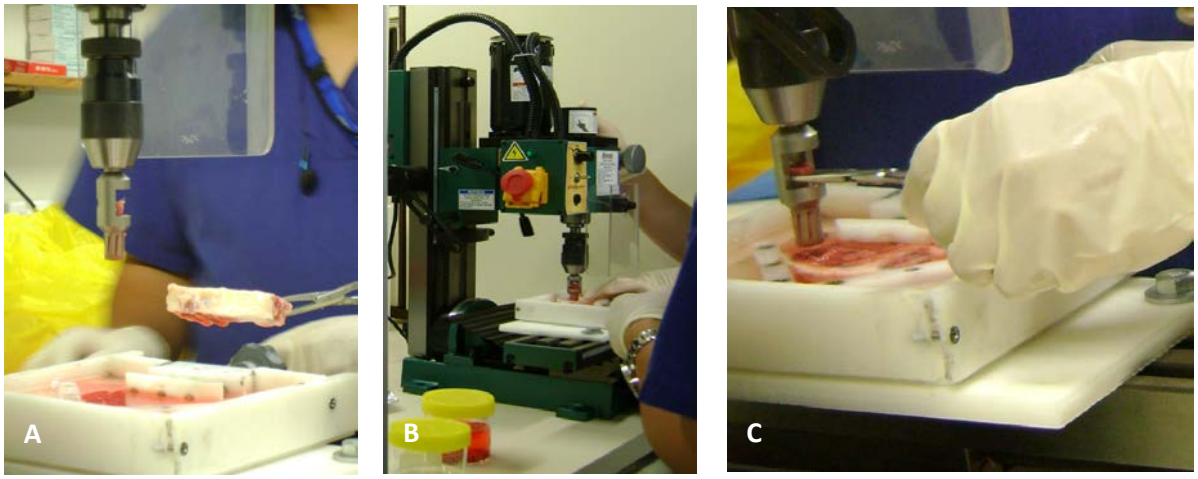

Figure 2.5 – Drilling Process

A) The prepared bone piece was transferred into the custom made drilling jig that was filled with cold sterile saline or PBS. **B)** The whole process was performed using an industrial milling machine. **C)** The bone cores that were drilled out were carefully removed from the slot of the custom made diamond coated coring drill bit before being placed in another clean container filled with the antibiotic containing prewash media.

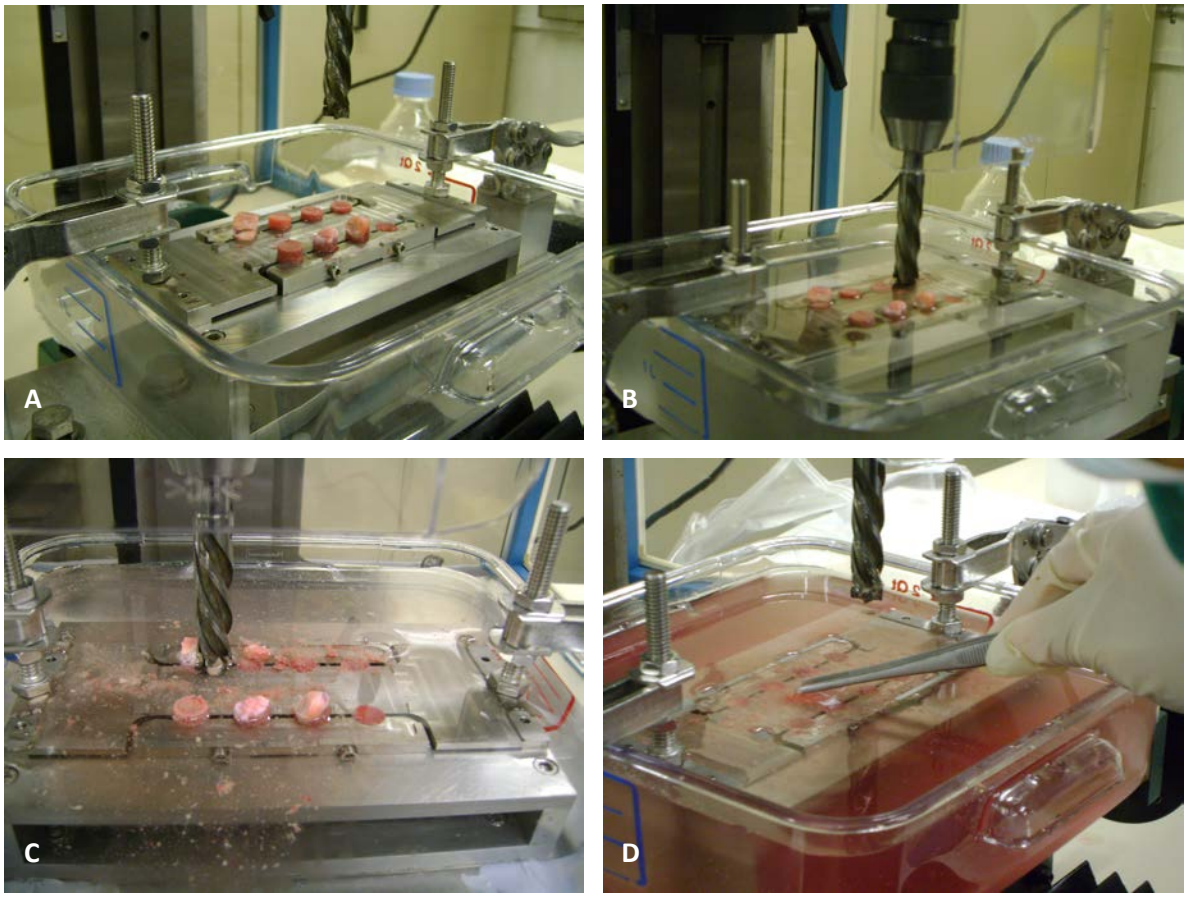

Figure 2.6 – Milling Process

A) The bone cores that were drilled out are held in place in the slots of the milling plate by tightening the screws on the sides before being put on the milling platform. **B)** The milling platform was then filled with sterile saline or PBS before the bone cores were milled down using the 4 fluted tungsten carbide milling bit. **C)** The milling plate enables the bone cores to be milled down to the correct height. **D)** The milling plate was then turned over and the process repeated to ensure that both sides of the bone cores are even and their heights are the same.

2.7.5 Measuring the bone cores

The diameter and height of the bone cores were measured three times each using a scientific calliper (micrometer), which is accurate to 0.02mm. Each bone core was numbered and kept in separate sterile containers filled with a nutrient rich mineralising media. The media was made up of Dulbecco's Modified Eagle Medium (DMEM)(Invitrogen Corporation, California) with 20mM 4-(2-Hydroxyethyl)-1-piperazineethanesulfonic acid (HEPES), 10% foetal calf serum (FCS), 1.8mM KH_2PO_4, 100µM L-ascorbate-2-phosphate, 2mM L-glutamine, 1.2 mg/mL benzyl-penicillin, 1.6 mg/mL gentamicin sulphate and 4 µg/mL Amphotericin B. The entire process was performed under sterile conditions in a Class II biohazard cabinet to prevent

microbial contamination of the prepared bone cores (Fig. 2.7). The mean diameter and height of each bone core were calculated from these measurements.

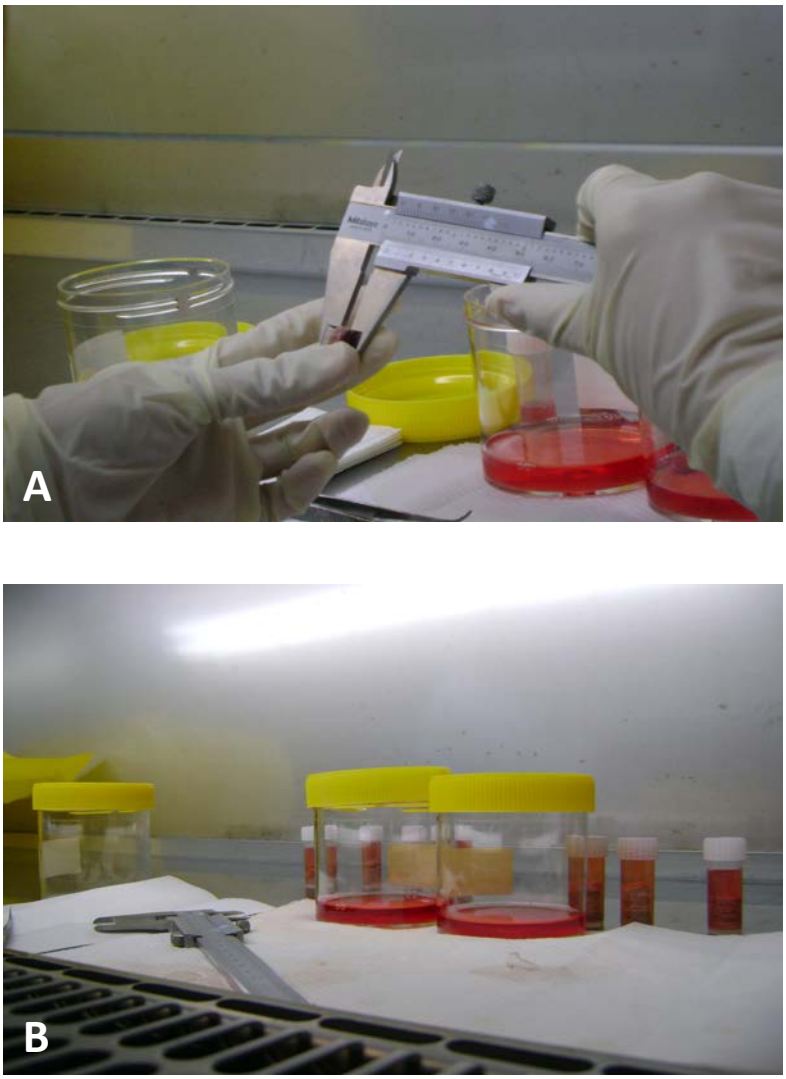

Figure 2.7 –Measuring the Bone Cores

Work on the bone cores was performed in a Class II biohazard cabinet at all times to maintain sterility and avoid contamination of the bone cores by any microorganisms. **A)** The diameter and height of each of the bone cores were measured thrice with a calliper (micrometer). **B)** The measured bone cores were transferred into numbered sterile containers before going for the pre-experimental micro-computed tomography (μCT) scanning. From this point onwards it is important not to mix bone cores up with each other.

2.7.6 Removal of bone marrow

Half (12) of the bone cores that were milled had their marrow removed using a cordless dental water jet (WP-450A, Water Pik Inc., Colorado, USA) device (Fig. 2.8). To maintain sterility 70% ethanol was run through the dental water jet first before using cold sterile saline or PBS

for this process. The whole procedure was, again, done in a Class II biohazard cabinet using sterile methods. Figure 2.9 is of a bone core before (A) and after (B) removal of its marrow.

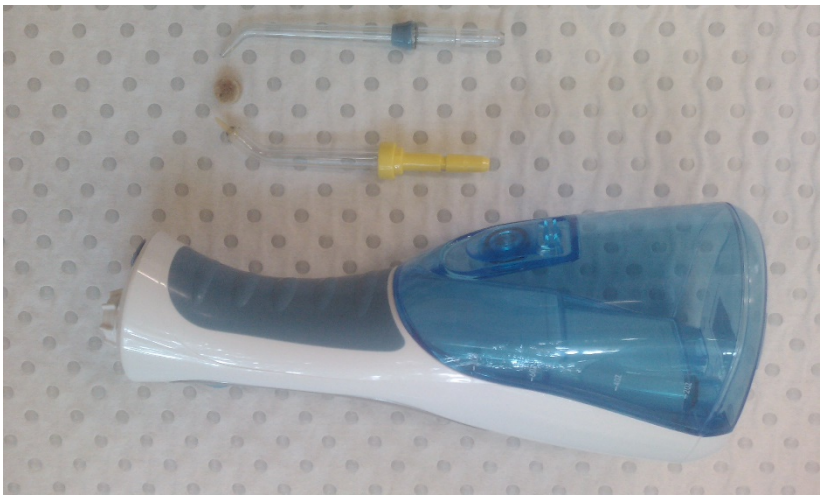

Figure 2.8 – Dental Water Jet Device
The cordless dental water jet device was used to remove marrow from some of the bone cores.

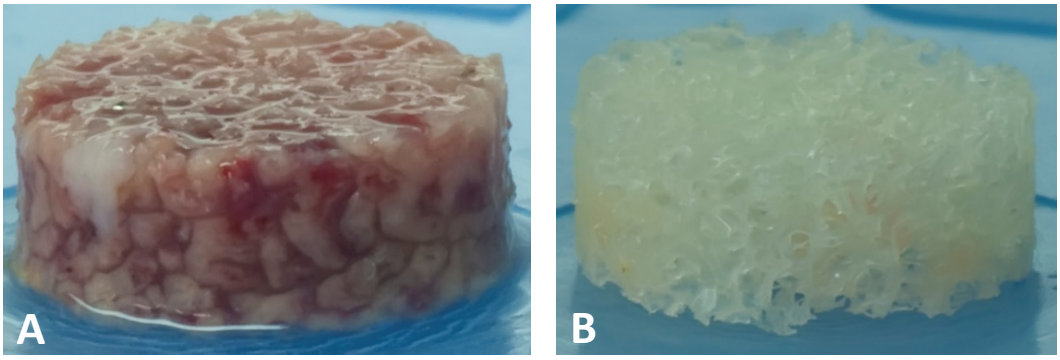

Figure 2.9 – Bone Core With and Without Marrow
A) Close up view of a bone core after drilling and milling with the marrow still in place. **B)** The same bone core after removal of its marrow.

2.7.7 Bone culture chamber assembly

The bone culture chambers for the Zetos™ system were made of cell culture plastic material with some accessories to enable a loading force to be applied to the bone cores within it but still maintain sterility and perfusion by the mineralising cell culture media. The complete chamber consists of two halves that can be screwed together with two X-rings, two O-rings and two sapphire pistons (Fig. 2.10). The sapphire pistons insert into the openings on the top and bottom ends of the chamber. Prevention of cell culture media leakage from inside the chamber while

allowing movement of the pistons is achieved with the X-rings and use of silicone-based grease applied to the sides of the pistons. Leakage of the cell culture media at the point where the two halves of the chamber are screwed together is prevented by the O-rings. The prepared bone cores are placed in the middle of the construct between the sapphire pistons. All components of the bone culture chamber, including the silicon-based grease were sterilised beforehand using low temperature hydrogen peroxide gas plasma (STERRAD®, Advances Sterilization Products, California, USA) and all assembly work was performed in a Class II biohazard cabinet.

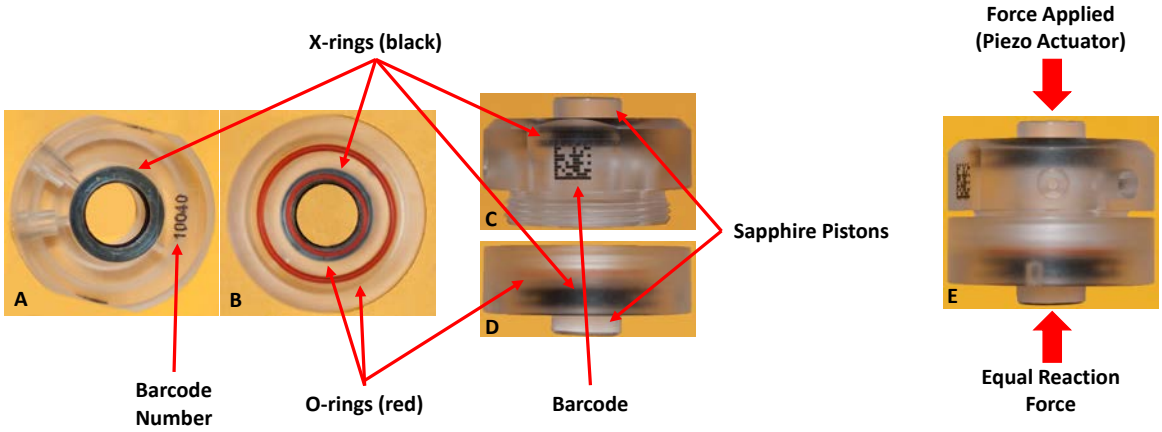

Figure 2.10 – Bone Culture Chamber Components
A) View of the top half of the bone culture chamber form above. **B)** View for the bottom half of the bone culture chamber from below. **C &D)** Side views of both halves of the bone culture chamber with the sapphire pistons inserted into the top and bottom openings. **E)** The fully assembled bone culture chamber showing how the application of a force at the top will result in equal pressures being applied to both ends of the bone core inside the chamber.

2.7.8 Assembly of closed perfusion system for bone culture chambers

While still in the Class II biohazard cabinet, the assembled bone culture chambers were each connected to two sterilised latex tubes in turn connected to the other end of a reservoir tube filled with the nutrient-rich mineralising cell culture media (DMEM (Invitrogen Corporation, California) with 20mM HEPES, 10% v/v FCS, 1.8mM KH_2PO_4, 100µM L-ascorbate-2-phosphate, 2mM L-glutamine, 1.2 mg/mL benzyl-penicillin, 1.6 mg/mL gentamicin sulphate and 4 µg/mL Amphotericin B). The completed apparatus constitutes a closed sterile environment for the bone cores. Once assembled the apparatus was connected to a running

planetary drive peristaltic pump (Ismatec IP 24, ISMATEC SA, Switzerland) to ensure timely perfusion of the bone core with the cell culture media (Fig. 2.11). The peristaltic pump was set to provide a flow rate of approximately 7ml/hr [67]. The peristaltic pump and bone culture systems were maintained in a 37°C chamber to simulate normal mammalian body temperature. The mineralising cell culture media supplying nutrients to the bone cores were changed daily.

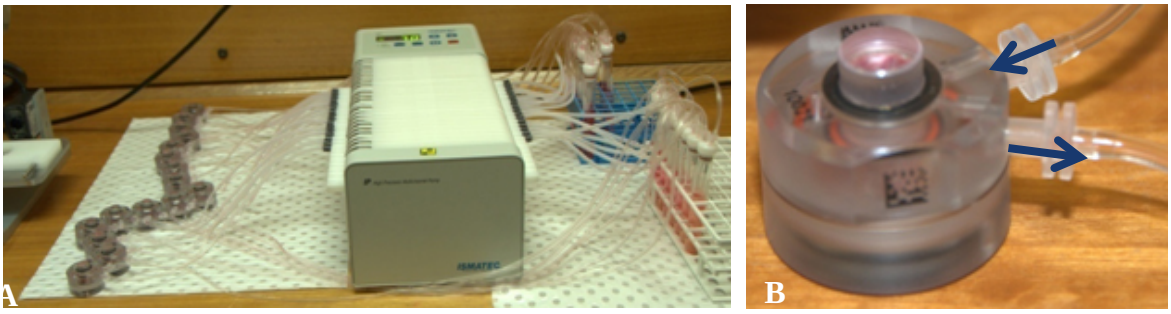

Figure 2.11 – Bone Culture Chamber Perfusion

A) The peristaltic pump with the fully assembled bone culture systems attached. All of the bone culture chambers were on the left while the media reservoirs were placed to the right **B)**. The flow of the cell culture media through the culture chambers provided by the pump was in one direction (arrows) only.

2.7.9 Analysis of pH and ionic calcium levels of the used media

The used mineralising cell culture media was kept in a 4°C fridge for further analysis of pH and ionic calcium ($Ca^{2+)}$ levels. Measurements of the pH of the used media were taken and recorded daily using a calibrated digital pH meter. Ca^{2+} levels of the mineralising cell culture media was performed on day 9, 10 and 11 using a direct Ca^{2+} assay method, whereby the absorbance at 630nm of 200µl of the media was measured on a microplate reader (MR7000, Dynatech Laboratories, Guernsey, Channel Islands) and compared to a standard curve created from freshly prepared calcium standards ($CaCl_2$, 0.0mM - 4.4mM) and measured on the same occasion. Unused mineralising cell culture media for day 10 and 11 was used as a control.

2.7.10 Mechanical loading of the bone cores

A second generation Zetos™ system was placed next to the bone culture system and peristaltic pump in the 37°C chamber (Fig. 2.12) to allow application of a specific loading regime to each of the bone cores within the bone culture chambers without having to detach them from the peristaltic pump. At the conclusion of the experiment, the bone cores were removed from the bone culture chambers and placed in 10% neutral buffered formalin for μCT scanning.

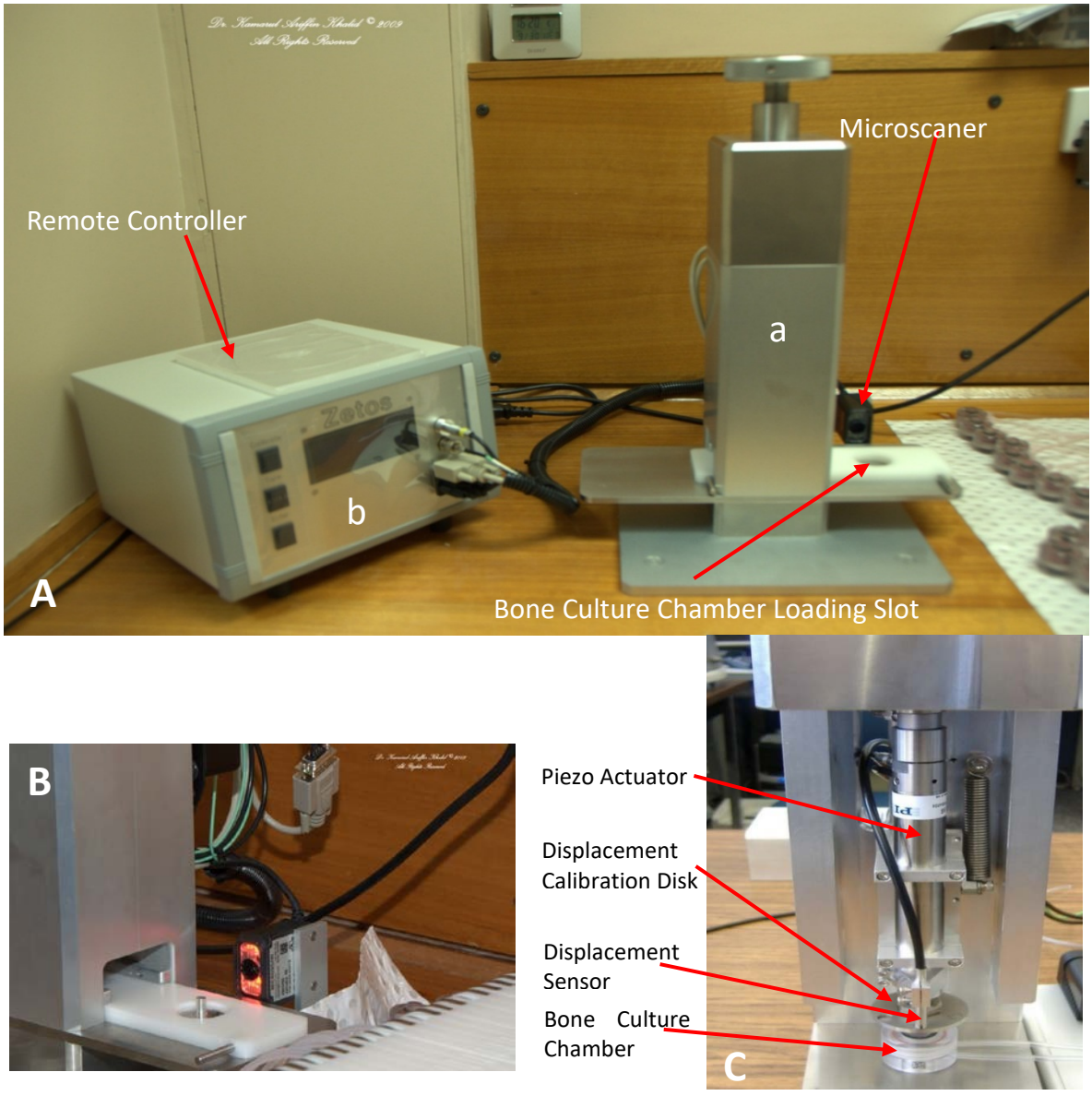

Figure 2.12 – Second Generation Zetos™ System

A) The Zetos™ system consisting of the loading device (**a**) and the remote controller (**b**) located just next to the peristaltic pump and bone culture chambers in the 37°C room. **B)** The barcode on the bone culture chamber is scanned by the micro scanner to ensure that the correct data is recorded by the Zetos™ system for each bone core. **C)** The insides of the loading device showing the piezo actuator that enables the accurate application of force and measurement of displacement. (Fig. 2.12C courtesy of Simplex Scientific LLC, Wisconsin, USA)

2.7.11 Bone loading regimes

The bone cores were distributed equally into 6 groups of 4. 1) Without marrow and not loaded (NMUL), 2); Without marrow and loaded 100 cycles three times a day (NM100x3); 3) Without marrow and loaded 300 cycles once a day (NM300x1); 4) With intact marrow and not loaded (MUL); 5) With intact marrow and loaded 100 cycles three times a day (M100x3); and 6) With marrow and loaded for 300 cycles once daily (M300x1). Each bone core was identified by a unique bar code displayed on the respective culture chamber (Table 2.3).

Table 2.3. Grouping of Bone Culture Chambers

Group	Chamber No.	Group	Chamber No.	Group	Chamber No.
NM100x3	10033	NM300x1	10038	NMUL	10030
	10034		10022		10044
	10032		10028		10027
	10040		10045		10021
M100x3	10024	M300x1	10039	MUL	10042
	10041		10037		10031
	10029		10043		10036
	10035		10025		10026

The Zetos ™ system was set to provide a load of 2,000 μstrain at 1 Hz, where strain is a dimensionless measurement of deformation in which 1 strain represents 100% deformation and 1 μstrain equals to 0.0001% [66]. Thus, 2,000 μstrain was equal to 0.2% deformation of the respective bone core. The bone cores are loaded in compression as the piezo actuator (Fig. 2.12C) applies the required amount of force down onto the sapphire piston at the top of the culture chamber, while the sapphire piston at the bottom provides an equal reaction force, (Fig.

2.10E) until the set amount of deformation to the bone core being loaded was achieved. The Zetos™ applies a triangular loading wave, giving rise to a sawtooth waveform for each loading session (see Appendix I page 4 and Appendix II page 5). The loading regime of 100 cycles three times a day (100x3) denotes that the bone cores will undergo 3 equal sessions of 100 cycles in a day with a rest interval of at least 4 hours between each. Similarly, 300x1 signifies that the bone cores are undergoing a single session of 300 cycles in in a 24h period. Unloaded bone cores were kept perfused as for loaded samples, and while no loading sessions were applied, their stiffness was measured daily, as for all other specimens. A preload of 20N was applied to the bone cores before they were loaded or the Young's Modulus measured, to ensure uniformity of the stresses being applied and good contact between the piezo actuator, loading pistons and bone core [63].

The calculation for the stiffness and Young's Modulus of the bone cores is based on the following calculation (see Appendix II pages 13-14):

$$E \text{ (in MPa)} = \frac{K \times \text{Length}}{\text{Area}}$$

$$= \frac{K \text{ (in N/micron)} \times (1000 \text{ micron/mm}) \times (\text{height of bone core in mm}}{\pi \times (\frac{1}{2} \text{ diameter of bone core})^2 \text{ (in mm}^2\text{)}}$$

K is the corrected stiffness (Kistler) value that is calculated based on the calibration curve for the system (Appendix III – Calibrating the Zetos™), whereby the uncorrected stiffness value equals to the slope of the force values versus the displacement values that the system calculates for each bone core.

All parameters were inputted into the Zetos™ software (version 2.0.0.1, Simplex Scientific LLC, Wisconsin, USA), installed into a Dell Latitude D420 laptop (Intel® Core™ Duo U2500 CPU) with processor speed of 1.20 GHz and with 2 GB RAM, The laptop PC was connected to the remote controller of the Zetos™ system via a USB 2.0 port, and as well as fully controlling the system, it also collected and stored all data generated by the system. The loading

apparatus was connected to the remote controller of the Zetos™ system via four high-speed USB channels. Software drivers for each of these channels were installed into the computer running the Zetos™ software before it is able to communicate with the system. The detailed procedure for creating a new experiment file that has all of the aforementioned parameters programmed into session files is illustrated in Appendix IV (Setting new experiment and sessions files for the Zetos™).

All relevant data and running parameters are able to be viewed in real-time via the graphical user interface (GUI) (Fig. 2.13). Details of the information that was shown on the GUI is illustrated by Figures 2.14 to 2.17. Figure 2.18 is of a GUI when a bone culture chamber was being loaded by the system.

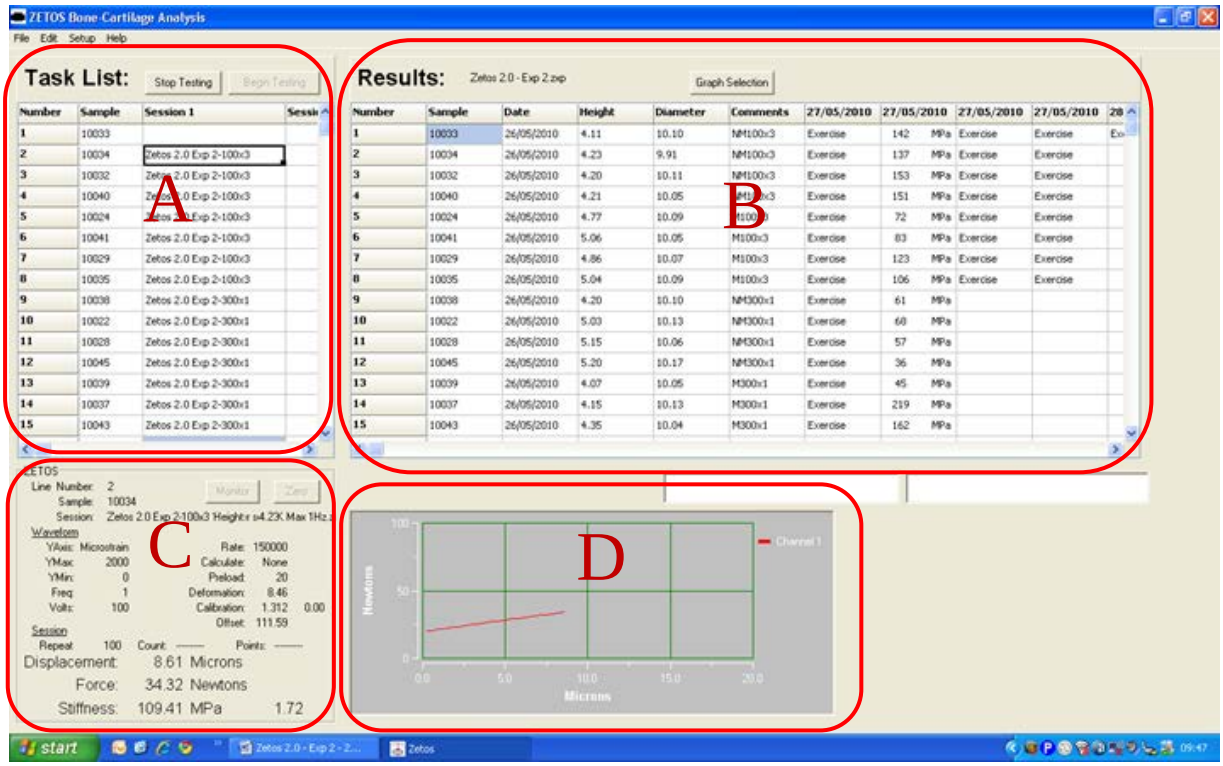

Figure 2.13 – Zetos™ Software Graphical User Interface (GUI)
The GUI of the Zetos™ software at the start of a loading session. It has four panels, which are **A**. Task List, **B**. Results, **C**. Real-time information panel, and **D**. Real-time stress/strain curve.

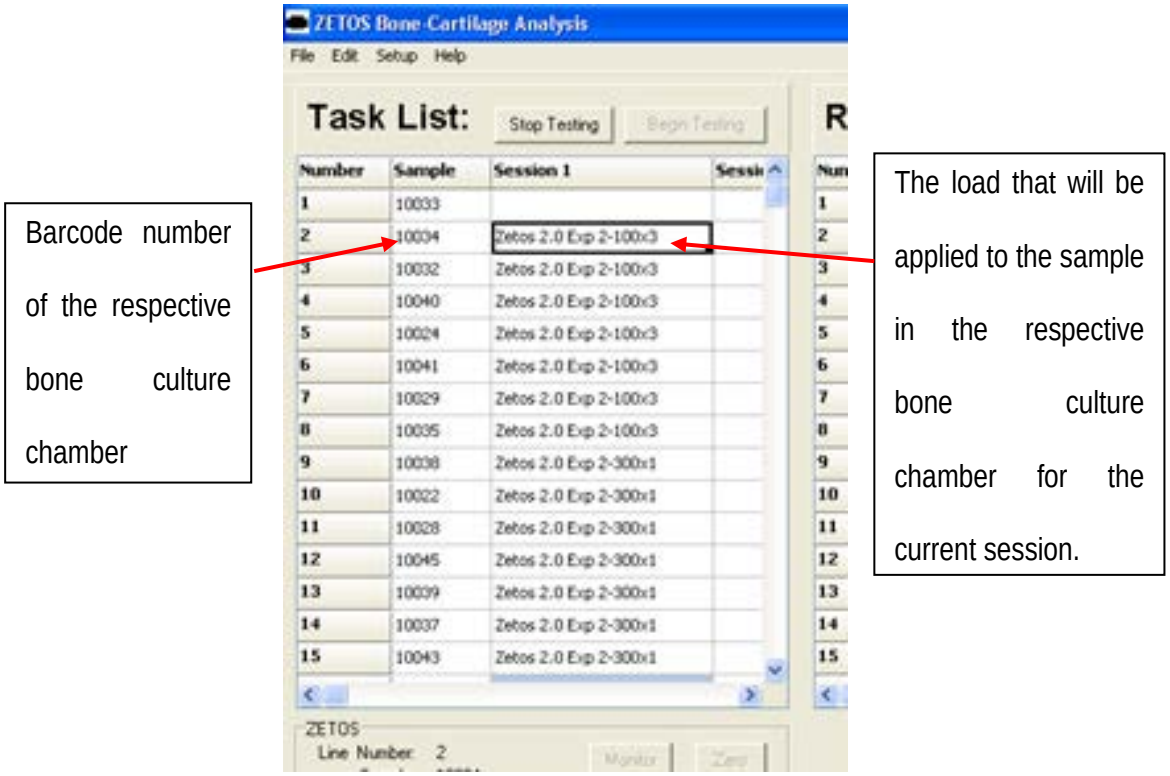

Figure 2.14 – GUI Task List Panel

Details of the Task List panel. The appropriate loading protocol that has been programmed into the software is chosen for each bone culture chamber in the respective column. Multiple sessions can be applied to the same sample by selecting the required session in the subsequent columns.

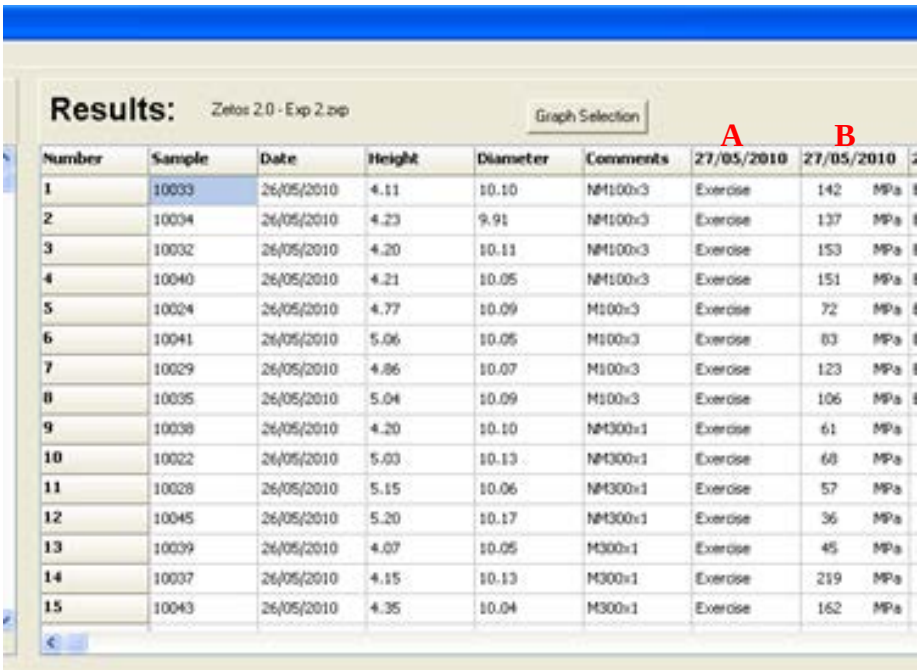

Figure 2.15 – GUI Results Panel

Results panel of the GUI displaying the contents of the experiment file (Zetos 2.0 - Exp 2.zxp) that was created at the start of the experiment. It shows the barcode number of each bone culture chamber (Sample column) together with the measured dimensions of the respective bone cores (Height and Diameter columns) in it, which was entered when the file was created. The Comments column was used to indicate which group the respective bone culture chamber is in. The column marked by **A** indicates that the bone cores were loaded accordingly with the chosen session protocol, while the column marked **B** showed the Young's Modulus that was measured by the system for each bone core.

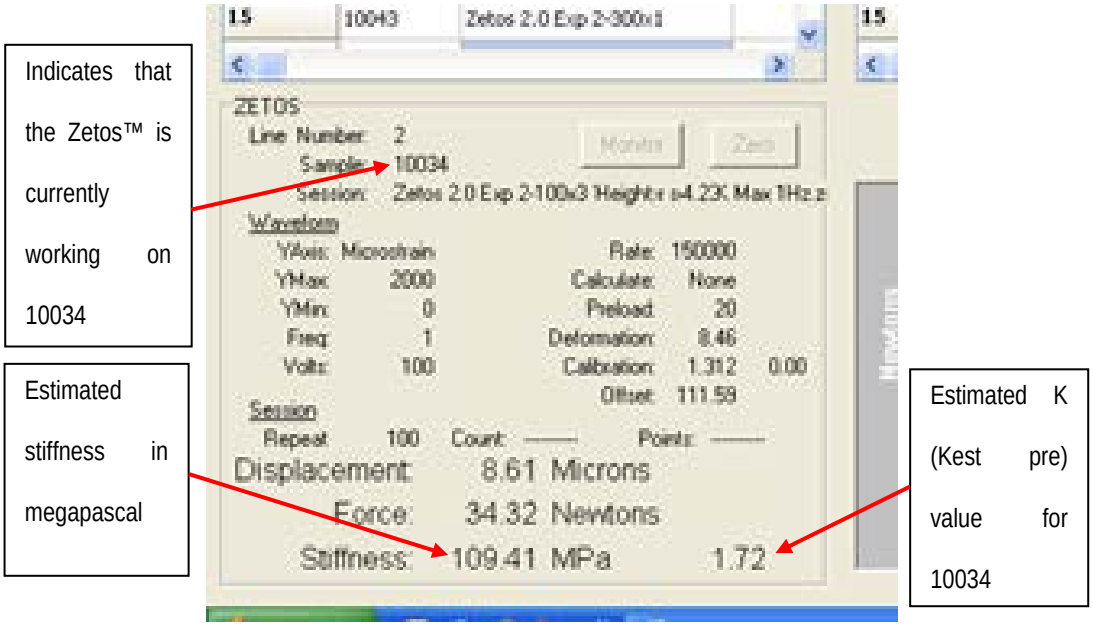

Figure 2.16 – GUI Real-Time Information Panel

The Real-Time Information panel at the left lower corner of the GUI provides the details of the bone culture chamber being loaded by the system together with the stress (Force) and strain (Displacement) being generated on the bone core within.

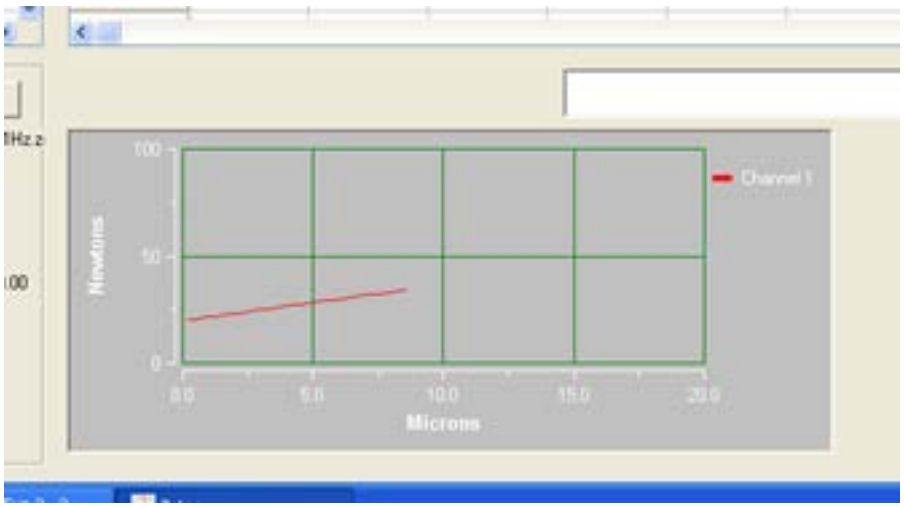

Figure 2.17 – GUI Real-Time Stress/Strain Curve Panel

The Real-Time Stress/Strain Curve panel of the GUI. The Zetos™ system performed a survey scan until displacement of 2,000 µstrain is reached before the loading regime is started and the generated stress/strain curve will be displayed here as shown.

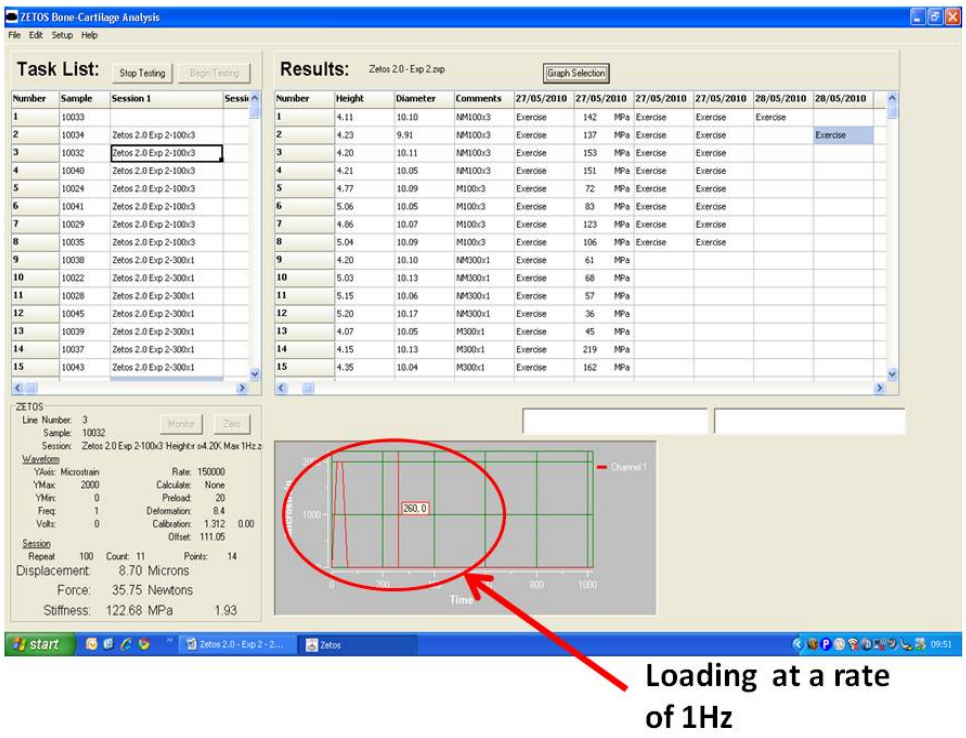

Figure 2.18 – GUI during Loading

The GUI of the Zetos™ software while the bone core is being loaded according to the pre-set loading protocol. The real-time stress/strain curve at the bottom right-hand panel depicts the characteristics of the load being applied.

2.7.12 Calibration of the Zetos™ system

The Zetos™ system requires regular calibration to ensure that the data generated are validated and reliable. In this experiment the system was calibrated each day before the stiffness was measured and the loading sessions started. The steps for the calibration process is illustrated in detail in Appendix III – Calibrating the Zetos™.

2.7.13 Measurement of stiffness using Young's Modulus

Young's modulus, also known as the tensile or elastic modulus, is a measure of the stiffness of an isotropic elastic material, such as bone. It is defined as the ratio of the uniaxial stress over the uniaxial strain in the range of stress, in which Hooke's Law holds. This is calculated automatically from the slope of a stress-strain curve created during tensile tests conducted on

each of the bone cores using the Young's Modulus setting in the Zetos™ system (Appendix II page 5). In this study, the forces applied is set to deform the individual bone cores by 2,000 μstrain (0.2%), which is equivalent to 0.2/100 x 5mm for a 5mm thick bone core. Hence, the amount of force required will differ for each bone core as their measurements differ slightly, giving rise to specific apparent stiffness values for each bone cores on each occasion (see equation on page 80 in section 2.7.11 above). Using this equation, the apparent stiffness (Young's modulus) that was calculated by the system has been normalised to come out with a value that does not depend on the dimensions of the bone cores as reported by Jones et al. [26]. This enable a value that can be associate with the mechanical properties of each bone core to be derived, thus allowing for comparison of subsequent loading and/or treatments to be made; such as if the stiffness of the bone cores has increased or reduced and how it is related to measured biochemical or histomorphometric changes. A quasi-static loading method was used to measure the apparent stiffness of the bone cores to avoid stimulating them dynamically during measurement of the Young's Modulus.

Each bone core, including those that do not have a load applied to them (groups NMUL and MUL), had their stiffness measured in mega-pascals (MPa) each day from Day 1 (start of loading session) until Day 11. The measurements were made before any loading regime was applied to the bone cores as it is surmised that any changes to the stiffness due to the applied load will only be apparent the following day.

2.7.14 μCT imaging and 3D analysis

The bone cores were subjected to pre and post experiment μCT imaging to detect any changes within their trabecular microarchitecture. The μCT instrument (SkyScan model 1174, Belgium) was able to scan 4 bone cores at a time (Fig. 2.19). The settings used were; resolution 26.01μm, rotation step 0.80° and a 0.25mm aluminium filter was used. Using the provided volumetric reconstruction software (NRecon ver1.6.3, Skyscan, Belgium), the angular projection images

of the scanned bone cores were converted to cross section slices through the bone cores and file conversion from TIFF to Bitmap format for easier handling by the subsequent software (Fig. 2.20). The NRecon software also enables ring artefact and beam hardening corrections to be made, which were set at 15 and 30% respectively (Fig. 2.21), while the dynamic range for the output was set to between 0.000 and 0.075 (Fig. 2.22).

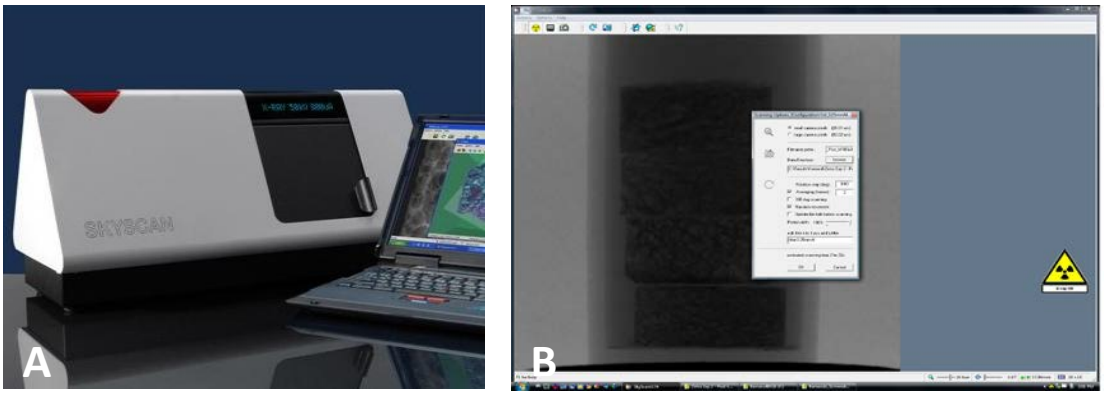

Figure 2.19 – µCT Imaging Device and Settings

A) The Skyscan 1174 micro-computed tomography machine. **B)** GUI of the Skyscan software with the Scanning Options panel opened for changing the settings. 4 bone cores were scanned simultaneously. Care is taken to ensure that the bone cores are not mixed up during this process.

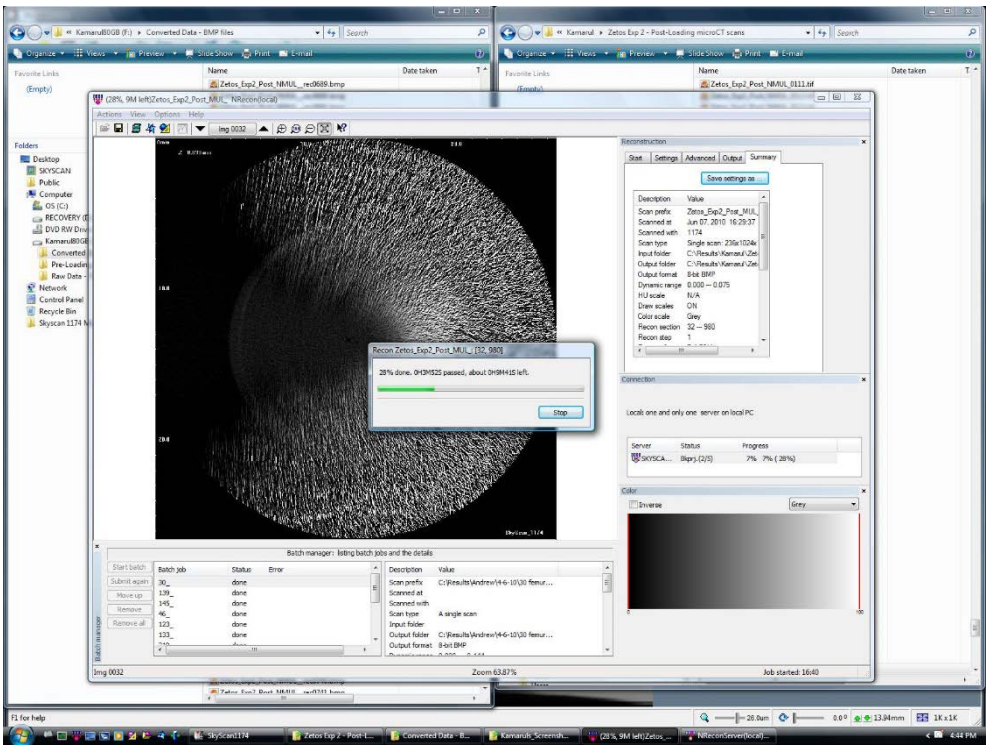

Figure 2.20 – Image Reconstruction Using NRecon Software

The NRecon software was used to reconstruct the images scanned and produced by the µCT scanner and to convert them to Bitmap format.

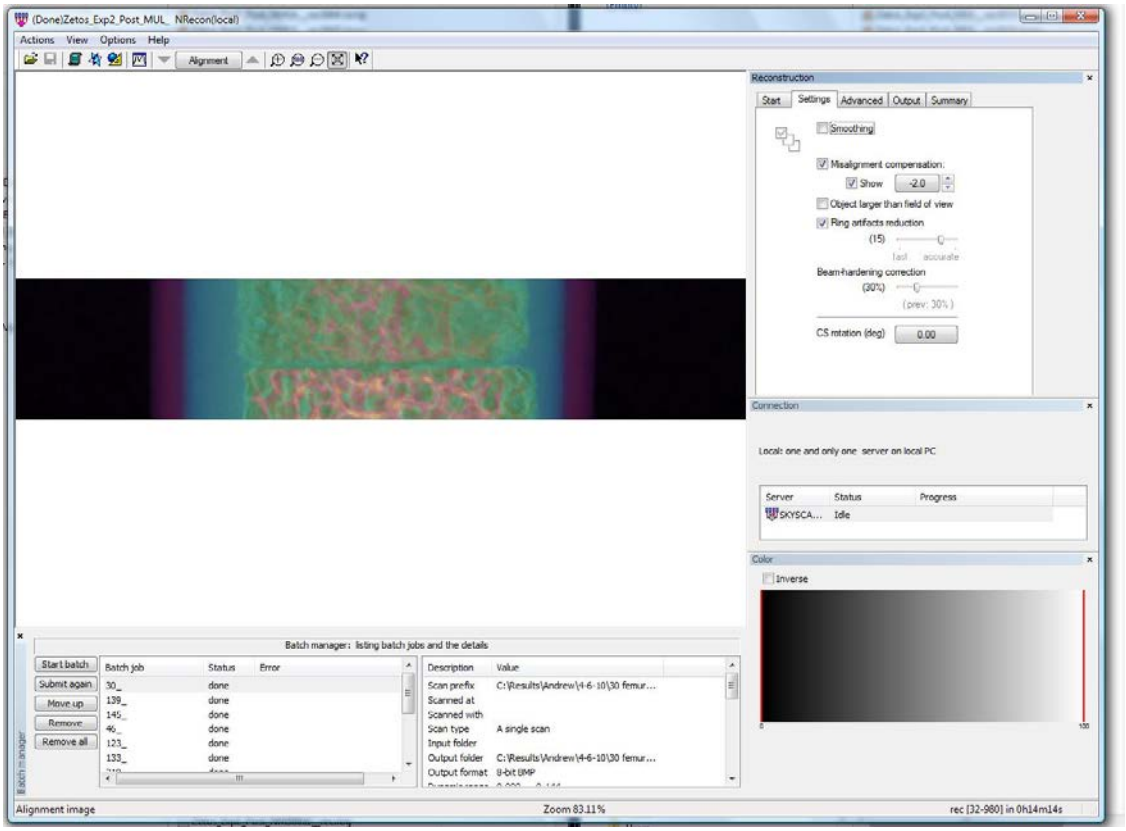

Figure 2.21 – NRecon Software GUI with Settings

The same settings must be used for the NRecon software both before and after bone cores are loaded, to ensure that the data generated are standardised.

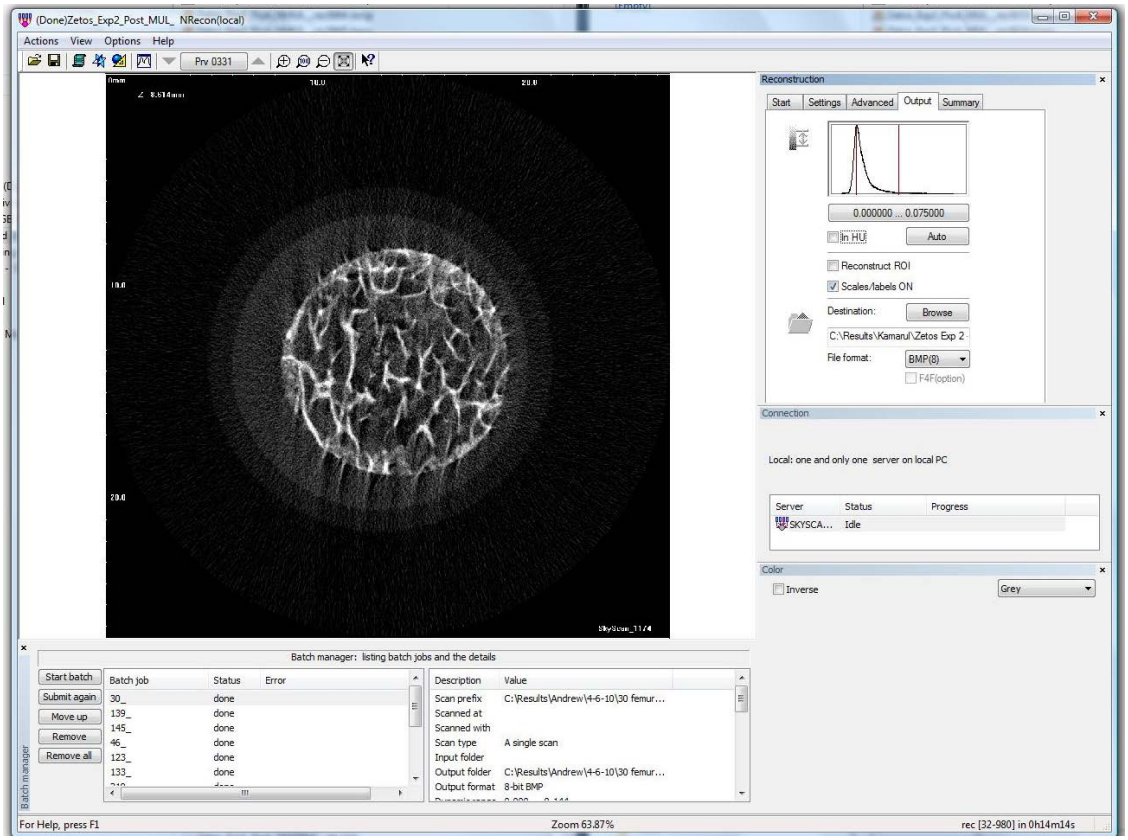

Figure 2.22 – NRecon Software Output Settings

The settings for the NRecon output must also be kept the same in all instances.

3D analysis of the images produced were performed using the proprietary software CT-Analyzer (version 1.10, Skyscan, Belgium), which enables the histomorphometric measurements of tissue volume (TV), bone volume (BV), percent bone volume (BV/TV), bone surface area (BS), intersection surface (iS), bone surface / volume ratio (BS/BV), bone surface density (BS/TV), trabecular pattern factor (Tb.Pf), structure model index (SMI), trabecular thickness (Tb.Th), trabecular number (Tb.N) and trabecular separation (Tb.Sp) for each bone core to be obtained (Fig. 2.23). Changes in these parameters are believed to be directed by the ability of the bone cells to sense the amount and direction of loading being applied and the resulting remodelling of the bone to accommodate these forces [78].

To ensure that the volume of bone being analysed is the same, each bone core is realigned using the Data Viewer (ver 1.4.3.0, Skyscan, Belgium) software and only the middle 101 layers (approximately 2.6 mm) and centre (approximately 9.5 mm diameter) of each bone core were analysed to keep the results consistent. This will effectively remove the area with non-viable osteocytes and debris known to be present at the sides of the bone cores [63]. Furthermore, it had been reported that the bone within 1mm from the top and bottom surfaces had the lowest amount of viable osteocytes [71]. 3D visualisation of the bone cores can be reproduced by the software CT-Volume (ver2.0, Skyscan, Belgium) (Fig. 2.24). The resultant data for each bone core, before and after the 10 days of loading is tabulated and statistically analysed and can be compared with the apparent stiffness that was measured as explained in the previous sections.

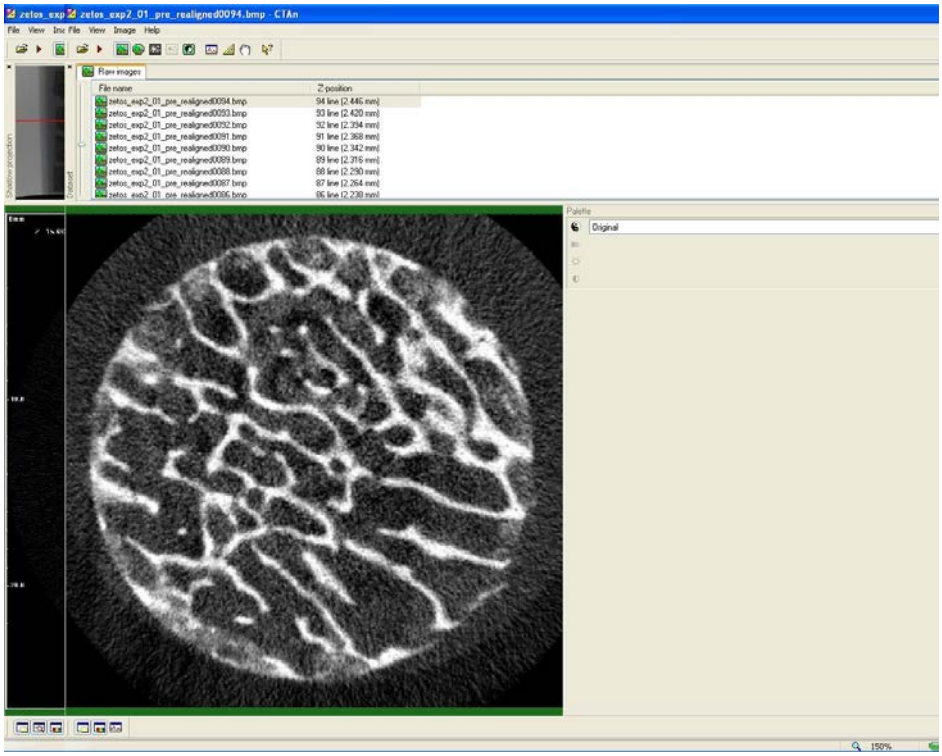

Figure 2.23 – CT Analyzer GUI

The CT-Analyzer software is able to measure and calculate the histomorphometric parameters of the bone cores.

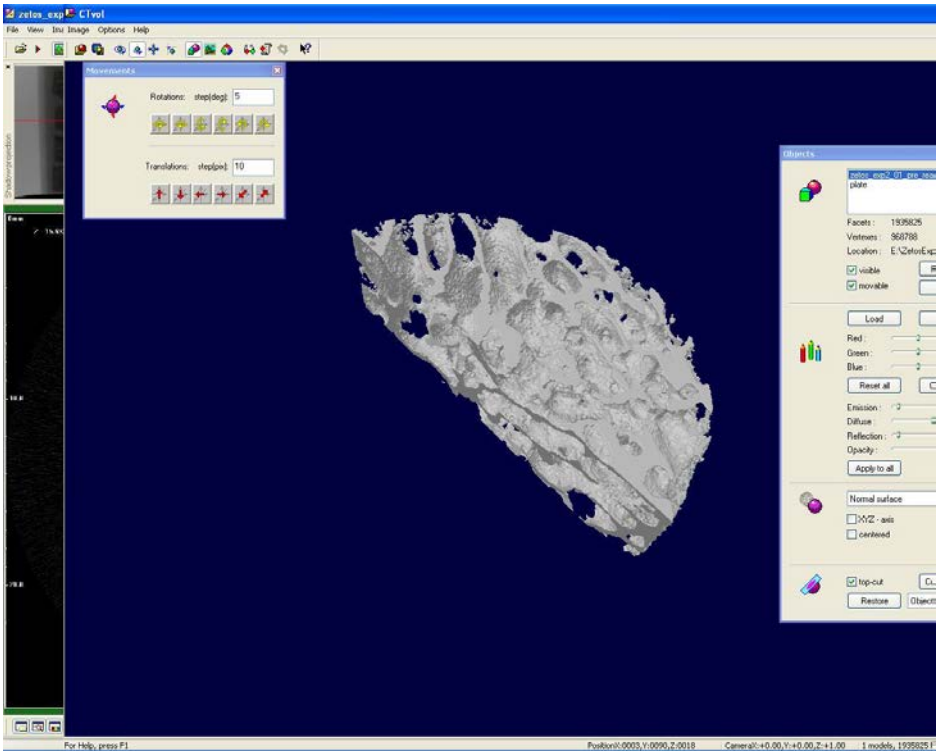

Figure 2.24 – CT-Volume GUI

The reconstructed 3D image of the bone core can be rotated and sliced in any direction using the CT-Volume software.

2.8 Statistics

All data tabulation and statistical analysis was made using Microsoft Office Excel (2007). More detailed statistical analysis was performed with GraphPad Prism (version 8.0.1 (244) for Windows. GraphPad Software, San Diego California USA, www.graphpad.com) when necessary. The graphs used for illustration of the data were made using either one of the software above.

Students paired t-test was used for the statistical analysis when comparing only one variable against each other. Correlation between two variables was demonstrated using a regression line on a scatter plot of the samples or groups being analysed.

Repeated measures two-way ANOVA was used when there are more than one variable that require analysis for each data point and the data are measurements of the same samples over a period of time. Tukey post tests were used whenever appropriate. The results of the two-way ANOVA will look at the following effects between the data and the variable for the columns (time between start (before loading) and end (after loading) of the experiment, which was 10 days) and rows (the different loading regimes):

1. The effect of the variables for the columns and rows, irrespectively, with the data being analysed where the null hypothesis being tested is defined as, “If the variable (for column or row) has no effect overall, there is an X% chance of randomly observing an effect this big (or bigger) in an experiment of this size”, with X = p value.
2. The interaction between the variable for the columns with the variable for the rows where the null hypothesis being tested is defined as, “If there is no interaction overall, there is an X% chance of randomly observing so much interaction in as experiment of this size” with X = p value. If the Interaction between the two factors is significant then the effect of one factor is readily influenced by the level of the other factor, e.g., the difference in the parameter tested in column 1 and parameter

tested in column 2 is not the same for each row. A high interaction P value suggests a consistent difference from one column to another among all rows, making the post-tests not particularly helpful. The effectiveness of sample matching in controlling for variability between samples where the null hypothesis being tested is defined as, "If the matching were not effective overall, there is an X% chance of randomly observing an effect this big (or bigger) in an experiment of this size", with X% = p value. If it is not significant then the matching of samples was not effective in controlling for variability between samples.

2.9 Results

2.9.1 Young's Modulus Measurements

Although the bone cores used in each experiment were from the sternum of one animal, and the orientation of the bone cores was kept the same during processing, the initial stiffness of the bone cores was varied, ranging from 36 MPa to 219 MPa, while the thickness of the bone cores varied from 4.07mm to 5.20mm (Fig. 2.25).

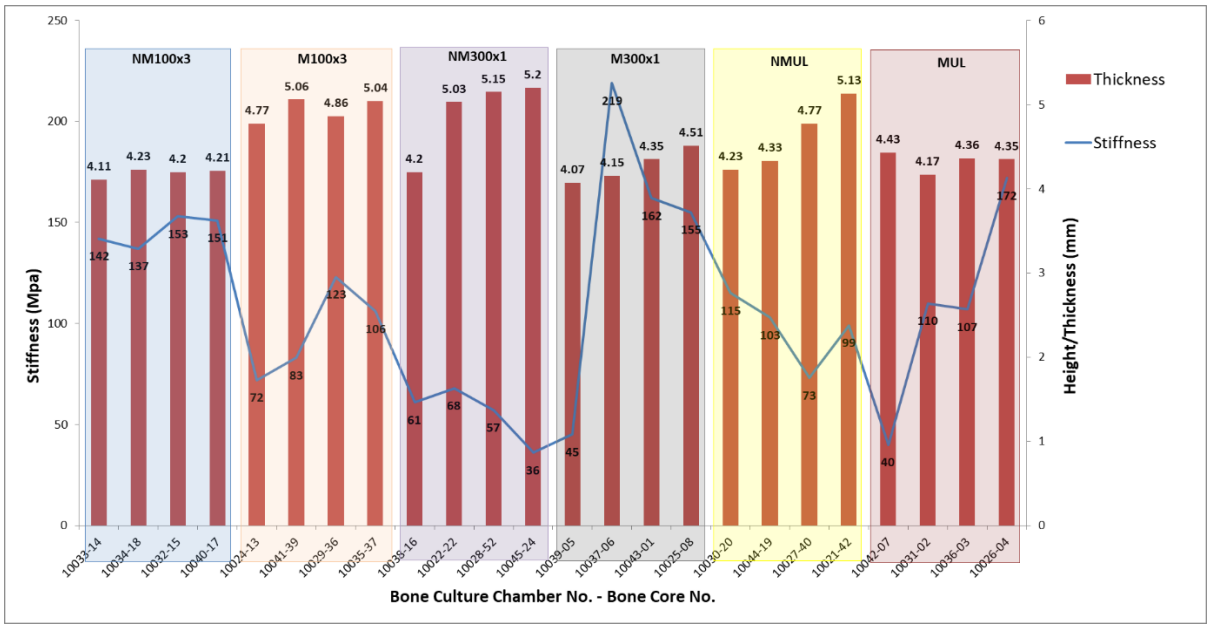

Figure 2.25 – Stiffness and Height of Individual Bone Cores Before Loading

Stiffness (primary-axis) and height/thickness (secondary axis) profile of each bone core prior to any loading being applied. (N.B.: The stiffness values are discrete values for each bone core and were depicted as a line graph for better illustration purposes only)

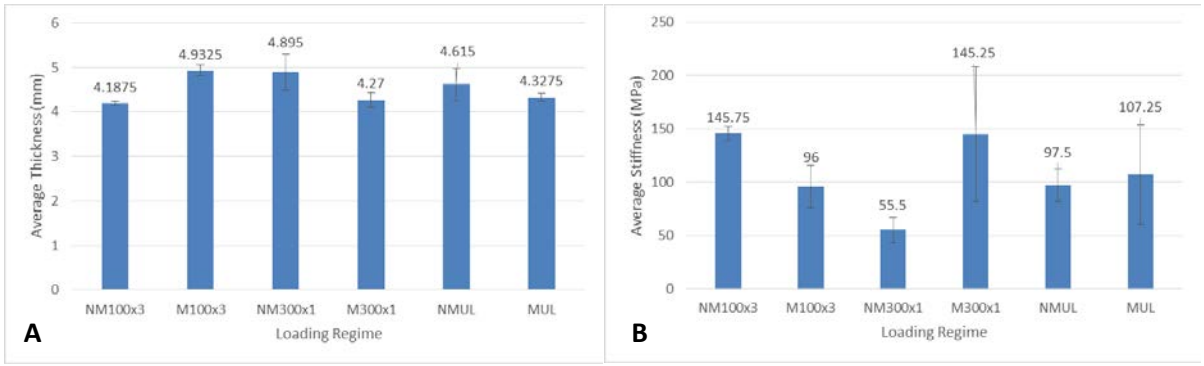

Figure 2.26 – Average Height and Stiffness of Groups Before Loading

A) Average thickness (height) and **B)** average stiffness of the bone cores within each group at the start of the experiment before any loading was applied. (Mean ± SD; n = 4)

The average bone core thickness and stiffness for each group and their standard deviation were calculated (Fig. 2.26). Due to the large variance in the measured stiffness of the bone cores, the standard deviation was found to be very large for groups M300x1 and MUL. Individually, the stiffness did not correlate very well with the thickness of the bone cores (R^2 = 0.236) (Fig. 2.27). However, when the average stiffness of each group was plotted against the average

thickness of the bone cores within (Fig. 2.28), there is an apparent trend observed with a strong correlation of $R^2 = 0.7752$.

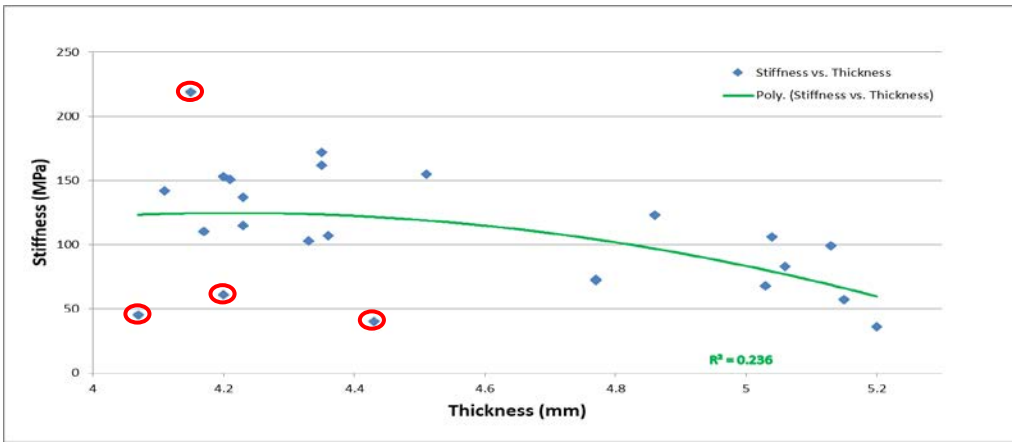

Figure 2.27 – Relationship of Bone Cores Stiffness and Height Before Loading

Distribution of the stiffness and height of each bone core with a polynomial regression line showing an R^2 value of 0.236, Even though the values circled red are furthest from the regression line, Grubb's test revealed that they are not significant outliers ($p > 0.05$).

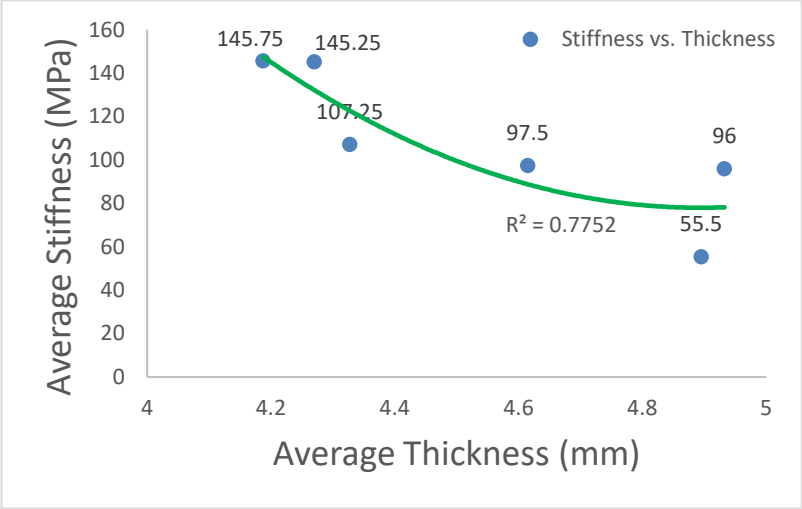

Figure 2.28 –Average Stiffness and Height Correlation Before Loading

Correlation of the average stiffness and average thickness (height) of each group at the start of the experiment before any loading was applied, with an R^2 value of 0.7752. (n = 4)

The average value for the Young's Modulus showed an initial drop on Day 2 for all bone groups except NM300x1. Subsequent to this, the stiffness of the bone cores increased gradually except for the group MUL, which hardly increased above the initial measurement (Fig. 2.29). On Day 11, approximately 24 hours after the last loading session, the bone cores showed a significant decrease in their stiffness (t-test = 0.0355).

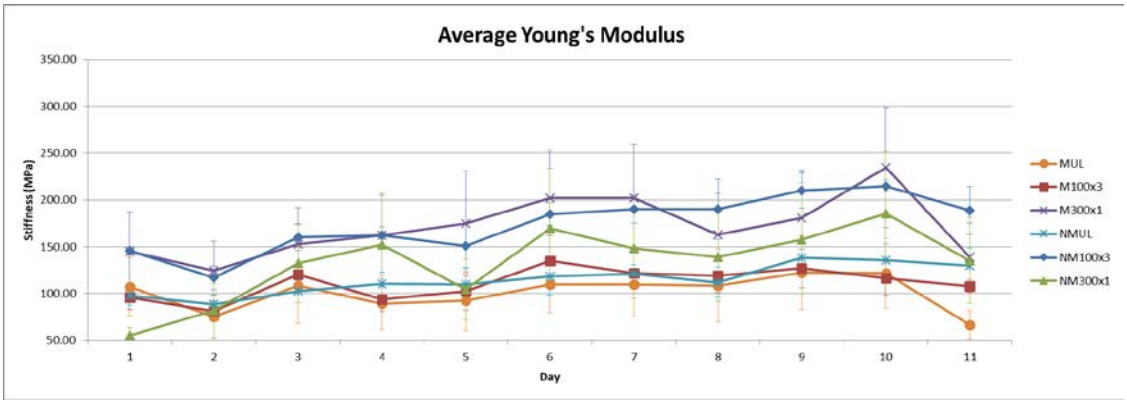

Figure 2.29 – Average Stiffness Over 10 Days of Loading

Average Young's Modulus (stiffness) for each of the 6 groups during the course of the experiment. (n = 4)

However, when the amount of change in the average stiffness was calculated (Fig. 2.30), the group NM300x1 showed an exceptionally high relative increase in stiffness with loading. Only the bone cores without marrow have significant increases in their stiffness over the duration of the experiment (NMUL, $p = 0.0001$; NM100x3, $p = 0.0005$; NM300x1, $p = 0.0140$), while the trend line for the bone cores with marrow (MUL, M100x3 & M300x1) were not significant. Further analysis using Tukey's multiple comparison test showed no significant difference between individual curves.

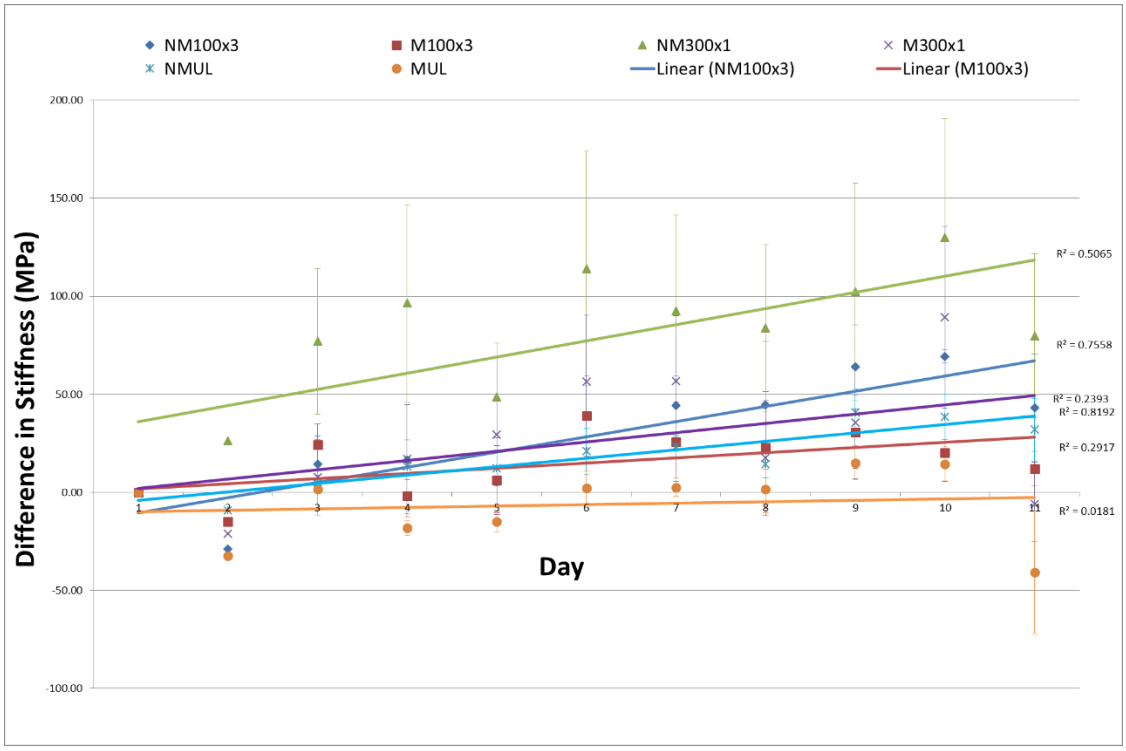

Figure 2.30 – Trend in Change of Average Stiffness

Amount of change in the average stiffness for each group of bone cores during the course of the study with a linear regression line for each group. (n = 4)

When the loading regime was analysed using two-way ANOVA independently for the bone cores with or without marrow, there was no significant change in stiffness over time (Fig. 2.31).

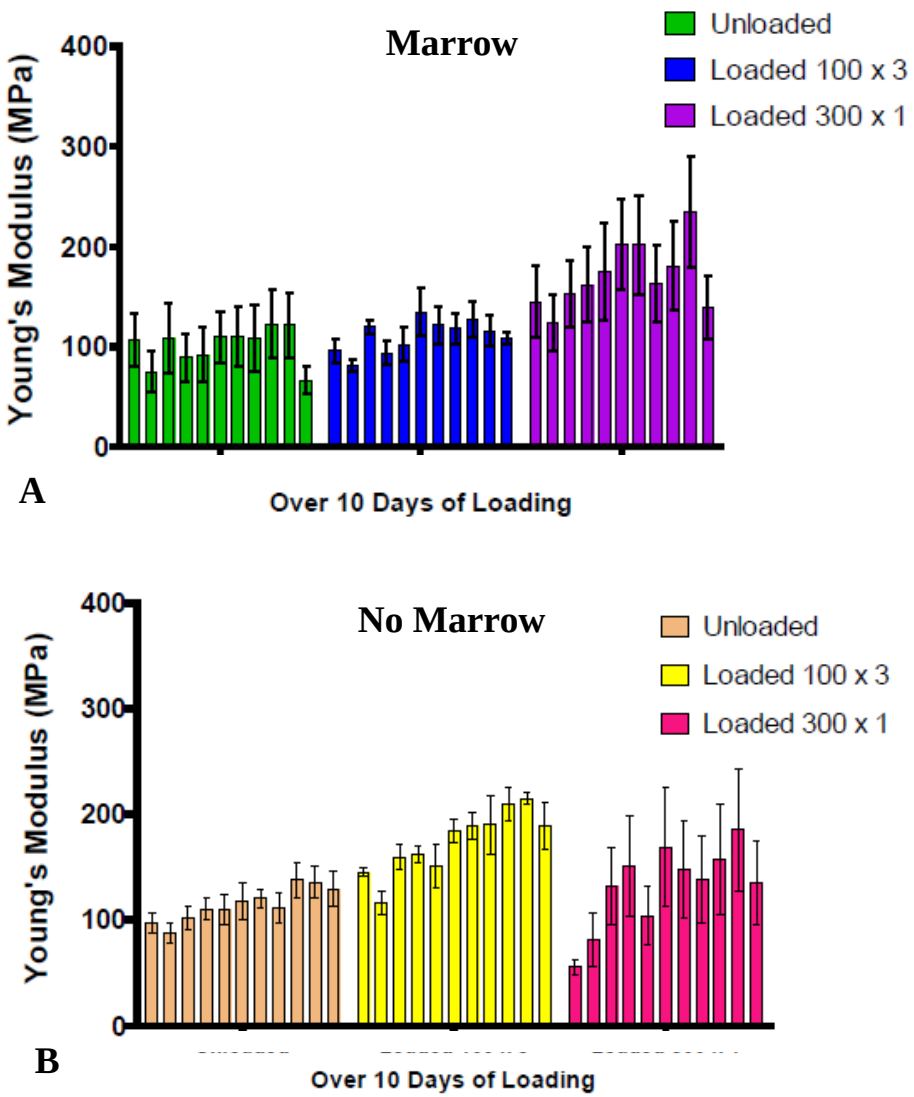

Figure 2.31 – Average Stiffness for Each Loading Regime

No significance seen between the different loading regime on the stiffness of the bone cores **A)** with marrow and **B)** without marrow over 10 days of loading (n = 4)

For each loading regime there was a time dependent increase in the average stiffness ($p < 0.0001$). However, only for the 100x3 bone cores was there a statistically significant effect in the stiffness between the groups having marrow (M100x3) and no marrow (NM100x3) ($p = 0.0075$). Further analysis showed that the difference is significant at Day 4, 7, 8, 9, 10 and 11 (Fig. 2.32).

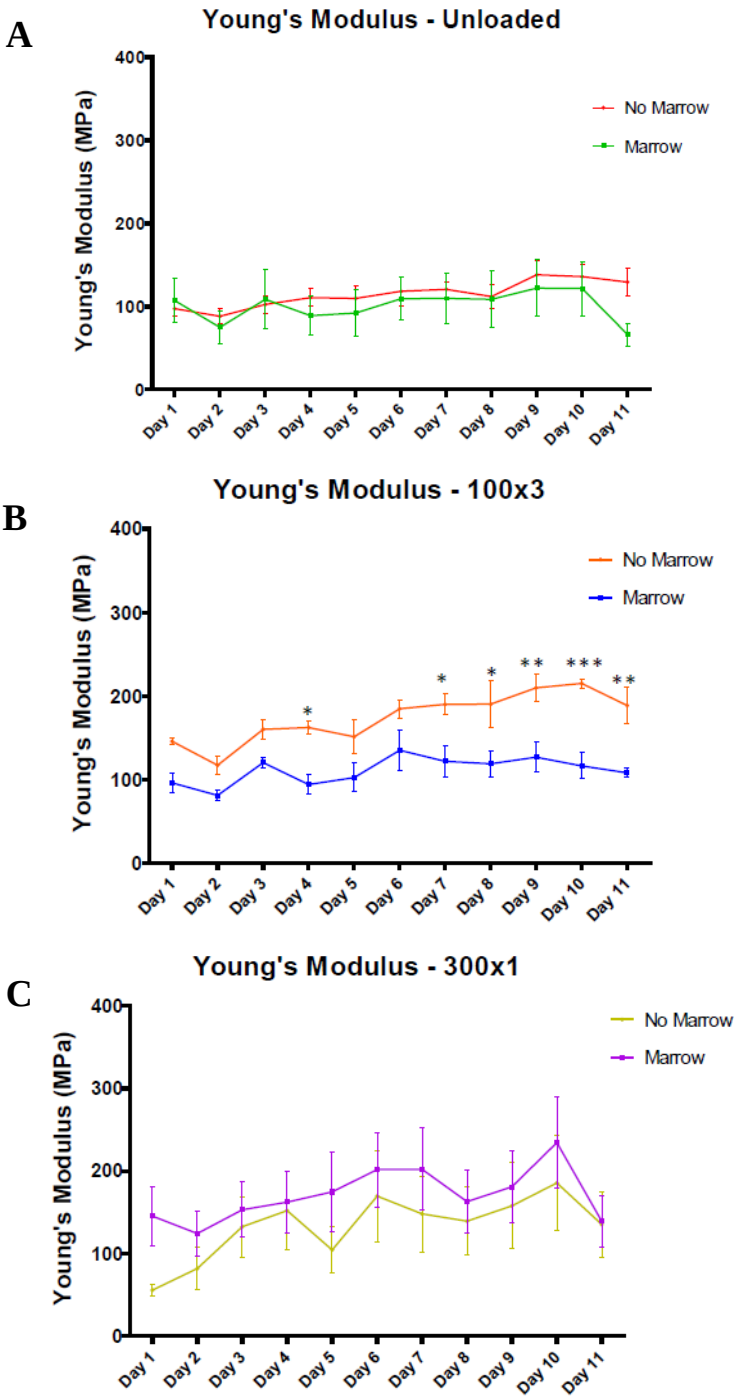

Figure 2.32 – Effect of Marrow Presence for Each Loading Regime

Comparing the effect of having marrow or not for each of the different loading regimes; **A)** unloaded, **B)** loaded 100 cycles thrice a day and **C)** loaded 300 cycles daily, over the duration of the experiment. (n = 4, whereby * = $p < 0.05$, ** = $p < 0.01$, *** = $p < 0.001$)

2.9.2 pH measurement

There was a consistent difference in the pH of the media collected at each 24-hour time point between the different loading regimes (Fig. 2.33).

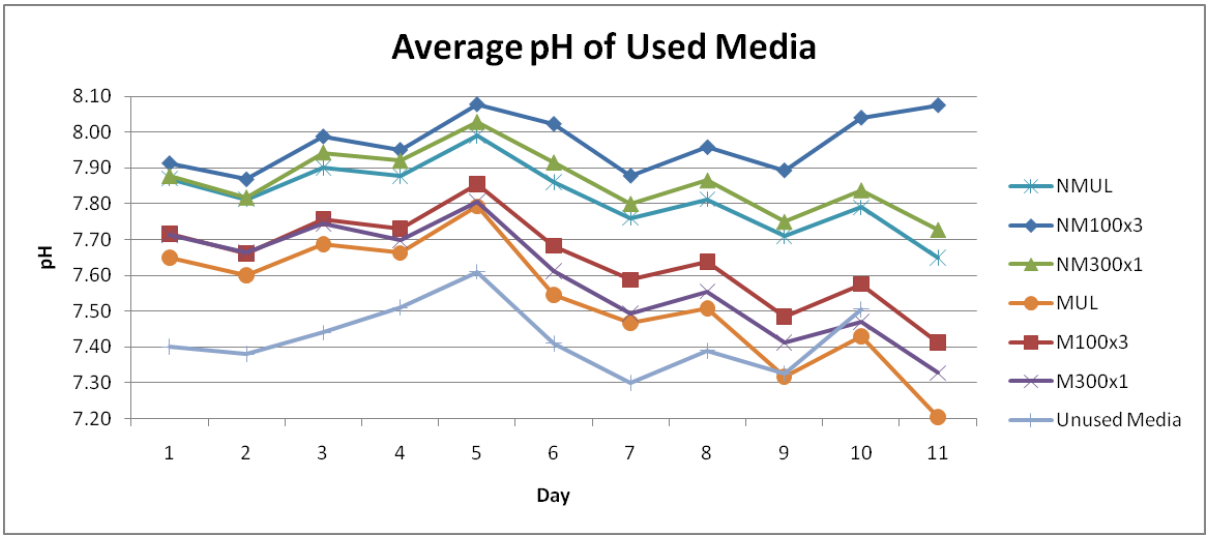

Figure 2.33 – Average pH of Used Media for Each Group

The average pH of the media for each group after it was changed daily. Media from the unloaded samples had the lowest pH values and that from the 100x3 samples the highest pH for bone cores with or without marrow. The pH of the new media that was prepared daily to replace the used media was also measured and shown as a control (n = 4)

The pH of the used media also showed a marked difference between the bone cores that had their marrow removed and those that retained it when they were looked at independently (Fig. 2.34). The difference in the pH was significant for every day of the experiment with $p < 0.01$ for Day 1 and Day 2 and $p < 0.001$ for the remaining days. Two-way ANOVA analysis also showed a highly significant interaction ($p < 0.0001$) between the average pH and the presence of marrow. The differences between the slopes were also extremely significant ($p < 0.0001$)

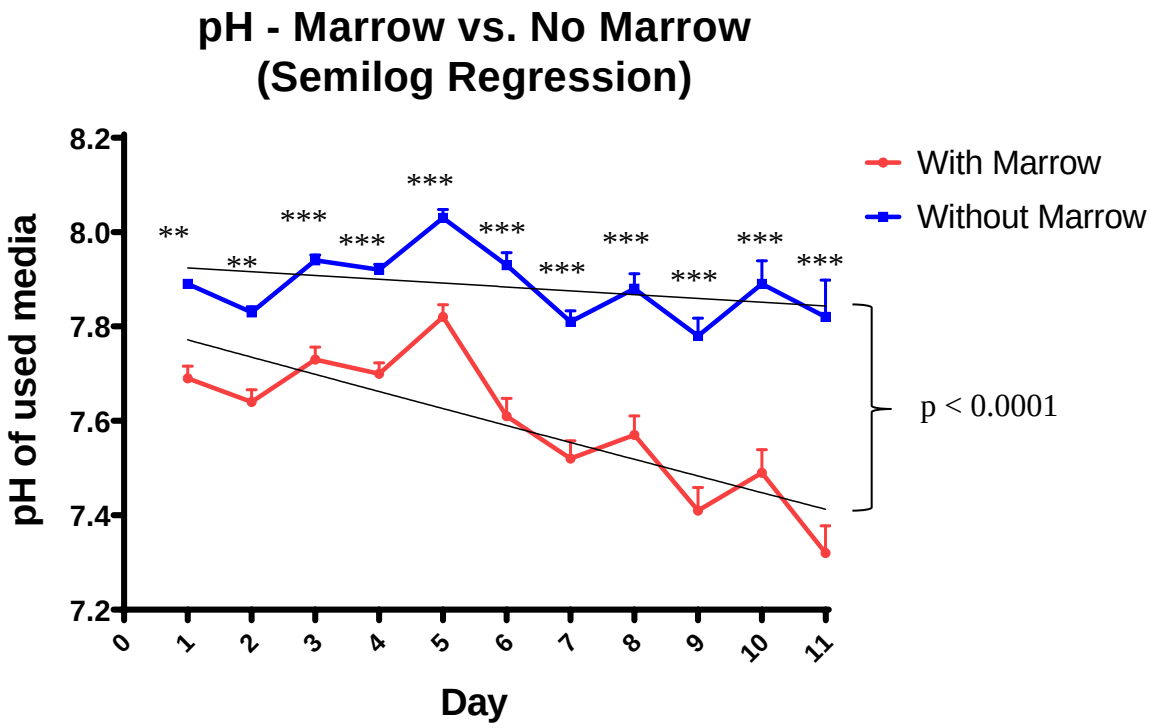

Figure 2.34 – Average pH for Bone Cores With and Without Marrow

Average pH of the used cell culture media that was changed daily for the bone cores with marrow and without marrow. The semilog regression line showed the difference in the amount of change in the pH between them over the course of the experiment. (n = 12, whereby ** = $p < 0.01$, *** = $p < 0.001$)

2.9.3 Ionic calcium (Ca^{2+}) levels

Measurement of the ionic calcium (Ca^{2+}) levels in the used media for Days 9, 10 and 11 showed that it was significantly reduced ($p < 0.05$ to $p < 0.001$) for all loading regimes when compared to those in the unused media (Fig. 2.35). The ionic calcium concentration was slightly higher for the bone cores with marrow (MUL, M100x3 and M300x1) compared to the average levels in the bone cores without marrow (NMUL, NM100x3 and NM300x1). Most of the groups showed an increasing trend in the Ca^{2+} levels except for the NMUL and NM100x3 groups. Further analysis showed a negative correlation between pH and Ca^{2+} levels ($R^2 = 0.5244$, $p < 0.05$) over these 3 days, which is consistent with a reduction in pH leading to increased mineral dissolution.

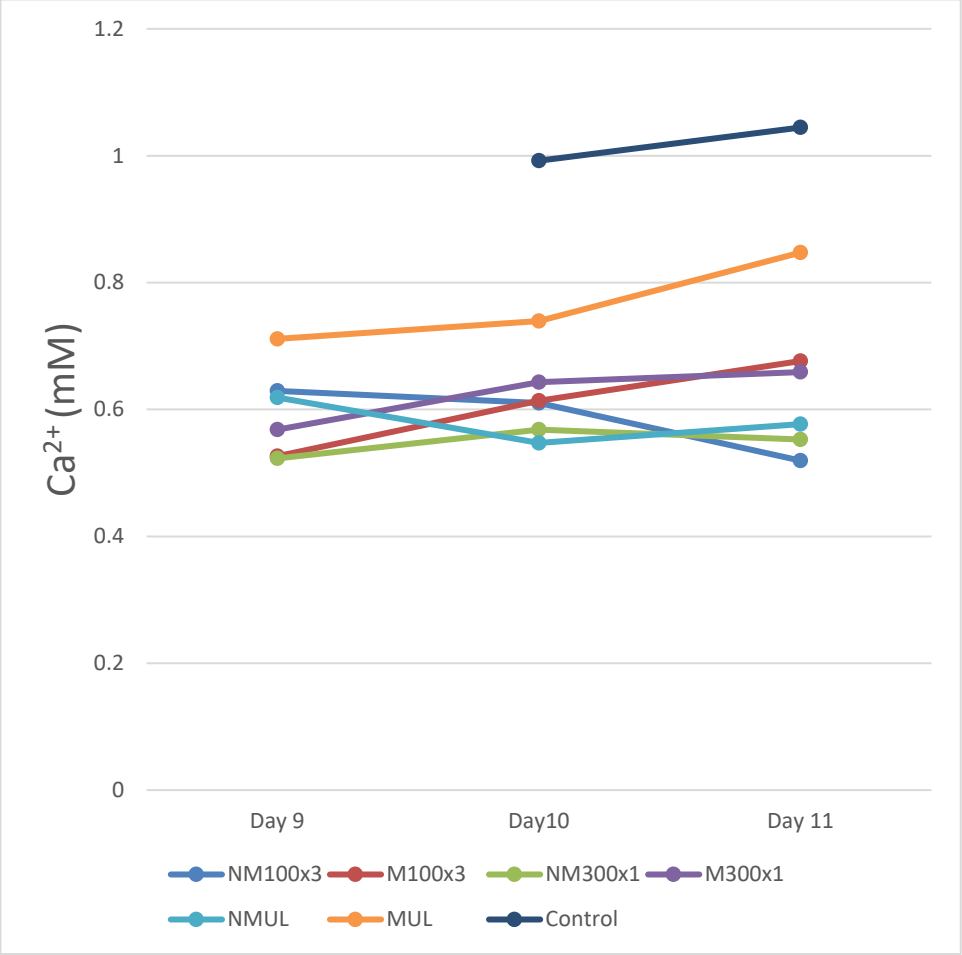

Figure 2.35 - Average Ca^{2+} Levels

Average Ca^{2+} levels of the used cell culture media on Days 9, 10 and 11 for all loading regimes, together with the measured levels of the newly prepared unused media as a control. (n = 4)

2.9.4 3D analysis of μCT images

The change in the histomorphometric parameters measured by analysis of the μCT images, before and after being loaded for 10 consecutive days, and .their relationship with stiffness were investigated.

2.9.4.1 Tissue volume (TV, unit = mm^3)

TV was unchanged as the volume that was analysed for each of the bone cores was kept the same, thickness of ~2.6mm and diameter of ~9.5mm, as described in the Materials and Methods

section above. The TV of the bone cores measured by the µCT machine (SkyScan 1174, Belgium) before and after 10 days of loading were 242.4 mm^3 and 243.5 mm^3 respectively.

2.9.4.2 Bone volume (BV, unit = mm^3)

There was a significant difference for BV after 10 days of loading for the bone cores that were loaded for 100 cycles thrice daily, regardless if marrow was present (M100x3, t-test = 0.0069) or not present (NM100x3, t-test = 0.0286) (Fig. 2.36). Further analysis using two-way ANOVA showed significant interaction between loading regime and duration of loading ($p = 0.0360$) and the loading regime affects BV significantly ($p = 0.0257$). However, Tukey's multiple comparisons test was only significant between M300x1 and. MUL ($p < 0.05$).

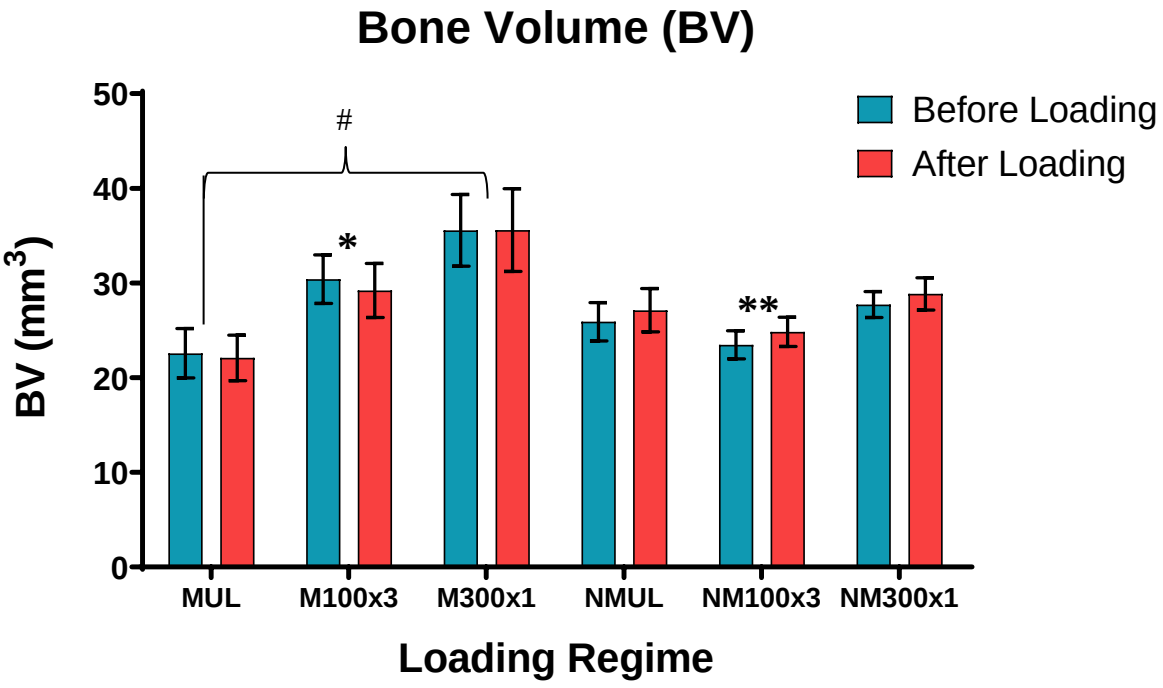

Figure 2.36 – Average Bone Volume (BV) Before and After Loading
(* = t-test < 0.05, ** = t-test < 0.01, # = p < 0.05, n = 4)

There was a positive correlation between stiffness and BV for the bone cores with marrow but it was negatively correlated for the bone cores without marrow (Fig. 2.37). The linear regression

line indicated a significant separation and increase (p = 0.0046) in the values for the bone cores without marrow at the end of the experiment.

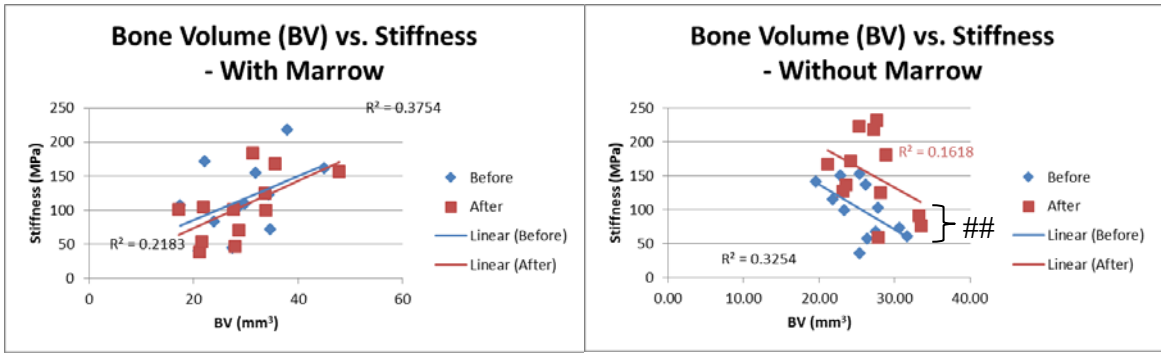

Figure 2.37 – Relationship of Stiffness with BV

Correlation between BV and stiffness of the bone cores, either with marrow or without marrow, before (blue) and after (red) 10 days of loading. (## = p < 0.01, n = 12)

2.9.4.3 Bone surface (BS, unit = mm^2)

Changes in BS were only significant after 10 days of loading for the bone cores without marrow that were loaded 100 cycles three times a day (NM100x3, t-test = 0.0456) or 300 cycles daily (NM300x1, t-test = 0.0191 (Fig. 2.38). Two-way ANOVA indicated a very significant effect of the duration of loading on BS (p = 0.0045) but there was no significant difference in the BS between the different loading regimes when compared to one another using Tukey's multiple comparison test.

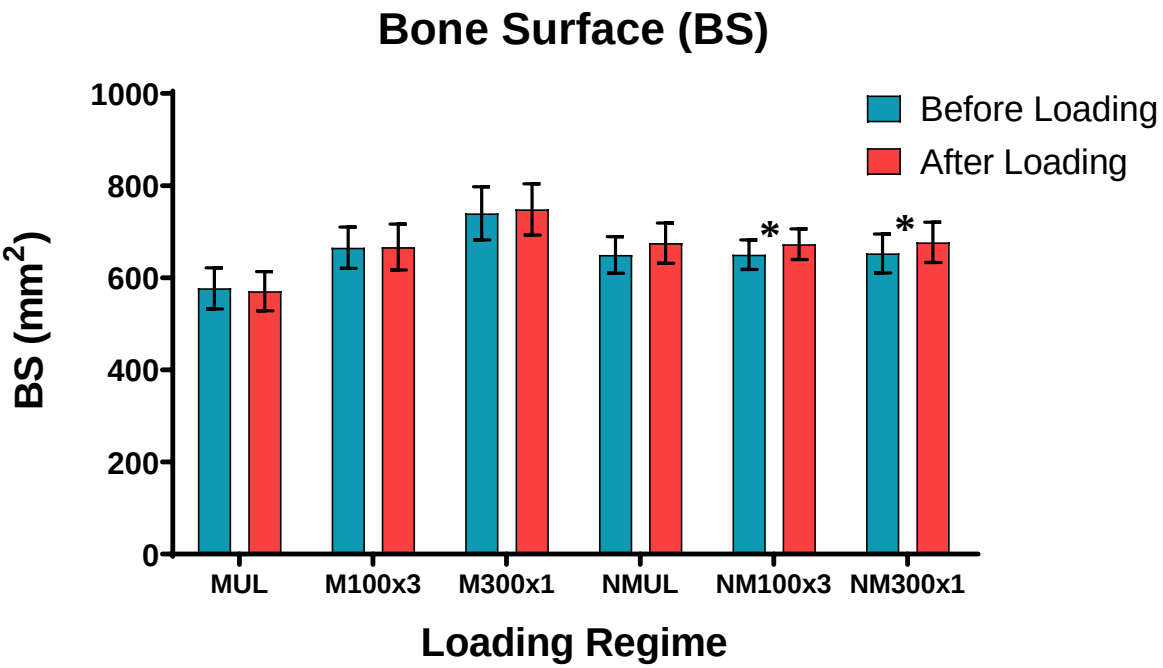

Figure 2.38 - Average Bone Surface (BS) Before and After Loading
(* = t-test < 0.05, n = 4)

The correlation between BS and stiffness of the bone cores before or after being loaded were much better for those with marrow (Fig. 2.39). However, a significant separation and apparent increase (p = 0.0206) in the linear regression line for the bone cores without marrow at the end of the experiment is also seen here. This is in contrast for the bone cores with marrow, whereby the regression line actually decreased slightly after 10 days of loading.

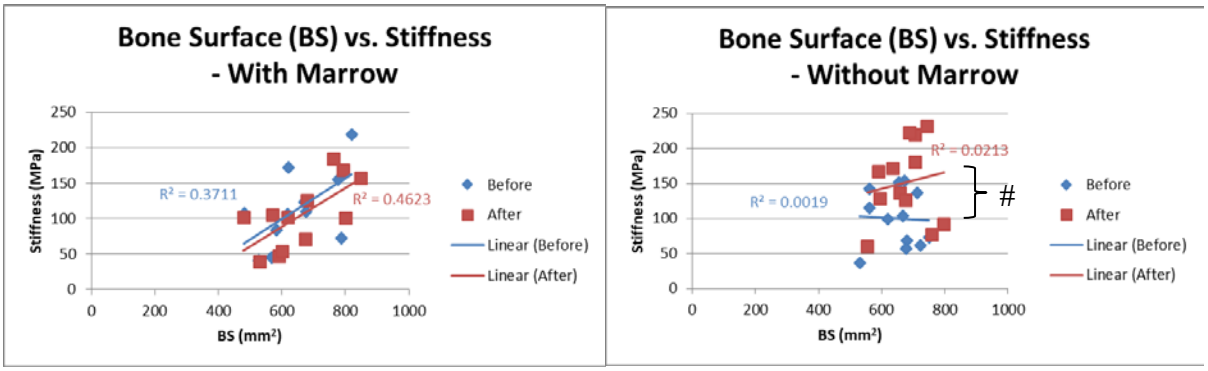

Figure 2.39 – Relationship of Stiffness with BS
Correlation between BS and stiffness of the bone cores, either with marrow or without marrow, before (blue) and after (red) 10 days of loading. (# = p < 0.05, n = 12)

2.9.4.4 Bone surface / volume ratio (BS/BV, unit = mm^{-1})

The change in the mean BS/BV was significant only for the bone cores with marrow that were loaded 100 cycles three times a day (M100x3, p = 0.0182), where it was slightly increased, and the bone cores without marrow loaded with the same regime (NM100x3, p = 0.0134), where it slightly decreased instead. (Fig. 2.40). Further analysis using two-way ANOVA showed a very significant interaction between loading regime and duration of loading (p = 0.0065) and the loading regime also affects BS/BV very significantly (p = 0.0065). Tukey's multiple comparisons test was significant for NM100x3 vs. M100x3 ($p < 0.05$) and NM100x3 vs. M300x1 ($p < 0.001$).

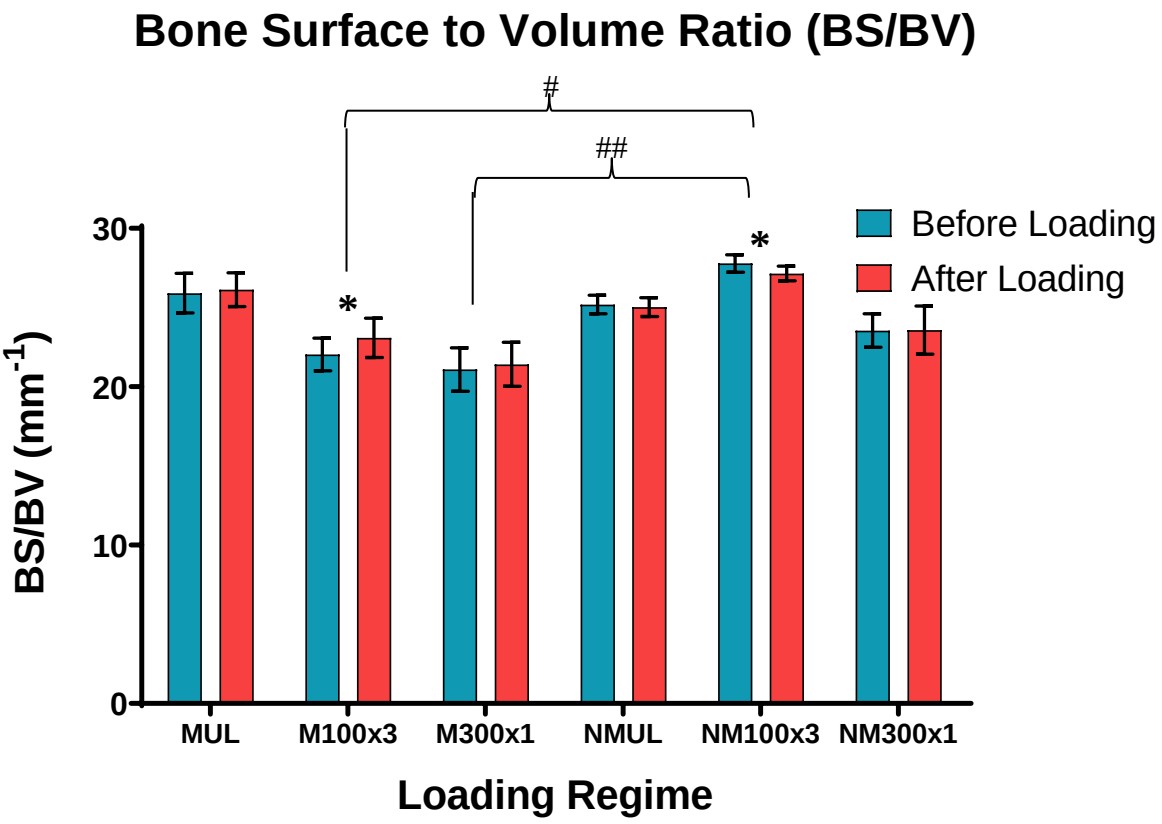

Figure 2.40 - Mean Surface/Volume Ratio (BS/BV) Before and After Loading
(* = t-test < 0.05, # = p < 0.05, ## = p < 0.01, n = 4)

The relationship between BS/BV and stiffness at the beginning and the end of the experiment was not significant for the bone cores with marrow. Conversely, in the absence of marrow, there

was strong correlations between stiffness and BS/BV before (R^2 = 0.7026) and after (R^2 = 0.5396) loading (Fig. 2.41). Similar to observations with stiffness against BV and BS above, distinct separation and an increase in the values for the bone cores without marrow at the end of the experiment was evident and extremely significant (p = 0.0004).

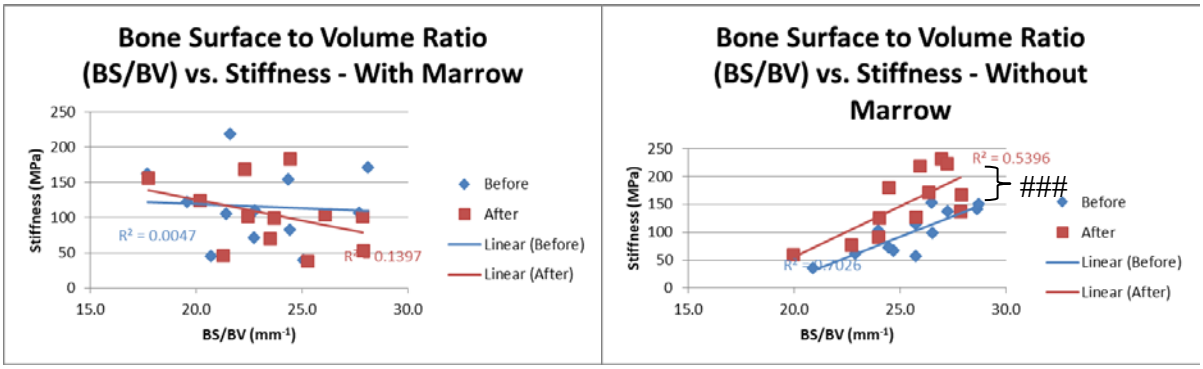

Figure 2.41 – Relationship of Stiffness with BS/BV
Correlation between BS/BV and stiffness of the bone cores, either with marrow or without marrow, before (blue) and after (red) 10 days of loading. (### = p < 0.001, n = 12)

2.9.4.5 Intersection surface (i.S, unit = mm^2)

There was no significant difference for i.S after 10 days of loading for any of the groups or when the groups were compared to each other using Tukey's multiple comparison test (Fig. 2.42). However, two-way ANOVA indicated a very significant effect on i.S by the duration of loading (p = 0.0074)

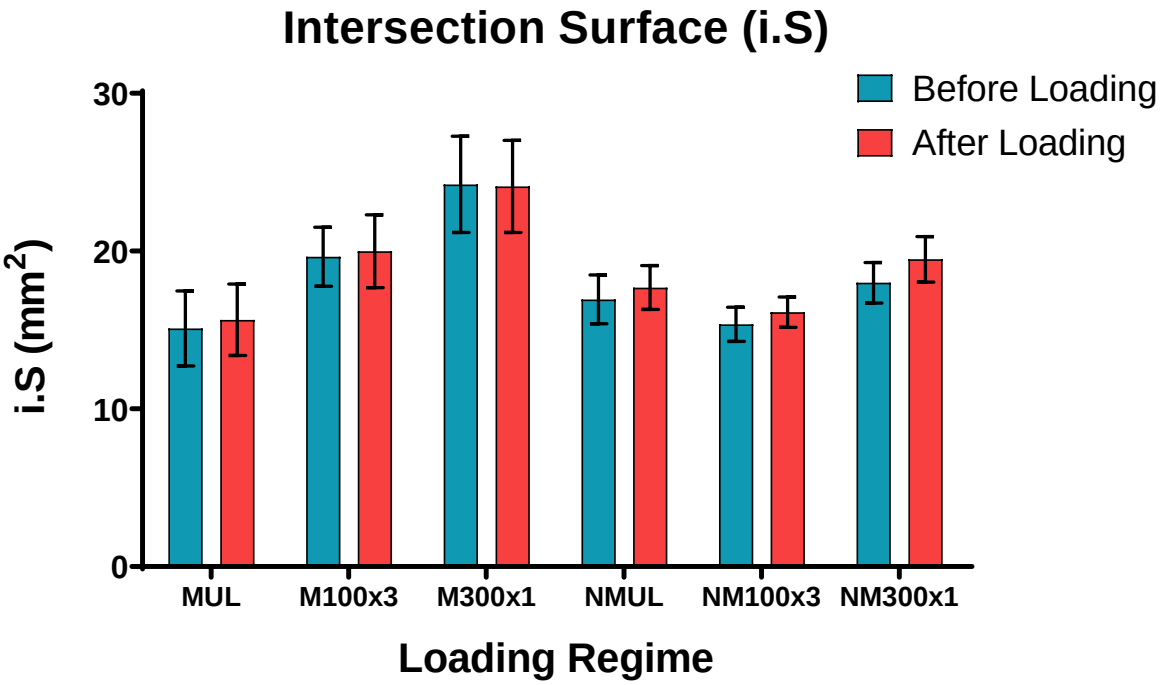

Figure 2.42 - Average Intersection Surface (i.S) Before and After Loading
(n = 4)

The relationship between i.S and stiffness were correlated positively with the presence of marrow but negatively when marrow was removed (Fig. 2.43). The same observations were made as with BV, BS and BS/BV previously, in which there was a separation and increase of the regression lines for the bone cores without marrow at the end of the experiment and it was very significant (p = 0.0058). However, in the presence of marrow, the regression line decreases slightly.

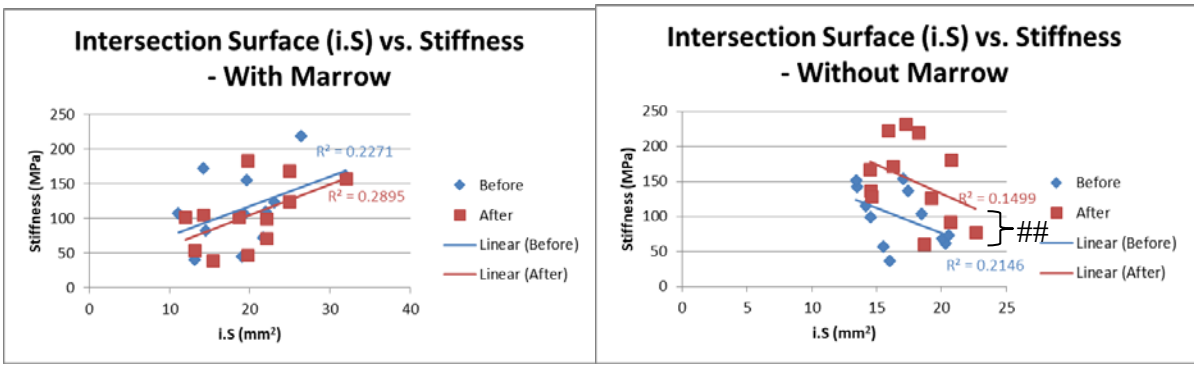

Figure 2.43 – Relationship of Stiffness with i.S
Correlation between i.S and stiffness of the bone cores, either with marrow or without marrow, before (blue) and after (red) 10 days of loading. (## = p < 0.01, n = 12)

2.9.4.6 Trabecular pattern factor (Tb.Pf, unit = mm^{-1})

The average Tb.Pf showed a significant reduction after 10 days of loading for the bone cores without marrow that were unloaded (NMUL, t-test = 0.0359) and loaded 100 cycles three times daily (NM100x3, t-test = 0.0007) (Fig. 2.44). Further analysis with two-way ANOVA indicated an extremely significant interaction between loading regime and duration of loading ($p = 0.0002$) with Tb.Pf being significantly affected by loading regime ($p = 0.0169$) and duration of loading ($p = 0.0229$). However, Tukey's multiple comparison test was only significant for NM100x3 vs. M300x1 ($p < 0.05$).

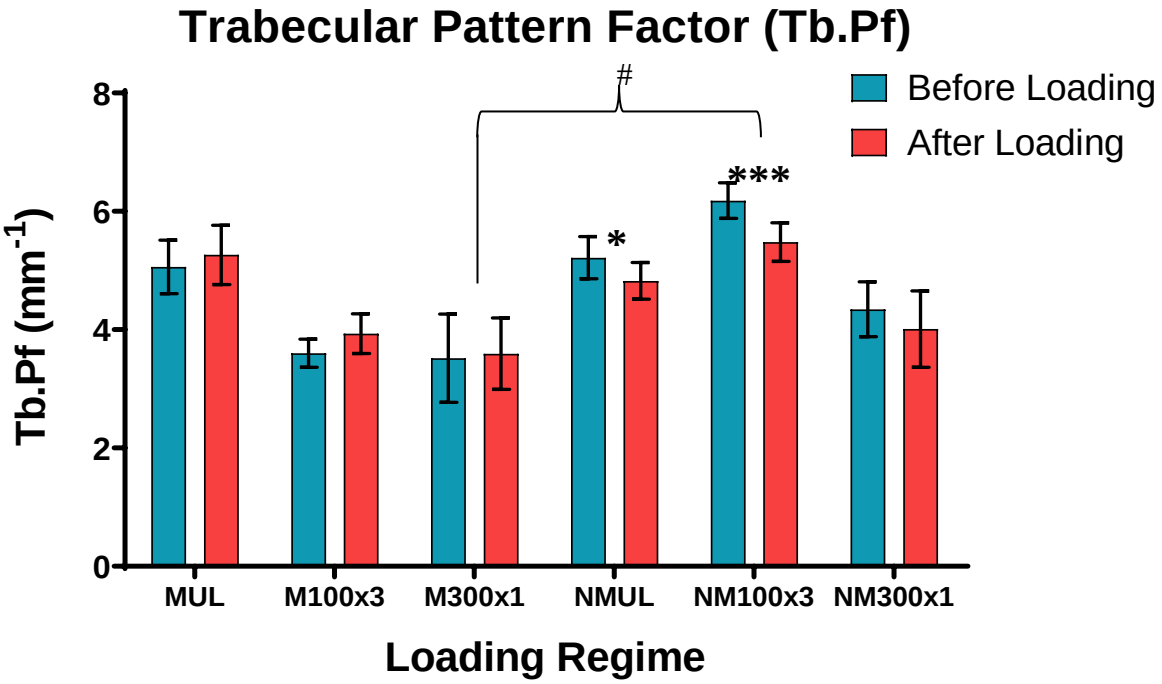

Figure 2.44 - Mean Trabecular Pattern Factor (Tb.Pf) Before and After Loading
Interestingly, the Tb.Pf increased when marrow is present but decreased when there is no marrow in the bone cores. (* = t-test < 0.05, *** = t-test < 0.001, # = $p < 0.05$, n = 4)

The correlation between Tb.Pf and stiffness of the bone cores before and after loading was applied was much better for the bone cores without marrow (Fig. 2.45). The distinct separation and increase of the regression lines for the bone cores without marrow was extremely significant ($p = 0.0004$) and consistent with the previous μCT parameters.

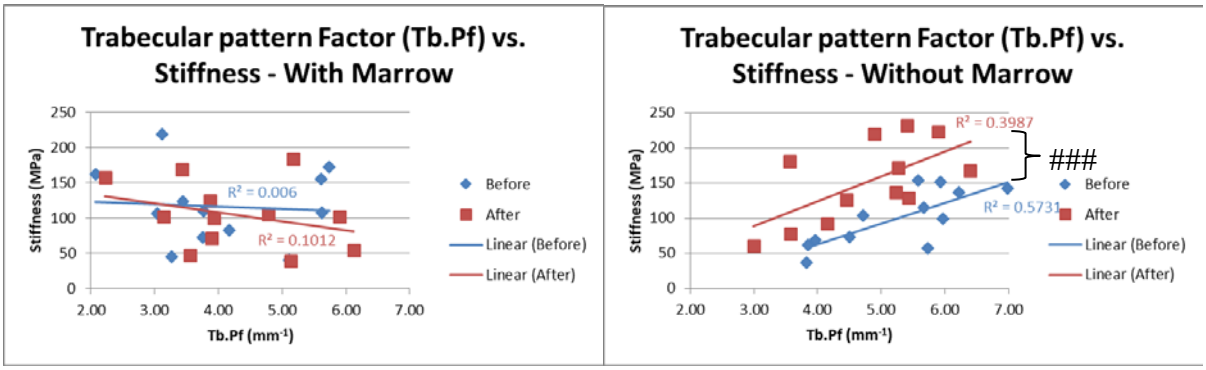

Figure 2.45 – Relationship of Stiffness with Tb.Pf

Correlation between Tb.Pf and stiffness of the bone cores, either with marrow or without marrow, before (blue) and after (red) 10 days of loading. (### = $p < 0.001$, $n = 12$)

2.9.4.7 Structure model index (SMI)

The mean SMI of the bone cores only showed a significant change after being loaded for 100 cycles three times a day for 10 days (Fig. 2.46). However, it was increased for the bone cores with marrow (M100x3, t-test = 0.0394) but decreased more significantly (t-test = 0.0012) for the bone cores without marrow (NM100x3). Two-way ANOVA analysis revealed an extremely significant interaction between loading regime and duration of loading ($p = 0.0007$) but SMI was only significantly affected by duration of loading ($p = 0.0153$). There was no significant difference for SMI when comparing the different groups to each other with Tukey's test.

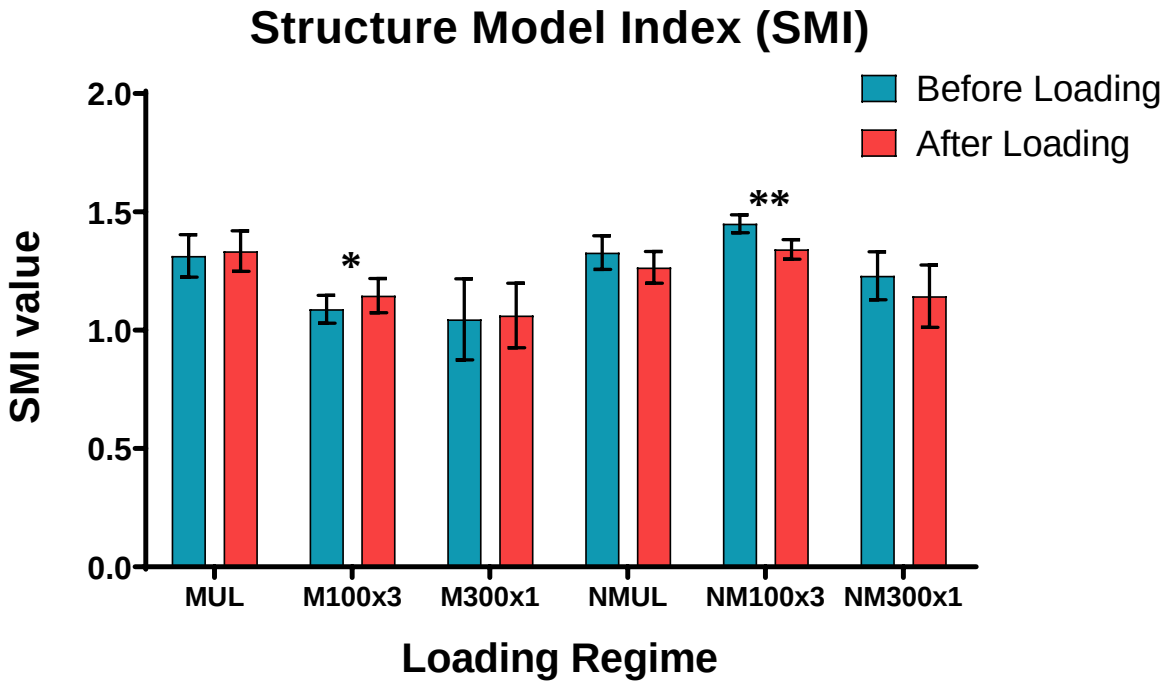

Figure 2.46 - Average Structure Model Index (SMI) Before and After Loading
Note that the SMI increased when marrow is present but decreased when there is no marrow. (* = t-test < 0.05, ** = t-test < 0.01, n = 4)

No significant relationship between SMI and stiffness was seen for the bone cores with marrow at the beginning of the experiment, which became more negatively correlated at the end of the experiment. Conversely, in the absence of marrow, the correlation between SMI and stiffness were strongly positive before ($R^2 = 0.3055$) and after ($R^2 = 0.3319$) loading (Fig. 2.47). Similar to observations with stiffness and previous μCT parameters, a very significant ($p = 0.0014$) separation and increase in the values for the bone cores without marrow was also evident after loading was applied.

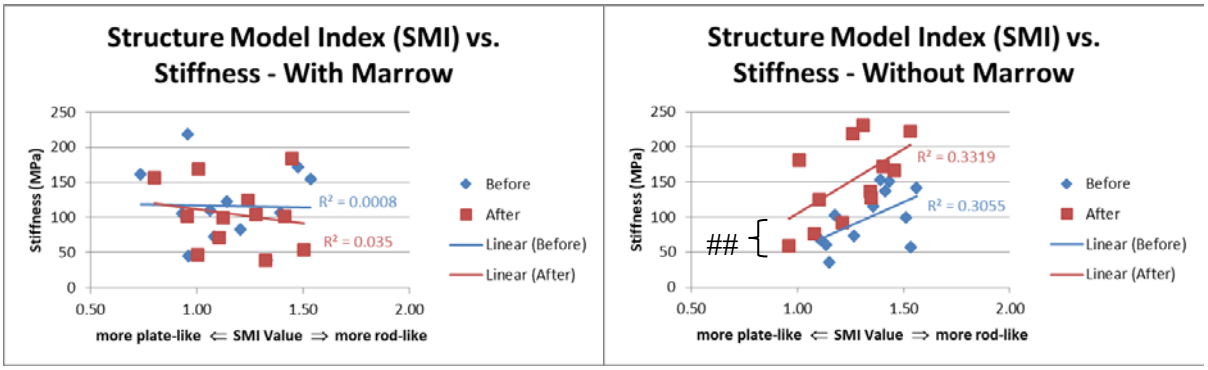

Figure 2.47 – Relationship of Stiffness with SMI
Correlation between SMI and stiffness of the bone cores, either with marrow or without marrow, before (blue) and after (red) 10 days of loading. (## = $p < 0.01$, n = 12)

2.9.4.8 Trabecular thickness (Tb.Th, unit = mm)

Only the bone cores with marrow that were loaded 100 cycles three times a day (M100x3) showed a significant decrease (t-test = 0.0212) in Tb.Th after 10 days of loading (Fig. 2.48). Further analysis with two-way ANOVA indicated only loading regime affects Tb.Th very significantly (p = 0.0092). Tukey's multiple comparison test was only significant (p = 0104) for NM100x3 vs. M300x1.

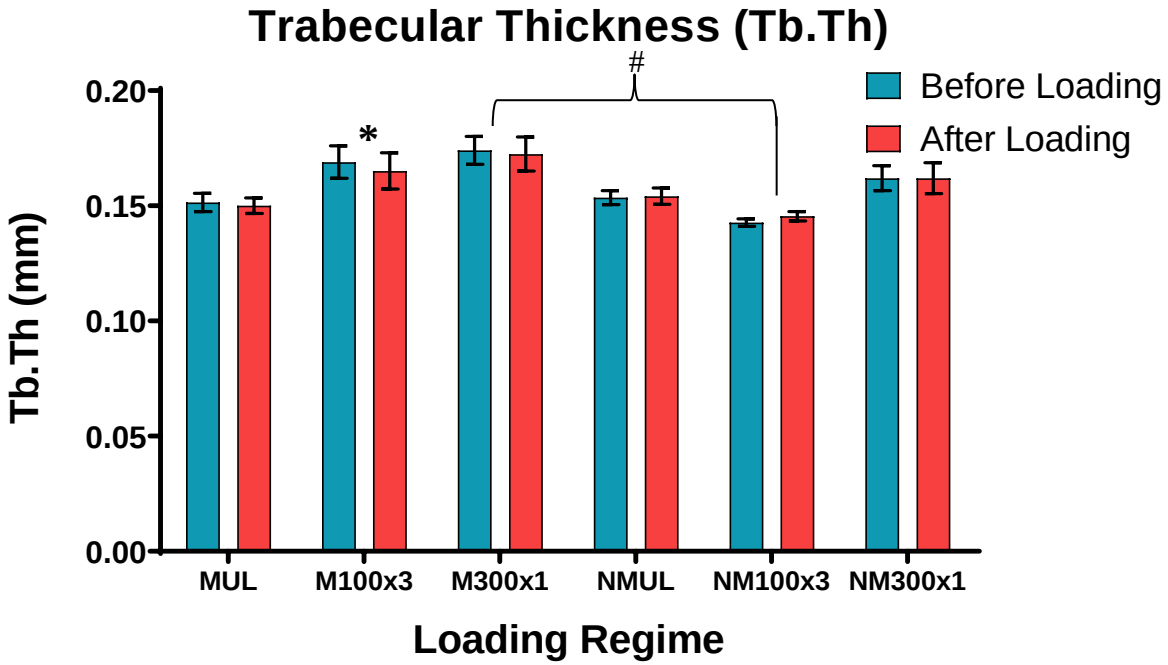

Figure 2.48 - Average Trabecular Thickness (Tb.Th) Before and After Loading
(* = t-test < 0.05, # = p < 0.05, n = 4)

The relationship between Tb.Th and stiffness was positive for the bone cores with marrow and negative for the bone cores without marrow. The correlation was much stronger for the bone cores without marrow before (R^2 = 0.7888) and after (R^2 = 0.4912) 10 days of loading (Fig. 2.49). The highly significant (p = 0.0005) separation and increase of these values for the bone cores without marrow at the end of the experiment was also observed, despite the reduced correlation after loading was applied.

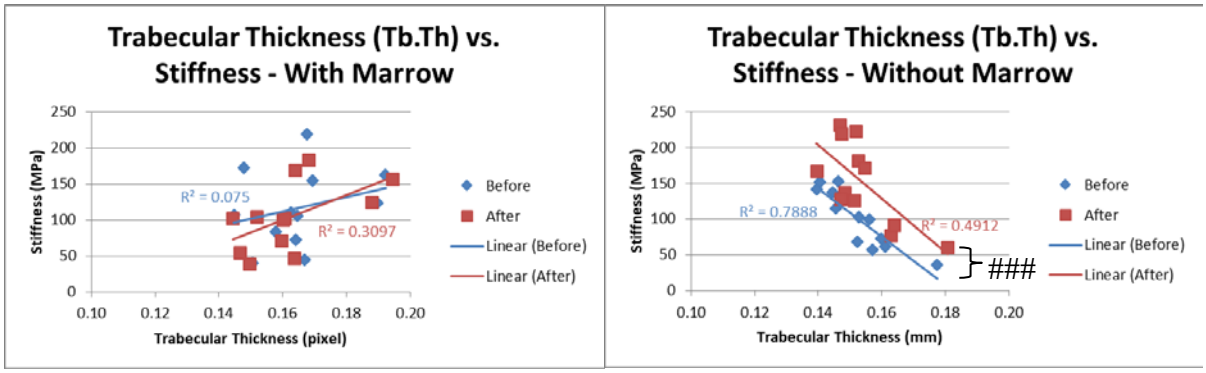

Figure 2.49 – Relationship of Stiffness with Tb.Th

Correlation between Tb.Th and stiffness of the bone cores, either with marrow or without marrow, before (blue) and after (red) 10 days of loading. (### = $p < 0.001$, n = 12)

2.9.4.9 Trabecular number (Tb.N, unit = mm^{-1})

Tb.N decreased after loading was applied for the bone cores with marrow that were not loaded (MUL) and loaded 100 cycles three times daily (M100x3) but it was increased slightly when loaded 300 cycles once a day (M300x1), which gave rise to a significant difference ($p = 0.0470$) between M300x1 and MUL using Tukey's multiple comparison test (Fig. 2.50). For the bone cores without marrow there was an increase in Tb.N, which was only significant for the unloaded ones (NMUL, t-test = 0.0224). Further analysis using two-way ANOVA revealed a significant interaction ($p = 0.0430$) between loading regime and duration of loading.

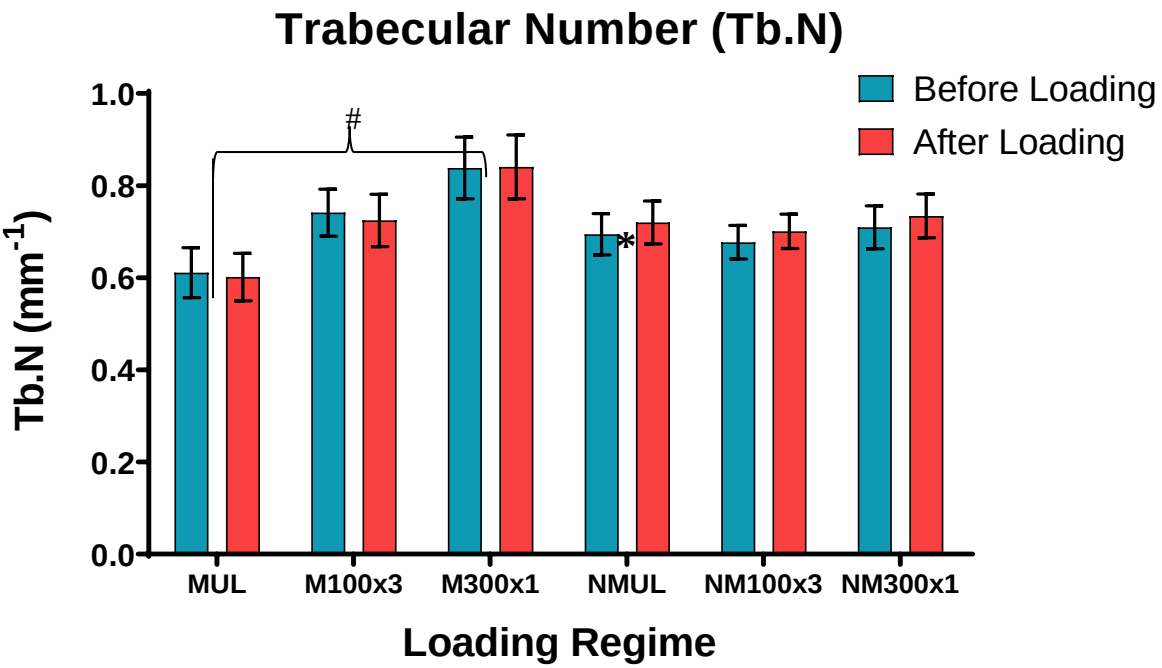

Figure 2.50 - Average Trabecular Number (Tb.N) Before and After Loading
(* = $p < 0.05$, n = 4)

The relationship between Tb.N and stiffness was positive when marrow was present but negative without the presence of marrow (Fig. 2.51) and the correlation was better for the bone cores with marrow before ($R^2 = 0.2486$) and after ($R^2 = 0.3469$) loading. However, there was a significant separation and apparent increase ($p = 0.0189$) in the linear regression line for the bone cores without marrow at the end of the experiment, similar to the previous μCT parameters. This is in contrast for the bone cores with marrow, whereby the regression line actually decreased slightly after 10 days of loading.

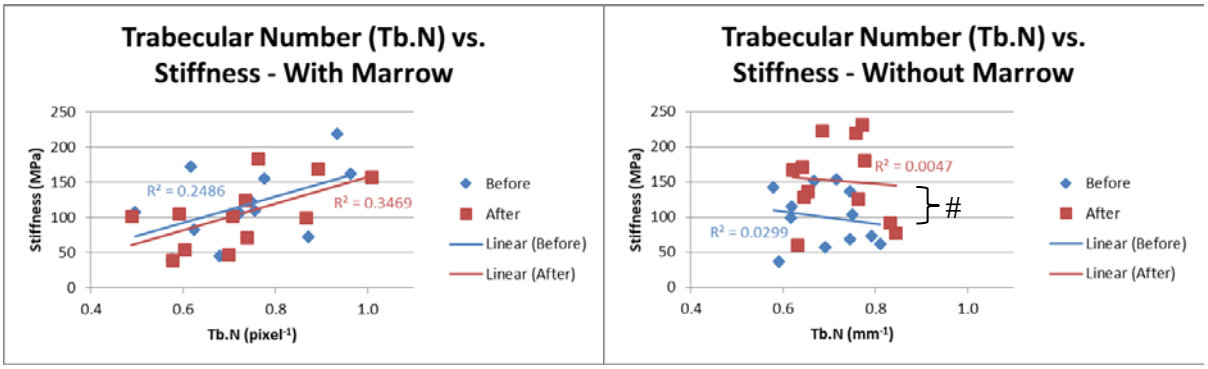

Figure 2.51 – Relationship of Stiffness with Tb.N
Correlation between Tb.N and stiffness of the bone cores, either with marrow or without marrow, before (blue) and after (red) 10 days of loading. (# = $p < 0.05$, n = 12)

2.9.4.10 Trabecular separation (Tb.Sp)

The difference in Tb.Sp of the bone cores was only significant (t-test = 0.0197) for those with no marrow that was loaded for 10 days 300 cycles once daily (NM300x1) (Fig. 2.52). Two-way ANOVA analysis revealed Tb.SP does not change after 10 days of loading and it does not depend on the loading regime. No significant differences were observed when the groups were compared to each other using Tukey's multiple comparison test.

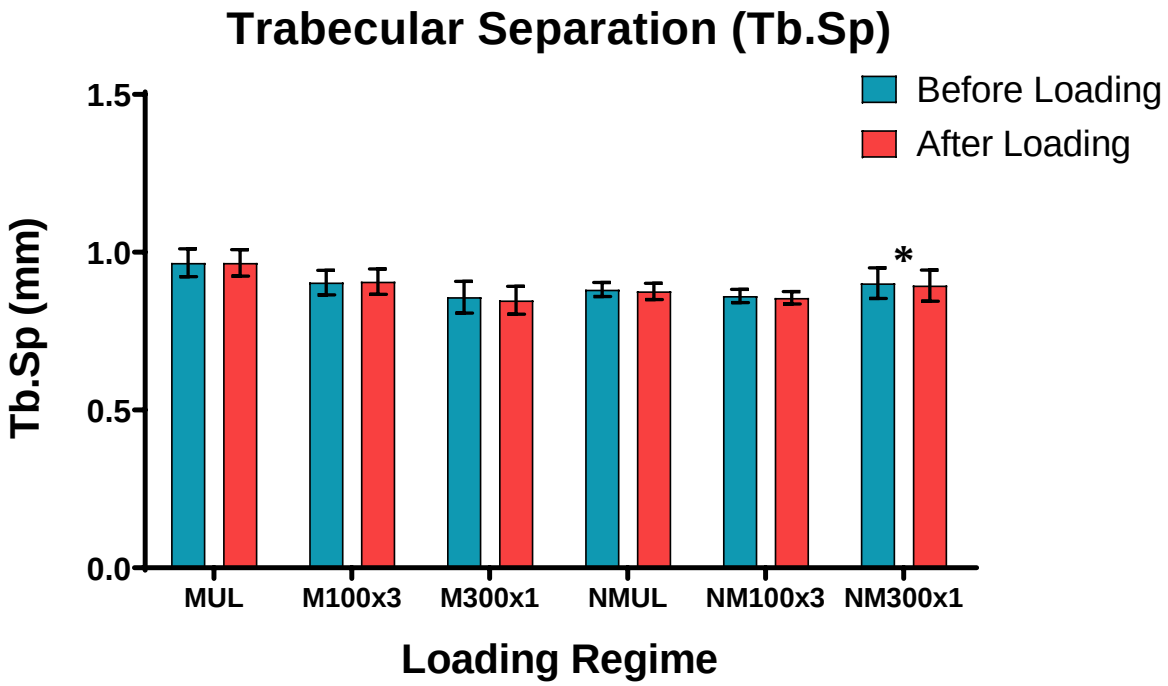

Figure 2.52 - Average Trabecular Separation (Tb.Sp) Before and After Loading
(* = t-test < 0.05, n = 4)

The relationship between stiffness and Tb.SP were positive, regardless marrow was present or not, both before and after loading was applied (Fig. 2.53). However, as with previous μCT parameters, the distinct separation and an increase in the regression line at the end of the experiment for the bone cores without marrow was also significant (p = 0.0187) here, in contrast to the bone cores with marrow where it reduced slightly.

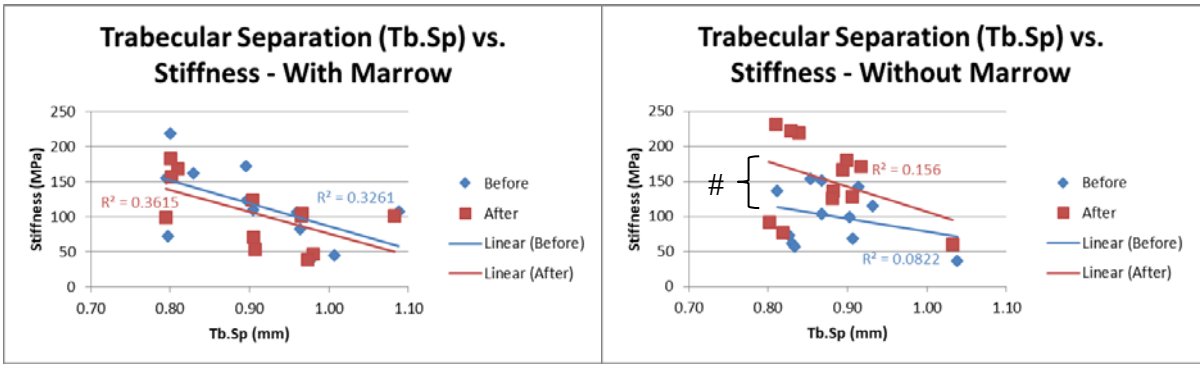

Figure 2.53 – Relationship of Stiffness with Tb.Sp

Correlation between Tb.Sp and stiffness of the bone cores, either with marrow or without marrow, before (blue) and after (red) 10 days of loading. (# = $p < 0.05$, n = 12)

A summary of the changes in the histomorphometric parameters at the beginning and end of the experiment, measured using the µCT system, was shown in Table 2.4 below.

Table 2.4 – Summary of Change in 3D Histomorphometric Parameters

µCT Parameters	Loaded 100x3		Loaded 300x1		Unloaded (UL)	
	NM	M	NM	M	NM	M
BV	↑ **	↓ *	↑	↑	↑	↓
BV/TV	↑ **	↓ *	↑	↓	↑	↓
BS	↑ *	↑	↑ *	↑	↑	↓
BS/BV	↓ *	↑ *	↑	↑	↓	↑
BS/TV	↑	↓	↑ *	↑	↑	↓
i.S	↑	↑	↑	↓	↑	↑
Tb.Pf	↓ ***	↑	↓	↑	↓ *	↑
SMI	↓ **	↑ *	↓	↑	↓	↑
Tb.Th	↑	↓ *	No change	↓	↑	↓
Tb.N	↑	↓	↑	↑	↑ *	↓
Tb.Sp	↓	↑	↓ *	↓	↓	↓

(* = t-test < 0.05, ** = t-test < 0.01, *** = t-test < 0.001)

2.10 Discussion

2.10.1 Young's Modulus Measurements

There was a large variance in the stiffness of the bone cores (Fig. 2.25), causing some of the groups (M300x1 and MUL) to have very large standard deviations (Fig. 2.26B). This was despite the same piece of bone (sternum) being used and the same orientation being maintained during the cutting, drilling and milling process to produce the bone cores as recommended by previous authors [63]. The average size of the trabeculae measured by the μCT was only 0.15 mm (Figs. 2.9B and 2.23), which was small enough that these small bone discs vary quite a lot in the number of their trabeculae and other histomorphometric parameters. Thompson first published in 1917 how the skeleton of a quadruped is likened to the structure of a bridge [79]. He also described how the trabecular structure of bone followed the stresses applied to it. It is likely that the forces acting on the sternum of a quadruped with a heavier front end are substantial and in multiple directions, resulting in very different trabecular structure at different parts of a large flat bone like the sternum (Fig. 2.54). Davies and colleagues also concluded the same from their work [63]

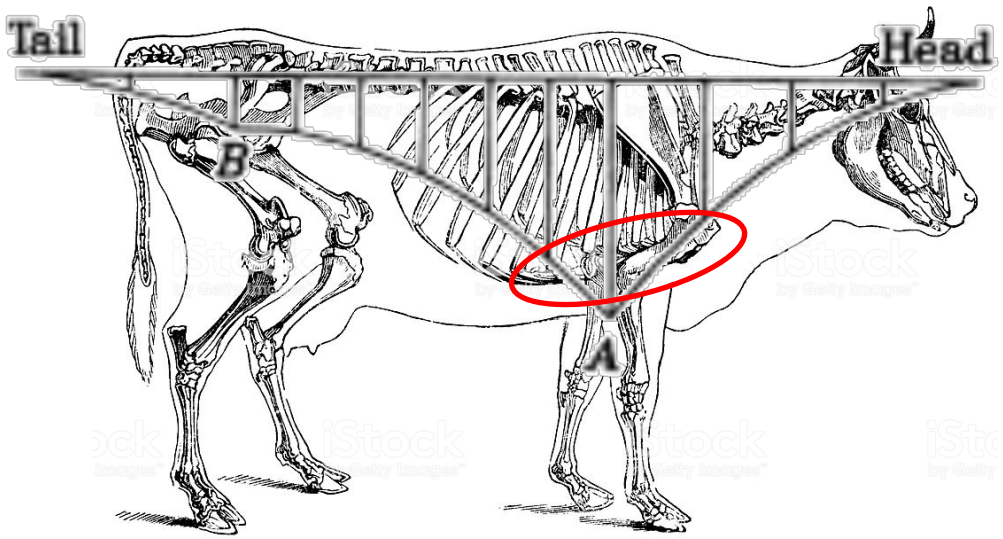

Figure 2.54 – Stresses on a Bovine Skeleton
Illustration of a stress diagram over a bovine skeleton and how the sternum (red circle) is at the area with the most stress. (Adapted from Thompson, 1917) (Diagram of bovine skeleton from http://media.istockphoto.com/illustrations/cow-skeleton-illustration-id184972282)

There was a strong correlation between height (thickness) of the bone cores and their initial stiffness (Fig. 2.27 and 2.28). From an engineering point of view, one of the variables for calculating the axial stiffness (K_{axial}) of a column, in this case the bone core, is the length (i.e. height) of the column (L), in the formula $K_{axial} = \frac{AE}{L}$, where A is area and E is the elastic modulus of the bone core. However, the microstructure of the trabecular bone itself contributes to the stiffness of bone [80] and the anisotropy of its mechanical properties [81], making the relationship between stiffness and height of the bone cores much more complex [82]. At the same time, the work done may be at the limit of the Zetos™ system sensitivity, thus, causing some variation to the measurements made during the course of the experiment. To reduce any bias in future experiments, it is important to keep the dimensions of the bone cores as near to each other as possible and increase the number of bone cores in each treatment group to 6 or more.

There was a drop in stiffness for all groups on day 2 (Fig. 2.29). The exception being the NM300x1 group, which also happened to have the lowest mean of initial stiffness at 55.5 MPa (Fig. 2.26), but with the greatest relative increase in its stiffness (Fig. 2.30). Despite attempts made to minimise thermal necrosis during the rigors of the processes required to cut, drill and mill the bone cores to size, some degree of osteocyte apoptosis probably occurred, especially nearer to the surface of the bone cores [63, 71]. However, the initial drop may not likely be due to the catabolic response of bone to damage as it requires localised osteoclast formation for targeted bone resorption [83], which will take more than 24 hours even with the presence of osteoclast precursors. Thus, it is more likely that this initial drop in stiffness is due to further compaction of the cut trabeculae free ends at the top and bottom of the prepared bone cores on day 2. For the NM300x1 group, it is probable that compaction was maximal already after the Young's Modulus was measured on day 1. It may also be due to development of microcracks initially in the bone cores, which did not propagate further either due to maximal compaction having been achieved or failure was not reached with the amount of loading applied during the course of the experiment. Bulk staining and histological examination of bone cores at different

time points during the course of future experiments will be an interesting observation to be made to elucidate the cause of this initial drop in stiffness further.

There was also another drop in stiffness on Day 11 for all groups, although it was not significant except for group M300x1 (Fig. 2.29). An experiment with a longer duration and looking at other parameters, such as markers for bone resorption and formation, should be performed to better understand what may cause this observation.

The stiffness of the bone cores did not show a steady rise as there were declines that occurred on Day 4 and Day 5 for some and on Day 8 for all (Fig. 2.29), even though the Zetos™ system was calibrated each day before the start of the loading sessions and Young's Modulus measurements. This may not be avoidable as previous published work using the first generation Zetos™ system demonstrated a similar looking non-linear and variable change in stiffness over a period of 22 days [67].

The bone cores without marrow seemed to respond better to loading when compared to those with marrow (Fig. 2.30). Even the unloaded bone cores (NMUL group) showed relatively better increase in stiffness over the duration of the experiment than the bone cores with marrow. The absence of marrow probably facilitates better perfusion of the osteocytes within the bone trabeculae, as alluded by Davies et al. [63], and, hence, the better response to mechanical loading.

Even the bone cores with marrow that was not loaded (MUL group, Fig. 2.30) showed a slight increase in stiffness. Past authors have shown that unloaded bone cores will also have an increase in their stiffness, albeit at a lower rate than loaded bone cores [73], which eventually plateaued [67]. Vivanco and colleagues hypothesised that this was due to the release of PGE_2 during preparation of the bone cores inducing osteoblastic bone formation [73]. It could also be that this is due to the underlying modelling activity (growth) in the bone of a young animal. Interestingly, Endres et al. showed that dead bone cores also have a significant increase in stiffness when they were loaded to a maximum of 3,000μstrain [67]. They considered the

possibility that mineralisation or some other process, such as passive uptake of calcium by the bone matrix mineral [84], contributed to the observation.

There was a significant difference in the Young's Modulus between the groups that were loaded 100 cycles thrice daily (M100x3 and NM100x3), where the NM100x3 group showed a persistent increase in stiffness leading to a more significant difference with the M100x3 group over time (Fig. 2.32B). Previous work in animals have shown that having a period of rest between loading sessions allowed the loaded bone to regain its mechanosensitivity and a further increase in bone formation in response to the loading [85, 86]. These observations are also in agreement with the first two of the three rules postulated by Turner [87] for the adaptation of bone to mechanical loading.

2.10.2 pH measurement

The average pH of the unused culture media was calculated to be 7.43, which was very near to the mammalian physiological pH. The higher pH of the used media by the bone cores with and without marrow (Fig. 2.33) was converse to what was generally known, whereby pH will decrease as metabolically active cells produced carbon dioxide (CO_2) via cellular respiration. This was most probably due to the diffusion of CO_2 out of the used media into the atmosphere, despite being kept in the refrigerator, because of the difference in the CO_2 partial pressure. For future studies using the Zetos™ system, pH of the used media will need to be measured immediately after it was changed.

It was observed that the bone cores without marrow have a significantly higher pH than the bone cores with marrow (Fig. 2.34). This observation probably reflects a larger number of metabolically active cells in the bone cores with marrow than those without. Although it was expected that most of the haemopoietic cells in the marrow will quickly undergo cell death within the 72 hours that it took to start loading the bone cores from the time the steer was

slaughtered, it may be that there are more than enough of fat cells and osteogenic cell precursors left alive to provide a larger response than in the bone cores without marrow. However, this will need to be checked using different metabolic markers in future experiments. The difference in the number and viability of the cells within the bone cores when the marrow was left intact or removed should also be studied.

2.10.3 Ionic calcium (Ca^{2+}) levels

A highly significant amount of Ca^{2+} was taken up from the prepared culture media by the bone cores (Fig. 2.35). However, the unloaded bone cores with marrow (MUL) took up the least amount of Ca^{2+} while it was comparatively more for the bone cores without marrow (NMUL). In general, all of bone cores without marrow (NMUL, NM 100x3 and NM300x1) took up more Ca^{2+}.

It is interesting to note that the concentration of serum ionised calcium in the body is tightly regulated within a physiologic range of 1.10 to 1.35 mM [88], which is higher than the levels measured in the culture media. In normal circumstances, access of water and ions to the bone matrix is very restricted, whereby calcium matrix deposition is driven primarily by phosphate production and requires regulated Ca^{2+} and H^{+} transport with alkalinisation at the site of deposition, while matrix removal is driven by acidification, which dissolves the mineral. When necessary, the skeleton is sacrificed to maintain the pH of the extracellular fluid [89]. The chemistry of the main bone mineral, hydroxyapatite (HA), necessitates that any mechanism of bone formation include a supply of ionic calcium and phosphate with some way to dispose of 1.4 proton for each calcium deposited, as per the equation:

$$10Ca + 6H_2PO_4^- + 2H_2O \leftrightarrow Ca_{10}(H_2PO_4)_6(OH)_2 + 14H^+$$

The exact stoichiometry depends on the pH at the deposition site, which determines the ratio of $H_2PO_4^{2-}$ to $H_2PO_4^-$ that is available. Thus, knowing the exact pH of the culture media may be an important criteria to be determined in future experiments.

(Neuman et al. 1982) Using chemical studies on bone without the inclusion of living or dead cells, it was demonstrated that noncollagenous proteins (e.g. osteocalcin and osteonectin) found on all bone mineral surfaces are able to maintain the concentration of Ca^{2+} in the media at around 1.25 mM [90], which is higher than the levels measured in this study. By inhibiting the formation and growth of HA crystals, the noncollagenous proteins are able to increase the calcium concentration to a maximum level of 2 mM, by dissolution of some of the HA crystals, with the subsequent release of both calcium and phosphate into the medium. Radiolabelled calcium and phosphate showed that a large amount of these two ions were rapidly fluxed into and out of bone instantaneously. Although bone acts as a temporary buffer to take up and release serum calcium, the mechanism is largely passive and driven by serum concentration itself at the bone surfaces. This activity is an equilibrium process between the influx of calcium in the ECF and the efflux of calcium from the bone mineral it comes into contact with [91]. Taking into account all of the above, it is will be interesting to investigate further the actual movement of calcium in the bone cores without marrow.

A recent review by Tsourdi et al. indicated the possible role of the osteocytes in removing and replacing the perilacunar matrix (i.e. osteocytic osteolysis) in response to mechanical loading, as well as for normal physiological needs [92]. By regulating the interaction between protein phosphate-regulating gene with homologies to endopeptidases on the X-chromosome (PHEX) and matrix extracellular phosphoglycoprotein (MEPE), preosteocytes was shown to be able to mineralise their surrounding matrix [93]. Furthermore, human primary osteoblastic cells differentiated to osteocyte-like stage (hOCy) and MLO-Y4 cells was able to degrade the surrounding bone matrix or mineralised substrate, respectively, via production of carbonic anhydrase 2 (CA2), resulting in a reduced pH and release of calcium locally [94]. Conversely,

osteocytes that were actively mineralising their perilacunar matrix will use up more of the available Ca^{2+} and have a lower pH. This uptake of Ca^{2+} occurs very rapidly on all accessible bone surfaces, regardless of cellular activity or degree of mineralization [84]. Marenzana and colleagues elegantly demonstrated that a steady Ca^{2+} influx occurs in living bone, which is reversed to an efflux when there is a Ca^{2+} deficiency [95]. The Ca^{2+} influx was an immediate and constant passive, concentration-dependent process, while the Ca^{2+} efflux from bone was a bone cell energy-dependent process. They suggested that the osteocyte-bone lining cell syncytium separates the extracellular fluid (ECF) into a systemic and an endocanaliculi network, with a strong Ca^{2+} gradient (1.5mM/L vs. 0.5mM/L) between them. The passive Ca^{2+} influx occurred when this syncytium was damaged, while the active Ca^{2+} efflux occurred when the ECF is calcium deficient. This will not only explain the observations above but also the strong correlation between pH and the remaining Ca^{2+} levels in the used media as mentioned. Future experiments using the second generation Zetos™ system will include a suitable method to demonstrate this rapid uptake of Ca^{2+} by viable osteocytes in the bone cores and the effect it has on osteocyte-induced osteocytic osteolysis, which had been reported in Chapter 4 of this thesis.

2.10.4 3D analysis of μCT images

The bone cores that were loaded 100 cycles thrice daily (NM100x3 and M100x3) showed more significant changes to their histomorphometric features (Table 2.4). However, for the most part, the changes were reversed between the bone cores without marrow (NM100x3) and those with marrow (M100x3). The cause for this difference in the measured μCT histomorphometric parameters of the bone cores, either with or without marrow, in response to mechanical loading is unclear and warrants further investigation in the future. BV, BV/TV and BS were significantly increased and BS/BV, Tb.Pf and SMI were significantly reduced for the NM100x3 group. But for the M100x3 group BV and BV/TV were significantly reduced, while BS/BV and

SMI were significantly increased. This is in agreement with Turners second rule and the *in vivo* observations made by previous authors (see section 1.9.2 in Chapter 1), whereby a period of rest between loading sessions resulted in better mechanical responses to the loading.

For the bone cores that were unloaded or loaded 300 cycles daily, only those without marrow (NMUL and NM300x1) showed any significant changes to their histomorphometric parameters (Table 2.4). The NM300x1 group had a significant increase in BS and BS/TV with a significant decrease in Tb.Sp, while the NMUL group only have a significant decrease in Tb.Pf. These changes were consistent with the NM100x3 group. This seems to indicate that removing the marrow from the bone cores was able to provide a better response in the histomorphometric parameters when mechanical loading was applied.

The structure model index (SMI) have a value between 0 and 3, where 0 is for an ideal plate structural model while 3 is for an ideal cylindrical rod structural model [96]. Thus, the trabeculae for the bone cores without marrow seemed to become more plate-like but for the bone cores with marrow their trabecular structure becomes more rod-like. Previous authors have also shown that SMI was the best predictor for Young's Modulus and percent bone volume (BV/TV) the second best predictor [97]. This is consistent with the better increase in stiffness for the bone cores without marrow as their SMI was reduced and BV/TV increased very significantly (Table 2.4). In a well-connected network the trabecular pattern factor (Tb.Pf) will be low [98] and this parameter was reduced extremely significantly in the bone cores without marrow after 10 days (Fig. 2.44). Furthermore, all histomorphometric parameters for the bone cores without marrow, when plotted against stiffness, showed a clear separation and increase in the linear regression lines before and after the 10 days of loading, (Fig. 2.37, 2.39, 2.41, 2.43, 2.45, 2.47, 2.49, 2.51 and 2.53). The above observations indicated that bone cores without marrow are able to show consistent changes to their trabecular microstructure, which correlated well with change in their stiffness, despite the small number of samples and shorter duration of this experiment when compared to previous work using the first generation Zetos™ system.

It is interesting to note that during the process of removing the marrow using the dental water jet (Section 2.7.6 and Fig. 2.9) most, if not all, of the bone cells on the surface of the trabeculae (osteoblasts, osteoclasts and lining cells) were likely removed also. This was clearly demonstrated in Chapter 4 of this thesis [99]. Thus, the changes in the histomorphometric parameters in the bone cores without marrow, as mentioned above, were independent of the normal bone remodelling process brought about by the coupled actions of osteoclasts and osteoblasts. As discussed in section 2.10.3, ionic calcium from the culture media was taken up significantly more by the bone cores without marrow and the remaining osteocytes within the lacuno-canaliculi network had been suggested as being able to do this [92, 100]. The actual mechanism of these changes remains unclear but the work done in Chapter 4 had also demonstrated an association between the clear uptake of ionic calcium from the culture media and the increased modulus in the loaded bone cores without marrow [99], which was probably due to the influx of calcium into the perilacunar matrix via the process of osteocytic osteolysis. This intriguing observation requires further study in future works with the second generation Zetos™ system.

2.11 Limitations

An important observation made was the limitation of the milling process in which the 4-fluted milling bit may also mill through the milling plate surrounding the bone cores. In other words, the adjustment of the heights of the bone cores is user-dependent. An overestimation or overzealous milling will cause the bone cores to be thinner than the 5 mm that was targeted for and this can introduce significant variability between the bone cores when measuring stiffness.

Some metal debris were also found to be embedded into the inter-trabecular spaces of the bone cores, as previously reported [63]. This metal debris can produce artefacts during μCT scanning of the bone cores, which was observed in a few of the bone cores in this experiment. This may affect the calculation of the parameters measured during 3D analysis. An improvement to the

design of the milling plate to prevent this from occurring should be looked into. However, this problem was minimised when only the central portion of the bone cores were analysed with the μCT scanner as was done in this study (see section 2.7.14 above).

It is clear from this experiment that having only 4 bone cores in each group may be insufficient to provide a statistically significant outcome for many of the parameters measured. The large variation in the baseline measurements of the parameters that were looked at further compounded this problem. It is important to ensure that the bone cores have very similar height (thickness), which should not be less than 5.0 mm, and the top and bottom surfaces must be as parallel to each other as possible to minimise this variation. However, a limitation of the Zetos™ system being used was that only 24 bone cores can be cultured and experimented on at any one time. This means that probably more than one experiment will need to be performed to better investigate all the parameters that were analysed in this study. This will further increase the variability of the bone cores since each experiment necessitates the use of a different animal to procure fresh bone from each time. Furthermore, as the bones were acquired from a nearby abattoir, it makes it difficult to minimise the variation between the animals that were slaughtered on each day. In the course of doing the trial experiments for optimising the Zetos™ system, there had been instances when it was possible to produce more than 50 bone cores from a single sternum of a larger animal. Thus, another way to overcome this limitation is to have another set of bone culture chambers and planetary drive peristaltic pump available so that a total of 48 bone cores can be used in a single experiment.

In this experiment, the use of bone from a young steer (male cow) may have compounded the observations made as it is still undergoing a significant amount of bone modelling (growth) and it will continue to form new bone regardless of the amount of loading, or lack thereof, which was being applied. However, this may not be an issue in the bone cores without marrow since most, if not all, of the cells on the bone surface has been removed. Still, it is probably better to

procure bone from an older animal, of at least two years in age, in future experiments to avoid this confounding factor.

2.12 Conclusions

Initial work was performed to make operational the software associated with the second generation Zetos™ system to enable an *ex vivo* bone study. From this *ex vivo* study, it was found that the removal of bone marrow may be beneficial in terms of optimal response to mechanical loading. Short-term loading of bone cores *ex vivo* to a peak strain of 2,000 μstrain at 150 kHz for 100 cycles thrice daily, with a 4 hours break in between loading sessions, was found to show more significant changes in many of the measured parameters. Mechanical loading was found to be associated with changes in the trabecular structure, by an as yet unknown mechanism.

2.13 Recommendations

Removal of marrow should be done for future experiments using the Zetos™ system to be able to attribute effect of loading on osteocytes and better nutrition perfusion to the available bone cells.

A loading regime to a maximum strain of 2,000 μstrain at 150 kHz for 100 cycles thrice daily, with a 4 hours break in between loading sessions, was able to produce significant change in the stiffness and histomorphometric features for future short term experiments.

It was postulated that the growing bone of a young steer may not be optimal for mechanotransduction experiments, due to the inherent variability of this tissue. Other trabecular bone sites should be investigated.

A minimum of six (6) bone cores in each treatment or control group would allow for inter-sample variability.

More work need to be done in the future to understand the response of trabecular bone to agents that affect bone.

With the optimisation of the Zetos™ system having been performed in this study, it would be of great interest to explore the use of human femoral head trabecular bone, in order to translate findings to human pathophysiology.

2.14 References

1. Robling, A.G., A.B. Castillo, and C.H. Turner, *Biomechanical and molecular regulation of bone remodeling.* Annu Rev Biomed Eng, 2006. **8**: p. 455-98.

2. Klein-Nulend, J., R.G. Bacabac, and M.G. Mullender, *Mechanobiology of bone tissue.* Pathol Biol (Paris), 2005. **53**(10): p. 576-80.

3. Turner, C.H., *Bone strength: current concepts.* Ann N Y Acad Sci, 2006. **1068**: p. 429-46.

4. Chen, J.H., et al., *Boning up on Wolff's Law: mechanical regulation of the cells that make and maintain bone.* Journal of Biomechanics, 2010. **43**(1): p. 108-18.

5. Katsimbri, P., *The biology of normal bone remodelling.* Eur J Cancer Care (Engl), 2017. **26**(6).

6. Rubin, C., S. Judex, and M. Hadjiargyrou, *Skeletal adaptation to mechanical stimuli in the absence of formation or resorption of bone.* J Musculoskelet Neuronal Interact., 2002. **2**(3): p. 264-7.

7. Bilezikian, J.P., et al., *Targeting bone remodeling for the treatment of osteoporosis: summary of the proceedings of an ASBMR workshop.* J Bone Miner Res, 2009. **24**(3): p. 373-85.

8. Kogianni, G. and B.S. Noble, *The biology of osteocytes.* Curr Osteoporos Rep, 2007. **5**(2): p. 81-6.

9. Noble, B.S., *The osteocyte lineage.* Arch Biochem Biophys, 2008. **473**(2): p. 106-11.

10. Klein-Nulend, J. and L. Bonewald, *The Osteocyte*, in *Principles of Bone Biology*, J.P. Bilezikian, L.G. Raisz, and T.J. Martin, Editors. 2008, Academic Press: San Diego. p. 153-174.

11. Chen, H., T. Senda, and K.Y. Kubo, *The osteocyte plays multiple roles in bone remodeling and mineral homeostasis.* Med Mol Morphol, 2015. **48**(2): p. 61-8.

12. Noble, B.S. and J. Reeve, *Osteocyte function, osteocyte death and bone fracture resistance.* Mol Cell Endocrinol, 2000. **159**(1-2): p. 7-13.

13. Knothe Tate, M.L., et al., *The osteocyte.* Int J Biochem Cell Biol, 2004. **36**(1): p. 1-8.

14. Bellido, T., *Osteocyte-driven bone remodeling.* Calcif Tissue Int, 2014. **94**(1): p. 25-34.

15. Fritton, S.P. and S. Weinbaum, *Fluid and Solute Transport in Bone: Flow-Induced Mechanotransduction.* Annu Rev Fluid Mech, 2009. **41**: p. 347-374.

16. Schaffler, M.B., et al., *Osteocytes: master orchestrators of bone.* Calcif Tissue Int, 2014. **94**(1): p. 5-24.

17. Uda, Y., et al., *Osteocyte Mechanobiology.* Curr Osteoporos Rep, 2017. **15**(4): p. 318-325.

18. Henriksen, K., et al., *Local communication on and within bone controls bone remodeling.* Bone, 2009. **44**(6): p. 1026-33.

19. Rubin, J., C. Rubin, and C.R. Jacobs, *Molecular pathways mediating mechanical signaling in bone.* Gene, 2006. **367**: p. 1-16.

20. Sun, Q., et al., *Ex vivo 3D osteocyte network construction with primary murine bone cells.* Bone Res, 2015. **3**: p. 15026.

21. Gu, Y., et al., *Microbeads-Guided Reconstruction of 3D Osteocyte Network during Microfluidic Perfusion Culture.* J Mater Chem B, 2015. **3**(17): p. 3625-3633.

22. Marino, S., et al., *Models of ex vivo explant cultures: applications in bone research.* Bonekey Rep, 2016. **5**: p. 818.

23. Sun, Q., et al., *Ex vivo construction of human primary 3D-networked osteocytes.* Bone, 2017. **105**: p. 245-252.

24. Takai, E., et al., *Osteocyte viability and regulation of osteoblast function in a 3D trabecular bone explant under dynamic hydrostatic pressure.* J Bone Miner Res, 2004. **19**(9): p. 1403-10.

25. Boukhechba, F., et al., *Human primary osteocyte differentiation in a 3D culture system.* J Bone Miner Res, 2009. **24**(11): p. 1927-35.

26. Jones, D.B., et al., *Development of a mechanical testing and loading system for trabecular bone studies for long term culture.* Eur Cell Mater, 2003. **5**: p. 48-59; discussion 59-60.

27. Raggatt, L.J. and N.C. Partridge, *Cellular and molecular mechanisms of bone remodeling.* J Biol Chem, 2010. **285**(33): p. 25103-8.

28. Takahashi, N., et al., *Osteoclast Generation*, in *Principles of Bone Biology*, J.P. Bilezikian, L.G. Raisz, and T.J. Martin, Editors. 2008, Academic Press: San Diego. p. 175-192.

29. Wada, T., et al., *RANKL-RANK signaling in osteoclastogenesis and bone disease.* Trends Mol Med, 2006. **12**(1): p. 17-25.

30. Seeman, E., *Modeling and Remodeling: The Cellular Machinery Responsible for the gain and Loss of Bone's Material and Structural Strength*, in *Principles of Bone Biology*, J.P. Bilezikian, L.G. Raisz, and T.J. Martin, Editors. 2008, Academic Press: San Diego. p. 2-27.

31. Cabahug-Zuckerman, P., et al., *Osteocyte Apoptosis Caused by Hindlimb Unloading is Required to Trigger Osteocyte RANKL Production and Subsequent Resorption of*

Cortical and Trabecular Bone in Mice Femurs. J Bone Miner Res, 2016. **31**(7): p. 1356-65.

32. Kennedy, O.D., et al., *Osteocyte apoptosis is required for production of osteoclastogenic signals following bone fatigue in vivo.* Bone, 2014. **64**: p. 132-7.

33. Atkins, G.J., et al., *RANK Expression as a cell surface marker of human osteoclast precursors in peripheral blood, bone marrow, and giant cell tumors of bone.* J Bone Miner Res, 2006. **21**(9): p. 1339-49.

34. Kong, Y.Y., W.J. Boyle, and J.M. Penninger, *Osteoprotegerin ligand: a common link between osteoclastogenesis, lymph node formation and lymphocyte development.* Immunol Cell Biol, 1999. **77**(2): p. 188-93.

35. Tsurukai, T., et al., *Roles of macrophage-colony stimulating factor and osteoclast differentiation factor in osteoclastogenesis.* J Bone Miner Metab, 2000. **18**(4): p. 177-84.

36. Hadjidakis, D.J. and Androulakis, II, *Bone remodeling.* Ann N Y Acad Sci, 2006. **1092**: p. 385-96.

37. Raisz, L.G., *Physiology and pathophysiology of bone remodeling.* Clin Chem, 1999. **45**(8 Pt 2): p. 1353-8.

38. Tang, S.Y. and T. Alliston, *Regulation of postnatal bone homeostasis by TGFbeta.* Bonekey Rep, 2013. **2**: p. 255.

39. Kawai, M. and C.J. Rosen, *Insulin-like growth factor-I and bone: lessons from mice and men.* Pediatr Nephrol, 2009. **24**(7): p. 1277-85.

40. Sims, N.A. and T.J. Martin, *Coupling Signals between the Osteoclast and Osteoblast: How are Messages Transmitted between These Temporary Visitors to the Bone Surface?* Front Endocrinol (Lausanne), 2015. **6**: p. 41.

41. Hill, P.A., *Bone remodelling.* Br J Orthod, 1998. **25**(2): p. 101-7.

42. Nguyen, J., et al., *Load regulates bone formation and Sclerostin expression through a TGFbeta-dependent mechanism.* PLoS One, 2013. **8**(1): p. e53813.

43. Imai, S., et al., *Osteocyte-derived HB-GAM (pleiotrophin) is associated with bone formation and mechanical loading.* Bone, 2009. **44**(5): p. 785-94.

44. Han, Y., et al., *Paracrine and endocrine actions of bone-the functions of secretory proteins from osteoblasts, osteocytes, and osteoclasts.* Bone Res, 2018. **6**: p. 16.

45. Mishra, S. and M.L. Knothe Tate, *Effect of lacunocanalicular architecture on hydraulic conductance in bone tissue: implications for bone health and evolution.* Anat Rec A Discov Mol Cell Evol Biol, 2003. **273**(2): p. 752-62.

46. Boyce, B.F., Z. Yao, and L. Xing, *Osteoclasts have multiple roles in bone in addition to bone resorption.* Crit Rev Eukaryot Gene Expr, 2009. **19**(3): p. 171-80.

47. Galli, C., G. Passeri, and G.M. Macaluso, *Osteocytes and WNT: the mechanical control of bone formation.* J Dent Res, 2010. **89**(4): p. 331-43.

48. Temiyasathit, S. and C.R. Jacobs, *Osteocyte primary cilium and its role in bone mechanotransduction.* Ann N Y Acad Sci, 2010. **1192**(1): p. 422-8.

49. Heino, T.J., et al., *Evidence for the role of osteocytes in the initiation of targeted remodeling.* Technol Health Care, 2009. **17**(1): p. 49-56.

50. Zhao, S., et al., *MLO-Y4 osteocyte-like cells support osteoclast formation and activation.* J Bone Miner Res, 2002. **17**(11): p. 2068-79.

51. Kogianni, G., V. Mann, and B.S. Noble, *Apoptotic bodies convey activity capable of initiating osteoclastogenesis and localized bone destruction.* J Bone Miner Res, 2008. **23**(6): p. 915-27.

52. Cheung, W.Y., et al., *Pannexin-1 and P2X7-Receptor Are Required for Apoptotic Osteocytes in Fatigued Bone to Trigger RANKL Production in Neighboring Bystander Osteocytes.* J Bone Miner Res, 2016. **31**(4): p. 890-9.

53. Prideaux, M., D.M. Findlay, and G.J. Atkins, *Osteocytes: The master cells in bone remodelling.* Curr Opin Pharmacol, 2016. **28**: p. 24-30.

54. Bonewald, L.F., *Mechanosensation and Transduction in Osteocytes.* Bonekey Osteovision, 2006. **3**(10): p. 7-15.

55. Nakashima, T., et al., *Evidence for osteocyte regulation of bone homeostasis through RANKL expression.* Nat Med, 2011. **17**(10): p. 1231-4.

56. Xiong, J., et al., *Osteocytes, not Osteoblasts or Lining Cells, are the Main Source of the RANKL Required for Osteoclast Formation in Remodeling Bone.* PLoS One, 2015. **10**(9): p. e0138189.

57. Palumbo, C., S. Palazzini, and G. Marotti, *Morphological study of intercellular junctions during osteocyte differentiation.* Bone, 1990. **11**(6): p. 401-6.

58. Kamioka, H., T. Honjo, and T. Takano-Yamamoto, *A three-dimensional distribution of osteocyte processes revealed by the combination of confocal laser scanning microscopy and differential interference contrast microscopy.* Bone, 2001. **28**(2): p. 145-9.

59. Honma, M., et al., *RANKL subcellular trafficking and regulatory mechanisms in osteocytes.* J Bone Miner Res, 2013. **28**(9): p. 1936-49.

60. Honma, M., et al., *Regulatory mechanisms of RANKL presentation to osteoclast precursors.* Curr Osteoporos Rep, 2014. **12**(1): p. 115-20.

61. Xiong, J., et al., *Matrix-embedded cells control osteoclast formation.* Nat Med, 2011. **17**(10): p. 1235-41.

62. Wijenayaka, A.R., et al., *Sclerostin stimulates osteocyte support of osteoclast activity by a RANKL-dependent pathway.* PLoS One, 2011. **6**(10): p. e25900.

63. Davies, C.M., et al., *Mechanically loaded ex vivo bone culture system 'Zetos': systems and culture preparation.* Eur Cell Mater, 2006. **11**: p. 57-75; discussion 75.

64. Garcia-Rodriguez, S., E.L. Smith, and H.-L. Ploeg, *A calibration procedure for a bone loading system.* Journal of Medical Devices, 2008. **2**: p. 011006-1-6.

65. David, V., et al., *Ex Vivo bone formation in bovine trabecular bone cultured in a dynamic 3D bioreactor is enhanced by compressive mechanical strain.* Tissue Eng Part A, 2008. **14**(1): p. 117-26.

66. Meyer, U., et al., *Design and performance of a bioreactor system for mechanically promoted three-dimensional tissue engineering.* Br J Oral Maxillofac Surg, 2006. **44**(2): p. 134-40.

67. Endres, S., et al., *Zetos: a culture loading system for trabecular bone. Investigation of different loading signal intensities on bovine bone cylinders.* J Musculoskelet Neuronal Interact, 2009. **9**(3): p. 173-83.

68. David, V., et al., *Mechanical loading down-regulates peroxisome proliferator-activated receptor gamma in bone marrow stromal cells and favors osteoblastogenesis at the expense of adipogenesis.* Endocrinology, 2007. **148**(5): p. 2553-62.

69. Dumas, V., et al., *The effect of dual frequency cyclic compression on matrix deposition by osteoblast-like cells grown in 3D scaffolds and on modulation of VEGF variant expression.* Biomaterials, 2009. **30**(19): p. 3279-88.

70. Stoddart, M.J., et al., *A comparison of non-radioactive methods for assessing viability in ex vivo cultured cancellous bone: technical note.* Eur Cell Mater., 2006. **12**: p. 16-25; discussion 16-25.

71. Mann, V., et al., *The influence of mechanical stimulation on osteocyte apoptosis and bone viability in human trabecular bone.* J Musculoskelet Neuronal Interact, 2006. **6**(4): p. 408-17.

72. Simpson, A.E., et al., *TGFbeta3 and loading increases osteocyte survival in human cancellous bone cultured ex vivo.* Cell Biochem Funct, 2009. **27**(1): p. 23-9.

73. Vivanco, J., et al., *Apparent elastic modulus of ex vivo trabecular bovine bone increases with dynamic loading.* Proc Inst Mech Eng H, 2013. **227**(8): p. 904-12.

74. Aw, M.S., et al., *Characterization of drug-release kinetics in trabecular bone from titania nanotube implants.* Int J Nanomedicine, 2012. **7**: p. 4883-92.

75. Rahman, S., et al., *Drug diffusion, integration, and stability of nanoengineered drug-releasing implants in bone ex-vivo.* J Biomed Mater Res A, 2016. **104**(3): p. 714-725.

76. Schnieders, J., et al., *Ex vivo human trabecular bone model for biocompatibility evaluation of calcium phosphate composites modified with spray dried biodegradable microspheres.* Adv Healthc Mater, 2013. **2**(10): p. 1361-9.

77. Chan, M.E., et al., *A Trabecular Bone Explant Model of Osteocyte-Osteoblast Co-Culture for Bone Mechanobiology.* Cell Mol Bioeng, 2009. **2**(3): p. 405-415.

78. Parfitt, A.M., et al., *Bone histomorphometry: standardization of nomenclature, symbols, and units. Report of the ASBMR Histomorphometry Nomenclature Committee.* J Bone Miner Res, 1987. **2**(6): p. 595-610.

79. Thompson, D.A.W., *On Growth and Form*. 1917, Cambridge: Cambridge University Press.

80. Rho, J.Y., L. Kuhn-Spearing, and P. Zioupos, *Mechanical properties and the hierarchical structure of bone.* Med Eng Phys, 1998. **20**(2): p. 92-102.

81. Rietbergen, v., B., Huiskes, R., Weinans, H., Odgaard, A., & Kabel, J., *The role of trabecular architecture in the anisotropic mechanical properties of bone,* in *Bone structure and remodeling*. 1995, World Scientific: Singapore. p. 137-45.

82. Oftadeh, R., et al., *Biomechanics and mechanobiology of trabecular bone: a review.* J Biomech Eng, 2015. **137**(1).

83. Komori, T., *Cell Death in Chondrocytes, Osteoblasts, and Osteocytes.* Int J Mol Sci, 2016. **17**(12).

84. Parfitt, A.M., *Misconceptions (3): calcium leaves bone only by resorption and enters only by formation.* Bone, 2003. **33**(3): p. 259-63.

85. Burr, D.B., A.G. Robling, and C.H. Turner, *Effects of biomechanical stress on bones in animals.* Bone, 2002. **30**(5): p. 781-6.

86. Robling, A.G., et al., *Improved bone structure and strength after long-term mechanical loading is greatest if loading is separated into short bouts.* J Bone Miner Res, 2002. **17**(8): p. 1545-54.

87. Turner, C.H., *Three rules for bone adaptation to mechanical stimuli.* Bone, 1998. **23**(5): p. 399-407.

88. Peacock, M., *Calcium metabolism in health and disease.* Clin J Am Soc Nephrol, 2010. **5 Suppl 1**: p. S23-30.

89. Blair, H.C., et al., *Calcium signalling and calcium transport in bone disease.* Subcell Biochem, 2007. **45**: p. 539-62.

90. Neuman, W.F., et al., *Blood:bone disequilibrium. VI. Studies of the solubility characteristics of brushite: apatite mixtures and their stabilization by noncollagenous proteins of bone.* Calcif Tissue Int, 1982. **34**(2): p. 149-57.

91. Talmage, R.V. and H.T. Mobley, *Calcium homeostasis: reassessment of the actions of parathyroid hormone.* Gen Comp Endocrinol, 2008. **156**(1): p. 1-8.

92. Tsourdi, E., et al., *Physiological and pathological osteocytic osteolysis.* J Musculoskelet Neuronal Interact, 2018. **18**(3): p. 292-303.

93. Atkins, G.J., et al., *Sclerostin is a locally acting regulator of late-osteoblast/preosteocyte differentiation and regulates mineralization through a MEPE-ASARM-dependent mechanism.* J Bone Miner Res, 2011. **26**(7): p. 1425-36.

94. Kogawa, M., et al., *Sclerostin regulates release of bone mineral by osteocytes by induction of carbonic anhydrase 2.* J Bone Miner Res, 2013. **28**(12): p. 2436-48.

95. Marenzana, M., et al., *Bone as an ion exchange organ: evidence for instantaneous cell-dependent calcium efflux from bone not due to resorption.* Bone, 2005. **37**(4): p. 545-54.

96. Ding, M. and I. Hvid, *Quantification of age-related changes in the structure model type and trabecular thickness of human tibial cancellous bone.* Bone, 2000. **26**(3): p. 291-5.

97. Ding, M., et al., *Mutual associations among microstructural, physical and mechanical properties of human cancellous bone.* Journal of Bone and Joint Surgery. British Volume, 2002. **84**(6): p. 900-7.

98. Chappard, D., et al., *Trabecular bone microarchitecture: a review.* Morphologie, 2008. **92**(299): p. 162-70.

99. Kogawa, M., et al., *Recombinant sclerostin antagonizes effects of ex vivo mechanical loading in trabecular bone and increases osteocyte lacunar size.* Am J Physiol Cell Physiol, 2018. **314**(1): p. C53-c61.

100. Atkins, G.J. and D.M. Findlay, *Osteocyte regulation of bone mineral: a little give and take.* Osteoporos Int, 2012. **23**(8): p. 2067-79.

CHAPTER 3. Characterization of drug-release kinetics in trabecular bone from titania nanotube implants

Moom Sinn Aw, Kamarul A Khalid, Karan Gulati, Gerald J Atkins, Peter Pivonka, David M Findlay, Dusan Losic

School of Chemical Engineering, The University of Adelaide, Adelaide, SA, Australia

Discipline of Orthopaedics and Trauma, The University of Adelaide, Adelaide, SA, Australia

Department of Orthopaedics, Traumatology and Rehabilitation, Faculty of Medicine, International Islamic University Malaysia, Kuantan, Pahang, Malaysia

Engineering Computational Biology Group, School of Computer Science and Software Engineering, The University of Western Australia, Perth, WA, Australia

International Journal of Nanomedicine (2012); 7:4883-92

Introduction

3.1 Summary of Chapter

In this chapter, the idea to study drug-release kinetics and drug distribution in *ex vivo* bone using the second generation Zetos™ system was introduced for the first time. Live trabecular bone of bovine origin, with their bone marrow removed, embedded with a novel drug-releasing implant, a nano-engineered titanium wire covered with titania nanotube arrays, was used in this study. The usefulness of the system in investigating the transport of drugs in bone and its drug-release kinetics was demonstrated as the release pattern and molecular disposition of drugs, with respect to time and location, can be estimated precisely. New understanding of drug distribution in the complex environment of viable bone can be made possible using the system. It has the potential to predict real drug concentration and distribution in trabecular bone, which was hereto not feasible using available *in vitro* models. The method can also be used to enhance current technologies for the local administration of drugs in bone for bone therapy and finding the solution to problems in bone therapy and orthopaedic implants.

3.2 Context and Contribution of Chapter

This paper demonstrated the usefulness of using the Zetos™ system for investigating drug release and distribution from a bone delivery system in an intact bone environment and the effect mechanical loading has on them, which was previously not possible. The function, integration and stability of the drug delivery system used in this chapter, the nano-engineered titanium wire covered with titania nanotube arrays, had been further investigated in the presence of marrow, which improved with the addition of an anticoagulant [1]. The potential application and customisation of the delivery system as a therapeutic bone implant had also been studied using a 3D collagen gel matrix containing human osteoblast-like cells and the Zetos™ system [2]. The Zetos™ system has also been used to study the biocompatibility of another

bone drug delivery system, which comprises of calcium phosphate bone cement composite modified with spray dried and drug loaded microspheres [3]. A number of published works on titania nanotubes and other drug delivery systems have also cited this paper [4-8]. To date, this paper has been cited by more than 40 other scholarly articles that are available online via Google Scholar (https://scholar.google.com/scholar?oi=bibs&hl=en&cites=12076154416609966967 accessed on 8 November 2019, 2.33 p.m.).

3.3 References

1. Rahman, S., et al., *Drug diffusion, integration, and stability of nanoengineered drug-releasing implants in bone ex-vivo.* J Biomed Mater Res A, 2016. **104**(3): p. 714-725.

2. Gulati, K., et al., *Drug-releasing nano-engineered titanium implants: therapeutic efficacy in 3D cell culture model, controlled release and stability.* Mater Sci Eng C Mater Biol Appl, 2016. **69**: p. 831-40.

3. Schnieders, J., et al., *Ex vivo human trabecular bone model for biocompatibility evaluation of calcium phosphate composites modified with spray dried biodegradable microspheres.* Adv Healthc Mater, 2013. **2**(10): p. 1361-9.

4. Daish, C., et al., *Estimation of anisotropic permeability in trabecular bone based on microCT imaging and pore-scale fluid dynamics simulations.* Bone Rep, 2017. **6**: p. 129-139.

5. Kern, C., et al., *Investigation of strontium transport and strontium quantification in cortical rat bone by time-of-flight secondary ion mass spectrometry.* J R Soc Interface, 2019. **16**(151): p. 20180638.

6. Malekar, S.A., et al., *Radio Frequency-Activated Nanoliposomes for Controlled Combination Drug Delivery.* AAPS PharmSciTech, 2015. **16**(6): p. 1335-43.

7. Wang, Q., et al., *Recent advances on smart TiO2 nanotube platforms for sustainable drug delivery applications.* Int J Nanomedicine, 2017. **12**: p. 151-165.

8. Li, Y., et al., *Surface Immobilization of TiO2 Nanotubes with Bone Morphogenetic Protein-2 Synergistically Enhances Initial Preosteoblast Adhesion and Osseointegration.* Biomed Res Int, 2019. **2019**: p. 5697250.

Statement of Authorship

Title of Paper	Characterization of drug-release kinetics in trabecular bone from titania nanotube implants
Publication Status	☑ Published ☐ Accepted for Publication ☐ Submitted for Publication ☐ Unpublished and Unsubmitted work written in manuscript style
Publication Details	Aw, M. S., Khalid, K. A., Gulati, K., Atkins, G. J., Pivonka, P., Findlay, D. M., & Losic, D. (2012). Int J Nanomedicine, 7, 4883-4892. DOI:10.2147/ijn.s33655

Principal Author

Name of Principal Author (Candidate)	Kamarul Ariffin Khalid		
Contribution to the Paper	Designed the study, development of methods, performed the experiments and analysis of the results, interpreted the data and critically revised the manuscript.		
Overall percentage (%)	40%		
Certification:	This paper reports on original research I conducted during the period of my Higher Degree by Research candidature and is not subject to any obligations or contractual agreements with a third party that would constrain its inclusion in this thesis. I am the primary author of this paper.		
Signature		Date	23 July 2019

Co-Author Contributions

By signing the Statement of Authorship, each author certifies that:

i. the candidate's stated contribution to the publication is accurate (as detailed above);

ii. permission is granted for the candidate in include the publication in the thesis; and

iii. the sum of all co-author contributions is equal to 100% less the candidate's stated contribution.

Name of Co-Author	Moom Sinn Aw		
Contribution to the Paper	Contributed to design of the study, development of methods, performed the experiments, data analysis and wrote the manuscript (Principal Supervisor signed on behalf of M.S.Aw due to the author moving institutions and proving uncontactable)		
Signature		Date	29/07/2019

Name of Co-Author	Karan Gulati		
Contribution to the Paper	Contributed to perform the experiments and critically revised the manuscript.		
Signature		Date	29/07/2019

Name of Co-Author	Gerald J Atkins		
Contribution to the Paper	Designed the study, interpreted the data, provided overall supervision and wrote the manuscript.		
Signature		Date	29/07/2019

Name of Co-Author	Peter Pivonka		
Contribution to the Paper	Designed the study, interpreted the data and drafted the manuscript.		
Signature		Date	29/07/2019

Name of Co-Author	David M Findlay		
Contribution to the Paper	Designed the study, interpreted the data, provided overall supervision, wrote the manuscript and acted as corresponding author.		
Signature		Date	24/07/2019

Name of Co-Author	Dusan Losic		
Contribution to the Paper	Designed the study, interpreted the data, provided overall supervision, wrote the manuscript and acted as corresponding author.		
Signature		Date	25/07/2019

International Journal of Nanomedicine

Dovepress

open access to scientific and medical research

Open Access Full Text Article

ORIGINAL RESEARCH

Characterization of drug-release kinetics in trabecular bone from titania nanotube implants

This article was published in the following Dove Press journal:
International Journal of Nanomedicine
11 September 2012
Number of times this article has been viewed

Moom Sinn Aw[1]
Kamarul A Khalid[2,3]
Karan Gulati[1]
Gerald J Atkins[2]
Peter Pivonka[4]
David M Findlay[2]
Dusan Losic[1]

[1]School of Chemical Engineering, [2]Discipline of Orthopaedics and Trauma, The University of Adelaide, Adelaide, SA, Australia; [3]Department of Orthopaedics, Traumatology and Rehabilitation, Faculty of Medicine, International Islamic University Malaysia, Kuantan, Pahang, Malaysia; [4]Engineering Computational Biology Group, School of Computer Science and Software Engineering, The University of Western Australia, Perth, WA, Australia

Correspondence: Dusan Losic
School of Chemical Engineering,
The University of Adelaide, Adelaide,
SA 5005, Australia
Tel +61 8 8302 6862
Fax +61 8 8302 3683
Email dusan.losic@adelaide.edu.au

David M Findlay
Level 4, Bice Building
Royal Adelaide Hospital
The University of Adelaide
SA 5005, Australia
Tel +61 8 8222 5621
Fax +61 8 8232 3065
Email david.findlay@adelaide.edu.au

Purpose: The aim of this study was to investigate the application of the three-dimensional bone bioreactor for studying drug-release kinetics and distribution of drugs in the ex vivo cancellous bone environment, and to demonstrate the application of nanoengineered titanium (Ti) wires generated with titania nanotube (TNT) arrays as drug-releasing implants for local drug delivery

Methods: Nanoengineered Ti wires covered with a layer of TNT arrays implanted in bone were used as a drug-releasing implant. Viable bovine trabecular bone was used as the ex vivo bone substrate embedded with the implants and placed in the bone reactor. A hydrophilic fluorescent dye (rhodamine B) was used as the model drug, loaded inside the TNT–Ti implants, to monitor drug release and transport in trabecular bone. The distribution of released model drug in the bone was monitored throughout the bone structure, and concentration profiles at different vertical (0–5 mm) and horizontal (0–10 mm) distances from the implant surface were obtained at a range of release times from 1 hour to 5 days.

Results: Scanning electron microscopy confirmed that well-ordered, vertically aligned nanotube arrays were formed on the surface of prepared TNT–Ti wires. Thermogravimetric analysis proved loading of the model drug and fluorescence spectroscopy was used to show drug-release characteristics in-vitro. The drug release from implants inserted into bone ex vivo showed a consistent gradual release of model drug from the TNT–Ti implants, with a characteristic three-dimensional distribution into the surrounding bone, over a period of 5 days. The parameters including the flow rate of bone culture medium, differences in trabecular microarchitecture between bone samples, and mechanical loading were found to have the most significant influence on drug distribution in the bone.

Conclusion: These results demonstrate the utility of the Zetos™ system for ex vivo drug-release studies in bone, which can be applied to optimize the delivery of specific therapies and to assist in the design of new drug delivery systems. This method has the potential to provide new knowledge to understand drug distribution in the bone environment and to considerably improve existing technologies for local administration in bone, including solving some critical problems in bone therapy and orthopedic implants.

Keywords: local drug delivery, Zetos bone bioreactor, drug-releasing implant, drug diffusion

Introduction

Bone diseases are a major health problem worldwide. They have a highly deleterious effect on both quality of life for patients and health expenditure, representing at least 10% of annual health care expenditure in many developed countries.[1] A number of therapeutic approaches have been developed to treat bone diseases, and these

are dominated by the use of systemic drug administration. However, conventional systemic drug therapies have many limitations, both in general and in bone, such as low efficacy, poor bioavailability and biodistribution, lack of selectivity, and drug overdose and toxicity in nontarget tissues.[2,3] To overcome these limitations, increase drug effectiveness, and reduce systemic side effects of drugs, localized delivery of therapeutics to bone has been recognized as a promising alternative.[4,5] Local drug delivery offers many potential advantages, leaving healthy cells or adjacent tissues at other sites unaffected and avoiding serious side effects, providing locally optimal concentrations of often expensive drugs without diluting them across the entire body, and optimizing bioavailability, without rapid breakdown and clearance of drugs, particularly through the liver uptake.[6]

The concept of a skeletal drug delivery system was first introduced by Buchholz et al[7] in the 1970s and has been extensively explored since. The development of biocompatible drug-releasing materials and appropriate models to study drug release from these systems, and their effectiveness in bone prior to in vivo study, are recognized as critical issues to be addressed.[8,9] Numerous biomaterials, either natural or synthetic, and either biodegradable or biologically inert, such as polymethyl methacrylate, poly(lactic-co-glycolic acid), collagen, hyaluronan, chitosan, fibrin, silk, hydroxyapatite, ceramics and injectable calcium phosphate cements, in the form of membranes, granules, hydrogels, matrices, coatings, fibers, sponges, and foams, have been explored in recent years as implants for the delivery of bone active agents.[10–15] These materials are mostly amorphous, with a large variation of porosity and nonreproducible preparation, which in turn makes the bone therapy nonreproducible.[15] In most cases, these implants are designed for the delivery of specific drugs and do not have the flexibility to be applied to a wide range of therapeutic agents, such as water-insoluble drugs, drug carriers, or labile agents (proteins and genes). To address these disadvantages, several new nanosynthetic and surface-engineered approaches have been applied for the development of advanced drug-releasing materials and devices with controllable pore size, porosity, and surface functionality at the nanoscale level.[5,6,16] Among them, titania nanotube (TNT) arrays, generated on titanium (Ti) surfaces by self-ordered electrochemical anodization, are recognized as a particularly promising solution.[17,18] TNTs have been proven to have many favorable features, including biocompatibility, excellent integration with bone tissue, an ability to promote the growth of hydroxyapatite, high surface area, controllable pore dimensions, surface chemistry, chemical stability, and mechanical rigidity.[18–21]

The second issue of local drug delivery in bone is that most studies of drug release relevant to bone therapies have been performed using in vitro conditions, where the drug-loaded implant is interfaced with the solution (buffer) or with cultured bone cells. However, bone is a complex porous material consisting of a solid bone matrix and pore spaces. Two types of bone can be distinguished: compact (or cortical) bone with small pore spaces (Haversian canals) and spongy (or cancellous) bone with large pore spaces filled with bone marrow. The three major types of bone cells are osteoblasts, osteoclasts, and osteocytes.[22] It is not known how drug release in solution relates to drug release in bone tissues, given that cancellous bone is a highly hydrated tissue, with abundant interstitial fluid surrounded by marrow with a high fat content.[5,23] Hence, in order to evaluate the potential of local drug delivery systems, the authors sought a suitable system. Because studies in live bone tissue in situ are technically difficult and expensive, the use of an ex vivo bone bioreactor, consisting of a trabecular bone explant, was explored as a suitable alternative. Recently, several three-dimensional (3D) bone reactors have been developed and explored to study the biological aspect of bone cell behavior and bioengineering of bone tissues, including the Zetos system.[23–25] The Zetos system, devised by David Jones (Department of Experimental Orthopaedics and Biomechanics, Philipps University of Marburg, Marburg, Germany) and Everett Smith (Medical Sciences Center, Madison, WI), enables discs of cancellous bone to be maintained for at least 3 weeks by continuous perfusion with culture medium and daily loading with physiologically relevant strains.[24–26]

The aim of this study was to assess the Zetos bone bioreactor for ex vivo study of drug distribution in bone and to demonstrate the application of nanoengineered Ti wires generated with TNT arrays (TNT–Ti wires) as drug-releasing implants for local drug delivery (Figure 1A and B). The TNT layer is composed of an array of highly ordered, vertically aligned nanotubes with the capacity to accommodate and release a considerable amount of drug.[18–20] In previous work, the authors have developed TNT–Ti wires with advanced properties to provide extended and sustained drug release with zero-order kinetics, multidrug delivery with sequential or delayed release, and stimuli-responsive release of drugs using a magnetic field.[27–31] In the present study, the TNT–Ti wires were loaded with the fluorescence dye (rhodamine B [RhB]) as a model drug and inserted into the middle of trabecular bone discs (Figure 1C), which were placed inside the bone bioreactor with continuous perfusion of culture medium (Figure 1D). The Xenogen IVIS® 100 BioPhotonic Imaging®

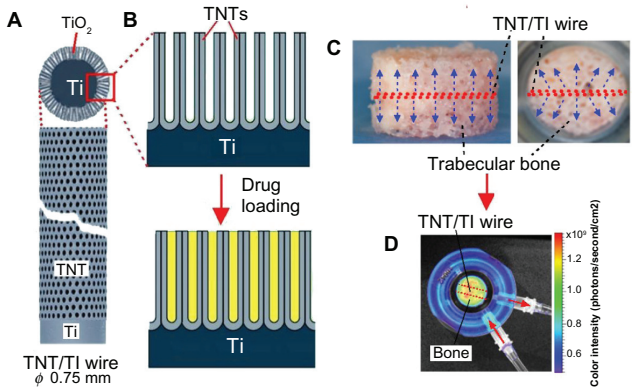

Figure 1 (**A**) Diagram of a titanium (Ti) wire with titania nanotube (TNT) arrays on the surface as a drug-releasing implant; (**B**) diagram of the TNT arrays formed by anodization of the Ti wire and the drug loading inside these nanotubes; (**C**) trabecular bone with the embedded TNT–Ti implant indicated in the center of the bone core (side and top views); (**D**) bioluminescence image of the bone core and the embedded TNT–Ti implant inside the perfusion chamber – the distribution of released drug inside the bone is also shown.
Abbreviation: TiO_2, titanium dioxide.

system (Caliper Life Sciences, Inc, Hopkinton, MA) was used to monitor in vivo drug release and distribution inside the bone matrix over time (from 1 hour to 5 days). The purpose was to demonstrate the capacity of the Xenogen system to provide in situ measurements of drug release from the implant and to determine the 3D spatial distribution of drugs in bone, the drug-release rate, and drug-release kinetics.

Materials and methods

Materials

Alfa Aesar (Ward Hill, MA) supplied the Ti (99.99%) wires (diameter 0.75 mm). Ethylene glycol, acetone, ammonium fluoride, and RhB ($C_{28}H_{31}ClN_2O_3$, with 97% dye content) were obtained from Sigma-Aldrich Pty Ltd (Sydney, Australia) and used without further purification. High-purity, ultra-grade Milli-Q® water (18.2 MΩcm resistivity) (EMD Millipore Corporation, Billerica, MA) with additional filtration (0.22 µm) was used for the preparation of all reagents.

Preparation of TNT–Ti wires as drug-releasing implants

Ti wires were cut to size (approximately 10 mm in length), polished, cleansed ultrasonically with acetone, rinsed thoroughly with deionized Milli-Q water, and air-dried. TNT layers were then prepared by a two-step electrochemical anodization of Ti wires in ammonium fluoride/ethylene glycol electrolyte (3% water and 0.3% ammonium fluoride) at 20°C, using a constant voltage of 100 V for 1 hour, as described previously.[32–34] Both pore diameter and length of the TNTs were determined by selecting the appropriate voltage (100 V) and anodization time (1 hour).

Structural characterization of prepared TNT–Ti wires

Structural characterization of the prepared TNT–Ti wires was performed before and after drug loading and drug-release experiments in bone using a field emission scanning electron microscope (SEM) (Philips XL 30; Philips Research Eindhoven, Eindhoven, The Netherlands). The samples were cut into small pieces, (approximately 5 mm in length) mounted on a holder with double-sided conductive tape, and coated with a layer of platinum 3–5 nm thick. Images, with a range of scan sizes at normal incidence and at a 30° angle, were acquired from the top surface, the bottom surface, and cross-sections.

Loading of the model drug

RhB, the model drug in this study, was dissolved in water (50 mg/mL) and used for loading into the TNT–Ti wires. TNT–Ti wires cut into 8 mm lengths were fully immersed in the RhB solution to ensure drugs were entirely loaded inside the nanotubes. The wires were rotated every 2–4 hours during RhB deposition. After 1–3 days of loading, the wires were removed, dried in air, and then kept under vacuum for 2 hours. Finally, to remove the excess of loaded drug from the TNT surfaces, samples were gently cleaned with a soft tissue after wetting with a small amount of phosphate buffered saline (pH 7.2). The wires were sterilized using low-temperature hydrogen peroxide gas plasma (Sterrad® 100NX™ System, Advanced Sterilization Products (ASP),Division of Ethicon Inc, a Johnson & Johnson company, Irvine, CA).

Quantification of drug loading

To quantify the amount of RhB loaded into the TNT–Ti wires, thermogravimetric analysis (TGA), which measures the mass change (weight loss) in a sample as a function of temperature, was performed using a Hi-Res Modulated TGA 2950 (TA Instruments, New Castle, DE). The drug-loaded TNT–Ti wire was mounted on the platinum pan and heated from room temperature (at 20°C) to 800°C in a furnace at a scanning rate of 10°C per minute under a nitrogen gas flow of 50 mL per minute. To find the correct decomposition range and peak of RhB model drugs, TGA of the pure RhB was performed in separate experiments. A thermogram showing a decrease in weight was identified from the TGA software (Q Series Thermal Analysis, Universal Analysis 2000; TA Instruments) and was used to calculate the loaded amount of RhB.

Preparation of bovine trabecular bone cores

The sternum of a 16-month-old steer was harvested from the freshly slaughtered animal and kept in cold sterile saline (0.85%) prior to processing. All soft tissues were removed from the sternum, which was then manually cut into sagittal sections using a hacksaw. Care was taken to maintain the sterility and viability of the samples at all times. Prepared sections were kept immersed in a prewash medium, consisting of high-glucose Dulbecco's Modified Eagle Medium (Life Technologies Corporation, Carlsbad, CA), with 20 mM of 4-(2-hydroxyethyl)-piperazineethanesulfonic acid, 2.4 mg/mL of benzylpenicillin, 3.2 mg/mL of gentamicin sulfate, and 4 µg/mL of amphotericin B. Bone cylinders, 10 mm in diameter, were prepared from the bone sections using an industrial drilling machine (Model G0517 Mill/Drill, Grizzly Industrial®, Inc, Muncy, PA) and a custom-made diamond drill bit (Figure 2A). Bone samples were continually immersed in cold sterile saline (0.85%) on a custom-made polyoxymethylene drilling jig to prevent desiccation and/or thermal necrosis. The bone cylinders were mounted onto a custom-made platform and milled to a 5 mm thickness using a 10 mm diameter tungsten carbide bit, with the bone pieces immersed throughout in cold sterile saline (0.85%). The resulting bone cores consisted of uniform trabecular bone without any visible cartilage. All bone cores had the marrow removed by washing under pressure using a dental water jet (WP-450A; Water Pik, Inc, Fort Collins, CO). The bone cores were stored in the prewash medium at 4°C prior to use.

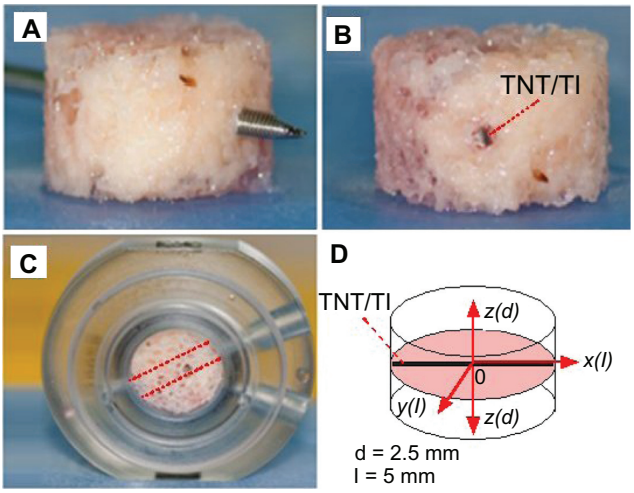

Figure 2 Steps for preparation of bovine trabecular bone cores for ex vivo studies using the Zetos three-dimensional bone bioreactor: (**A**) bone core with marrow removed and a hole in the center drilled with a surgical Kirschner wire; (**B**) drug-releasing implant, based on a titanium (Ti) wire with titania nanotube (TNT) arrays on the surface, embedded in the center of the bone; (**C**) the bone core with implant placed inside the chamber with the same orientation (angle) to the flow of prelusion medium into the bone; (**D**) diagram of bone core showing inserted implant in the middle and the directions (with different axes) used to monitor drug concentration.
Note: In this work, only drug distribution from the central point of the implant (0) at the bottom vertical plane (*x*-*z*) and the horizontal plane (*x*-*y*) is presented.

In vitro drug release from TNT–Ti implants

The RhB-loaded TNT–Ti wires were immersed in 5 mL of phosphate buffered saline (pH 7.2) at room temperature and an in vitro drug-release study was performed, using a procedure described previously.[27] Briefly, aliquots of buffer solution were analyzed every 5–15 minutes and then twice daily until the release reached completion. The aliquots were placed in a quartz cuvette and the concentration of released RhB was measured using a Cary Eclipse fluorescence spectrophotometer (Varian, Inc, Palo Alto, CA) with excitation and emission wavelengths of 510 and 625 nm, respectively.

Insertion of TNT–Ti wires into the bovine bone cores

A hole was drilled through each bone core using a sterilized 1.1 mm diameter Kirschner wire (surgical grade stainless steel sharp pin) (Figure 2A). A TNT–Ti wire was carefully inserted into the hole, fitting tightly into the center of the bone core (Figure 2B), and the bone was secured in the custom-made culture chamber, as shown in Figure 2C. The orientation of the implants inside the bones connected to the inlets and outlets of the bioreactor was kept the same for all samples (Figure 2C). Bone cores were then loaded into the sterile perfusion chambers that were compatible with the Zetos™ loading system (Figure 3). The study was performed with and without different mechanical loading, but only results without loading have been presented, because of data congestion.

Ex vivo drug release in trabecular bone

Six trabecular bone cores, four with TNT–Ti wires loaded with RhB and two with TNT–Ti wires without RhB, were prepared and perfused with culture medium during the course of this study. The study was performed in triplicate. The 3D bone bioreactor comprises a set of cross-flow culture chambers, allowing a constant perfusion of bone samples with culture medium at a rate of 7 mL per hour (Figure 3). The entire apparatus was maintained at 37°C. The color intensity of the dye from the TNT–Ti wires and into the bone core was measured at 1, 4, and 24 hours and 4 and 5 days (Figure 1D) using the Xenogen IVIS 100 (In vivo imaging system). This measurement provided an accurate estimate of the amount of dye released, as this amount is directly proportional to

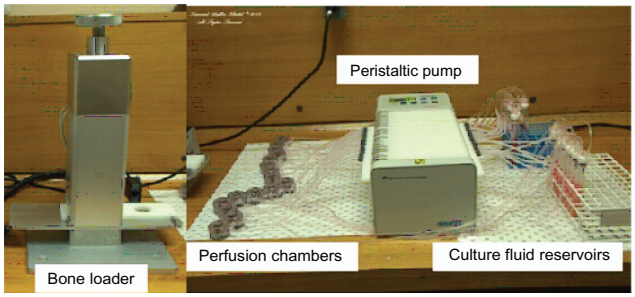

Figure 3 The Zetos three-dimensional bone bioreactor (devised by David Jones [Department of Experimental Orthopaedics and Biomechanics, Philipps University of Marburg, Marburg, Germany] and Everett Smith [University of Wisconsin, WI]) used for the ex vivo study of drug distribution inside trabecular bone.

the color intensity (photons/second/cm2). The luminescence imaging mode was set at an exposure time of 1 minute, with medium-size binning, open emission filter, and 25 cm view field. The dimension of the pixel count was 2 × 2 (width by height), with a subject area of 0.76 cm^2. The photon count rate per unit area, based on the control samples with dye and no dye, was used as the benchmark for the diffusion measurement in terms of the time and spatial distance across the bone. The drug concentration values from the collected images were obtained by calibration, using the known concentration of the model drug on the TNT–Ti wire surface and the control wire with no drug. The parameter mass flux ($mg/cm^2 \cdot$ second) was calculated from the number of photons collected as the RhB dye passed through a unit area by a linear conversion of units. Molar flux ($mol/cm^2 \cdot$ second), mass flow (mg/second), and volumetric flow rate (mL/second) can also be derived from the primary data available from the results. From these images, the values of drug concentration in bone at different distances along the *x*, *y*, and *z* axes from the center of the bone (position of the implant) over time (from 1 hour to 5 days) were obtained. These results can be used to create 3D drug distribution graphs, but in this study only two-dimensional concentration profiles in the horizontal and vertical directions from the TNT–Ti implant surface are presented to demonstrate the capability of the system.

Results and discussion

Structural characterization of TNT–Ti wires

The structure of prepared TNT–Ti wires was characterized by SEM and the typical morphology of the wires is summarized in Figure 4. Figure 4A shows the whole TNT–Ti wire (12 mm) (inset) and a low-resolution SEM image confirming the growth of a TNT film on the curved surface of the Ti wire. The SEM image shows randomly dispersed vertical

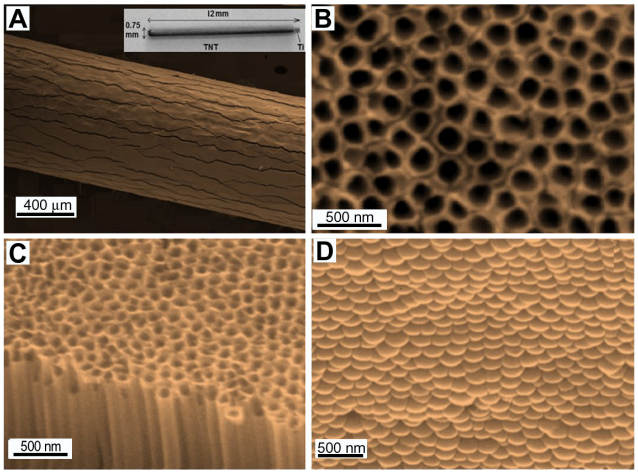

Figure 4 Scanning electron microscope images of (**A**) a drug-releasing implant based on a titanium (Ti) wire with titania nanotube (TNT) arrays on the surface (whole wire shown in inset), (**B**) the top surface of the TNTs, (**C**) a cross-sectional view showing hollow nanotube structures, and (**D**) the bottom surface, showing closed ends of the nanotube structures (the TNT layer was removed from the underlying Ti for imaging purposes).

cracks across the entire length of the wire, caused by the radial growth of TNTs on the curved surface and mechanical stress through volume expansion. These cracks have not been observed on TNT films grown on planar Ti surfaces. However, the generation of TNTs on wire did not significantly change the original mechanical stability and adherence of the TNT layer on Ti. High-resolution SEM images of the top surface, cross-section, and bottom surface of the TNT layer show a vertically aligned and densely packed array of uniform nanotubes, with diameters of 140 ± 10 nm and lengths of 50 ± 2 µm, across the entire structure (Figure 4B–D). TNT–Ti wires occupy a very small amount of space and are easy to implant into bone and be removed. These features show many advantages for implantable orthopedic applications in comparison with existing commercial bone implants such as polymer gels and bone cements.

The in vitro drug-release characterization

TGA was performed to determine the amount of drug loaded into the nanotubular structures of the TNT–Ti wires. A total RhB loading of 0.27 mg was found per 8 mm length of TNT–Ti wire. However, the drug loading of TNT–Ti wires can be optimized by selecting appropriate TNT dimensions and applying surface modifications.[35] Thus, it is possible to customize TNT–Ti platforms to meet specific requirements for implantable drug delivery in bone, depending on the required dosage, properties of drugs, and proposed bone therapy (infections, bone cancer, and so forth).

In vitro drug release of the model drug (RhB) loaded into the TNT–Ti wires in buffer solution is presented in Figure 5. The drug-release kinetics can be described in two phases, the first phase showing an initial burst release during the first 6 hours, followed by the second phase with a slow release of the remaining drug. The initial burst denoted by the straight portion of the curve, with a release of about 65% in buffer solution, is regarded as a first-order release. The fast initial release accounts for the fast diffusion of the drug molecules physisorbed on the top and upper parts of the TNTs. In the second phase, drug release from the TNT–Ti implant was very slow and underwent a linearly increasing cumulative release over a period of 3 days. The release mechanism of this phase is controlled by diffusion from the long nanotube structures.[36,37] The best-fitting model for this phase was obtained using the Higuchi equation followed by the zero-order release, which describe drug release from an insoluble matrix.[38] The square root of a time-dependent process is based on the Fickian diffusion law, where the diffusion-controlled release rate of drug molecules decreases as a function of time due to a reduction in concentration gradient. The pharmaceutical dosage following a zero-ordered pattern is the ideal profile of drug release because it provides the same amount of drug elution per unit of time.[30] These results confirmed previous reports showing suitable drug-releasing characteristics of TNT–Ti implants as drug-releasing platforms for local drug delivery applications.[39,40] In the following section, the authors investigate the performance of the TNT–Ti implants when implanted in trabecular bone in a bioreactor environment.

The characterization of drug diffusion in trabecular bone ex vivo

The structure of bone is complex and is expected to have a significant impact on both drug-release kinetics and drug distribution in bone. Bioluminescence images created at different times (ie, 1, 4, 24, and 120 hours) for the 5-day experiment on drug-release studies using the Xenogen IVIS (in vivo imaging system) are presented in Figure 6. Results clearly show an increasing concentration of the model drug within the bone model. To demonstrate drug release in the 3D bone matrix, a series of drug concentration profiles were collected from these images. These profiles show the changes of drug concentration in bones across all directions (*x*, *y*, and *z* axes) from the TNT–Ti implant. To simplify the presentation of results, only two-dimensional concentration profiles of the drug in vertical (*x*-*z*) and horizontal (*x*-*y*) directions from the implant are presented in this work (Figure 7). The graphs show significant changes in RhB concentration in bone over time, confirming that both processes, ie, the diffusion of RhB from the TNT–Ti implants and the diffusion of RhB into bone, occurred. Initially, the release of RhB from the TNT–Ti implants followed burst release kinetics (Figure 5), and the highest concentration of RhB was observed at locations close to the implant surface, with zero concentration at greater distances from the implant. Over time, as more RhB was released, the concentration increased further from the implant, showing the spread of RhB across the bone tissue in all directions (results for only two directions, vertical and horizontal, are presented). After 4 and 5 days of release, the highest concentration was observed at the outer locations of the bone, which was 3.5–5 mm away from the surface of the implant, showing a concentration of nearly 15–20 µg. After 5 days of release, there was no measurable drug remaining in the TNT–Ti wires, as confirmed by TGA, which is consistent

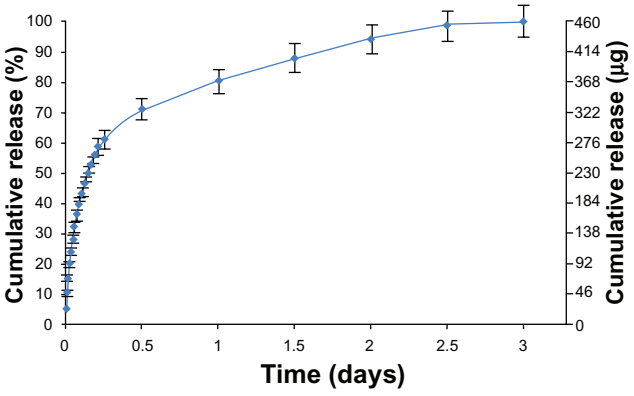

Figure 5 In vitro drug release from implants (based on titanium wires with titania nanotube arrays on their surfaces) into phosphate buffer.

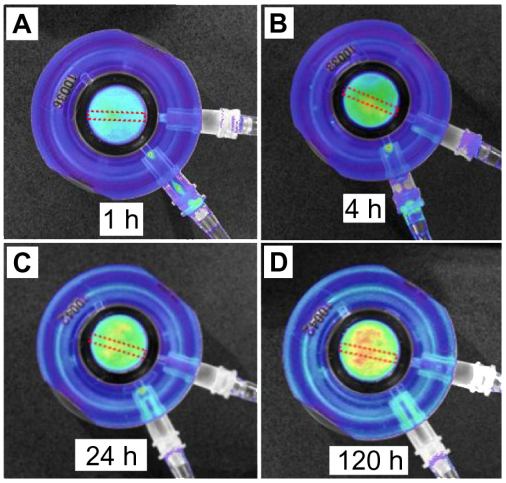

Figure 6 Bioluminescence images of bone with inserted drug-releasing implant (based on a titanium wire with titania nanotube arrays on the surface) for local drug delivery: distribution of released model drug (rhodamine B) taken at (**A**) 1, (**B**) 4, (**C**) 24, and (**D**) 120 hours (h) using the Xenogen IVIS® 100 (Caliper Life Sciences, Inc, Hopkinton, MA) in vivo imaging system.

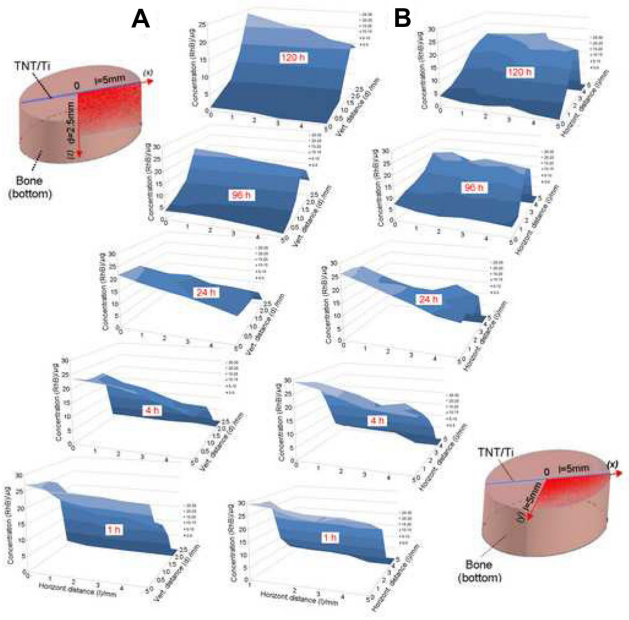

Figure 7 Two-dimensional concentration graphs of the model drug (rhodamine B [RhB]) released from implants based on titania nanotube (TNT) arrays on the surface of titanium (Ti) wires. The graphs show spatial distribution in the trabecular bone samples: drug distribution is presented at (**A**) the vertical (vert) plane (*x*-*z*) of the bottom part of the bone and (**B**) the horizontal (horizont) plane (*x*-*y*) from the implant surface at different release times (1, 4, 24, 96, and 120 hours [h]).
Note: The concentration changes are presented only for a selected area of bone (one quadrant), as illustrated in the bone diagrams (left and right).

with the diffusion of RhB into the bone tissue. The graphs also show that the spatial RhB distribution in bone is not uniform, which is likely explained by the variable nature of the internal bone microarchitecture and the influence of culture medium flow inside the bone chamber.[23]

The effects of perfusion of culture medium on the drug diffusion pattern

A continuous flow chamber with culture medium was used in the bone bioreactor to simulate in vivo conditions, mimicking bone fluid flow and maintaining bone viability. It is reasonable to expect that the flow of culture medium at the interface between bone and the TNT–Ti implant will influence the release kinetics of the drug from the TNTs and have a significant impact on drug distribution. To confirm the impact of flow on drug transport in the bone, the authors performed a control experiment without culture flow. The comparative concentration graphs obtained at different distances from the implant at vertical and horizontal directions unequivocally show a difference in diffusion kinetics when external flow is not applied (Figure 8). The drug concentration at both horizontal and vertical directions when perfusion was used was significantly greater than in static conditions, where drug distribution was generated not only by the free diffusion of the drug. This result suggests that the diffusion of drug in bone is a very slow process and should be considered in drug delivery for bone therapy where the access of a drug to bone sites without blood supply is required.

Data analysis of the concentration patterns of RhB in bone from a number of samples showed some unexpected differences and inconsistencies that cannot be linked to the influence of medium flow. The authors assumed these differences were attributed to differences in trabecular microarchitecture between bone samples; addressing this issue is outside the scope of this paper and will be presented in the next publication. When bone samples containing TNT–Ti implants were loaded by applying physiologically relevant mechanical strains, drug diffusion was increased (data not shown); these results will also be presented in a following publication. Therefore, bone loading, together with the presence of the vasculature, is likely to change the drug diffusion kinetics, although in vivo models will be required to fully investigate drug release and diffusion in situ.

The ex vivo study of drug-release kinetics in a 3D bone environment

Finally, to demonstrate the utility of the Zetos bone bioreactor for studying drug-release kinetics in bones, two examples showing changes of cumulative drug release in bone over time are presented in Figure 9. The graphs show cumulative drug release in bone over a period of time (from 1 hour to 5 days) at three different distances in vertical (z) and horizontal (x) directions from the surface of the TNT–Ti implant. The drug-release kinetics in buffer solution showed significant differences compared with release from TNT–Ti implants in the ex vivo bone. An initial burst release (6 hours), with 65% of the cumulative release and the first-order release kinetics, was observed for in vitro release of RhB into the buffer solution (Figure 5). In comparison, ex vivo release in bone showed considerably lower initial release (<20%), without burst release. Drug release over this time was slow, with a continuous and gradual cumulative increase over time. This behavior is likely governed by the diffusion of drug from the TNTs, flow rate of culture medium at the TNT–Ti interface, and flow rate of culture medium across the bone. The release pattern of drug inside the bone follows first-order kinetics in all directions from the implant surface, but some anomalies were shown after 3 days in the vertical direction ($z = 0$). This is possibly the result of the accumulation of RhB at the edge of the bone sample. At this stage, the authors cannot quantitatively explain the drug-release

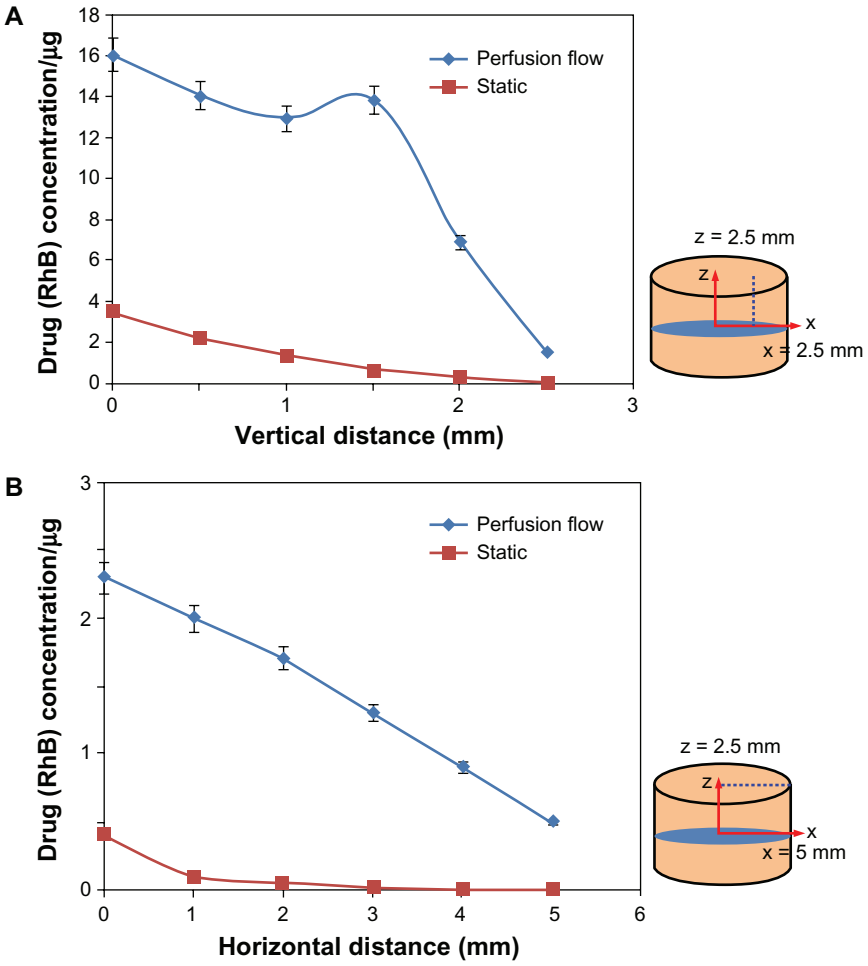

Figure 8 Influence of the physiological solution (culture medium) flow rate in the bone bioreactor on the distribution of the model drug (rhodamine B [RhB]) released from implants based on titania nanotube arrays on the surface of titanium wires. The flow rate of 7 mL/hour was compared with the static condition (no flow) after 24 hours of drug release. The bone diagrams on the right indicate the locations at (**A**) horizontal (5 mm) and (**B**) vertical distances (2.5 mm) from the surface of the implant where concentration measurements were taken.

kinetics and transport of the model drug in the trabecular bone samples, owing to the complex interactions of transport mechanisms, including the diffusive and advective components. The importance of this current study is to demonstrate the capability of the ex vivo bone system to generate valuable experimental data. These data can not only be used to define the transport kinetics of drugs in bone but also to optimize drug-release characteristics of bone implants using TNT technology. Future work will include a statistical analysis of repeated experiments, the

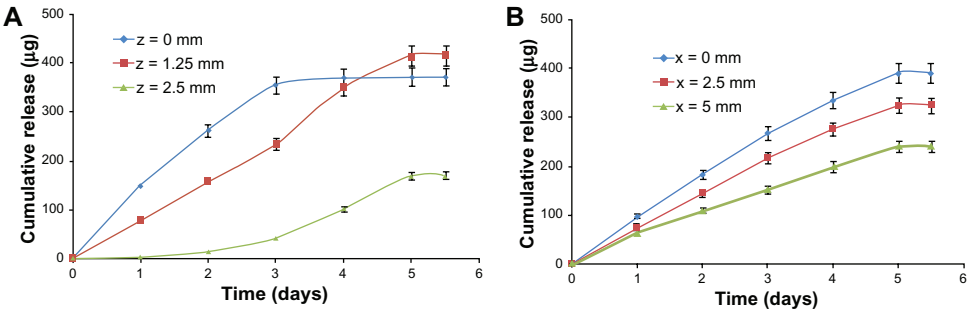

Figure 9 Cumulative release of the model drug (rhodamine B) from drug-releasing implants (based on titania nanotube arrays on the surface of titanium wires) in trabecular bone, showing changes of concentration at different times (from 1 hour to 5 days). The concentration changes over time are presented for selected locations at (**A**) vertical (*x*-*z*) and (**B**) horizontal (*x*-*y*) distances from the surface of the implant.

influence of flow rate, mechanical loading, an optimization of the design of the bioreactor.

Conclusion

In summary, the concept of using a Zetos three-dimensional bone bioreactor as a characterization tool for the ex vivo study of drug-release kinetics and drug distribution in bone was introduced. Viable bovine trabecular bone was used as the ex vivo bone substrate embedded with a drug-releasing implant based on nanoengineered Ti wires covered with a layer of TNT arrays. The utility of the Zetos system for studying drug-release kinetics and transport of drugs in bones is demonstrated for the first time. Successful ex vivo experiments lead to the conclusion that the release pattern and molecular disposition of drugs can be precisely estimated in the bone core with respect to time and location, showing the potential of this technology to predict a real drug concentration and distribution in bone, which is not possible with existing in vitro models. This method has the potential to provide new knowledge to understand drug distribution in complex bone environment and to considerably improve existing technologies for local administration in bone, including solving some critical problems in bone therapy and orthopedic implants. TNT–Ti wire can be considered as a safe drug-releasing implant for localized drug delivery in bone with the potential for clinical application in a range of bone therapies, including those for bone infection, bone inflammation, and bone cancer.

Acknowledgments

The authors gratefully acknowledge the financial support of the Australian Research Council (DP 120101680) and the National Health and Medical Research Council (ID 565375). DL receives funding from the Australian Research Council as a Future Fellow (FT110100711). KAK receives funding from the International Islamic University Malaysia and the Malaysian Government.

Disclosure

The authors report no conflicts of interest in this work.

References

1. Rodan GA, Martin TJ. Therapeutic approaches to bone diseases. *Science*. 2000;289(5484):1508–1514.
2. Mainardes RM, Silva LP. Drug delivery systems: past, present, and future. *Curr Drug Targets*. 2004;5(5):449–455.
3. LaVan DA, McGuire T, Langer R. Small-scale systems for in vivo drug delivery. *Nat Biotechnol*. 2003;21(10):1184–1191.
4. Jain AK, Panchagnula R. Skeletal drug delivery systems. *Int J Pharm*. 2000;206(1–2):1–12.
5. Porter JR, Ruckh TT, Popat KC. Bone tissue engineering: a review in bone biomimetics and drug delivery strategies. *Biotechnol Prog*. 2009; 25(6):1539–1560.
6. Wu P, Grainger DW. Drug/device combinations for local drug therapies and infection prophylaxis. *Biomaterials*. 2006;27(11):2450–2467.
7. Buchholz HW, Elson RA, Engelbrecht E, Lodenkämper H, Röttger J, Siegel A. Management of deep infection of total hip replacement. *J Bone Joint Surg Br*. 1981;63-B(3):342–353.
8. Soundrapandian C, Sa B, Datta S. Organic-inorganic composites for bone drug delivery. *AAPS Pharm Sci Tech*. 2009;10(4):1158–1171.
9. Simchi A, Tamjid E, Pishbin F, Boccaccini AR. Recent progress in inorganic and composite coatings with bactericidal capability for orthopaedic applications. *Nanomedicine*. 2011;7(1):22–39.
10. Zhao L, Chu PK, Zhang Y, Wu Z. Antibacterial coatings on titanium implants. *J Biomed Mater Res B Appl Biomater*. 2009;91(1):470–480.
11. Tran PA, Sarin L, Hurt RH, Webster TJ. Opportunities for nanotechnology-enabled bioactive bone implants. *J Mater Chem*. 2009;19:2653–2659.
12. Zilberman M, Elsner JJ. Antibiotic-eluting medical devices for various applications. *J Control Release*. 2008;130(3):202–215.
13. Lewis G. Alternative acrylic bone cement formulations for cemented arthroplasties: present status, key issues, and future prospects. *J Biomed Mater Res B Appl Biomater*. 2008;84(2):301–319.
14. Arcos D, López-Noriega A, Ruiz-Hernández E, Terasaki O, Vallet-Regí M. Ordered mesoporous microspheres for bone grafting and drug delivery. *Chem Mater*. 2009;21(6):1000–1009.
15. Hoppe A, Güldal NS, Boccaccini AR. A review of the biological response to ionic dissolution products from bioactive glasses and glass-ceramics. *Biomaterials*. 2011;32(11):2757–2774.
16. Liu H, Webster TJ. Nanomedicine for implants: a review of studies and necessary experimental tools. *Biomaterials*. 2007;28(2):354–369.
17. Ghicov A, Schmuki P. Self-ordering electrochemistry: a review on growth and functionality of TiO(2) nanotubes and other self-aligned MO(x) structures. *Chem Commun (Camb)*. 2009;(20): 2791–2808.
18. Losic D, Simovic S. Self-ordered nanopore and nanotube platforms for drug delivery applications. *Expert Opin Drug Deliv*. 2009;6(12): 1363–1381.
19. Roy P, Berger S, Schmuki P. TiO(2) nanotubes: synthesis and applications. *Angew Chem Int Ed Engl*. 2011;50(13):2904–2939.
20. Popat KC, Eltgroth M, LaTempa TJ, Grimes CA, Desai TA. Titania nanotubes: a novel platform for drug-eluting coatings for medical implants? *Small*. 2007;3(11):1878–1881.
21. Rani S, Roy SC, Paulose M, et al. Synthesis and applications of electrochemically self-assembled titania nanotube arrays. *Phys Chem Chem Phys*. 2010;12(12):2780–2800.
22. Sikavitsas VI, Temenoff JS, Mikos AG. Biomaterials and bone mechanotransduction. *Biomaterials*. 2001;22(19):2581–2593.
23. Davies CM, Jones DB, Stoddart MJ, et al. Mechanically loaded ex vivo bone culture system 'Zetos': systems and culture preparation. *Eur Cell Mater*. 2006;11:57–75.
24. David V, Guignandon A, Martin A, et al. Ex vivo bone formation in bovine trabecular bone cultured in a dynamic 3D bioreactor is enhanced by compressive mechanical strain. *Tissue Eng Part A*. 2008;14(1): 117–126.
25. Endres S, Kratz M, Wunsch S, Jones DB. Zetos: a culture loading system for trabecular bone. Investigation of different loading signal intensities on bovine bone cylinders. *J Musculoskelet Neuronal Interact*. 2009;9(3): 173–183.
26. David V, Martin A, Lafage-Proust MH, et al. Mechanical loading down-regulates peroxisome proliferator-activated receptor gamma in bone marrow stromal cells and favors osteoblastogenesis at the expense of adipogenesis. *Endocrinology*. 2007;148(5):2553–2562.
27. Gulati K, Ramakrishnan S, Aw MS, Atkins GJ, Findlay DM, Losic D. Biocompatible polymer coating of titania nanotube arrays for improved drug elution and osteoblast adhesion. *Acta Biomater*. 2012;8(1): 449–456.

28. Simovic S, Losic D, Vasilev K. Controlled drug release from porous materials by plasma polymer deposition. *Chem Commun (Camb)*. 2010; 46(8):1317–1319.
29. Aw MS, Addai-Mensah J, Losic D. A multi-drug delivery system with sequential release using titania nanotube arrays. *Chem Commun (Camb)*. 2012;48(27):3348–3350.
30. Aw MS, Simovic S, Addai-Mensah J, Losic D. Polymeric micelles in porous and nanotubular implants as a new system for extended delivery of poorly soluble drugs. *J Mater Chem*. 2011;21:7082–7089.
31. Aw MS, Addai-Mensah J, Losic D. Magnetic-responsive delivery of drug-carriers using titania nanotube arrays. *J Mater Chem*. 2012;22: 6561–6563.
32. Vasilev K, Poh Z, Kant K, Chan J, Michelmore A, Losic D. Tailoring the surface functionalities of titania nanotube arrays. *Biomaterials*. 2010;31(3):532–540.
33. Kant K, Losic D. A simple approach for synthesis of TiO(2) nanotubes with through-hole morphology. *Phys Status Solidi RRL*. 2009;3(5): 139–141.
34. Gulati K, Aw MS, Losic D. Drug-eluting Ti wires with titania nanotube arrays for bone fixation and reduced bone infection. *Nanoscale Res Lett*. 2011;6:571.
35. Popat KC, Leoni L, Grimes CA, Desai TA. Influence of engineered titania nanotubular surfaces on bone cells. *Biomaterials*. 2007;28(21): 3188–3197.
36. Roy P, Kim D, Lee K, Spiecker E, Schmuki P. TiO(2) nanotubes and their application in dye-sensitized solar cells. *Nanoscale*. 2010;2(1):45–59.
37. Wang S. Ordered mesoporous materials for drug delivery. *Micropor Mesopor Mater*. 2009;117(1–2):1–9.
38. Singhvi G, Singh M. Review: in-vitro drug release characterization models. *Int J Pharm Studies Res*. 2011;2(1):77–84.
39. Alpaslan E, Ercan B, Webster TJ. Anodized 20 nm diameter nanotubular titanium for improved bladder stent applications. *Int J Nanomedicine*. 2011;6:219–225.
40. Gulati K, Aw MS, Losic D. Nano-engineered Ti wires for local delivery of chemotherapeutics in brain. *Int J Nanomedicine*. 2012;7: 2069–2076.

CHAPTER 4. Recombinant sclerostin antagonizes effects of ex vivo mechanical loading in trabecular bone and increases osteocyte lacunar size

M. Kogawa, K. A. Khalid, A. R. Wijenayaka, R. T. Ormsby, A. Evdokiou, P. H. Anderson, D. M. Findlay, and G. J. Atkins

Biomedical Orthopaedic Research Group, Centre for Orthopaedic and Trauma Research, University of Adelaide, Adelaide, South Australia, Australia;

Discipline of Surgery, Breast Cancer Research Unit, Basil Hetzel Institute, University of Adelaide, Woodville, South Australia, Australia;

School of Pharmacy and Medical Sciences, University of South Australia, Adelaide, South Australia, Australia

American Journal of Physiology - Cell Physiology (2018); 314:C53-61,

Introduction

4.1 Summary of Chapter

In this chapter, the second generation Zetos™ system was used in conjunction with available *in vitro* methods to demonstrate the role of osteocytes in maintaining calcium homeostasis via the passive uptake of calcium by bone. Mechanical loading was shown to elevate the appropriation of calcium into the perilacunar matrix. This effect was diminished when exogenous sclerostin was added, whereby the osteocytes within the bone cores releases bone matrix resorption molecules through an as yet unknown mechanism. The findings elicited may represent either physiological or pathological processes but are likely pertinent to deducing sclerostin-targeting treatments mechanism of action.

4.2 Context and Contribution of Chapter

The work in this chapter represents an important addition to current knowledge on the role of osteocytes in bone and the effect of sclerostin on calcium uptake in the perilacunar matrix via osteocytic osteolysis. It adds to the evidence that osteocytes are able to rapidly increase the amount of calcium in the perilacunar matrix in response to mechanical loading, which results in increased mechanical strength of the bone. Conversely, sclerostin was demonstrated to act directly on osteocytes, causing it to catabolise the perilacunar matrix and blunting its response to mechanical loading. The published article has been cited in a few recent review publications on the actions of sclerostin on bone [1], physiological and pathological osteocytic osteolysis [2], and the study of osteocytes in native 3D matrix versus *in vitro* 2D models [3]. It was also cited in a recent paper that looked at trabecular bone loss after tibial plateau fractures in humans [4].

4.3 References

1. Holdsworth, G., S.J. Roberts, and H.Z. Ke, *Novel actions of sclerostin on bone.* J Mol Endocrinol, 2019. **62**(2): p. R167-r185.

2. Tsourdi, E., et al., *Physiological and pathological osteocytic osteolysis.* J Musculoskelet Neuronal Interact, 2018. **18**(3): p. 292-303.

3. Zhang, C., et al., *Studies on Osteocytes in Their 3D Native Matrix Versus 2D In Vitro Models.* Curr Osteoporos Rep, 2019. **17**(4): p. 207-216.

4. Solomon, L.B., et al., *Time dependent loss of trabecular bone in human tibial plateau fractures.* J Orthop Res, 2018. **36**(11): p. 2865-2875.

Statement of Authorship

Title of Paper	Recombinant sclerostin antagonizes effects of ex vivo mechanical loading in trabecular bone and increases osteocyte lacunar size
Publication Status	☑ Published ☐ Accepted for Publication ☐ Submitted for Publication ☐ Unpublished and Unsubmitted work written in manuscript style
Publication Details	Kogawa, M., Khalid, K. A., Wijenayaka, A. R., Ormsby, R. T., Evdokiou, A., Anderson, P. H., Findlay, D. M., Atkins, G. J. (2018). American Journal of Physiology: Cell Physiology, 314(1), C53-c61. DOI:10.1152/ajpcell.00175.2017

Principal Author

Name of Principal Author (Candidate)	Kamarul Ariffin Khalid		
Contribution to the Paper	Designed the study, development of methods, performed the experiments and analysis of the results, interpreted the data and critically revised the manuscript.		
Overall percentage (%)	40%		
Certification:	This paper reports on original research I conducted during the period of my Higher Degree by Research candidature and is not subject to any obligations or contractual agreements with a third party that would constrain its inclusion in this thesis. I am the primary author of this paper.		
Signature		Date	23 July 2019

Co-Author Contributions

By signing the Statement of Authorship, each author certifies that:

i. the candidate's stated contribution to the publication is accurate (as detailed above);

ii. permission is granted for the candidate to include the publication in the thesis; and

iii. the sum of all co-author contributions is equal to 100% less the candidate's stated contribution.

Name of Co-Author	Masakazu Kogawa		
Contribution to the Paper	Contributed to design of the study, development of methods, performed the experiments, data analysis and wrote the manuscript		
Signature		Date	28/07/2019

Name of Co-Author	Asiri R Wijenayaka		
Contribution to the Paper	Contributed to perform the experiments and critically revised the manuscript.		
Signature		Date	27/07/2019

Name of Co-Author	Renee T Ormsby		
Contribution to the Paper	Contributed to perform the experiments and critically revised the manuscript.		
Signature		Date	24/07/2019

Name of Co-Author	Andreas Evdokiou		
Contribution to the Paper	Designed the study, interpreted the data, provided overall supervision and wrote the manuscript.		
Signature		Date	27/07/2019

Name of Co-Author	Paul H Anderson		
Contribution to the Paper	Developed micro-CT methodologies; Interpreted the data; Provided supervision; Contributed to manuscript preparations.		
Signature		Date	23/07/2019

Name of Co-Author	David M Findlay		
Contribution to the Paper	Designed the study, interpreted the data, provided overall supervision and wrote the manuscript.		
Signature		Date	24/07/2019

Name of Co-Author	Gerald J Atkins		
Contribution to the Paper	Designed the study, interpreted the data, provided overall supervision, wrote the manuscript and acted as corresponding author.		
Signature		Date	29/07/2019

Am J Physiol Cell Physiol 314: C53–C61, 2018.
First published October 4, 2017; doi:10.1152/ajpcell.00175.2017.

RESEARCH ARTICLE

Recombinant sclerostin antagonizes effects of ex vivo mechanical loading in trabecular bone and increases osteocyte lacunar size

M. Kogawa,[1] K. A. Khalid,[1] A. R. Wijenayaka,[1] R. T. Ormsby,[1] A. Evdokiou,[2] P. H. Anderson,[3] D. M. Findlay,[1]* and G. J. Atkins[1]*

[1]*Biomedical Orthopaedic Research Group, Centre for Orthopaedic and Trauma Research, University of Adelaide, Adelaide, South Australia, Australia;* [2]*Discipline of Surgery, Breast Cancer Research Unit, Basil Hetzel Institute, University of Adelaide, Woodville, South Australia, Australia; and* [3]*School of Pharmacy and Medical Sciences, University of South Australia, Adelaide, South Australia, Australia*

Submitted 4 August 2017; accepted in final form 2 October 2017

Kogawa M, Khalid KA, Wijenayaka AR, Ormsby RT, Evdokiou A, Anderson PH, Findlay DM, Atkins GJ. Recombinant sclerostin antagonizes effects of ex vivo mechanical loading in trabecular bone and increases osteocyte lacunar size. *Am J Physiol Cell Physiol* 314: C53–C61, 2018. First published October 4, 2017; doi: 10.1152/ajpcell.00175.2017.—Sclerostin has emerged as an important regulator of bone mass. We have shown that sclerostin can act by targeting late osteoblasts/osteocytes to inhibit bone mineralization and to upregulate osteocyte expression of catabolic factors, resulting in osteocytic osteolysis. Here we sought to examine the effect of exogenous sclerostin on osteocytes in trabecular bone mechanically loaded ex vivo. Bovine trabecular bone cores, with bone marrow removed, were inserted into individual chambers and subjected to daily episodes of dynamic loading. Cores were perfused with either osteogenic media alone or media containing human recombinant sclerostin (rhSCL) (50 ng/ml). Loaded control bone increased in apparent stiffness over time compared with unloaded bone, and this was abrogated in the presence of rhSCL. Loaded bone showed an increase in calcein uptake as a surrogate of mineral accretion, compared with unloaded bone, in which this was substantially inhibited by rhSCL treatment. Sclerostin treatment induced a significant increase in the ionized calcium concentration in the perfusate and the release of β-CTX at several time points, an increased mean osteocyte lacunar size, indicative of osteocytic osteolysis, and the expression of catabolism-related genes. Human primary osteocyte-like cultures treated with rhSCL also released β-CTX from their matrix. These results suggest that osteocytes contribute directly to bone mineral accretion, and to the mechanical properties of bone. Moreover, it appears that sclerostin, acting on osteocytes, can negate this effect by modulating the dimensions of the lacunocanalicular porosity and the composition of the periosteocyte matrix.

sclerostin; mechanical loading; osteocyte; osteocytic osteolysis; bone mineralization

INTRODUCTION

Bone is a metabolically active organ that undergoes continuous remodeling (20, 44), which is necessary to maintain the structural integrity of the skeleton (8, 50). A lack of loading causes an imbalance of this remodeling, favoring bone resorption over bone formation. Accumulated evidence suggests that osteocytes play key roles in the regulation of bone remodeling by controlling the function of the other cell types in bone, such as activating osteoblastogenesis or osteoclastogenesis in response to increased or decreased strains, respectively, imposed by mechanical loading (1, 21, 22, 24, 33, 34, 42). In particular, osteocytes have a key role in mechanotransduction, the mechanism by which mechanical load applied to bone is converted to biological signals for maintaining appropriate strength and mechanical integrity of the bone (15, 16, 47). Although it is well established that loading has anabolic effects on bone, inducing endosteal and periosteal bone formation, the effects of loading on the bone matrix are less clear.

Mature osteocytes embedded in the mineralized bone matrix secrete sclerostin, the product of the sclerosteosis (*SOST*) gene (38), which is a potent anti-anabolic factor of bone formation (9, 25–27, 51, 55). The *SOST* gene appears to be mechanosensitive, with sclerostin production reported to be suppressed in a mouse ulnar loading model (45). Tu and coworkers (49) reported that cyclic ulnar loading-induced bone formation in mice did not occur in animals transgenic for human *SOST* expression, where effective sclerostin levels remained abnormally high after loading, indicating that the downregulation of sclerostin expression was a prerequisite for loading-induced bone growth. Consistent with this, Moustafa and colleagues (31) reported in a mouse tibial axial loading model that the suppression of *Sost* colocalized with regions of increased strain and increased bone formation. In contrast, *Sost* expression was reported to increase in response to unloading of bone (31, 45). Lin and coworkers (28) reported that unloading-induced bone loss was sclerostin-dependent, as Sost-*null* mice were resistant to this effect. A study by Macias and colleagues (30) suggested that the relationship between *Sost* expression and loading is more complex, as in a rat hindlimb unloading model, whereas *Sost* mRNA levels increased in diaphyseal cortical bone in response to unloading, they decreased in metaphyseal cortical and trabecular bone. Despite this, it appears that pharmacological inhibition of sclerostin prevents and reverses unloading-induced bone loss in both cortical and trabecular bone compartments, as shown in the mouse hindlimb tail suspension model (48).

* D. M. Findlay and G. J. Atkins are joint senior authors.

Address for reprint requests and other correspondence: G. J. Atkins, Level 7, Adelaide Health and Medical Sciences (AHMS) Building, Univ. of Adelaide, North Terrace and George St., Adelaide, SA 5000, Australia (e-mail: gerald.atkins@adelaide.edu.au).

Recent evidence from our group suggests that, in bone formation, mature cells of the late osteoblast to osteocyte stages are key cellular targets for the action of sclerostin (2, 23, 54). We reported that sclerostin induced the expression of mineralization inhibitory peptides, termed MEPE-ASARM (acidic, serine, aspartate-rich, MEPE-associated) peptides, derived from the proteolytic processing of matrix extracellular phosphoglycoprotein (MEPE) (2). We also showed that sclerostin could act as a catabolic agent by stimulating osteocyte support of osteoclastic activity via the receptor-activated nuclear factor kappa-B ligand (RANKL) signaling pathway (54), which could explain the rapid and marked effect on bone resorption when sclerostin is inhibited clinically using a sclerostin-neutralizing antibody (36). We also demonstrated a direct catabolic action of sclerostin in promoting osteocytic osteolysis, increasing osteocyte expression of carbonic anhydrase II (CA2) (23), cathepsin K (CTSK), and matrix metallopeptidase-13 (MMP13). Treatment with exogenous sclerostin resulted in an increase in the size of osteocyte lacunae in human trabecular bone over 7 days in static, mechanically nonloaded culture ex vivo (23). Together, these findings provide evidence that sclerostin acts on osteocytes to control bone volume via bone formation and bone remodeling, and on bone matrix mineralization by regulating osteocytic osteolysis.

In this study, we further investigated the effects of sclerostin on osteocytes in the context of their natural conformation within bone matrix, largely free of other cell types and where the effects of bone loading were separated from the influence of the circulation and other organ systems. Isolated cores of cancellous bone were perfused with culture fluid and loaded using the Zetos culture/loading system (18). Although daily episodes of loading induced mineral accretion and increased apparent stiffness compared with unloaded bone, the addition of exogenous recombinant sclerostin inhibited these changes. Concomitantly, exogenous sclerostin increased the expression of bone resorption marker genes, such as *CA2* and *CTSK* mRNA and increased mean osteocyte lacunar size, indicative of osteocytic osteolysis. Our findings suggest that sclerostin can block response to mechanical loading in part via direct actions on osteocyte-controlled mineral accretion and the promotion of osteocytic osteolysis.

MATERIALS AND METHODS

Sample preparation and culture conditions. Cancellous bovine bone was obtained fresh from the sternum of male cattle less than 2 yr of age courtesy of a local slaughterhouse. Using a specially designed diamond-coated hollow drill (Grizzly Industrial, Bellingham, WA), bone cores with a diameter of 10 mm were drilled out of the bone slices under sterile conditions. The bone cores were then machined to 5 mm thickness using a plane-parallel saw (5). During the entire procedure, the saw, drill, and bone were continuously cooled with sterile saline to prevent thermal necrosis and desiccation. The bone cores were washed with sterile saline using a dental cleaning device (Water Pik, Fort Collins, CO) to remove the bone marrow, and then placed in sterile bone chambers and connected to individual culture media reservoirs, at 37°C. They were perfused with the mineralizing cell culture media (7 ml/sample) consisting of Dulbecco's Modified Eagle Medium (DMEM) (Invitrogen, Carlsbad, CA) with 20 mM HEPES, 10% fetal calf serum, 1.8 mM KH_2PO_4, 100 μM L-ascorbate-2-phosphate, 2 mM L-glutamine, 1.2 mg/ml benzyl-penicillin, 1.6 mg/ml gentamicin sulfate, and 4 μg/ml amphotericin B, at a rate of 7 ml/h using a 24-channel planetary drive peristaltic pump (Ismatec IP 24, Ismatec SA, Switzerland). After equilibration for 24 h, bone cores were perfused in the absence or additional presence of 50 ng/ml human recombinant sclerostin (rhSCL; R&D Systems, Minneapolis, MN). The dose of 50 ng/ml rhSCL was chosen based on that we had already demonstrated to have near-maximal effects on osteoblast/osteocyte lineage cells in vitro (2, 54). Media with all supplements, including rhSCL where used, were changed daily throughout the experimental period and eluates stored at 4°C for analysis.

Mechanical stimulation and measurement of stiffness. Bone cores were loaded using a second-generation Zetos device, running proprietary software (Zetos version 2.0.0.1, Simplex Scientific). Loaded bone cores received a single episode of 300 cycles of loading per day at 2,000 microstrain at 1 Hz. The apparent stiffness measured in megapascals (Young's modulus) was determined for all bone samples immediately before applying each daily loading episode, using the in-built Zetos protocol (18) over a 16- to 18-day experimental period, as indicated. This consisted of applying a 10-N preload to the bone cores and then increasing loading to a maximum of 4,000 microstrain, acquiring 50 measurements of deformation. An additional control group of bone cores (unloaded control) was cultured identically to the other groups but without either loading or the addition of rhSCL.

Biochemical analyses. The ionized calcium concentrations in the culture media were measured using a micro calcium ion electrode (Lazar Research Laboratories) and a direct UV method (10), respectively, as per manufacturer's instructions (ThermoFisher Scientific). The absorbance at 650 nm and 340 nm was measured on a Konelab 30 (ThermoFisher Scientific), respectively. Levels of COOH-terminal telopeptide of type I collagen (β-CTX) in the culture media were measured by enzyme-linked immunosorbent assay (ELISA) (Immunodiagnostic Systems, Boldon, UK).

Bone histology. Specimens for histology were fixed with 10% formalin (Asia Pacific Specialty Chemicals) and decalcified with PBS (pH 8.0) including 1% ethylenediaminetetraacetic acid (EDTA) disodium salt (Chem-Supply) and 0.5% paraformaldehyde (PFA; ThermoFisher Scientific) to decalcify samples slowly for tartrate-resistant acid phosphatase (TRAP) conservation. The samples were infiltrated and embedded in paraffin after decalcification. Sections, 5 μm thick, were stained by hematoxylin-eosin (H&E), toluidine blue, and TRAP staining. Images were captured by a Leica DM6000B microscope (Leica Microsystems, Wetzlar, Germany). Toluidine blue-stained sections were used to measure osteocyte lacuna size, which was quantified from images using a Quantimet imaging system (Leica) and ImageJ software, as de-

Table 1. *Sequences of oligonucleotide primers for real-time RT-PCR designed on the basis of published bovine gene sequences and predicted PCR product sizes*

Target Gene	Sense	Primer Sequence (5′→3′)	Expected Product Size, bp
BACT	S	ACCGTGAGAAGATGACCCAGA	127
	AS	TCACCGGAGTCCATCACG	
SOST	S	CCCTTTGAGACCAAAGACGC	244
	AS	CAGGACACAACAGCTGCACC	
CA2	S	GGAAGAAATATGCTGCCGAGC	194
	AS	GAAGTCGGTGCTCTTACCCTTTG	
TRAP	S	GCAGCCAAGGAGGACTACGTG	176
	AS	CCATTCTCATCCTGAAGGTACTGC	
CTSK	S	CCTATCCATATGTTGGACAGGATG	169
	AS	AAGGAGGTCAGGCTTGCATC	
RANKL	S	CTACTTCCGAGCGCAGATGG	90
	AS	TCCGTGTTTTCATGGAGCTTG	
MEPE	S	TGACCCTGGCAGCACCAAC	219
	AS	GCTCTTGACTTCTCTTGCCAGAATG	
PHEX	S	GGGTGTTCGATGGGCCTTTA	217
	AS	ATACTTGCCGGTTTGCAGGA	

S, sense; AS, antisense.

scribed previously (23). These sections were also used to determine the percentage of occupied osteocyte lacunae, according to the number of visible nuclei, stained purple and located within the lacunae (35).

To visualize the calcium incorporation, bone cores were incubated with medium containing 3 μg/ml calcein (Sigma Chemical, St. Louis, MO) for 24 h on *days 7* and *13* of the experiment. Specimens were fixed and embedded in methylmethacrylate. Bone blocks were trimmed and sectioned by microtome (Polycut-E, Leica SP 2600, Cambridge Instruments, Cambridge, UK). Calcein-labeled regions were imaged using the Quantimet (Leica) and the degree of calcein staining was also measured at 9–17 regions of each section, in 3–5 samples for each treatment. Fluorescence intensity was quantified using ImageJ software.

Osteocyte-like cell cultures. Human primary osteoblast-like cells were isolated from femoral trabecular bone taken from patients undergoing primary total hip replacement surgery and cultured ex vivo, as described previously (3). Samples were obtained with written, informed consent and approval by the Human Ethics Committee of the Royal Adelaide Hospital. Cells were cultured under differentiating conditions for a period of 28 days, which gives rise to cells that phenotypically resemble mature osteocytes (2, 4, 23, 35). Mature osteocyte-like cells were cultured for a further 72 h, either untreated or with the addition of rhSCL, as indicated. Supernatants were assayed for β-CTX levels, as above.

RNA extraction and real-time polymerase chain reaction (PCR). Extraction of RNA from bone and real-time RT-PCR was conducted, as described previously (23) with some modifications. Briefly, following the experimental protocol (ex vivo culture with or without mechanical loading or in the additional presence of rhSCL) bovine trabecular bone samples were rinsed in PBS, and cut into small pieces using sterile instruments cleaned with diethylpyrocarbonate (DEPC)-treated water. Trizol reagent (Life Technologies, Gaithersburg, MD) was added and the bone pieces were transferred to sterile 1.5-ml centrifuge tubes and further crushed using the blunt end of a pair of surgical steel scissors. The samples were frozen at −80°C overnight, then thawed and centrifuged at 1,000 *g* for 5 min to pellet any insoluble material. Total RNA was then isolated as per manufacturer's instructions (Life Technologies). Complementary DNA (cDNA) was synthesized using iScript reagent (Bio-Rad Laboratories, Hercules, CA), and gene expression was analyzed by real-time RT-PCR using the SYBR Green incorporation technique. Relative gene expression between samples was calculated using the comparative cycle threshold method, using bovine actin-beta (ACTB) as a housekeeping gene. Oligonucleotide primers were designed in-house to flank intron-exon boundaries, and were purchased from Geneworks (Thebarton). Sequences of oligonucleotide primers used are shown in Table 1.

Statistical analysis. Statistical differences between data sets were assessed using one-way analysis of variance (ANOVA) followed by

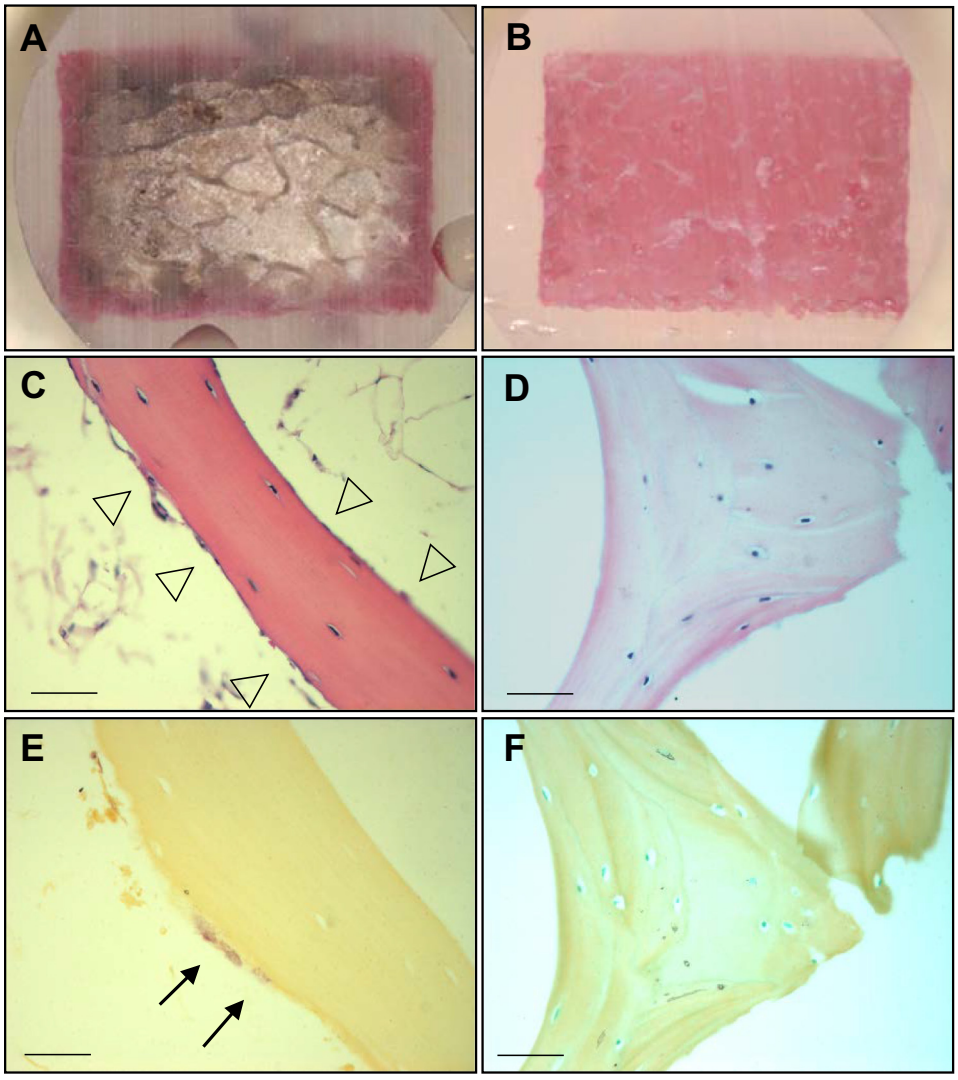

Fig. 1. The effect of bone marrow on perfusion. Bone cores with and without bone marrow (n = 3/group) were seated in individual chambers and continuously perfused with media including Reactive red 120 for 24 h. Sagittal sections were obtained through the center of the bone cores with bone marrow (*A*) and without bone marrow (*B*). Specimens with and without bone marrow were fixed in 10% formaldehyde and decalcified with phosphate-buffered saline (pH 8.0) including 1% EDTA and 0.5% PFA, and cut into 5-μm-thick sections. Samples stained by H&E and TRAP with bone marrow (*C* and *E*) and without bone marrow (*D* and *F*). Arrowheads indicate osteoblasts and lining cells. Arrows indicate TRAP-positive osteoclasts. Scale bar, 200 μm.

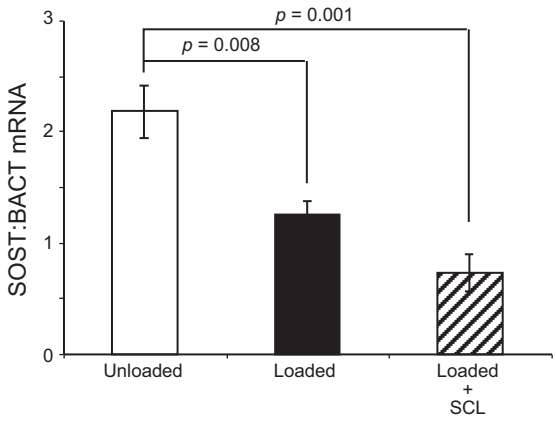

Fig. 2. *SOST* mRNA expression in response to loading in the presence or absence of rhSCL. Bone cores were divided into 3 groups: unloaded, loaded, and loaded in the presence 50 ng/ml of rhSCL over 7 days. Total RNA of bone was extracted and real-time RT-PCR was performed for *SOST* mRNA. Data are mean mRNA levels normalized to *BACT* mRNA ± SD of triplicate wells. Significant difference from the unloaded control is indicated.

Tukey's post hoc test (GraphPad Prism). A value for $P < 0.05$ was considered significant.

RESULTS

Bone organ culture. The Zetos system comprises a piezoelectric controlled bone loading device, together with a continuous flow chamber that perfuses bone samples with culture medium to maintain bone viability (12). Since the Zetos device allows controlled physiological loading to be applied to large animal trabecular bone, we considered it a suitable system, in which to investigate the effects of sclerostin on mineral accrual induced by mechanical loading. Since we have established that osteocytes are target cells for the action of sclerostin (2, 23, 54), we first performed a control experiment to test whether osteocytes would be exposed to the perfusate. Bone cores with either an intact marrow or with marrow physically removed using a dental flossing device were perfused with Reactive Red 120 stain solution. After perfusion for 24 h, the bone cores were sectioned transversely and longitudinally. Poor dye penetration in bone cores with intact marrow suggested that perfusion was limited to the periphery (Fig. 1*A*), whereas complete dye penetration in cores with marrow removed showed that cores were perfused throughout (Fig. 1*B*). Marrow was therefore removed for all subsequent experiments. Histological analysis indicated that the flushing of bone marrow resulted in the removal of most bone lining cells, osteoblasts (Fig. 1*C*) and osteoclasts (Fig. 1*E*), with a significant enrichment of osteocytes in the bone cores (Fig. 1, *D* and *F*).

The effect of mechanical loading on SOST mRNA expression. The expression of sclerostin in bone is reported to be influenced by the local strain perceived by osteocytes, with low expression under load and higher expression in the unloaded state (31, 32, 45). This has mainly been examined in cortical bone in mice. Thus we sought to test whether loading of large animal trabecular bone also regulates endogenous *SOST* mRNA levels. Bone cores were divided into three groups, unloaded, loaded, and loaded with rhSCL (50 ng/ml) for periods of 4 h and 7 days, and mRNA of each sample was prepared for RT-PCR analysis. We observed that 4 h after a single period of mechanical loading there was a trend for decreased *SOST* mRNA expression in comparison to unloaded bone (data not shown), and after 7 consecutive days of daily loading *SOST* expression was reduced by approximately half compared with unloaded bone samples (Fig. 2). The addition of exogenous rhSCL had no additional effect on the reduction of *SOST* mRNA expression in loaded bone.

Effect of sclerostin on loading-induced stiffness. It has been demonstrated previously in the Zetos system that loading changes the mechanical properties of the bone (11, 13, 53). To elucidate the direct effects of sclerostin on the loading response, cores were perfused with medium alone or medium containing added recombinant sclerostin, and mechanical load was applied daily. A third group of cores were cultured without daily loading or the addition of rhSCL. The stiffness (Young's modulus) of each bone core was determined each day and in the case of the loaded groups, before applying mechanical load. The apparent stiffness in the unloaded group increased slightly with time, as reported previously (13, 53). In response to daily loading, the apparent stiffness increased to a greater extent throughout the experimental period (Fig. 3), as reported previously (13, 53). However, the effect of loading was significantly abrogated by rhSCL treatment. These data show that sclerostin could attenuate the response to bone loading, most likely by a direct effect on osteocytes.

Ionic calcium levels in culture media. We have recently reported that rhSCL promotes osteocyte-mediated release of calcium from bone (23). To investigate whether these effects of sclerostin could occur in the context of mechanical loading, changes in the ionic calcium levels of the culture media were measured for each individual bone core. There was no detectable difference between groups during the first 2 wk of observation (data not shown), perhaps because of the relatively large volume of media perfused (7 ml) and the relatively short period (24 h), over which each sample was collected. However, media from the loaded + rhSCL group collected in the third week of culture showed significantly increased ionic cal-

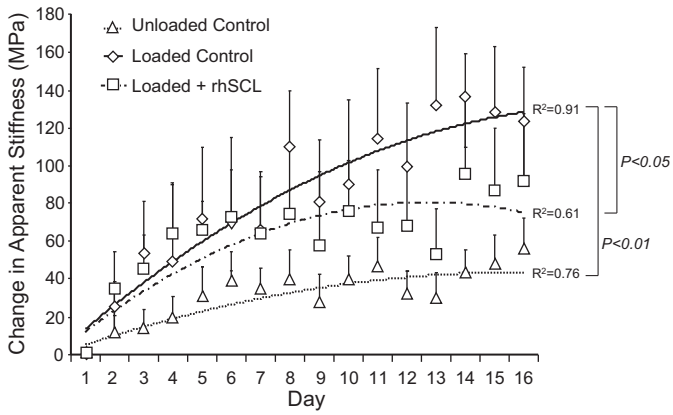

Fig. 3. Effects of sclerostin on apparent stiffness. The bone cores were divided into 3 groups: unloaded controls, loaded controls, and loaded + rhSCL (50 ng/ml). The loading procedure was 300 cycles/day of 2,000 microstrain applied at a frequency of 1 Hz for 3 wk. The apparent stiffness of each bone sample was determined daily immediately before the load was applied as described in MATERIALS AND METHODS. Data are means ± SE of 8 samples per group, all obtained from the same bovine sternum. Similar data were obtained from 3 independent experiments. The regression coefficients (R^2) for each group and significant difference between the groups are indicated.

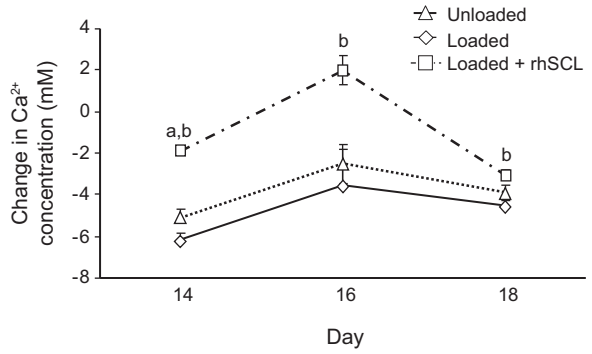

Fig. 4. Effects of mechanical stimulation and rhSCL on calcium concentration in the culture medium. Ionic calcium in the culture media was measured 24 h after loading or an equivalent time point for the unloaded control group. Data are means ± SE (8 samples per group) of the change in calcium concentration during 1 day culture; significant differences: [a]between rhSCL group and unloaded Controls; [b]between rhSCL group and loaded Controls ($P < 0.05$).

cium levels compared with the loaded and unloaded control samples (Fig. 4).

Calcein incorporation. We reported that treatment of human mineralizing osteocyte-like cultures with rhSCL in vitro resulted in the inhibition of mineral incorporation into the cell layer (2). To test the effect of sclerostin on mineral accrual in the bone cores, calcein was added to perfusates on *days 7* and *13* for a period of 24 h in each case and the bone cores processed for analysis after the 16-day experiment. Calcein was incorporated into the trabecular bone surfaces in all groups (Fig. 5). The overall fluorescence intensity of the loaded bone cores was significantly higher than that in the unloaded group, indicative of increased dynamic calcium uptake in response to loading (Fig. 5*D*). The incorporation of calcein into the bone cores in the presence of rhSCL (Fig. 5*B*) was significantly lower than in the cores perfused with medium alone (Fig. 5*A*). Higher power microscopy revealed that calcein labeling was most prominent on the surfaces of bone, including those of vascular pores, and within osteocyte lacunae (Fig. 5*C*), the latter consistent with osteocytes directly regulating perilacunar mineral in this system.

Histology. As stated, the predominant cell type remaining in the trabecular bone cores after flushing was osteocytes (Fig. 1*D*) and this remained the case after of culture ex vivo, with histological analysis revealing an apparent absence of both TRAP-positive osteoclasts (not shown) and osteoblasts (Fig. 6*A*). Osteocytes showed an evenly spread, noncondensed nucleus, consistent with cell viability, with the cell body often positioned eccentrically within the lacunae (Fig. 6*A*). To determine the viability of the remaining osteocytes, we measured the osteocyte lacunar occupancy. There was ~80% occupancy of osteocyte lacunae overall, with no significant differences observed between groups (Fig. 6*B*). Analysis revealed that the size of lacunae increased significantly with rhSCL treatment, in comparison to the cores perfused in medium alone, either loaded or unloaded (Fig. 6*C*).

The effect of sclerostin on markers of bone resorption and formation. To investigate bone resorption in this system, we analyzed the culture media for the presence of carboxy-terminal cross-linking telopeptides of type I collagen (β-CTX). β-CTX levels decreased after the first week of culture, and increased thereafter (Fig. 6*D*). After prolonged culture, the level of β-CTX was significantly elevated in the presence of rhSCL, compared with either unloaded or loaded control cores, suggesting that rhSCL could enhance the degradation of the bone matrix. The absence of observable osteoclasts implied that osteocytes were mediating this process. To test this, we generated human primary osteocyte-like cultures, consisting of differentiated cells residing in an endogenous mineralized type I collagen matrix (2, 4, 23, 35), and treated these cells for 72

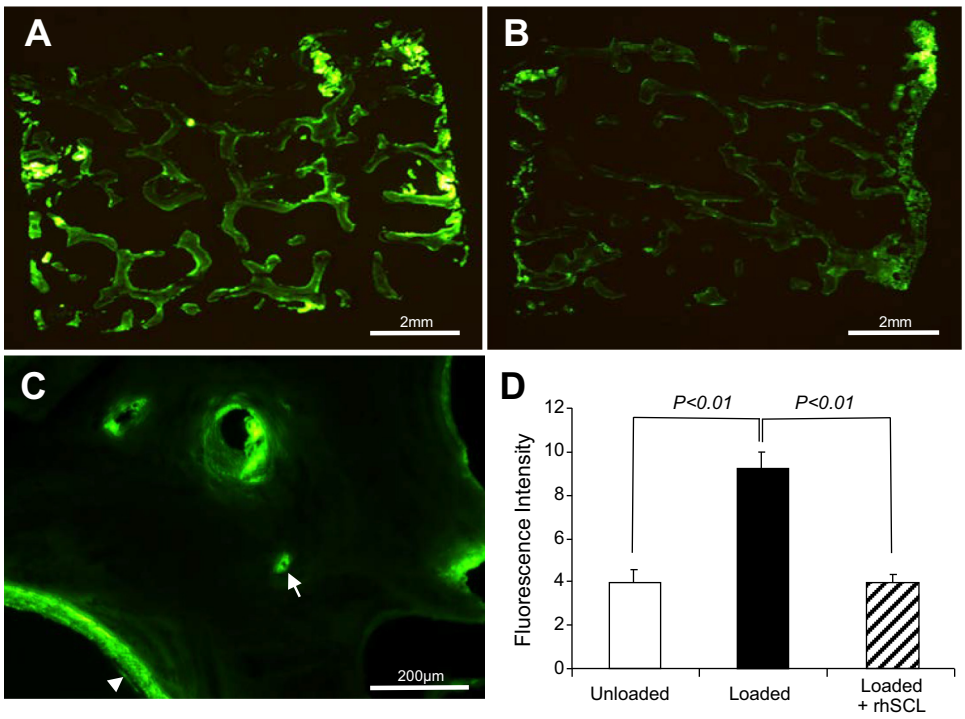

Fig. 5. Effects of rhSCL on bone mineralization. Bovine bone cores were perfused with calcein and processed for sectioning as described in MATERIALS AND METHODS. *A*: a cross section of a whole bone core (dimensions 10 mm × 5 mm) cultured with daily mechanical loading. *B*: an example of a bone core loaded in the presence of rhSCL. *C*: labeling at a higher magnification (20× objective) showing an example of calcein labeling at the trabecular surface (arrowhead) and a labeled osteocyte lacuna (arrow). *D*: quantification of total calcein labeling; data shown are means of fluorescence intensity ± SE. $n = 5$ bone cores group, all obtained from the same bovine sternum. Similar results were obtained for 2 independent experiments.

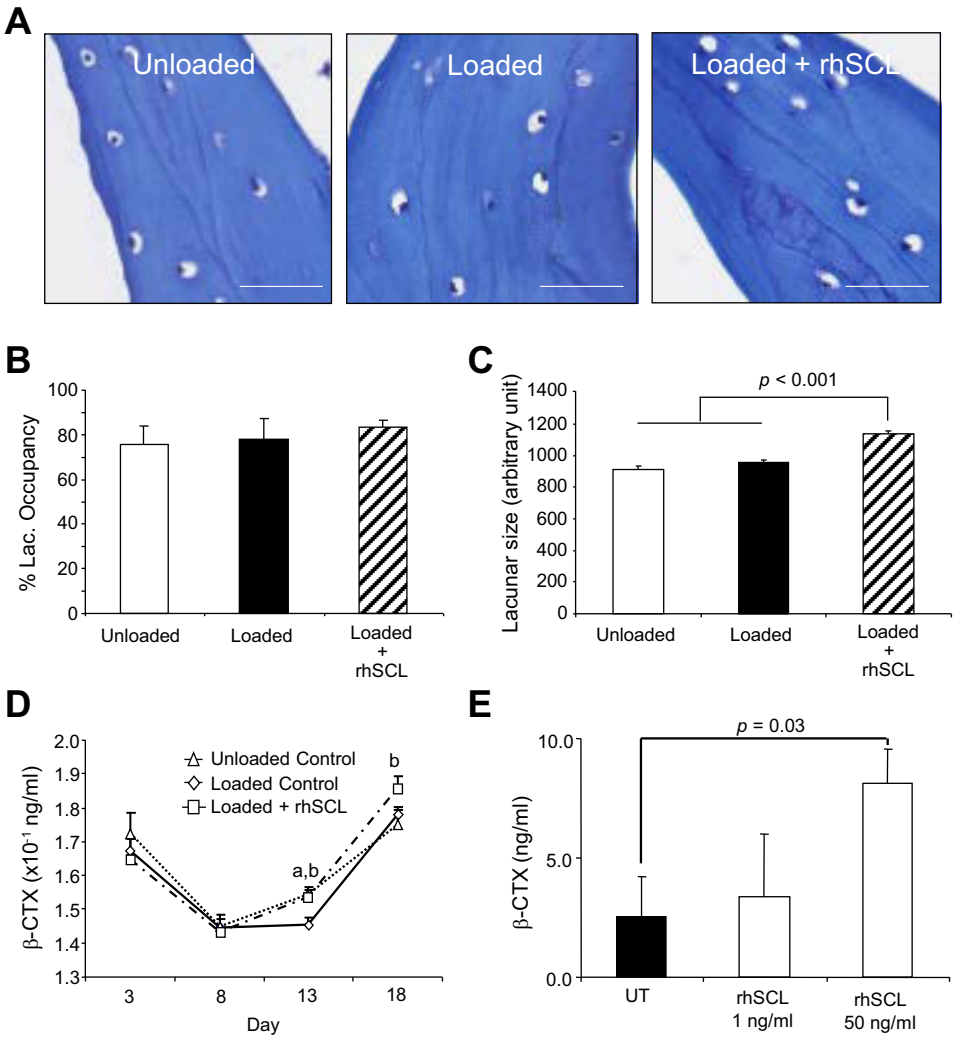

Fig. 6. Effects of mechanical stimulation and rhSCL on lacunar occupancy and osteocytic osteolysis. Bone cores were processed for analysis after an 18-day experimental period. *A*: representative toluidine blue-stained sections from each group of bone cores (20× objective; scale bars represent 100 μm). *B*: the occupancy of osteocyte lacunae was measured from toluidine blue-stained sections; data shown are means ± SE. *C*: the osteocyte lacunar size at the end of the experiment was measured from toluidine blue-stained sections imaged using a Quantimet imaging system analyzed using ImageJ software. Data shown are means (5 independent sections; at least 100 lacunae/section) ± SE. *D*: β-CTX levels were measured in culture eluates by commercial ELISA, with each time point representing the concentration of β-CTX in 7 ml of medium after 24 h of perfusion. Data shown are means ± SE. Significant difference: [a]between unloaded and loaded controls; [b]between loaded control and loaded + rhSCL groups ($P < 0.05$). *E*: β-CTX levels in culture supernatant of human primary osteocyte-like cultures treated or untreated with rhSCL for 72 h. Data represent means ± SD of triplicate wells.

h with rhSCL. As shown in Fig. 6*E*, measurably increased β-CTX was released into the culture supernatant in response to rhSCL at 50 ng/ml.

To investigate the effect of sclerostin on resorption marker gene expression, we cultured bone cores for 3 days with rhSCL at concentrations from 1 to 50 ng/ml. Consistent with our findings in human osteocyte-like cells, MLO-Y4 osteocytes and in human trabecular bone (23, 54), rhSCL induced the mRNA expression of the resorption-associated genes *TRAP*, cathepsin K, and *RANKL* (Fig. 7, *A–D*). Recombinant human sclerostin treatment also induced the expression of the mineralization inhibitory gene *MEPE* in a dose-dependent manner (Fig. 7*E*) and decreased the expression of the mineralization promoting gene, phosphate regulating gene with homologies to endopeptidases on the X-chromosome (*PHEX*), at concentrations between 1 and 50 ng/ml (Fig. 7*F*), consistent with our findings in osteocytes in vitro and ex vivo (2).

DISCUSSION

Accumulating evidence indicates that sclerostin, which is predominantly secreted from mature osteocytes, is a local regulator of bone metabolism. Osteocytes, including preosteocytes, constitute the major cell type in bone and are likely targets for the activity of sclerostin, based both on in vitro studies that demonstrate osteocyte sensitivity to sclerostin and its very localized and regulated expression pattern in bone (2, 23, 54). The expression of sclerostin appears to reflect local strains perceived by osteocytes, with low production under mechanical load and high production in the unloaded condition (31, 32, 45). Sclerostin is known to negatively regulate bone mass by inhibiting the Wingless integration (Wnt)/β-catenin pathway. Javaheri and colleagues (17) showed that bone formation induced by mechanical loading did not occur in mice lacking an allele of the β-catenin gene, indicating the importance of the Wnt/β-catenin signaling pathway for the effect of loading. Furthermore, transgenic expression of *SOST* also antagonized loading-induced bone formation in mice (49). However, the function of sclerostin in mechanical loading has been less well characterized in trabecular bone, particularly from large animals. Here, we sought to determine the effect of exogenous sclerostin on the response of bovine cancellous bone to daily episodes of loading. We used a concentration of rhSCL that we showed previously was near maximal for its effects on human osteocytes in vitro (2, 54). Although this is ~50–60-fold higher than levels typically found in the circula-

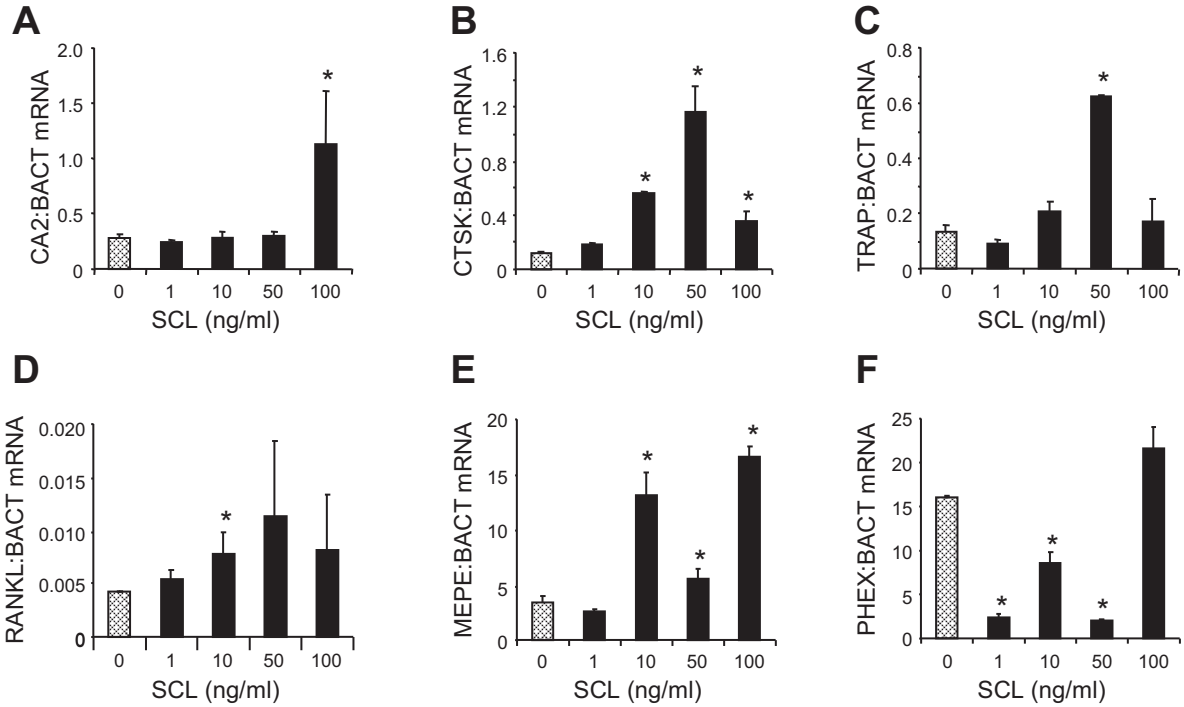

Fig. 7. Effects of sclerostin on gene expression. Bovine trabecular bone was prepared as described in MATERIALS AND METHODS and cultured ex vivo (without loading) with different doses of rhSCL (0–100 ng/ml). Total RNA was extracted at 72 h and real-time RT-PCR performed for *CA2* (*A*), *CTSK* (*B*), *TRAP* (*C*), *RANKL* (*D*), *MEPE* (*E*), and *PHEX* mRNA (*F*). Data are mean expressions normalized to that of the housekeeping gene *BACT* mRNA ± SD for triplicate RT-PCR reactions from quadruplicate bone samples/group. Difference in expression from the untreated control is indicated (*$P < 0.05$).

tion, the local bone fluid concentration of sclerostin deriving from osteocytes, and to which the responding cells are exposed, is unknown but is likely to be considerably higher than the circulating level. Consistent with previous reports using a similar system (13, 53), we observed a significant increase in stiffness in cyclically loaded bovine trabecular bone ex vivo compared with baseline and to identically cultured unloaded controls. In the present study, this was observed in a reductionist system, with removal of bone marrow and detectable bone surface cells, and in the absence of functional vasculature, neural, and endocrine systems. Furthermore, suppression of endogenous *SOST* mRNA expression in response to load was observed, at least over the first 7 days, consistent with in vivo models (31, 32, 45). Notably, perfusion of bone with rhSCL suppressed the positive effect of mechanical loading on bone stiffness.

In seeking a mechanistic explanation for changes in stiffness, we observed, using a calcein surrogate as a marker, a decreased uptake of calcium in bone loaded in the presence of exogenous rhSCL compared with loaded control samples. It is likely that additional mineralization within the bone matrix had a measurable effect on the stiffness of the bone cores, since bone mineralization and modulus have been shown to be positively correlated (14). Parfitt (37) reviewed the literature relating to calcium exchange between the bone and the extracellular fluid, citing experiments using radiolabeled calcium, which showed "immediate rapid uptake at all bone surfaces accessible to the circulation, regardless of their cellular activity or degree of mineralisation." This is consistent with the common observation that bone explants in culture take up calcium from the medium, likely by simple physicochemical mechanisms. Parfitt (37) described a pool of calcium that is exchangeable with bone surfaces, and it has subsequently been experimentally demonstrated that an osteocyte-mediated mechanism, driven for example by parathyroid hormone (PTH) (39), can mobilize calcium (and phosphate) from this pool into the circulation. Calcium uptake into bone may therefore proceed by a simple physicochemical mechanism, with its release being controlled by osteocytes, which are in turn regulated by mediators, such as PTH and, as we have shown previously (2), sclerostin. This mechanism relies on viable osteocytes and it has been shown that osteocyte death is associated with mineralizing osteocyte lacunae (6, 7).

We have recently demonstrated that rhSCL induced the expression by osteocytes of a number of mediators previously associated with bone resorption by osteoclasts. These included RANKL, carbonic anhydrase 2, cathepsin K, and TRAP (23). A similar panel of genes was shown to be associated with osteocytic osteolysis during lactation (41). We have identified that sclerostin also regulates osteocyte-mediated bone mineralization through regulation of the PHEX/MEPE axis, and that the upregulation by sclerostin of MEPE and MEPE-ASARM peptides was critical to the inhibitory effect of sclerostin (2). Sclerostin treatment of bovine bone upregulated the expression of *MEPE* mRNA and inhibited the expression of *PHEX* mRNA, consistent with our report in human bone (2). The combined regulation of these mineralization-associated proteins by sclerostin could provide cell-mediated control of the perilacunar mineralization and serve as a prelude to removal of the organic matrix, the latter evidenced by the release of β-CTX from the bone cores. Strong confirmatory evidence for this was obtained using differentiated cultures of human pri-

mary osteocyte-like cells, where we show for the first time the release of β-CTX by the activity of osteocytes in response to sclerostin. This is consistent with, and appears to result in, the enlargement of the osteocyte lacuna size in the rhSCL-treated bone. This is also consistent with our previous observations of the effect of sclerostin in human trabecular bone (23), and provides the first direct evidence that sclerostin can effect collagen breakdown by its actions on osteocytes and can do so even when trabecular bone is mechanically loaded. Interestingly, the osteocyte lacunar size in loaded + rhSCL-treated samples was significantly larger than that in both loaded and unloaded groups, and indeed there was no difference in this parameter in these two groups, consistent with the reports by others that significant osteocytic osteolysis does not seem to occur in response to mechanical unloading (29, 41). On the other hand, dramatic changes in osteocyte morphology occurred after spinal cord injury in rats, which could be prevented by treatment with neutralizing sclerostin antibodies (40). It appears that altered lacunocanalicular morphology has implications for the mechanical properties of bone. For example, it was elegantly shown in lactating rats that the bone elastic modulus decreased inversely with the increase in osteocyte lacunocanalicular porosity (19), consistent with the reduced gain in modulus seen in the present experiments with rhSCL treatment. Thus it is conceivable that the mechanical loading-induced reduction of endogenous sclerostin expression serves to stabilize the perilacunar matrix.

In summary, we propose that our observations are consistent with the notion of passive uptake by bone of calcium, which is maintained in balance by osteocytes, and that loading results in increased mineral incorporation into the periosteocyte matrix. Sclerostin, by an as yet undetermined mechanism, causes the release by osteocytes of bone matrix resorptive molecules, thereby reducing the effects of loading on mineral accrual. It is not known whether these experimental observations with exogenous sclerostin are reflective of physiological or pathological processes. However, increased levels of sclerostin in bone, as might be caused by inflammation (52) for example, could reduce the anabolic effects of mechanical loading. The contribution of osteocytes to circulating β-CTX, a major serum bone turnover marker, in vivo is an interesting area of future research. Our findings are of potential relevance to the mechanism of action of sclerostin-targeting therapies, since β-CTX levels are strongly suppressed in individuals receiving sclerostin-neutralizing antibodies (36, 43).

ACKNOWLEDGMENTS

We thank Dr. Everett Smith (Univ. of Wisconsin) for help in establishing the Zetos device.

GRANTS

This work was funded by National Health and Medical Research Council of Australia (NHMRC) Project Grant Scheme (Grant No. 1004871). G. J. Atkins is a NHMRC Senior Research Fellow.

DISCLOSURES

No conflicts of interest, financial or otherwise, are declared by the authors.

AUTHOR CONTRIBUTIONS

D.M.F. and G.J.A. conceived and designed research; M.K., K.A.K., A.R.W., and R.T.O. performed experiments; M.K., K.A.K., A.R.W., R.T.O., P.H.A., and G.J.A. analyzed data; M.K., A.R.W., A.E., P.H.A., D.M.F., and G.J.A. interpreted results of experiments; M.K., R.T.O., and G.J.A. prepared figures; M.K., R.T.O., D.M.F., and G.J.A. drafted manuscript; A.E., P.H.A., D.M.F., and G.J.A. edited and revised manuscript; M.K., K.A.K., A.R.W., R.T.O., A.E., P.H.A., D.M.F., and G.J.A. approved final version of manuscript.

REFERENCES

1. **Atkins GJ, Findlay DM.** Osteocyte regulation of bone mineral: a little give and take. *Osteoporos Int* 23: 2067–2079, 2012. doi:10.1007/s00198-012-1915-z.
2. **Atkins GJ, Rowe PS, Lim HP, Welldon KJ, Ormsby R, Wijenayaka AR, Zelenchuk L, Evdokiou A, Findlay DM.** Sclerostin is a locally acting regulator of late-osteoblast/preosteocyte differentiation and regulates mineralization through a MEPE-ASARM-dependent mechanism. *J Bone Miner Res* 26: 1425–1436, 2011. doi:10.1002/jbmr.345.
3. **Atkins GJ, Welldon KJ, Halbout P, Findlay DM.** Strontium ranelate treatment of human primary osteoblasts promotes an osteocyte-like phenotype while eliciting an osteoprotegerin response. *Osteoporos Int* 20: 653–664, 2009. doi:10.1007/s00198-008-0728-6.
4. **Atkins GJ, Welldon KJ, Wijenayaka AR, Bonewald LF, Findlay DM.** Vitamin K promotes mineralization, osteoblast-to-osteocyte transition, and an anticatabolic phenotype by gamma-carboxylation-dependent and -independent mechanisms. *Am J Physiol Cell Physiol* 297: C1358–C1367, 2009. doi:10.1152/ajpcell.00216.2009.
5. **Aw MS, Khalid KA, Gulati K, Atkins GJ, Pivonka P, Findlay DM, Losic D.** Characterization of drug-release kinetics in trabecular bone from titania nanotube implants. *Int J Nanomedicine* 7: 4883–4892, 2012. doi:10.2147/IJN.S33655.
6. **Bell LS, Kayser M, Jones C.** The mineralized osteocyte: a living fossil. *Am J Phys Anthropol* 137: 449–456, 2008. doi:10.1002/ajpa.20886.
7. **Busse B, Djonic D, Milovanovic P, Hahn M, Püschel K, Ritchie RO, Djuric M, Amling M.** Decrease in the osteocyte lacunar density accompanied by hypermineralized lacunar occlusion reveals failure and delay of remodeling in aged human bone. *Aging Cell* 9: 1065–1075, 2010. doi:10.1111/j.1474-9726.2010.00633.x.
8. **Chen JH, Liu C, You L, Simmons CA.** Boning up on Wolff's Law: mechanical regulation of the cells that make and maintain bone. *J Biomech* 43: 108–118, 2010. doi:10.1016/j.jbiomech.2009.09.016.
9. **Choi HY, Dieckmann M, Herz J, Niemeier A.** Lrp4, a novel receptor for Dickkopf 1 and sclerostin, is expressed by osteoblasts and regulates bone growth and turnover in vivo. *PLoS One* 4: e7930, 2009. doi:10.1371/journal.pone.0007930.
10. **Daly JA, Ertingshausen G.** Direct method for determining inorganic phosphate in serum with the "CentrifiChem". *Clin Chem* 18: 263–265, 1972.
11. **David V, Guignandon A, Martin A, Malaval L, Lafage-Proust MH, Rattner A, Mann V, Noble B, Jones DB, Vico L.** Ex Vivo bone formation in bovine trabecular bone cultured in a dynamic 3D bioreactor is enhanced by compressive mechanical strain. *Tissue Eng Part A* 14: 117–126, 2008. doi:10.1089/ten.a.2007.0051.
12. **Davies CM, Jones DB, Stoddart MJ, Koller K, Smith E, Archer CW, Richards RG.** Mechanically loaded ex vivo bone culture system "Zetos": systems and culture preparation. *Eur Cell Mater* 11: 57–75, 2006. doi:10.22203/eCM.v011a07.
13. **Endres S, Kratz M, Wunsch S, Jones DB.** Zetos: a culture loading system for trabecular bone. Investigation of different loading signal intensities on bovine bone cylinders. *J Musculoskelet Neuronal Interact* 9: 173–183, 2009.
14. **Follet H, Boivin G, Rumelhart C, Meunier PJ.** The degree of mineralization is a determinant of bone strength: a study on human calcanei. *Bone* 34: 783–789, 2004. doi:10.1016/j.bone.2003.12.012.
15. **Fritton SP, Weinbaum S.** Fluid and solute transport in bone: flow-induced mechanotransduction. *Annu Rev Fluid Mech* 41: 347–374, 2009. doi:10.1146/annurev.fluid.010908.165136.
16. **Henriksen K, Neutzsky-Wulff AV, Bonewald LF, Karsdal MA.** Local communication on and within bone controls bone remodeling. *Bone* 44: 1026–1033, 2009. doi:10.1016/j.bone.2009.03.671.
17. **Javaheri B, Stern AR, Lara N, Dallas M, Zhao H, Liu Y, Bonewald LF, Johnson ML.** Deletion of a single β-catenin allele in osteocytes abolishes the bone anabolic response to loading. *J Bone Miner Res* 29: 705–715, 2014. doi:10.1002/jbmr.2064.
18. **Jones DB, Broeckmann E, Pohl T, Smith EL.** Development of a mechanical testing and loading system for trabecular bone studies for long term culture. *Eur Cell Mater* 5: 48–59, 2003. doi:10.22203/eCM.v005a05.

19. **Kaya S, Basta-Pljakic J, Seref-Ferlengez Z, Majeska RJ, Cardoso L, Bromage TG, Zhang Q, Flach CR, Mendelsohn R, Yakar S, Fritton SP, Schaffler MB.** Lactation-induced changes in the volume of osteocyte lacunar-canalicular space alter mechanical properties in cortical bone tissue. *J Bone Miner Res* 32: 688–697, 2017. doi:10.1002/jbmr.3044.
20. **Klein-Nulend J, Bacabac RG, Mullender MG.** Mechanobiology of bone tissue. *Pathol Biol (Paris)* 53: 576–580, 2005. doi:10.1016/j.patbio.2004.12.005.
21. **Klein-Nulend J, Bonewald L.** The osteocyte. In: *Principles of Bone Biology* (3rd ed.), edited by Bilezikian JP, Raisz LG, Martin TJ. San Diego, CA: Academic, 2008, p. 153–174. doi:10.1016/B978-0-12-373884-4.00028-8.
22. **Knothe Tate ML, Adamson JR, Tami AE, Bauer TW.** The osteocyte. *Int J Biochem Cell Biol* 36: 1–8, 2004. doi:10.1016/S1357-2725(03)00241-3.
23. **Kogawa M, Wijenayaka AR, Ormsby RT, Thomas GP, Anderson PH, Bonewald LF, Findlay DM, Atkins GJ.** Sclerostin regulates release of bone mineral by osteocytes by induction of carbonic anhydrase 2. *J Bone Miner Res* 28: 2436–2448, 2013. doi:10.1002/jbmr.2003.
24. **Kogianni G, Noble BS.** The biology of osteocytes. *Curr Osteoporos Rep* 5: 81–86, 2007. doi:10.1007/s11914-007-0007-z.
25. **Krause C, Korchynskyi O, de Rooij K, Weidauer SE, de Gorter DJ, van Bezooijen RL, Hatsell S, Economides AN, Mueller TD, Löwik CW, ten Dijke P.** Distinct modes of inhibition by sclerostin on bone morphogenetic protein and Wnt signaling pathways. *J Biol Chem* 285: 41614–41626, 2010. doi:10.1074/jbc.M110.153890.
26. **Leupin O, Piters E, Halleux C, Hu S, Kramer I, Morvan F, Bouwmeester T, Schirle M, Bueno-Lozano M, Fuentes FJ, Itin PH, Boudin E, de Freitas F, Jennes K, Brannetti B, Charara N, Ebersbach H, Geisse S, Lu CX, Bauer A, Van Hul W, Kneissel M.** Bone overgrowth-associated mutations in the LRP4 gene impair sclerostin facilitator function. *J Biol Chem* 286: 19489–19500, 2011. doi:10.1074/jbc.M110.190330.
27. **Li X, Zhang Y, Kang H, Liu W, Liu P, Zhang J, Harris SE, Wu D.** Sclerostin binds to LRP5/6 and antagonizes canonical Wnt signaling. *J Biol Chem* 280: 19883–19887, 2005. doi:10.1074/jbc.M413274200.
28. **Lin C, Jiang X, Dai Z, Guo X, Weng T, Wang J, Li Y, Feng G, Gao X, He L.** Sclerostin mediates bone response to mechanical unloading through antagonizing Wnt/beta-catenin signaling. *J Bone Miner Res* 24: 1651–1661, 2009. doi:10.1359/jbmr.090411.
29. **Lloyd SA, Loiselle AE, Zhang Y, Donahue HJ.** Evidence for the role of connexin 43-mediated intercellular communication in the process of intracortical bone resorption via osteocytic osteolysis. *BMC Musculoskelet Disord* 15: 122, 2014. doi:10.1186/1471-2474-15-122.
30. **Macias BR, Aspenberg P, Agholme F.** Paradoxical *Sost* gene expression response to mechanical unloading in metaphyseal bone. *Bone* 53: 515–519, 2013. doi:10.1016/j.bone.2013.01.018.
31. **Moustafa A, Sugiyama T, Prasad J, Zaman G, Gross TS, Lanyon LE, Price JS.** Mechanical loading-related changes in osteocyte sclerostin expression in mice are more closely associated with the subsequent osteogenic response than the peak strains engendered. *Osteoporos Int* 23: 1225–1234, 2012. doi:10.1007/s00198-011-1656-4.
32. **Moustafa A, Sugiyama T, Saxon LK, Zaman G, Sunters A, Armstrong VJ, Javaheri B, Lanyon LE, Price JS.** The mouse fibula as a suitable bone for the study of functional adaptation to mechanical loading. *Bone* 44: 930–935, 2009. doi:10.1016/j.bone.2008.12.026.
33. **Noble BS.** The osteocyte lineage. *Arch Biochem Biophys* 473: 106–111, 2008. doi:10.1016/j.abb.2008.04.009.
34. **Noble BS, Reeve J.** Osteocyte function, osteocyte death and bone fracture resistance. *Mol Cell Endocrinol* 159: 7–13, 2000. doi:10.1016/S0303-7207(99)00174-4.
35. **Ormsby RT, Cantley M, Kogawa M, Solomon LB, Haynes DR, Findlay DM, Atkins GJ.** Evidence that osteocyte perilacunar remodelling contributes to polyethylene wear particle induced osteolysis. *Acta Biomater* 33: 242–251, 2016. doi:10.1016/j.actbio.2016.01.016.
36. **Padhi D, Jang G, Stouch B, Fang L, Posvar E.** Single-dose, placebo-controlled, randomized study of AMG 785, a sclerostin monoclonal antibody. *J Bone Miner Res* 26: 19–26, 2011. doi:10.1002/jbmr.173.
37. **Parfitt AM.** Misconceptions (3): calcium leaves bone only by resorption and enters only by formation. *Bone* 33: 259–263, 2003. doi:10.1016/j.bone.2003.05.002.
38. **Poole KE, van Bezooijen RL, Loveridge N, Hamersma H, Papapoulos SE, Löwik CW, Reeve J.** Sclerostin is a delayed secreted product of osteocytes that inhibits bone formation. *FASEB J* 19: 1842–1844, 2005.
39. **Powell WF, Jr, Barry KJ, Tulum I, Kobayashi T, Harris SE, Bringhurst FR, Pajevic PD.** Targeted ablation of the PTH/PTHrP receptor in osteocytes impairs bone structure and homeostatic calcemic responses. *J Endocrinol* 209: 21–32, 2011. doi:10.1530/JOE-10-0308.
40. **Qin W, Li X, Peng Y, Harlow LM, Ren Y, Wu Y, Li J, Qin Y, Sun J, Zheng S, Brown T, Feng JQ, Ke HZ, Bauman WA, Cardozo CC.** Sclerostin antibody preserves the morphology and structure of osteocytes and blocks the severe skeletal deterioration after motor-complete spinal cord injury in rats. *J Bone Miner Res* 30: 1994–2004, 2015. doi:10.1002/jbmr.2549.
41. **Qing H, Ardeshirpour L, Pajevic PD, Dusevich V, Jähn K, Kato S, Wysolmerski J, Bonewald LF.** Demonstration of osteocytic perilacunar/canalicular remodeling in mice during lactation. *J Bone Miner Res* 27: 1018–1029, 2012. doi:10.1002/jbmr.1567.
42. **Razi H, Birkhold AI, Weinkamer R, Duda GN, Willie BM, Checa S.** Aging leads to a dysregulation in mechanically driven bone formation and resorption. *J Bone Miner Res* 30: 1864–1873, 2015. doi:10.1002/jbmr.2528.
43. **Recker RR, Benson CT, Matsumoto T, Bolognese MA, Robins DA, Alam J, Chiang AY, Hu L, Krege JH, Sowa H, Mitlak BH, Myers SL.** A randomized, double-blind phase 2 clinical trial of blosozumab, a sclerostin antibody, in postmenopausal women with low bone mineral density. *J Bone Miner Res* 30: 216–224, 2015. doi:10.1002/jbmr.2351.
44. **Robling AG, Castillo AB, Turner CH.** Biomechanical and molecular regulation of bone remodeling. *Annu Rev Biomed Eng* 8: 455–498, 2006. doi:10.1146/annurev.bioeng.8.061505.095721.
45. **Robling AG, Niziolek PJ, Baldridge LA, Condon KW, Allen MR, Alam I, Mantila SM, Gluhak-Heinrich J, Bellido TM, Harris SE, Turner CH.** Mechanical stimulation of bone in vivo reduces osteocyte expression of Sost/sclerostin. *J Biol Chem* 283: 5866–5875, 2008. doi:10.1074/jbc.M705092200.
47. **Rubin J, Rubin C, Jacobs CR.** Molecular pathways mediating mechanical signaling in bone. *Gene* 367: 1–16, 2006. doi:10.1016/j.gene.2005.10.028.
48. **Spatz JM, Ellman R, Cloutier AM, Louis L, van Vliet M, Suva LJ, Dwyer D, Stolina M, Ke HZ, Bouxsein ML.** Sclerostin antibody inhibits skeletal deterioration due to reduced mechanical loading. *J Bone Miner Res* 28: 865–874, 2013. doi:10.1002/jbmr.1807.
49. **Tu X, Rhee Y, Condon KW, Bivi N, Allen MR, Dwyer D, Stolina M, Turner CH, Robling AG, Plotkin LI, Bellido T.** Sost downregulation and local Wnt signaling are required for the osteogenic response to mechanical loading. *Bone* 50: 209–217, 2012. doi:10.1016/j.bone.2011.10.025.
50. **Turner CH.** Bone strength: current concepts. *Ann N Y Acad Sci* 1068: 429–446, 2006. doi:10.1196/annals.1346.039.
51. **van Bezooijen RL, Svensson JP, Eefting D, Visser A, van der Horst G, Karperien M, Quax PH, Vrieling H, Papapoulos SE, ten Dijke P, Löwik CW.** Wnt but not BMP signaling is involved in the inhibitory action of sclerostin on BMP-stimulated bone formation. *J Bone Miner Res* 22: 19–28, 2007. doi:10.1359/jbmr.061002.
52. **Vincent C, Findlay DM, Welldon KJ, Wijenayaka AR, Zheng TS, Haynes DR, Fazzalari NL, Evdokiou A, Atkins GJ.** Pro-inflammatory cytokines TNF-related weak inducer of apoptosis (TWEAK) and TNFalpha induce the mitogen-activated protein kinase (MAPK)-dependent expression of sclerostin in human osteoblasts. *J Bone Miner Res* 24: 1434–1449, 2009. doi:10.1359/jbmr.090305.
53. **Vivanco J, Garcia S, Ploeg HL, Alvarez G, Cullen D, Smith EL.** Apparent elastic modulus of ex vivo trabecular bovine bone increases with dynamic loading. *Proc Inst Mech Eng H* 227: 904–912, 2013. doi:10.1177/0954411913486855.
54. **Wijenayaka AR, Kogawa M, Lim HP, Bonewald LF, Findlay DM, Atkins GJ.** Sclerostin stimulates osteocyte support of osteoclast activity by a RANKL-dependent pathway. *PLoS One* 6: e25900, 2011. doi:10.1371/journal.pone.0025900.
55. **Winkler DG, Sutherland MK, Geoghegan JC, Yu C, Hayes T, Skonier JE, Shpektor D, Jonas M, Kovacevich BR, Staehling-Hampton K, Appleby M, Brunkow ME, Latham JA.** Osteocyte control of bone formation via sclerostin, a novel BMP antagonist. *EMBO J* 22: 6267–6276, 2003. doi:10.1093/emboj/cdg599.

CHAPTER 5. Summary and Future Directions

5.1 General Discussion

At one point in time, osteocytes were thought to be the dormant remnant of some osteoblasts that were trapped in the bone matrix secreted by neighbouring osteoblasts. However, a virtual explosion of research publications on osteocyte biology, and their accessibility online, in the last couple of decades has led to the validation of many observations on bone and osteocytes made by researchers many years prior [1], such as Wolff's Law [2, 3], Frost's mechanostat [4, 5] and osteocytic osteolysis [6-8]. The study of osteocytes has also grown exponentially in recent years with the advent of new techniques and methods to culture osteocytes [9-12], which correspond to different stages of its development, and to investigate their interactions with other bone cells [13-15]. Most recently, a new osteocyte cell line called OCY454, which was also derived from murine long bones, showed great promise as mature osteocyte cells for the *in vitro* investigation of osteocyte mechanobiology [16]. With the use of these *in vitro* methods, specific questions on osteocytes differentiation, its gene and protein expression responses, and its contribution to matrix mineralisation can be investigated. It is now widely accepted that osteocytes are the bone cells responsible for detecting mechanical signals (mechanosensation) and transducing these signals (mechanotransduction) into the biological responses necessary for bone remodelling [17].

Research on osteocytes was previously very limited due to them being embedded in the mineralised bone matrix. Much of the early work to decipher how bone responded to load and the role that osteocytes played was performed using *in vivo* mechanical loading models that either requires surgical or non-invasive methods [18]. New *in vivo* extrinsic bone loading models are being developed to provide more evidence on osteocyte function. For example, Lewis and colleagues recently reported a novel method to directly observe individual osteocyte calcium signalling events in relation to simultaneous whole bone loading *in vivo* [19].

Methods using *ex vivo* organ culture of bone can provide many of the advantages of both *in vitro* and *in vivo* methods with valuable insight into osteocyte functions in bone biology [20].

With *ex vivo* bone it is possible to investigate the response of osteocytes within its natural lacuno-canaliculi network to various stimuli, including mechanical loading. A number of devices and methods have been developed to enable the application of mechanical loads onto viable bone samples over time (see section 1.1). However, with the Zetos™ system, it is also possible to perform real-time measurement of the deformation from the load being applied and the stiffness of the bone sample. This makes the Zetos™ system a very useful tool in investigating the mechanobiology of trabecular bone. With the improvements made in the second generation Zetos™ system its application in bone research has been improved further. It can also be used to study the release and effects of drug delivery devices in bone.

The ability to study *ex vivo* trabecular bone that still has viable osteocytes within the lacuno canalicular network but without any other cell types to be found on the bone surface or within the marrow spaces represents a new research model. It has the potential to push forward osteocyte research within its native 3D environment [21]. Since all other cells have been removed, any response in the bone cores should be due to the remaining osteocytes within the bone matrix or some other cell-independent process. Further investigation into this is warranted. It is known that apoptotic osteocytes release ATP from pannexin 1 channels [22], which induces the receptor activator of nuclear factor κB ligand (RANKL) expression from neighbouring osteocytes and the subsequent increase in osteoclast recruitment and activity [23]. Osteocyte death ultimately results in necrosis; leading to the release of danger-associated molecular patterns (DAMPs) to the bone surface that promote the production of proinflammatory cytokines from macrophages, dendritic cells, monocytes, and neutrophils, which then induce RANKL expression in osteoblast lineage cells and further enhancement of osteoclastogenesis [24]. Thus, any changes in the behaviour of the bone cores without marrow will be due to the actions of remaining viable osteocytes, rather than the apoptotic or dead osteocytes. Future experiments with the addition of the pan-caspase apoptosis inhibitor, QVD (quinolyl-valyl-O-methylaspartyl-[-2,6-difluorophenoxy]-methylketone) [25] may provide new insights on the role of osteocyte apoptosis in this *ex vivo* model.

Even though the Zetos™ system was able to maintain the viability of the trabecular bone cores for up to 30 days [26], and it could apply real-time mechanical loading to the bone cores together with the measurement of its stiffness, it is still not able to fully replicate the actual conditions *in vivo*. Thus, the information garnered when using the system may not be fully applicable in real life. The osteogenic culture media used is able to maintain the metabolic and osteogenic activity during the course of the experiment but it does not mimic the complexity and functions of the vascular system found in bone *in vivo*. Additions of the myriad of factors that are found or can be transported in blood to the media used will offer interesting insights to bone function and the role osteocytes play. Chan et al. [27] had developed a method to seed osteoblasts onto the surface of the bone cores to co-culture with the remaining osteocytes in the bone matrix. No reports on seeding with any other cell types, including osteoclasts, had been reported to date. This will be another avenue of research that could be further explored in the future.

Not much is known about the role of the bone lining cells normally found on the surface of bone. They are believed to be inactive quiescent cells formed by a subpopulation of osteocytes once bone matrix formation had been completed [28]. Bone lining cells are proposed to play a role in the formation of bone remodelling compartments (BRCs), to prevent the inappropriate interaction of osteoclast precursors with the bone surface [29], and are also responsible for the RANK/RANKL interactions on osteoclast precursors, as they had been shown to express RANKL and other osteoblastic markers when lining active BRCs [30]. More recently, bone lining cells are believed to be a major source of osteoblasts and proliferating preosteoblasts during normal bone turnover in adults [31]. They have also been postulated to play a key role in mediating the effects of oestrogen deficiency on bone, whereby they may actually work as the cellular integrators of hormonal signals from the extracellular fluid (ECF) outside and the mechanotransduction signals from osteocytes inside the bone [32]. It has long been contended that the primary site of calcium exchange between the ECF and bone is on the quiescent surface of both cortical and cancellous bone [33]. However, taking into account the much larger surface

area of the lacuno-canalicular network (see Section 1.4 Osteocyte Processes and the Canaliculi, page 16 paragraph 5) it probably has a much larger role in this aspect. Furthermore, the osteocyte-bone lining cell system had been suggested to form a functional syncytium that regulates ion exchange between systemic and bone ECF in response to both metabolic requirements and mechanical loading [34]. However, this is probably not the case as it had been demonstrated the movement of calcium and phosphate in and out of bone is a passive process that occurs on all bone surfaces independent of the osteocyte-bone lining cell system [35]. It is not clear at this time how does the removal of the bone lining cells in the bone cores without marrow affect this ionic flux nor the quantum of the effect, and whether there is also an effect on osteocyte survival. Developing a method to remove only the marrow without disturbing the bone lining cells in the bone cores could provide the opportunity to shed some light on these questions and further elucidate the role of bone lining cells.

Sclerostin is widely believed to be a protein secreted by mature osteocytes only. It is now known to also be expressed by other cells within the musculoskeletal system, such as hypertrophic chondrocytes and cementocytes and by many other non-mineralised tissues [36]. It is also associated with a number of disease states, although the role sclerostin has in them are mostly unknown at this time. Sclerostin expression by osteocytes is regulated by mechanical stimuli, whereby it is upregulated with reduced mechanical loading leading to reduced bone formation via negative modulation of the canonical Wnt signalling in osteoblasts. However, the role sclerostin has in the osteogenic response of bone to mechanical loading is more complex and is not fully understood yet. The previous assumption that its downregulation with mechanical loading led to increased bone formation, via reduced inhibition of osteoblasts canonical Wnt signalling and the suppression of osteoclastic bone resorption directly, or indirectly via OPG regulation, is oversimplified and warrants further investigation [37] as bone surface strains does not seem to reflect osteocyte-perceived strains [38]. The work done in this thesis and the discussions above raises the possibility that sclerostin has an effect on the movement of calcium at the trabecular bone surface, independent of its effect on the surviving osteocytes. Whether it

is via interaction with the noncollagenous proteins or by some other mechanism will need to be further investigated and will be an interesting area of study.

The osteocyte lacunae may have a role in modulating osteocyte mechanosensation [39] and osteocytes are able to induce changes to its perilacunar matrix via sclerostin [40, 41]. Application of mechanical loading is associated with increased osteocyte lacunae size but changes due to immobilisation and unloading are still controversial. This reversible process of osteocytic osteolysis is probably the mechanism by which calcium homeostasis is maintained by bone in the short-term when serum ionic calcium levels changes with physiological needs [8]. Osteocyte intracellular Ca^{2+} *in vivo* fluctuated in response to physiological mechanical loading in an all-or-none fashion and that the number of responding osteocytes was very much influenced by the magnitude of the strain applied and also the loading frequency [19]. These calcium fluxes due to mechanical loading in live bone *in situ* have also previously been reported using *ex vivo* mouse tibia [42] and femur [43]. Aging is also associated with changes in the osteocyte lacunae shape and size and this may contributed to the altered response to mechanical loading in the aged.

5.2 Overview of Study Findings

The beta-testing of the second generation Zetos™ software was performed while running a trial experiment before the system was optimised as described in Chapter 2 of the thesis. Version 2.0.0.1 of the Zetos™ software was developed based on the issues encountered during beta-testing and it was able to perform well during the optimisation study. Removing the marrow from the bone cores gave a better response to mechanical loading despite the relatively short period of the study. Analysis of the perfusate also showed a consistent and more rapid uptake of Ca^{2+}, with a lower decrease in pH, by the bone cores without marrow, which was probably due to osteocyte-induced osteocytic osteolysis (see Chapter 4) [44]. It was postulated that the

better perfusion of the osteocytes, the mechanosensory cells of bone, within their lacuno-canalicular network by the culture medium contributed to these effects and their uniformity.

The usefulness of the second generation Zetos™ system for investigating a novel drug delivery system, nano-engineered titanium wires with a layer of titania nanotube arrays (TNT-Ti), in trabecular bone was demonstrated for the first time in Chapter 3 of this thesis. The use of *ex vivo* trabecular bone cores, with the marrow removed, in the bone culture chambers provided greater insight into the characterisation of the drug-release kinetics and drug distribution from the TNT-Ti than possible using *in vitro* methods. Culture medium flow rate, mechanical loading and differences in the trabecular microstructure significantly influenced the drug distribution in the bone cores. Various aspects of the TNT-Ti implant had been further investigated in bone cores with marrow [45] and as a customisable therapeutic bone implant with potential application in complex bone conditions [46]. The use of the Zetos™ system is believed to an important addition to the investigation of drug delivery in bone as there is a need for better understanding of drug distribution within the complex microarchitecture of bone and to further improve existing local drug delivery systems in bone [26, 47, 48].

In Chapter 4, exogenous sclerostin added to the culture medium of *ex vivo* bone without marrow that were mechanically loaded in the second generation Zetos™ system, abrogated the effect of loading, which were an increase in apparent stiffness and mineral accretion of the bone, with a concomitant reduction of Ca^{2+} concentration in the culture media. Addition of sclerostin also increased the osteocyte lacunar size, the release of β-CTX from the perilacunar matrix into the perfusate and the expression of genes related to bone catabolism by the osteocytes. These findings are consistent with the current concept of osteocytes being responsible for maintaining calcium homeostasis in response to immediate changes in the ECF concentration [7]. However, the mechanism by which sclerostin caused osteocytes to release peptides that are able to catabolise the perilacunar matrix are as yet uncertain [8].

5.3 Strengths and Limitations

The beta-testing of the proprietary Zetos™ software and optimisation of the Zetos™ system is one of the strengths of this work. It led to the ability to use the system in various research applications as demonstrated in Chapters 3 and 4 of this thesis. It has great potential to contribute to the study of osteocyte and trabecular bone biology in response to various stimuli and the effect of mechanical loading to these responses.

Another strength of these studies is the validation of using trabecular bone cores with the marrow removed to study osteocytes in isolation in their native lacuno-canalicular network. This method can provide further information to bridge the gap in knowledge between research work using osteocytes *in vitro* with *ex vivo* studies using whole bone and *in vivo* research in animals and human, as demonstrated in Chapter 4. The findings that sclerostin acts directly on osteocytes to modulate bone mineral accretion and the mechanical properties of bone via osteocytic osteolysis is the first to be reported, which further contributed to the accumulating knowledge on osteocyte and bone mechanobiology.

A limitation of the studies is that only bovine bone from the sternum was used in all experiments. Although new knowledge was able to be acquired using the Zetos™ system, its translation to human bone biology may be limited. Studies using human bone samples will have to be conducted in the future but getting enough bone to produce a sufficient number of bone cores to allow statistically meaningful conclusions to be drawn will potentially be another limitation of the system. Furthermore, available human bone samples are mostly from the surgical removal of bone during arthroplasty surgery, which are bone with severe osteoarthritic changes and, therefore, with different responses to mechanical loading and other stimuli. One way to overcome this is to collaborate with an organ donor harvesting team to procure viable human bone post-mortem.

A further limitation is the time-sensitive multi-layered processes involved to produce the bone cores for use with the Zetos™ system, which are the procurement, cutting, drilling and milling

of fresh viable bone and the removal of marrow from the bone cores. Extensive preparation has to be done beforehand to ensure the timely execution of each process and the bone cores produced are suitable for use. Furthermore, the need to run the elastic modulus measurement and mechanical loading sessions while staying in the 37°C chamber add to the difficulty faced when using this system. To overcome these issues, it may be beneficial to have a team of researchers that are well-trained with the system available whenever running an experiment. A small 37°C cabinet that can house the Zetos™ system might avoid the need to be bodily at 37°C. These limitations will be more evident should viable human bone samples need to be procured either from the operating theatre or elsewhere. Other limitations on using the Zetos™ system had been discussed in Chapter 2 (section 2.11 – Limitations, pages 123-4).

Lastly, another limitation of these studies is the lack of data on the viability and characterisation of the cells within the lacuno-canalicular network of the trabecular bone cores. Previous authors using the first generation Zetos™ system have noted that some of the cells in their bone cores were not viable due to the drilling process, most probably due to the trauma and heat necrosis during the drilling process because of inefficient irrigation on the sides of the bone cores [49], and after 7 days of loading, although the percentage is much less than in the unloaded bone cores [50]. It was also demonstrated by Mann et al. that the middle portion of the bone cores, between 1 mm to 2.5 mm from the top and bottom surfaces, showed the greatest osteocyte viability. It would be interesting to more closely examine the viability of the remaining osteocytes after going through all of the processes to produce the bone cores and remove the marrow. However, in the experiments performed, there were generally a high percentage of osteocyte lacunar occupancy, as was demonstrated in Chapter 4 [44].

5.4 Areas for Further Research

As indicated earlier, future work using human bone with the Zetos™ system will have a greater impact on the knowledge gap in existence regarding osteocyte and bone mechanobiology.

Should there be an opportunity to obtain viable bone from cadaveric organ donors, who previously had no co-morbid diseases, it can provide information on normal adult (or juvenile) bone and osteocyte responses to mechanical and biochemical stimuli. The use of bone from elderly patients with proximal femur fracture requiring arthroplasty surgery can elucidate further the changes in these responses in aged and osteoporotic bone. Even using diseased bone procured from joint replacement surgery can add to the better understanding of the disease process and its effects on the mechanobiology of bone and osteocytes.

The studies presented in this thesis were able to demonstrate the usefulness of the second generation Zetos™ system as it can be used in many different areas in bone research. Future studies that measure the expression of mechanosensitive genes and proteins and the factors known to be released by osteocytes in response to mechanical loading in the perfusate can add to the body of knowledge from the numerous *in vitro* and *in vivo* studies reported in the literature. Furthermore, the correlation between osteocytic osteolysis and the mechanobiology of bone and osteocytes can be further explored as an extension of the work done in Chapter 4. Elucidating further the short-term responses to loading by osteocytes and the relationship between sclerostin, osteocytic calcium fluxes, perilacunar matrix and aging using the Zetos™ system will be an interesting area to study. Osteocytic plasma membrane disruption was very recently postulated as another mechanosensory mechanism in bone [51] and its investigation using this system can produce some interesting findings. There is also potential for the development of new methods to investigate the role of bone lining cells, interaction of sclerostin with noncollagenous proteins on the bone mineral surface, and the passive movement of calcium and phosphate into bone with the Zetos™ system, as had been discussed previously.

As had been demonstrated in Chapter 3, the Zetos™ system can also be used to study other small implantable devices in bone, such as biosensors and other drug delivery devices.

5.5 Conclusions

The software beta-testing and optimisation of the second generation Zetos™ system described in Chapter 2 of this thesis have made it possible for it to be used in a variety of ways to advance bone research. Not only can it be used to better study small implantable devices in bone, as illustrated in Chapter 3, it can also be used, in conjunction with available *in vitro* methods, to better investigate osteocyte mechanobiology, as described in Chapter 4. The demonstration that sclerostin was able to abrogate bone mineral accretion and mechanical properties of bone by regulating osteocytic osteolysis could be of relevance in determining the mechanism of action of sclerostin in human physiology and have implications for the mechanism of action of sclerostin-neutralising antibodies, currently in phase 3 clinical trials [52]. Future work using the second generation Zetos™ system will be able to fill some of the important gaps in the knowledge currently available on the role of osteocytes [53].

5.6 References

1. Bonewald, L.F., *The amazing osteocyte.* J Bone Miner Res, 2011. **26**(2): p. 229-38.

2. Wolff, J., *The law of bone remodelling*. 1986: Springer-Verlag. 126.

3. Chen, J.H., et al., *Boning up on Wolff's Law: mechanical regulation of the cells that make and maintain bone.* J Biomech, 2010. **43**(1): p. 108-18.

4. Frost, H.M., *Bone "mass" and the "mechanostat": a proposal.* Anatomical Record, 1987. **219**(1): p. 1-9.

5. Hughes, J.M. and M.A. Petit, *Biological underpinnings of Frost's mechanostat thresholds: the important role of osteocytes.* J Musculoskelet Neuronal Interact, 2010. **10**(2): p. 128-35.

6. Belanger, L.F., *Osteocytic osteolysis.* Calcif Tissue Res, 1969. **4**(1): p. 1-12.

7. Teti, A. and A. Zallone, *Do osteocytes contribute to bone mineral homeostasis? Osteocytic osteolysis revisited.* Bone, 2009. **44**(1): p. 11-6.

8. Tsourdi, E., et al., *Physiological and pathological osteocytic osteolysis.* J Musculoskelet Neuronal Interact, 2018. **18**(3): p. 292-303.

9. Prideaux, M., et al., *Isolation of osteocytes from human trabecular bone.* Bone, 2016. **88**: p. 64-72.

10. Bonewald, L.F., *Establishment and characterization of an osteocyte-like cell line, MLO-Y4.* J Bone Miner Metab, 1999. **17**(1): p. 61-5.

11. Rosser, J. and L.F. Bonewald, *Studying osteocyte function using the cell lines MLO-Y4 and MLO-A5.* Methods Mol Biol, 2012. **816**: p. 67-81.

12. Kalajzic, I., et al., *In vitro and in vivo approaches to study osteocyte biology.* Bone, 2013. **54**(2): p. 296-306.

13. Yellowley, C.E., et al., *Functional gap junctions between osteocytic and osteoblastic cells.* J Bone Miner Res, 2000. **15**(2): p. 209-17.

14. Takai, E., et al., *Osteocyte viability and regulation of osteoblast function in a 3D trabecular bone explant under dynamic hydrostatic pressure.* J Bone Miner Res, 2004. **19**(9): p. 1403-10.

15. Wijenayaka, A.R., et al., *Sclerostin stimulates osteocyte support of osteoclast activity by a RANKL-dependent pathway.* PLoS One, 2011. **6**(10): p. e25900.

16. Xu, L.H., et al., *OCY454 Osteocytes as an in Vitro Cell Model for Bone Remodeling Under Mechanical Loading.* J Orthop Res, 2019.

17. Uda, Y., et al., *Osteocyte Mechanobiology.* Curr Osteoporos Rep, 2017. **15**(4): p. 318-325.

18. Hinton, P.V., S.M. Rackard, and O.D. Kennedy, *In Vivo Osteocyte Mechanotransduction: Recent Developments and Future Directions.* Curr Osteoporos Rep, 2018. **16**(6): p. 746-753.

19. Lewis, K.J., et al., *Osteocyte calcium signals encode strain magnitude and loading frequency in vivo.* Proc Natl Acad Sci U S A, 2017. **114**(44): p. 11775-11780.

20. Staines, K.A., G. Brown, and C. Farquharson, *The Ex Vivo Organ Culture of Bone.* Methods Mol Biol, 2019. **1914**: p. 199-215.

21. Zhang, C., et al., *Studies on Osteocytes in Their 3D Native Matrix Versus 2D In Vitro Models.* Curr Osteoporos Rep, 2019. **17**(4): p. 207-216.

22. Cheung, W.Y., et al., *Pannexin-1 and P2X7-Receptor Are Required for Apoptotic Osteocytes in Fatigued Bone to Trigger RANKL Production in Neighboring Bystander Osteocytes.* J Bone Miner Res, 2016. **31**(4): p. 890-9.

23. Kennedy, O.D., et al., *Osteocyte apoptosis is required for production of osteoclastogenic signals following bone fatigue in vivo.* Bone, 2014. **64**: p. 132-7.

24. Komori, T., *Cell Death in Chondrocytes, Osteoblasts, and Osteocytes.* Int J Mol Sci, 2016. **17**(12).

25. Cabahug-Zuckerman, P., et al., *Osteocyte Apoptosis Caused by Hindlimb Unloading is Required to Trigger Osteocyte RANKL Production and Subsequent Resorption of Cortical and Trabecular Bone in Mice Femurs.* J Bone Miner Res, 2016. **31**(7): p. 1356-65.

26. Schnieders, J., et al., *Ex vivo human trabecular bone model for biocompatibility evaluation of calcium phosphate composites modified with spray dried biodegradable microspheres.* Adv Healthc Mater, 2013. **2**(10): p. 1361-9.

27. Chan, M.E., et al., *A Trabecular Bone Explant Model of Osteocyte-Osteoblast Co-Culture for Bone Mechanobiology.* Cell Mol Bioeng, 2009. **2**(3): p. 405-415.

28. Franz-Odendaal, T.A., B.K. Hall, and P.E. Witten, *Buried alive: how osteoblasts become osteocytes.* Dev Dyn, 2006. **235**(1): p. 176-90.

29. Hauge, E.M., et al., *Cancellous bone remodeling occurs in specialized compartments lined by cells expressing osteoblastic markers.* J Bone Miner Res, 2001. **16**(9): p. 1575-82.

30. Kular, J., et al., *An overview of the regulation of bone remodelling at the cellular level.* Clin Biochem, 2012. **45**(12): p. 863-73.

31. Matic, I., et al., *Quiescent Bone Lining Cells Are a Major Source of Osteoblasts During Adulthood.* Stem Cells, 2016. **34**(12): p. 2930-2942.

32. Streicher, C., et al., *Estrogen Regulates Bone Turnover by Targeting RANKL Expression in Bone Lining Cells.* Sci Rep, 2017. **7**(1): p. 6460.

33. Parfitt, A.M., *Misconceptions (3): calcium leaves bone only by resorption and enters only by formation.* Bone, 2003. **33**(3): p. 259-63.

34. Rubinacci, A., et al., *Bone as an ion exchange system: evidence for a link between mechanotransduction and metabolic needs.* Am J Physiol Endocrinol Metab, 2002. **282**(4): p. E851-64.

35. Talmage, D.W. and R.V. Talmage, *Calcium homeostasis: how bone solubility relates to all aspects of bone physiology.* J Musculoskelet Neuronal Interact, 2007. **7**(2): p. 108-12.

36. Weivoda, M.M., S.J. Youssef, and M.J. Oursler, *Sclerostin expression and functions beyond the osteocyte.* Bone, 2017. **96**: p. 45-50.

37. Galea, G.L., L.E. Lanyon, and J.S. Price, *Sclerostin's role in bone's adaptive response to mechanical loading.* Bone, 2017. **96**: p. 38-44.

38. Moustafa, A., et al., *Mechanical loading-related changes in osteocyte sclerostin expression in mice are more closely associated with the subsequent osteogenic response than the peak strains engendered.* Osteoporos Int, 2012. **23**(4): p. 1225-34.

39. Bonivtch, A.R., L.F. Bonewald, and D.P. Nicolella, *Tissue strain amplification at the osteocyte lacuna: a microstructural finite element analysis.* Journal of Biomechanics, 2007. **40**(10): p. 2199-206.

40. Kogawa, M., et al., *Sclerostin regulates release of bone mineral by osteocytes by induction of carbonic anhydrase 2.* J Bone Miner Res, 2013. **28**(12): p. 2436-48.

41. Prideaux, M., D.M. Findlay, and G.J. Atkins, *Osteocytes: The master cells in bone remodelling.* Curr Opin Pharmacol, 2016. **28**: p. 24-30.

42. Jing, D., et al., *In situ intracellular calcium oscillations in osteocytes in intact mouse long bones under dynamic mechanical loading.* Faseb j, 2014. **28**(4): p. 1582-92.

43. Hu, M., et al., *Dynamic fluid flow induced mechanobiological modulation of in situ osteocyte calcium oscillations.* Arch Biochem Biophys, 2015. **579**: p. 55-61.

44. Kogawa, M., et al., *Recombinant sclerostin antagonizes effects of ex vivo mechanical loading in trabecular bone and increases osteocyte lacunar size.* Am J Physiol Cell Physiol, 2018. **314**(1): p. C53-c61.

45. Rahman, S., et al., *Drug diffusion, integration, and stability of nanoengineered drug-releasing implants in bone ex-vivo.* J Biomed Mater Res A, 2016. **104**(3): p. 714-725.

46. Gulati, K., et al., *Drug-releasing nano-engineered titanium implants: therapeutic efficacy in 3D cell culture model, controlled release and stability.* Mater Sci Eng C Mater Biol Appl, 2016. **69**: p. 831-40.

47. Porter, J.R., T.T. Ruckh, and K.C. Popat, *Bone tissue engineering: a review in bone biomimetics and drug delivery strategies.* Biotechnol Prog, 2009. **25**(6): p. 1539-60.

48. Newman, M.R. and D.S. Benoit, *Local and targeted drug delivery for bone regeneration.* Curr Opin Biotechnol, 2016. **40**: p. 125-132.

49. Davies, C.M., et al., *Mechanically loaded ex vivo bone culture system 'Zetos': systems and culture preparation.* Eur Cell Mater, 2006. **11**: p. 57-75; discussion 75.

50. Mann, V., et al., *The influence of mechanical stimulation on osteocyte apoptosis and bone viability in human trabecular bone.* J Musculoskelet Neuronal Interact, 2006. **6**(4): p. 408-17.

51. Yu, K., et al., *Mechanical loading disrupts osteocyte plasma membranes which initiates mechanosensation events in bone.* J Orthop Res, 2018. **36**(2): p. 653-662.

52. McClung, M.R., *Clinical utility of anti-sclerostin antibodies.* Bone, 2017. **96**: p. 3-7.

53. Bonewald, L.F., *The Role of the Osteocyte in Bone and Nonbone Disease.* Endocrinol Metab Clin North Am, 2017. **46**(1): p. 1-18.

CHAPTER 6. Appendices

6.1 Appendix I – Zetos Manual v1.0.0.1

Zetos

Installation and setup

Plug the Zetos remote USB cable into the computer. When prompted, insert the Zetos CD to install the USB drivers.

Manual Software installation

Create a folder called Zetos and Copy the Zetos.exe file and Zetos.ini file from the CD to the Folder.

Note: A software installer will eliminate this step in the next version

Quick Start Guide for Zetos

1) **Open an Experiment**
2) **Select the Sessions to perform**
3) **Press the Begin Testing button**
4) **When prompted by the screen, scan and load the sample**

The rest of the manual will go the details of creating experiments and other functions and further explanation of the steps above.

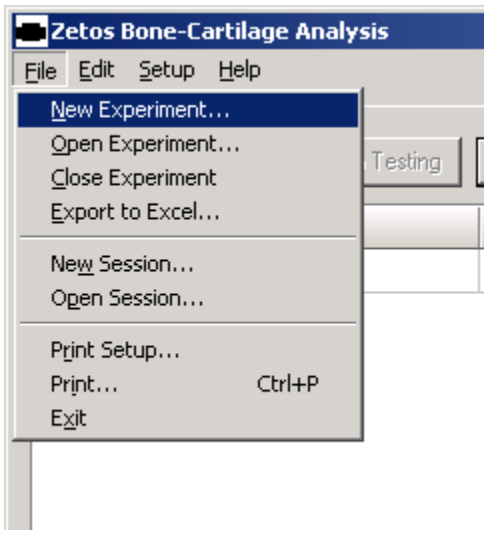

New Experiment

The Experiment Setup screen is used to begin a new experiment. This is where the numbers of the chambers are associated with the measurements of the bone samples they contain.

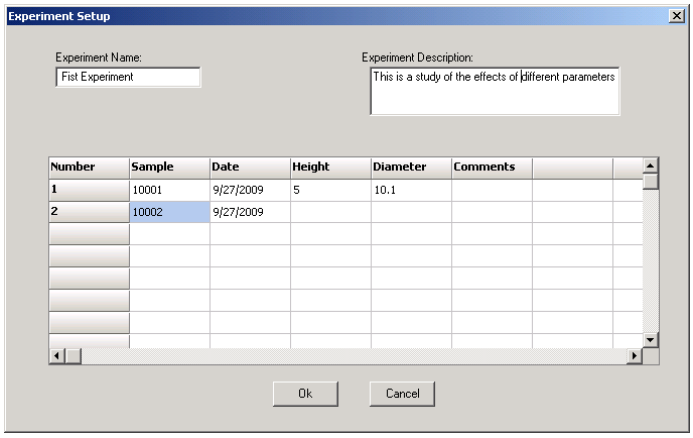

Selecting the Ok button will save the file as a type ZXP file (Zetos Experiment file) in a proprietary file format.

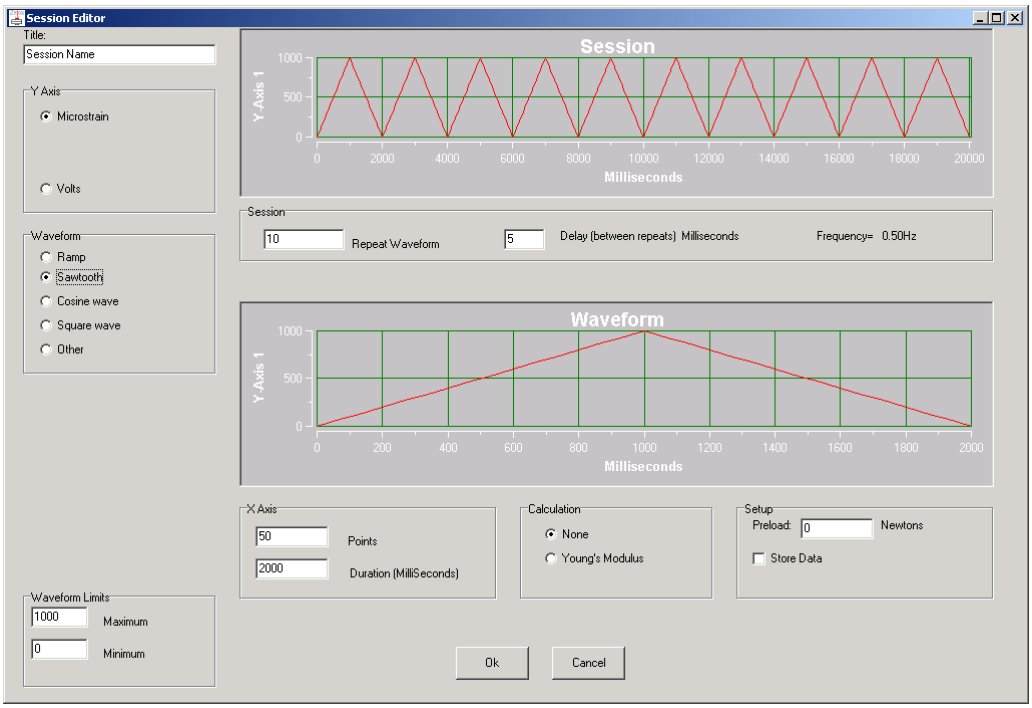

The Session screen allows selection of the session parameters.

Calibrate Force
A Kistler load cell detects the force in Newtons. It can be calibrated or using the Calibrate Force function can check the calibration.

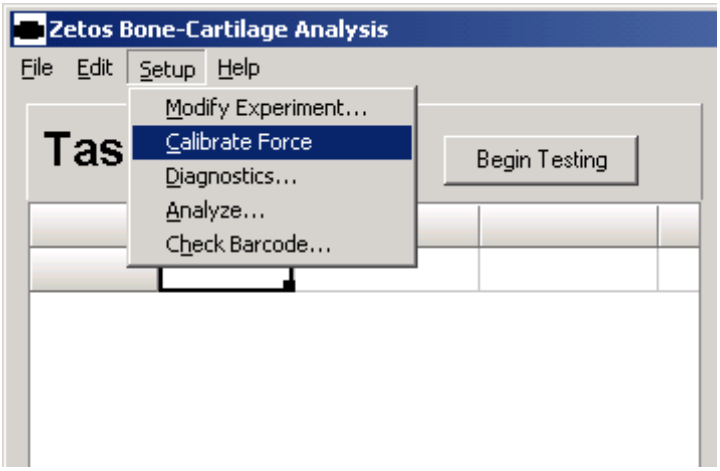

While at the PC running the Zetos software, select the Calibrate Force located under Setup.

Now walk to the Zetos system to do the calibration.

The screen on the Zetos remote controller will show the message as shown in the picture. Load the shipping restraint, adjust the position knob located on the top of the Zetos to contact the sample, and then reverse ¼ so the Zetos is just above and not touching the Shipping restraint. Now push the Enter button on the bottom left of the Zetos controller.

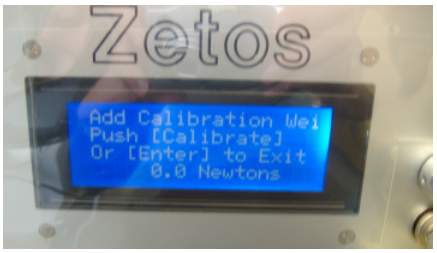

The message with now read as shown above.

To add the calibration weight, place the calibration rod into the hole on the top of the adjustment knob. Now slide on the stainless steel weight plate then carefully place the gold calibration weight on the top as shown above.

The current force readout located on the bottom row of the display will show the detected force. For Unit number 2, the force of the calibration weight and the holder is 56.70 Newtons. To calibrate, push the Calibrate Button located on the upper left of the Remote or push the Enter button to exit without calibrating.

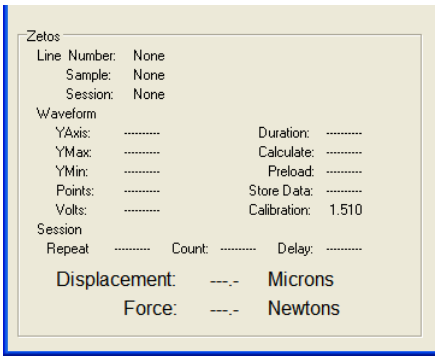

The current calibration factor is displayed on the bottom left of the Zetos software on the PC.

The calibration factor is automatically stored and reloaded each time the Zetos software is restarted.

Allow the Zetos system to be powered up for a minimum of one hour prior to calibrating.

Open Experiment

Is used each day to exercise or analyze the samples in an experiment. Select the Open Experiment and select the experiment to open

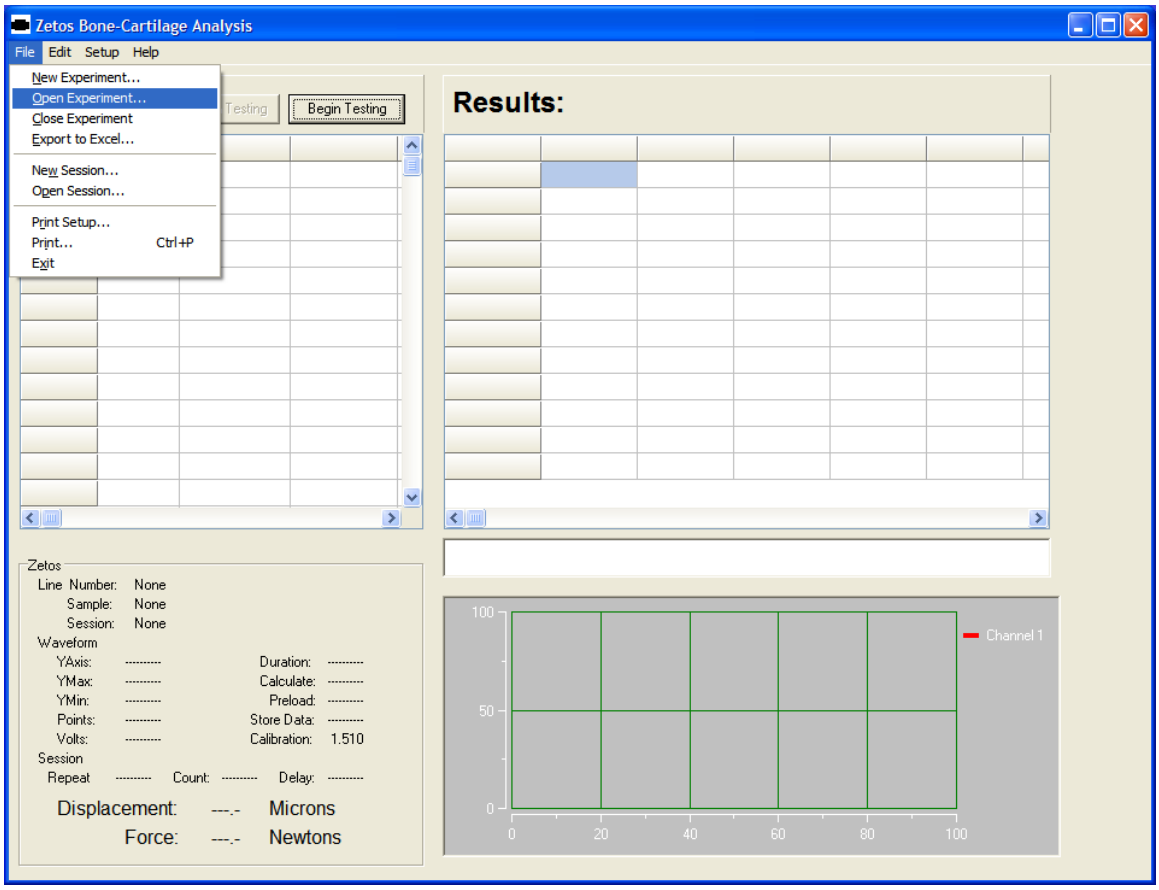

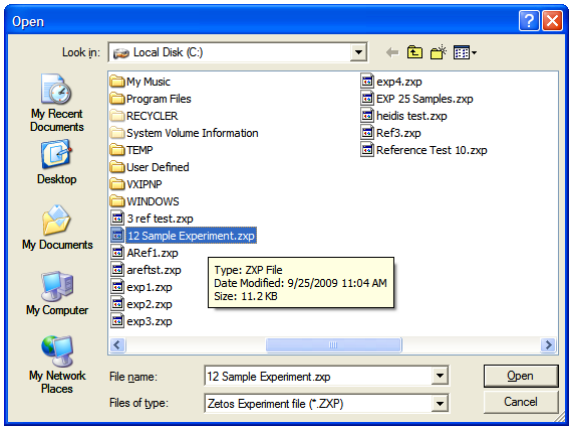

Zetos experiments end the extension ZXP.

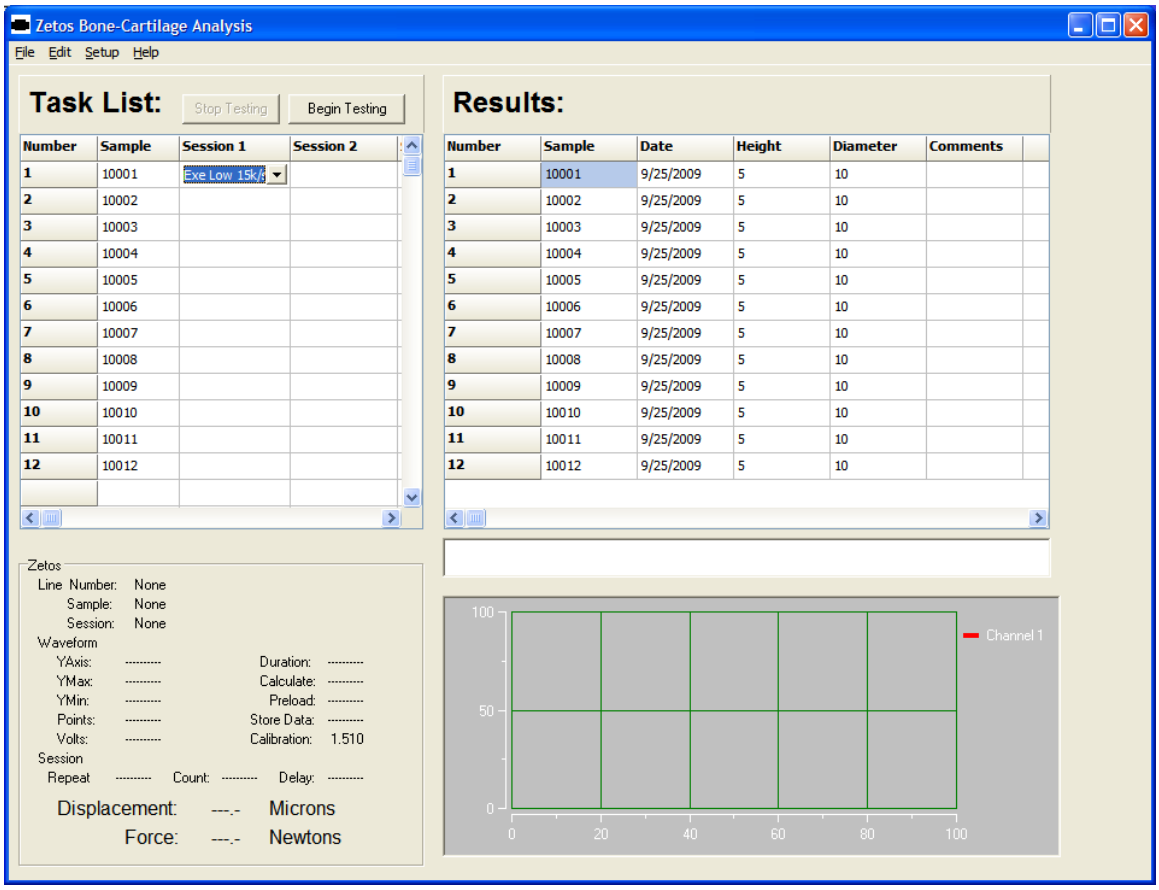

When the experiment has been opened, the information is loaded in the Task list and Results windows. To exercise the samples, Click on the box located after the first sample in the first session box. A drop down menu with show the available sessions that have previously been added to the experiment.

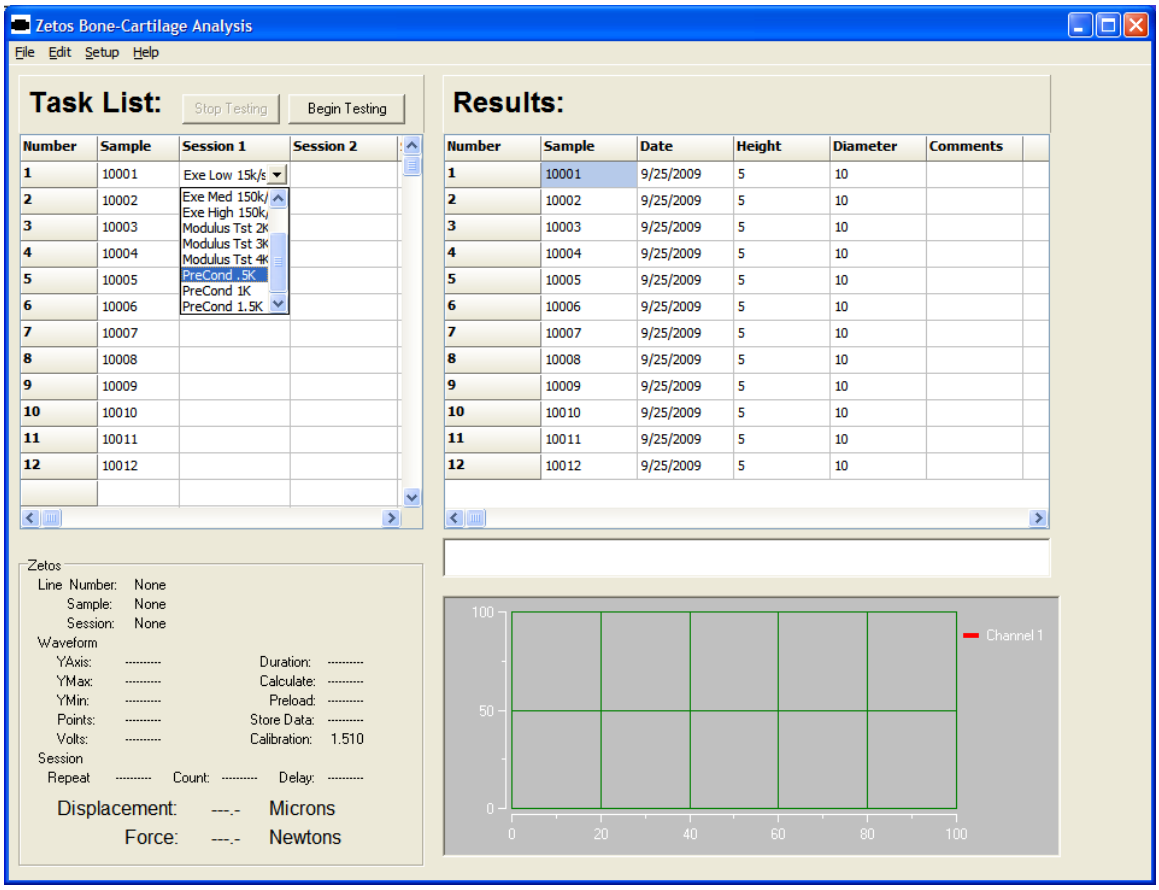

Scroll through the available selections to the one you want to use for this session. In this case one of the Precondition sessions has been selected.

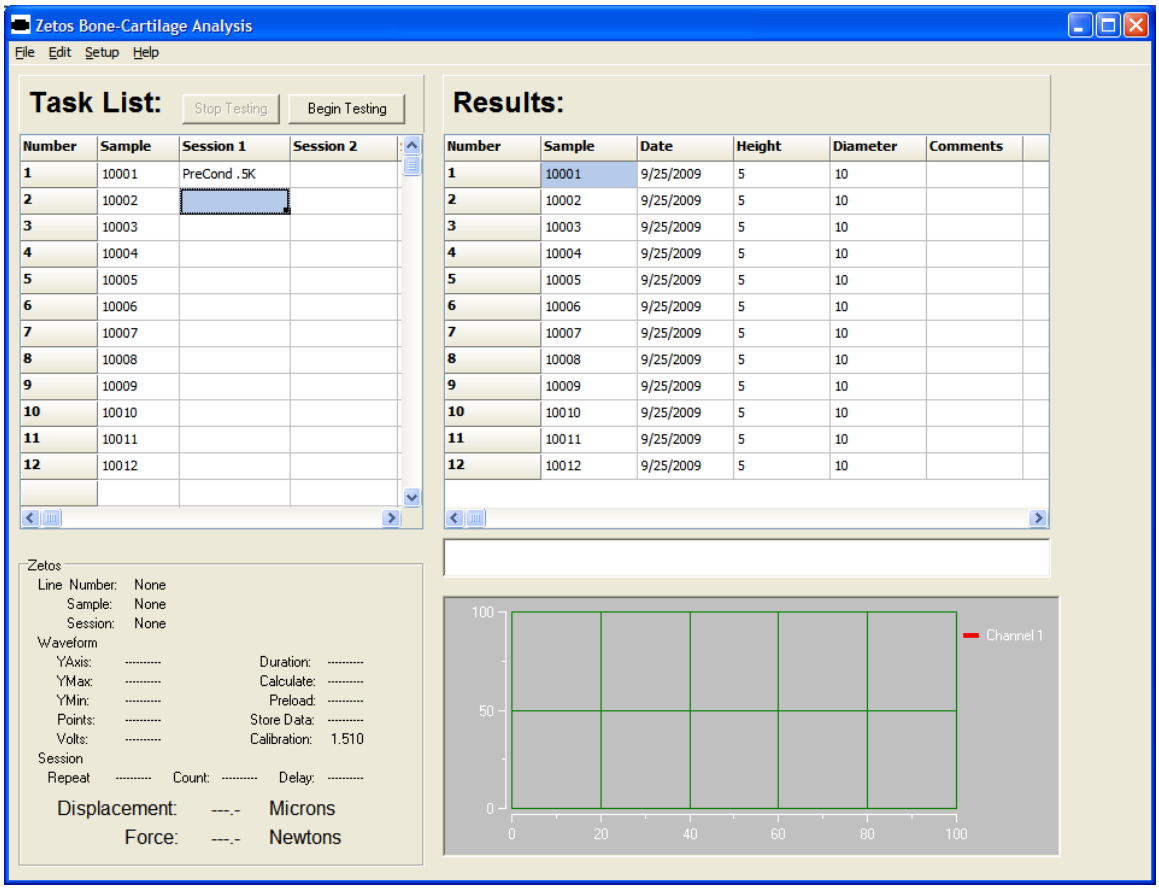

You can click and select for the rest of the boxes in case you want to have different sessions for each of the Samples.

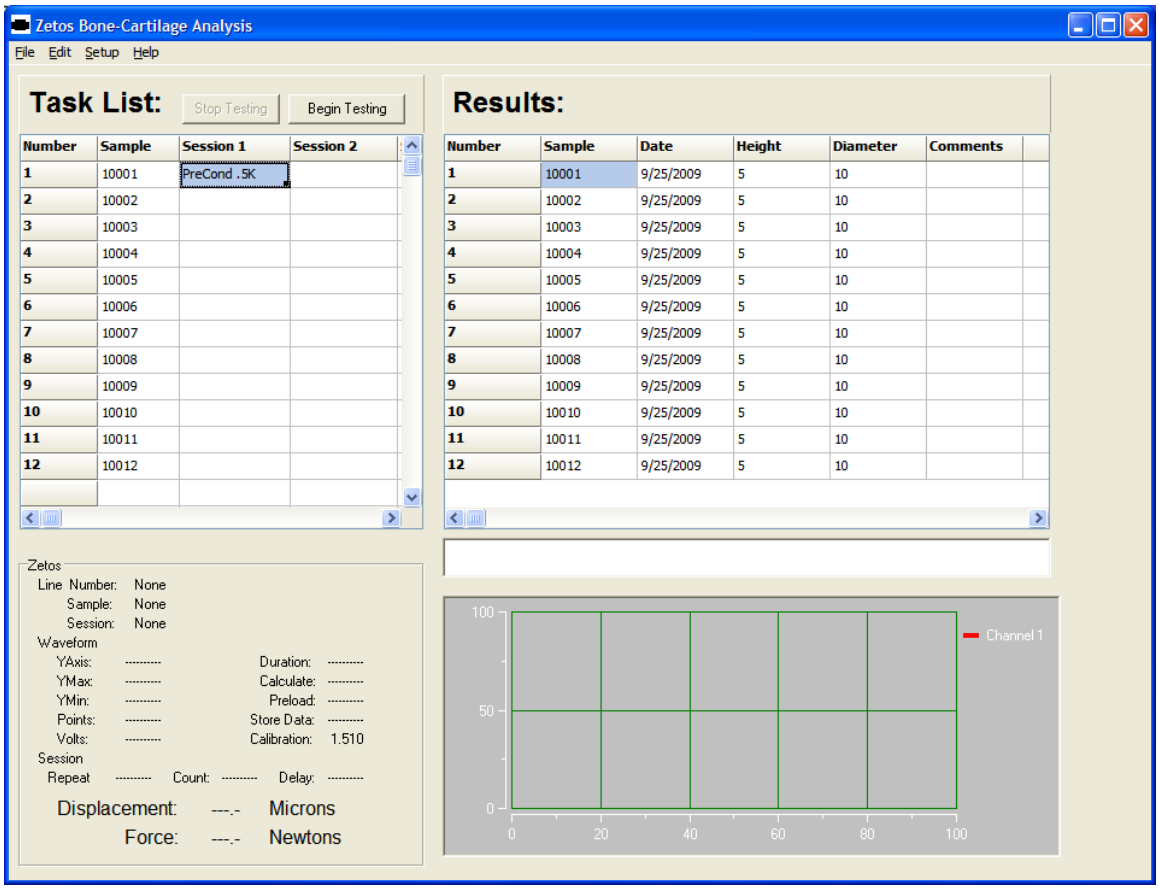

If you want to do the same session for all the samples, click on of the empty boxes, then click the first box again so instead of the drop down with the arrow you saw before you see a box like in the picture above. Now use the mouse to click on the small black box in the lower right and drag it over the rest of the cells you wish to have set to that session.

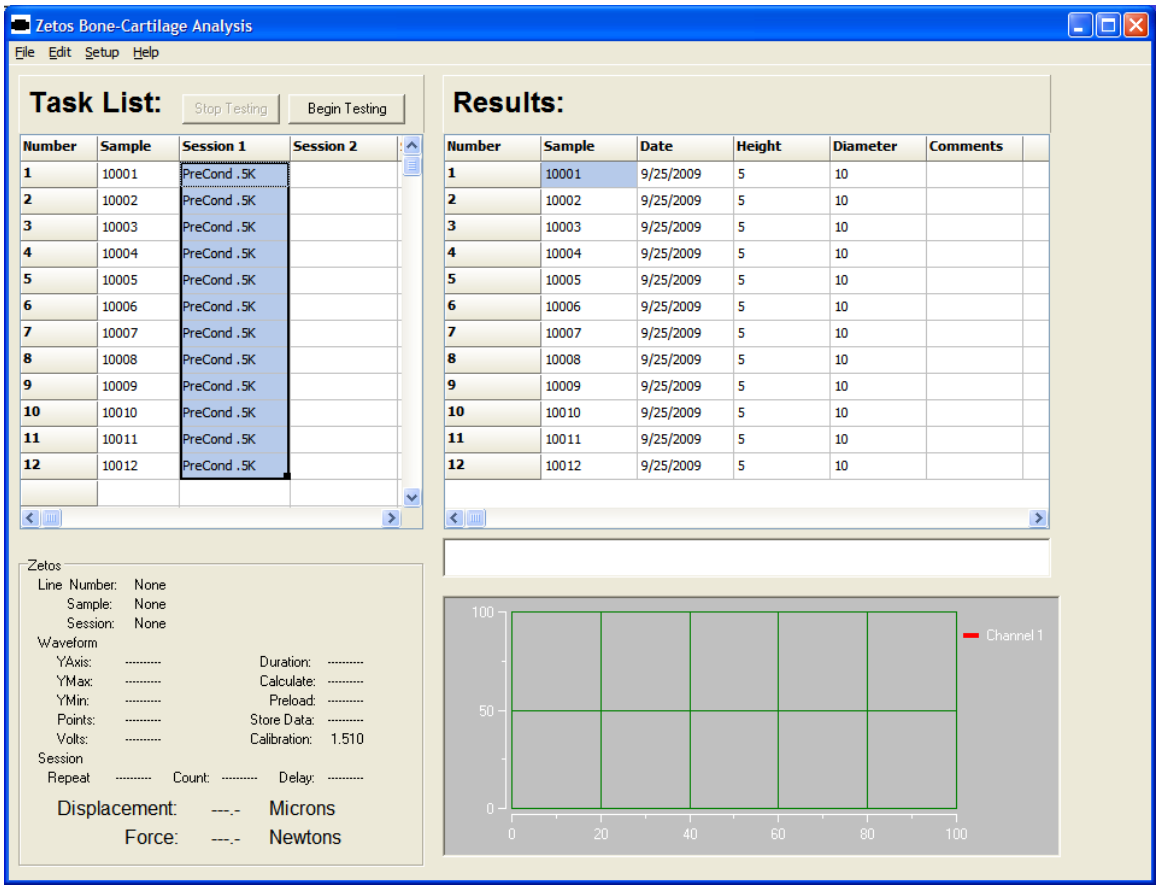

Here all the cells have been set to the same PreCond session as the first.

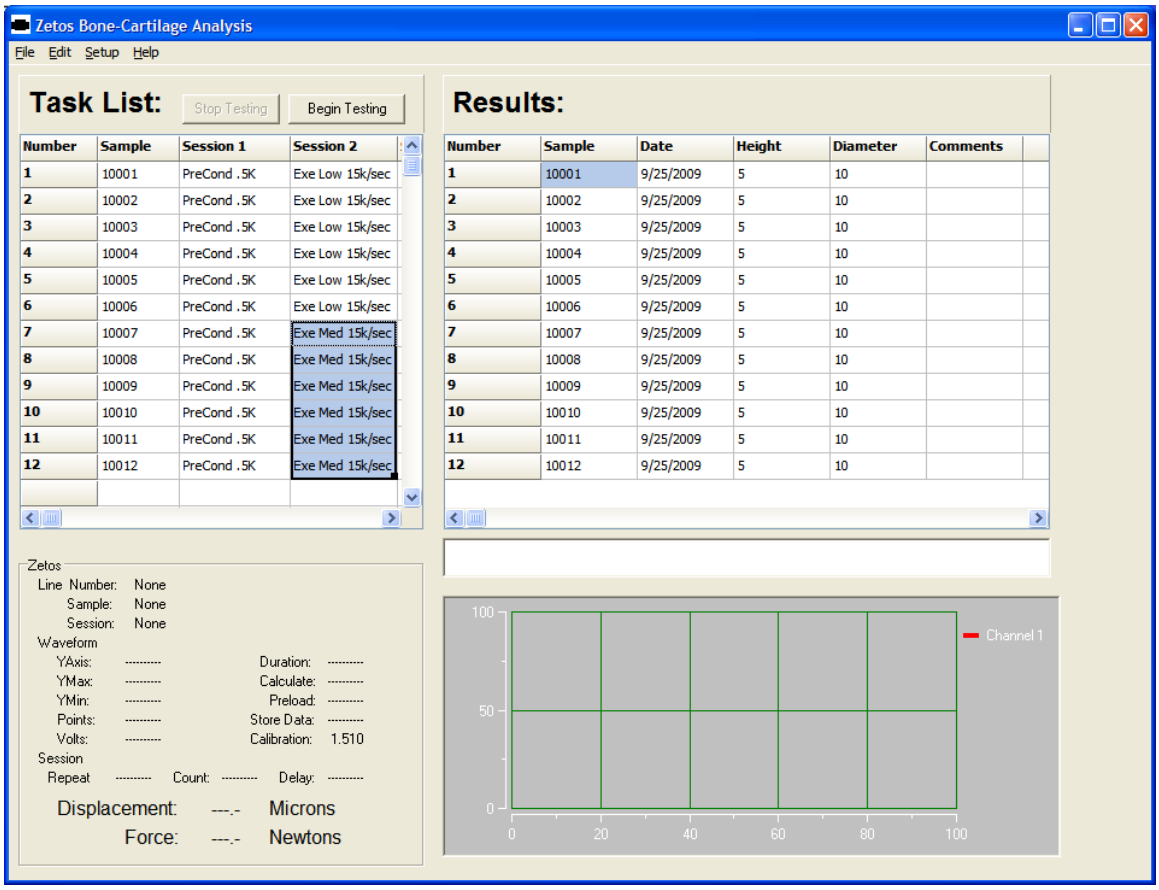

This example shows two sessions have been programmed in for each sample and the second session show different sessions have been selected for different samples.

NOTE: The Sessions are programmed and named for each experiment. A new experiment will not have any sessions until programmed.

6.2 Appendix II – Zetos Manual v2.0.0.1

ZETOS™

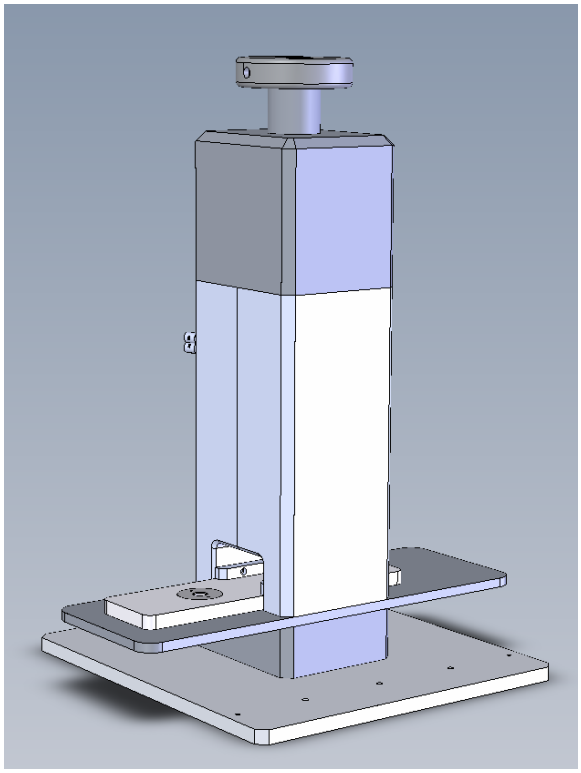

Bone Loading and Testing System
Software Manual

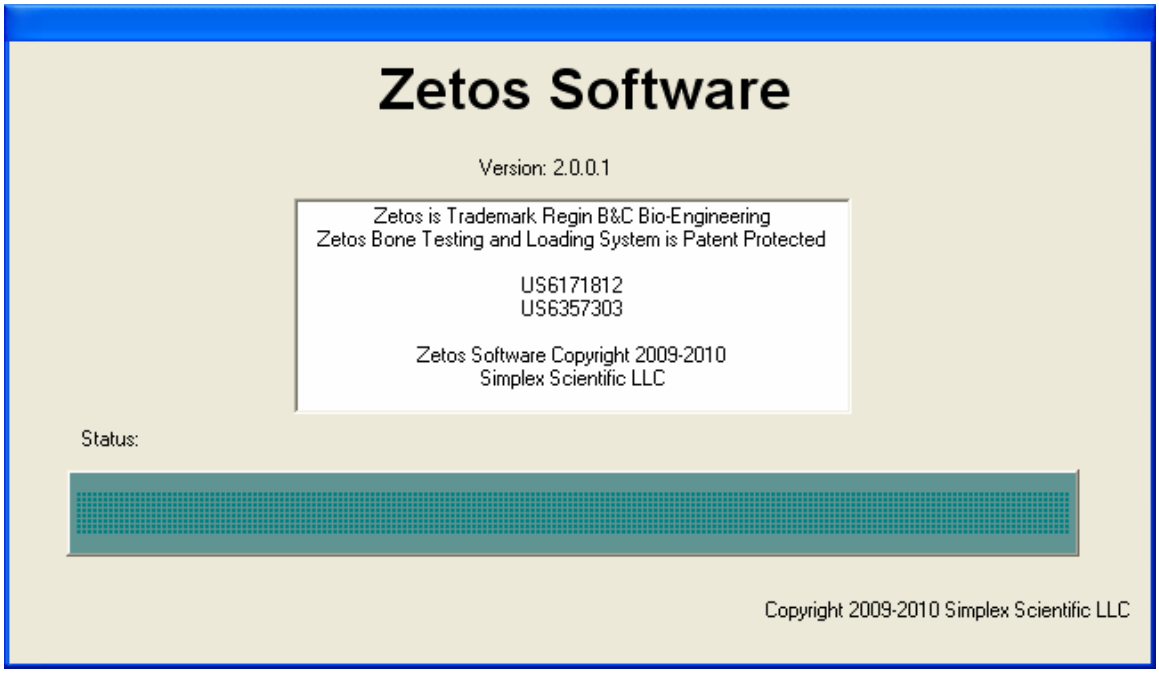

Quick Start: Daily Testing

The following is a description of the steps to be taken to either exercise (stimulate) or test the samples.

1) **Start the Zetos software**
2) **Push the monitor button**
3) **Push the Zero button to zero the force and displacement sensors**
4) **Open an experiment**
5) **Select the needed session for each sample**
6) **Push the begin testing button**

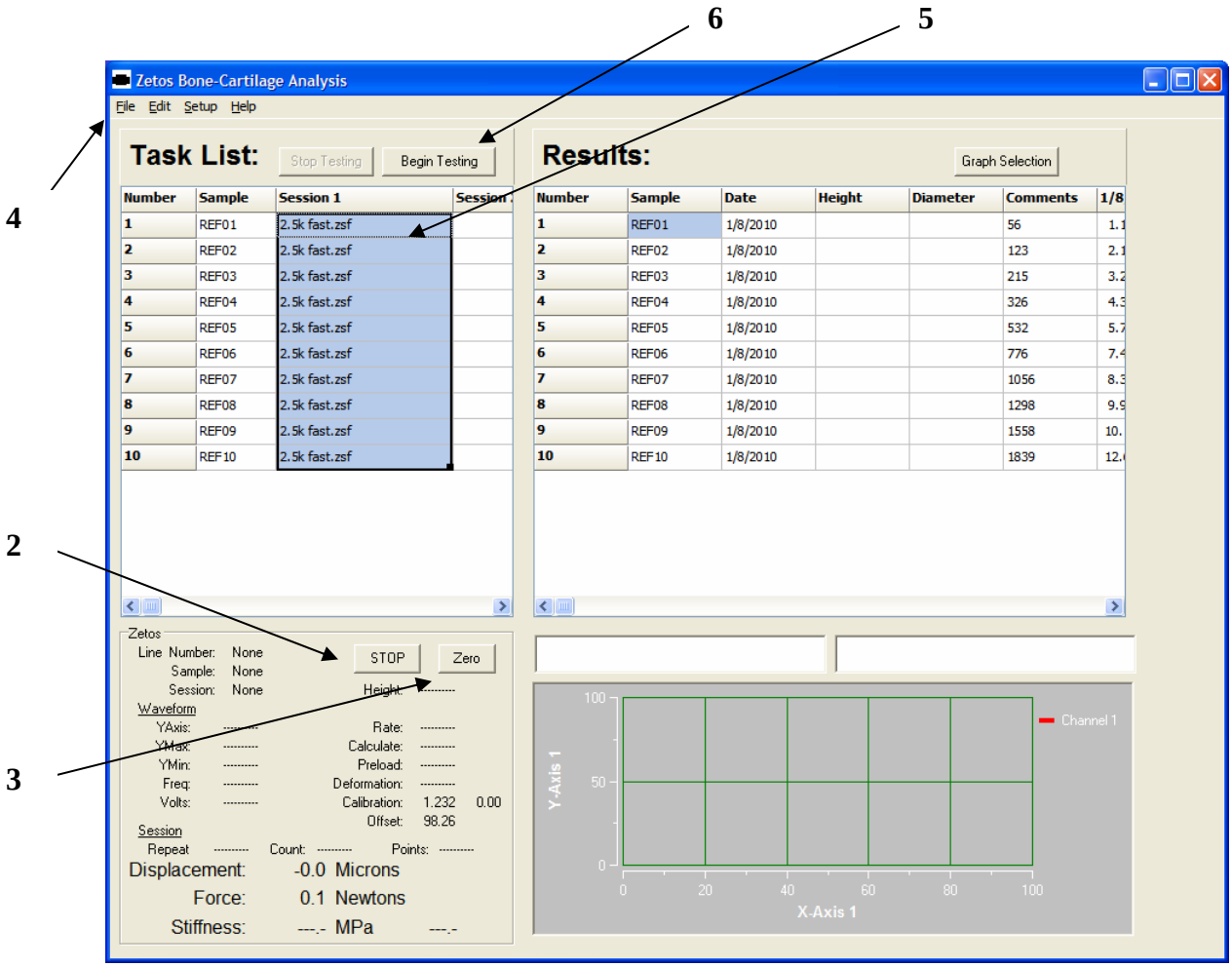

Introduction

The Zetos software controls the Zetos bone Testing and Loading system and logs experimental data. The basis for the program is the Experiment file, which contains the samples used in the experiment. The actions to be preformed on each sample are defined in the session files. These files can be created or modified when desired. They are selected for use in the task list and their parameters and results are logged in the Experiment file.

To begin an a new experiment, create a new Experiment file, then define the session files that are to be used or use the default session files shipped with the software.

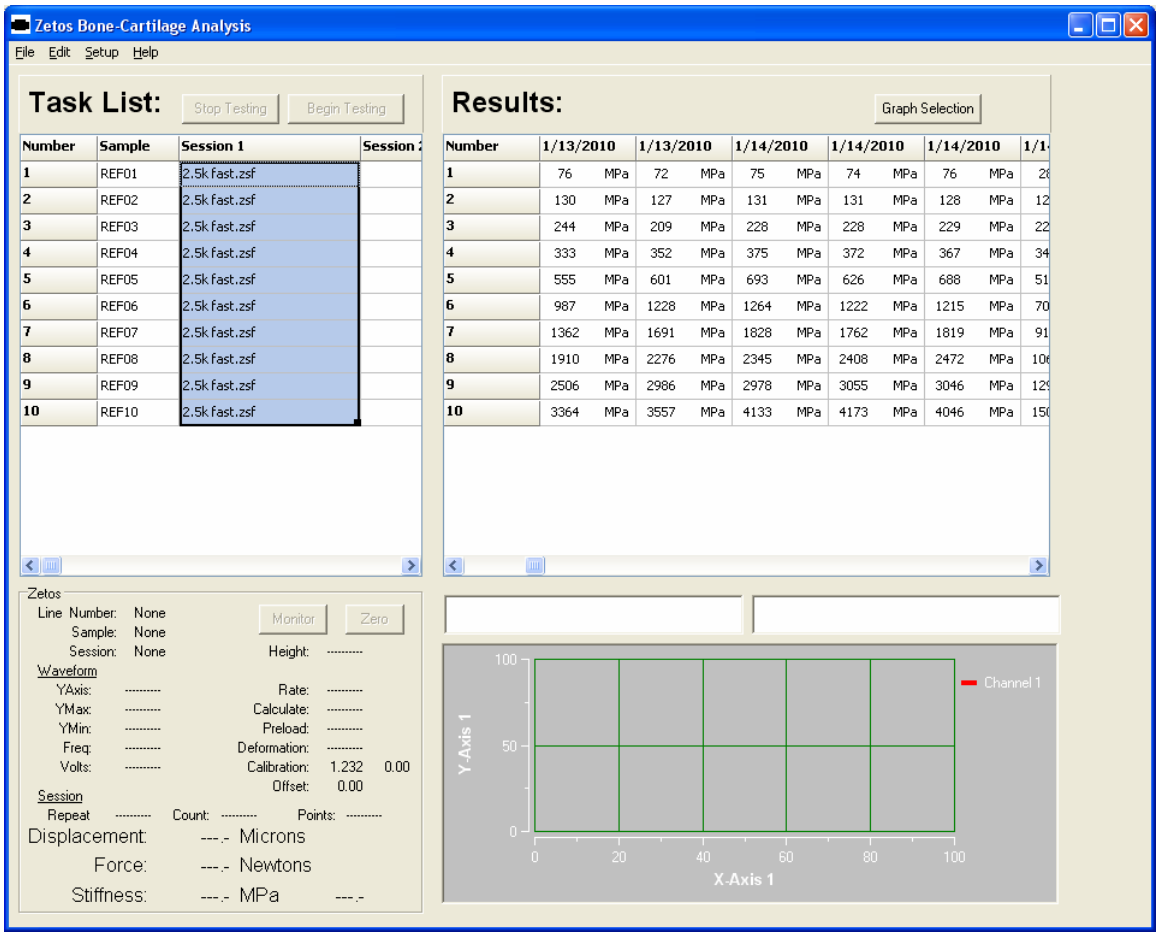

Zetos Main window

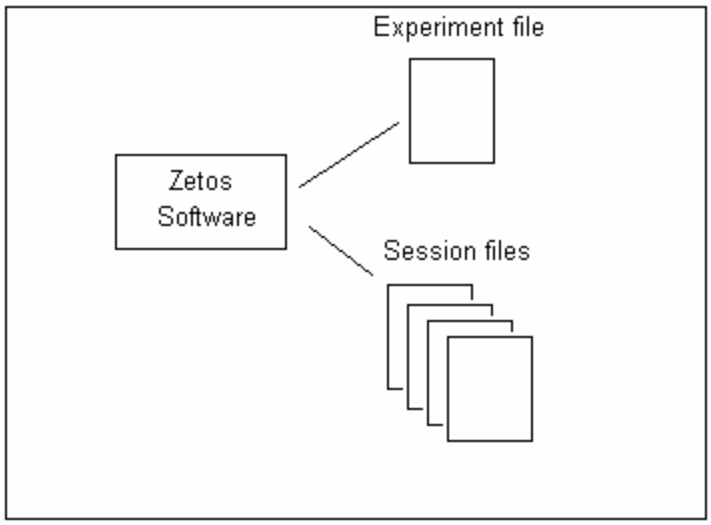

Zetos software with the Experiment and Session files

Creating a new Experiment

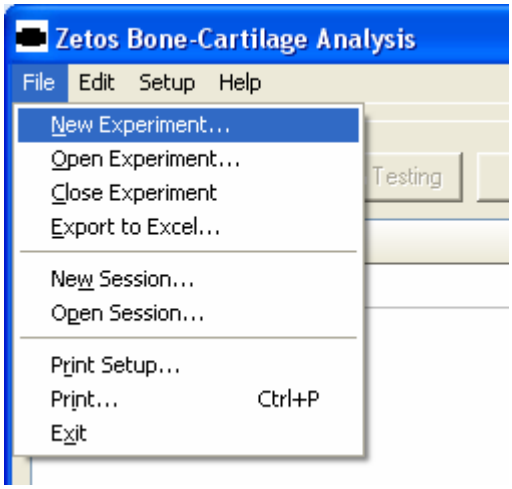

Select New Experiment from the File menu to create an Experiment.

You will need to know the number of each chamber or reference body your experiment will contain along with the height and diameter of each bone sample.

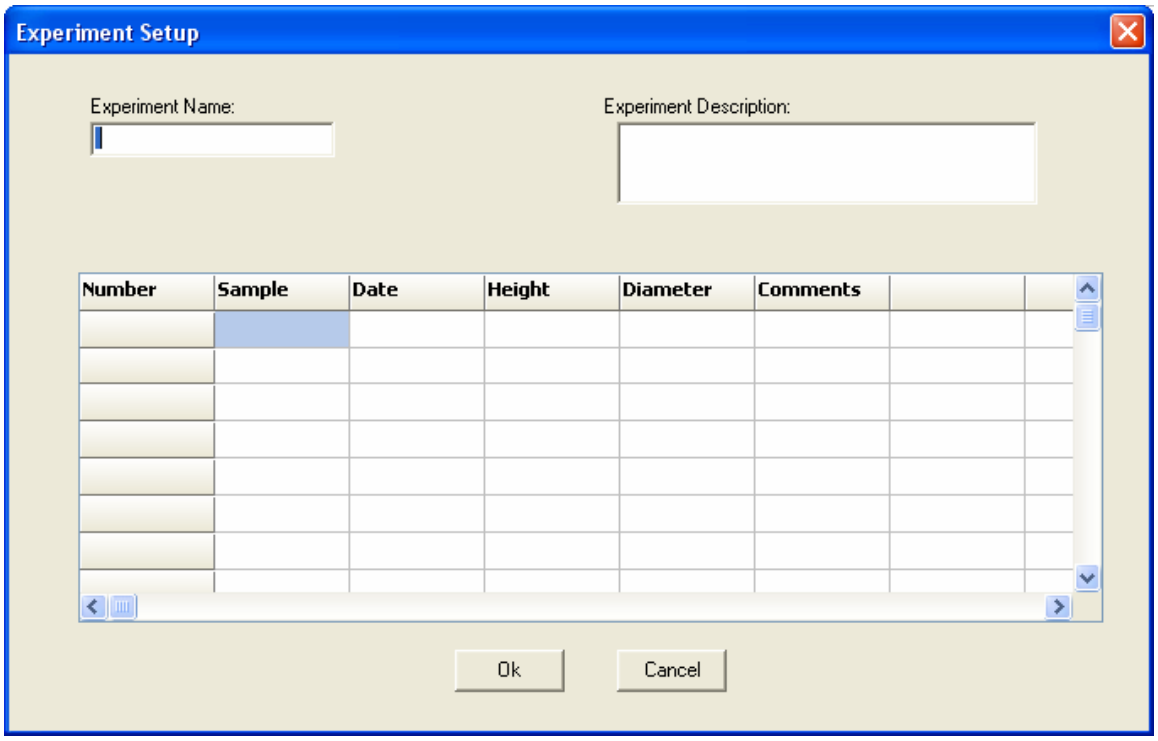

Enter the barcode number of the sample in the **Sample** column, the number and date will automatically be entered. The barcode numbers must be entered exactly as on the barcode to be recognized by the barcode reader.

Next enter the height and diameter in the next two columns in mm (millimeters). If no values are entered, default values of 5mm height and 10mm diameter is used.

Click to Ok button to close and save the file or cancel to close without saving

NOTE:
It is not possible to edit the experiment file once it is created.

Setting up a Session

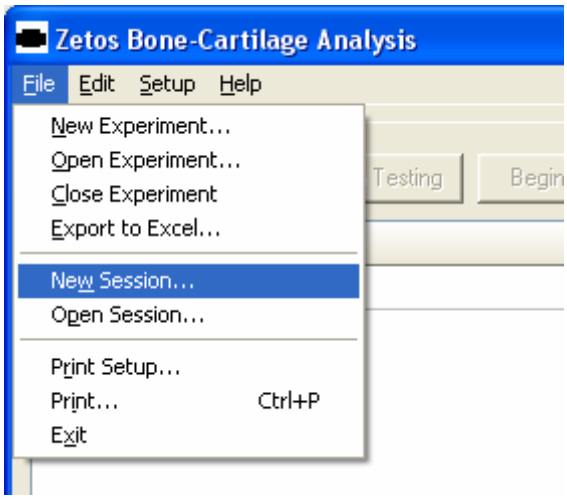

The Session Editor is used to create the sessions to be preformed on each sample. Access the editor by selecting New Session from the File menu.

Sessions can be either an exercise (bone stimulation) session or a calculation of Young's modulus.

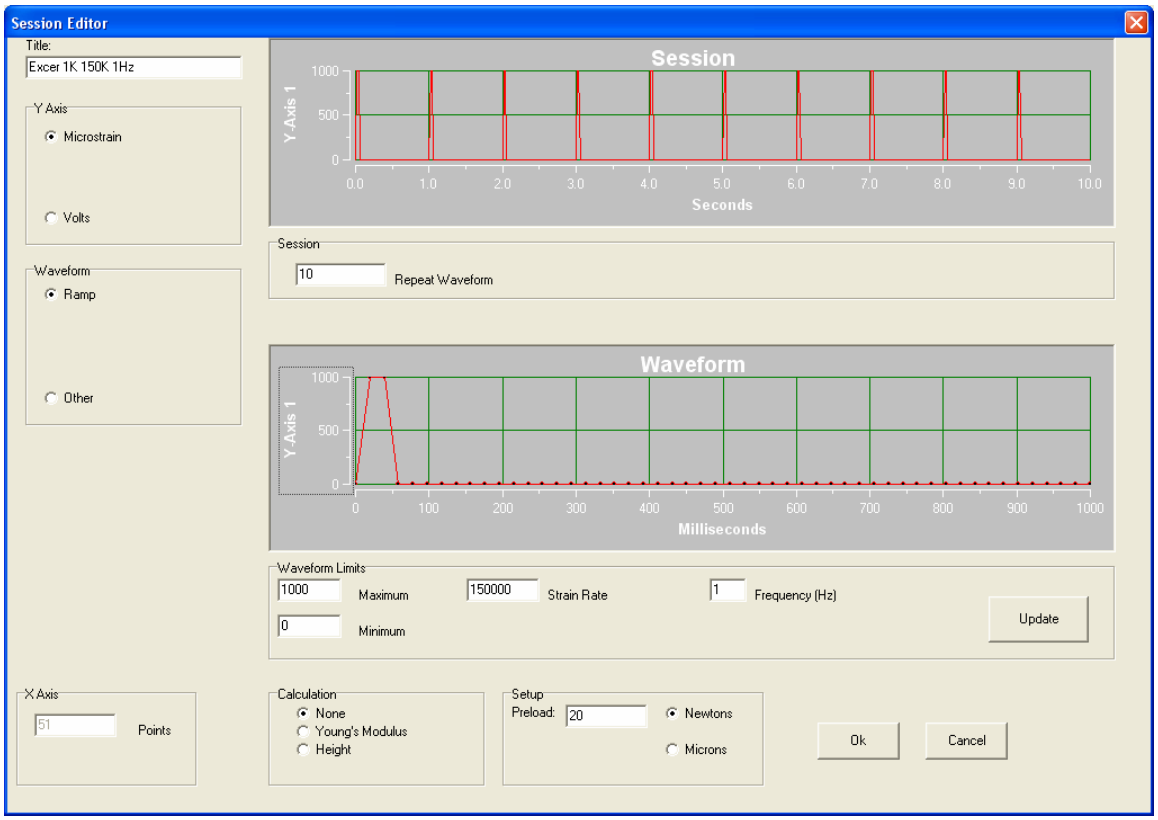

The Editor allows experimentation with different settings and displays the results. The information entered in the Waveform Limits box is displayed in the Waveform chart by pushing the Update button. The Session Chart displays the waveform the number of times defined by the repeat Waveform box.

The **Calculation** section allows selection of none or the Young's Modulus. High speed Exercise sessions must select None.

Selection of the Young's Module will automatically set several parameters to reduce the speed of the system to avoid simulating the samples.

In the **Setup** section Enter the desired Preload value in Newtons. 20 Newtons is recommended.

Operations

With each sample the Zetos software first does a survey scan to determine an estimated K (stiffness) value to be used in the following Young's Modulus calculation or exercise session. This scan slowly increases the force on the sample until it reaches the uncorrected displacement value set in the session. The chart displays the data during the scan. From the K estimate, the corrected displacement value is calculated and used by the next step of the session.

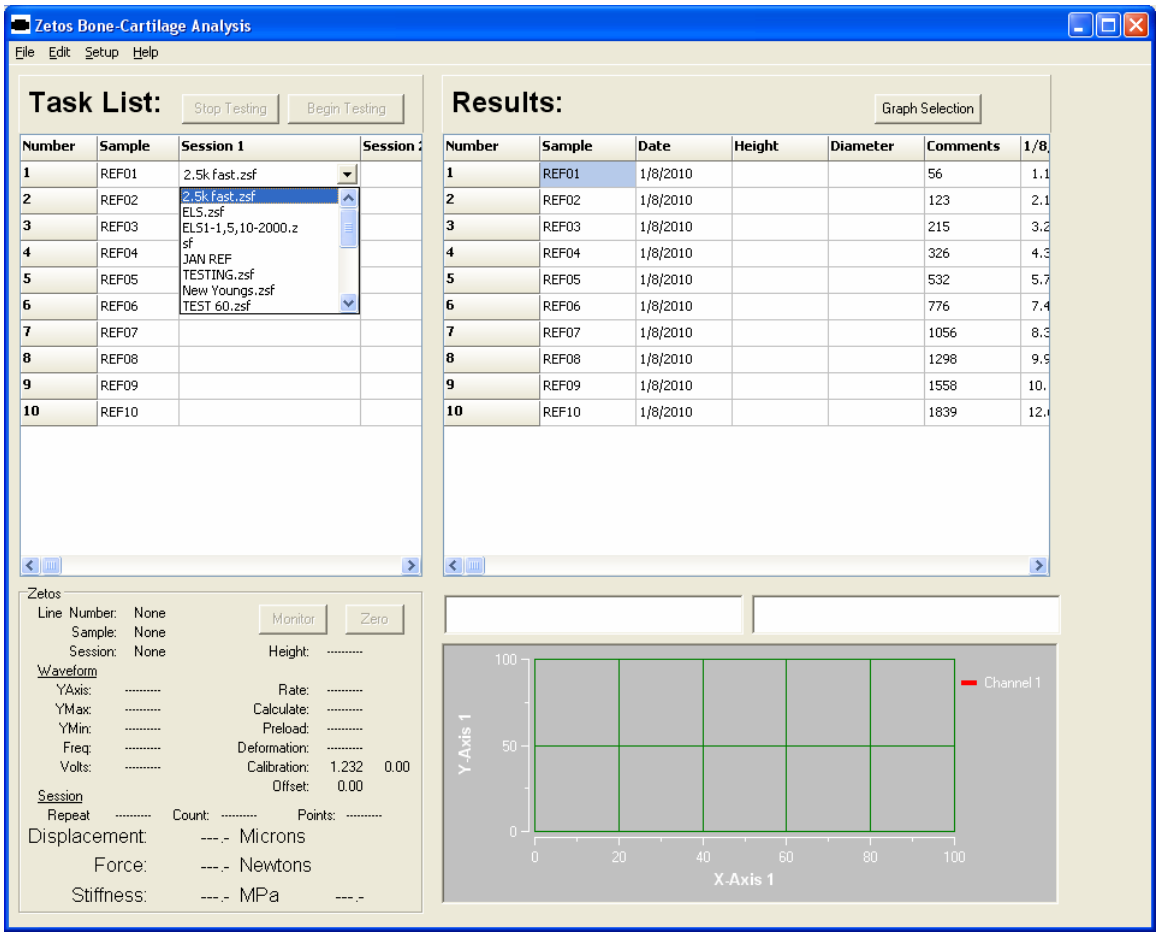

Calibration

The force sensor should be periodically checked with the reference weight set and calibrated when needed.

To calibrate or weight the reference weight, place a reference body with the sapphire crystal to act as a stop. Turn the knob on the top of the Zetos to touch the top of the reference then back 1/8 of a turn so the Zetos is not touching it.

Push the monitor then the Zero buttons. Next slide the weight holder into the top of Zetos then carefully add the reference weight.

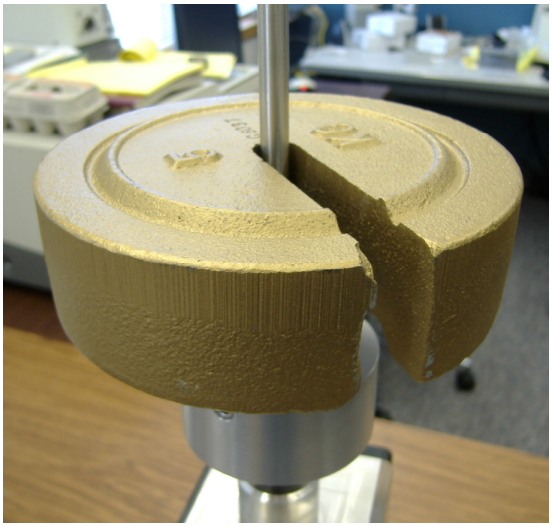

If the weight is within 0.5 N of the standard weight then nothing further is needed. If not, then remove the weight and holder and start the calibration.

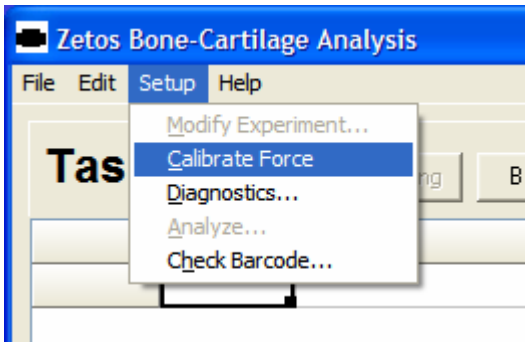

Start the calibration function by selecting Calibrate force from the Setup menu.

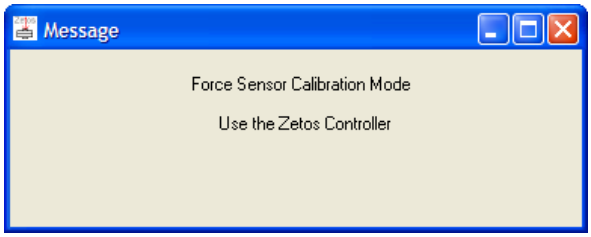

Calibration is done completely from the Zetos and the Zetos PC displays a message screen while this is occurring.

The Zetos Remote will display the following:

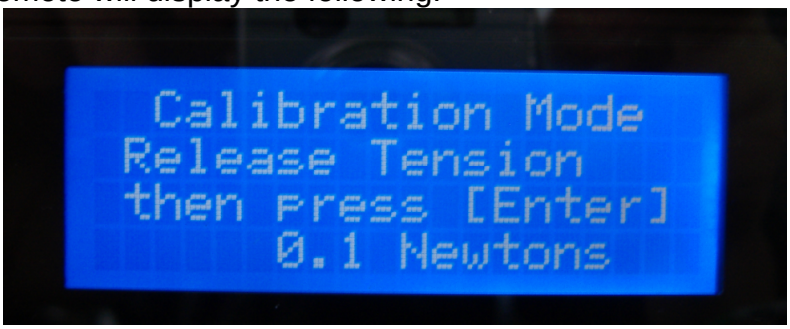

Place a reference body and crystal in the system and with the Zetos adjusted so it is close, but not touching as was described above, you should see the message as above. The Reference Weight should not be installed at this point. Don't worry about the reading, it will be zeroed when the Enter button is pushed.

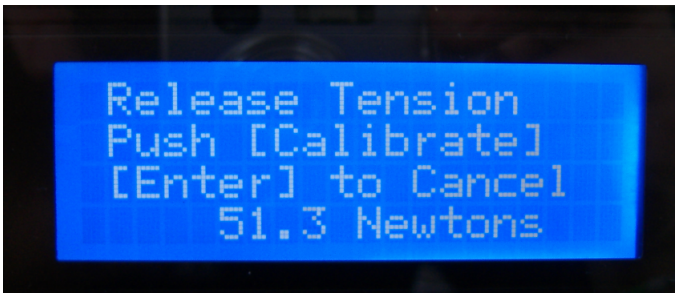

Add the weight holder and calibration weight as described previously. Push the Calibrate button to calculate a new calibration factor, or the Enter to exit without making a change.

Check Barcode

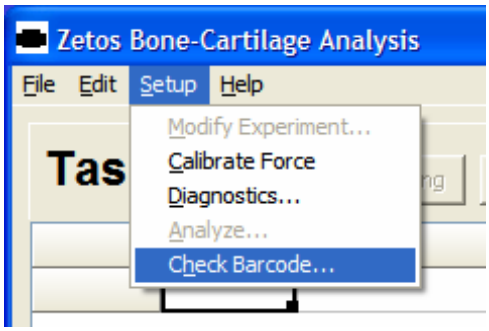

As barcode can be checked using the Barcode function. The barcode reader will be turned on and the read barcodes will be displayed on the remote screen.
Push the Enter button, or close the window displayed by the Zetos software to exit.

Excel

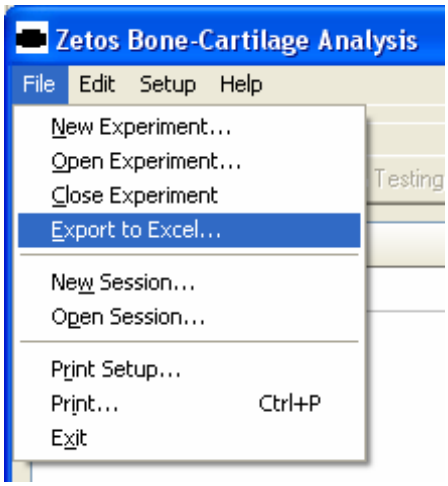

The experiment file can be exported to Excel at the conclusion of the experiment or in the course of the investigation for further analysis of the data.

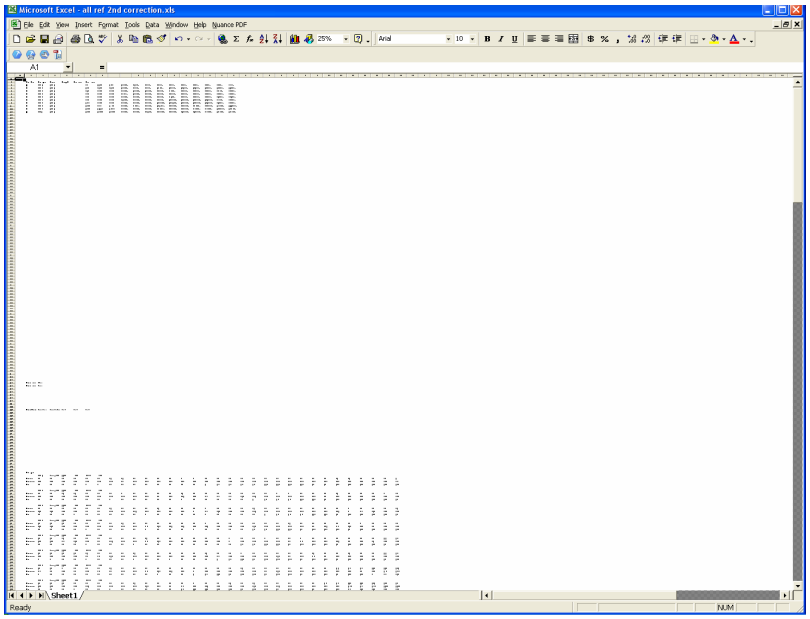

Zoomed out view of the layout of the data in Excel

In the picture above shows the data in Excel. The very top portion is the same as the Results graph in the Zetos software. Scrolling down below line 100 reveals the logged data.

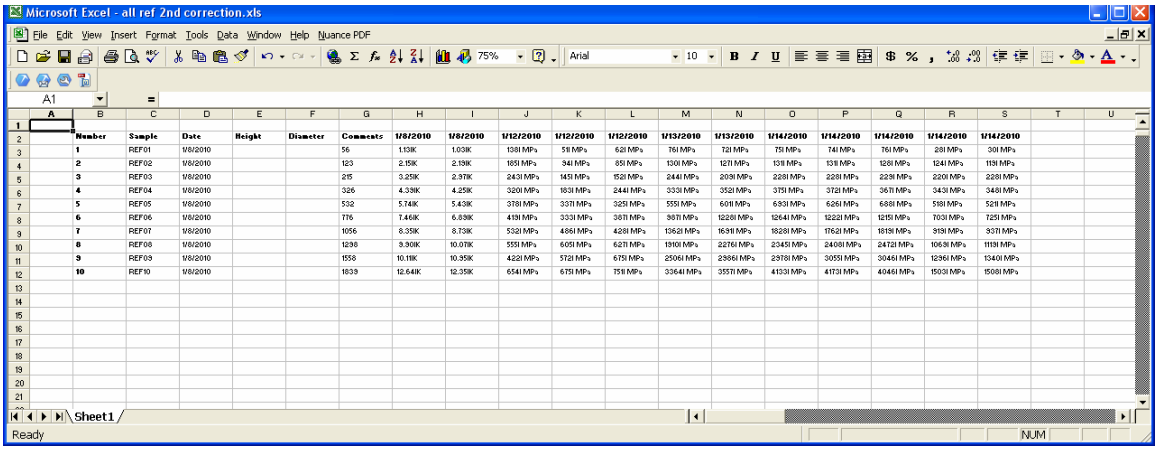

Results portion

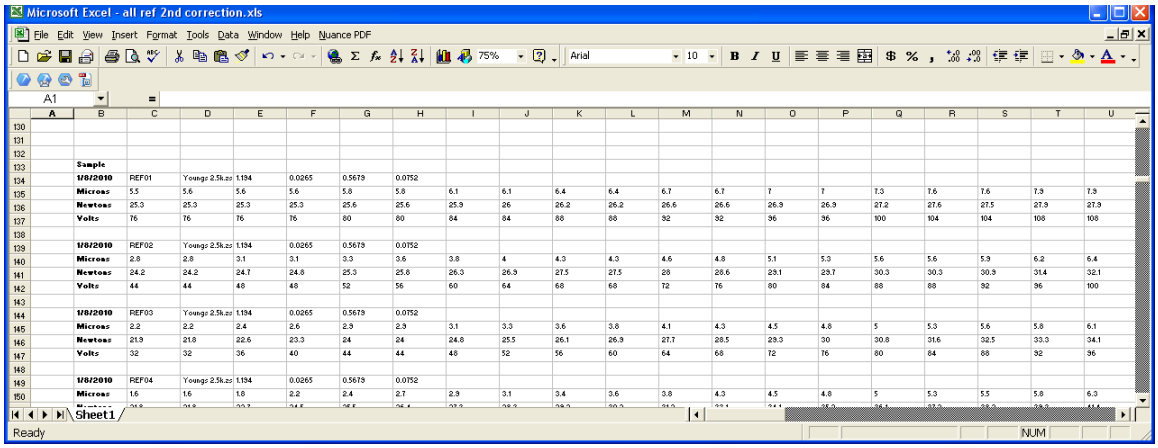

Log portion

Calculations

Correction curve.

The Zetos software uses a 3rd order polynomial for correcting the Estimated K values. The equation is:

Kcorr=(TermA * Kest^3) + (TermB * Kest^2) + (TermC *Kest)

Kcorr: corrected stiffness value
Kest : uncorrected stiffness value equals slope of force values vs the displacement values

The curve is forced to zero so there is no fourth term.

The terms are stored in the Zeto.ini file located in the Zetos program folder. Manually changing any of the values will change the results of the program. The current setting for each of this values is logged with the data in the experiment file. The Zetos software must be restarted to begin using any modified values.

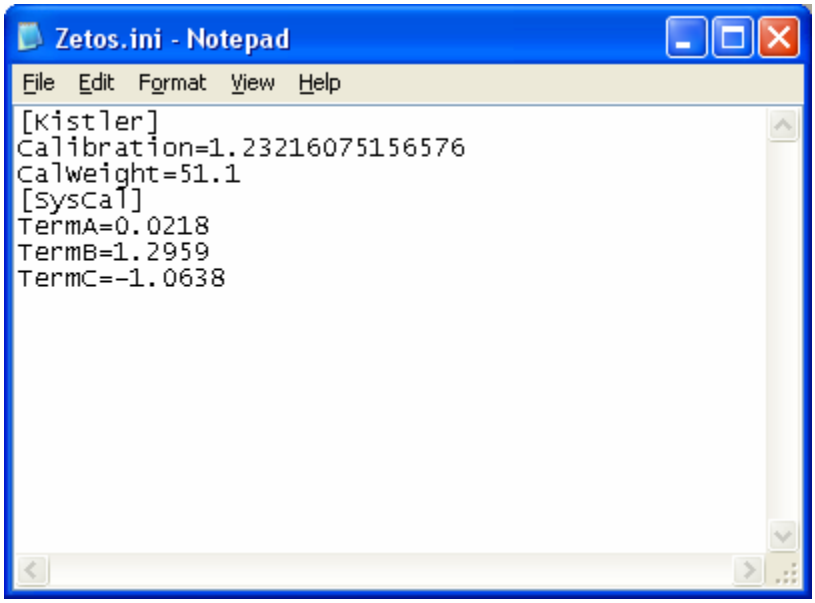

Megapascal Calculation

The stiffness value is converted to a MPa (Mega Pascal) value by the following:

E (in Mpa) = K * Length / Area
= K (in N/micron) * (1000 micron/mm) * (5 mm) / 3.1415 * 25 mm^2
= K * 63.66

6.3 Appendix III – Calibrating the Zetos™

Kamarul

CALIBRATING THE ZETOS™

Startup

- Connect USB cable to laptop
- Power on laptop
- Turn on Zetos™ machine
- Start Zetos™ software on laptop

Click Monitor (on software)

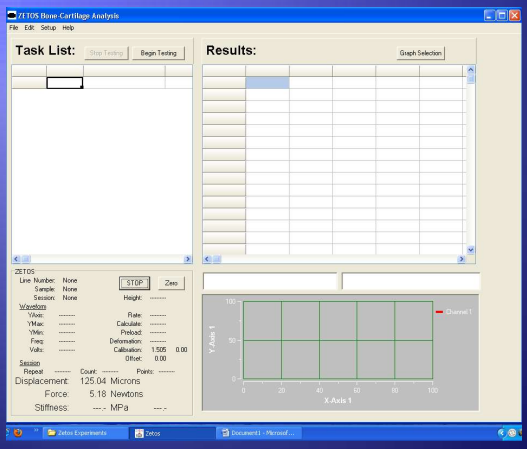

Click Zero (on software)

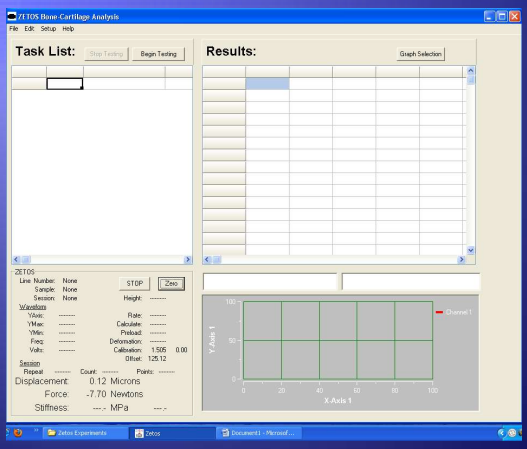

Initial Setup

- Release and remove transportation body
- Put in one of the standard reference bodies
  - i.e. any one of REF01 to REF10
- Turn knob till force sensor is on reference body
- Release tension by turning knob counter-clockwise 1/8 turn
  - So that force sensor is just off the top surface of the reference body)

Readings after initial setup

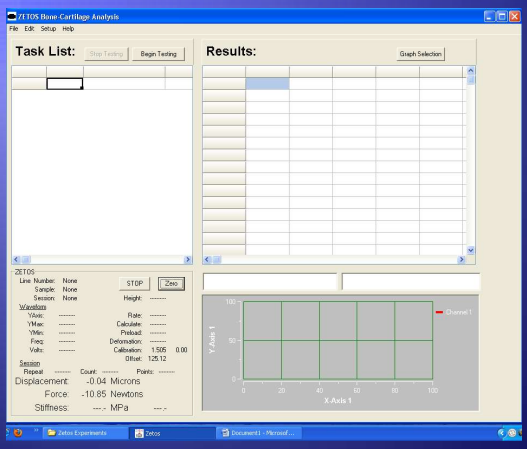

Click Zero (on software)

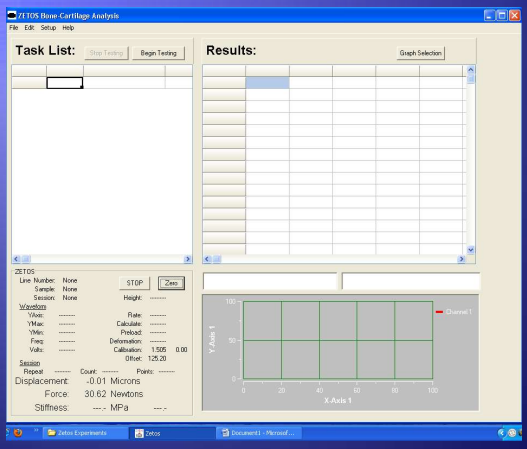

Click Zero (again)

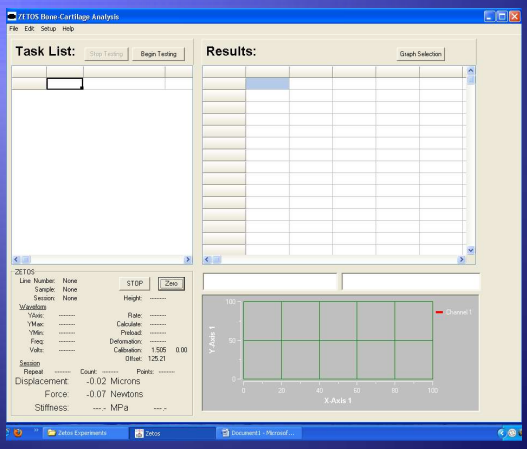

Add calibration weight

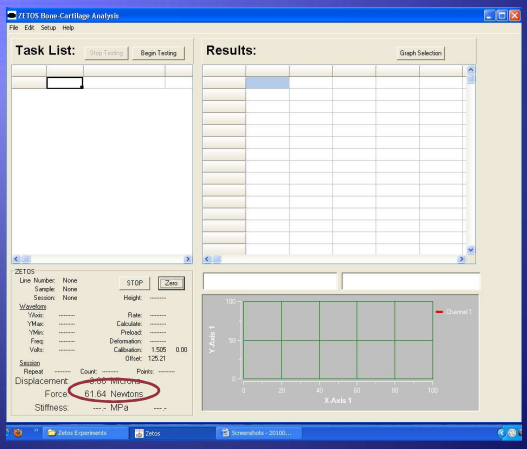

- OK if ± 0.5N of actual weight (56.70N), otherwise proceed to calibrating force sensor

CALIBRATING THE FORCE SENSOR

Remove weight

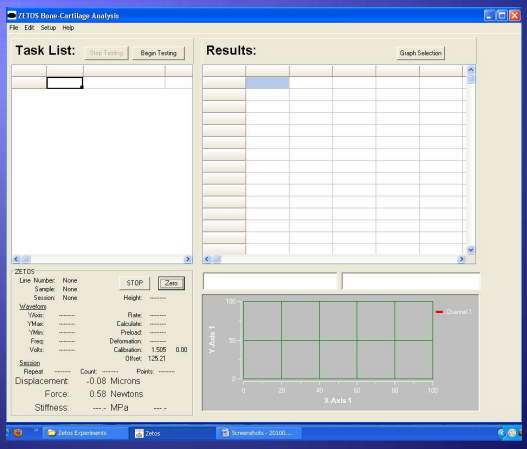

Put in reference body and release tension

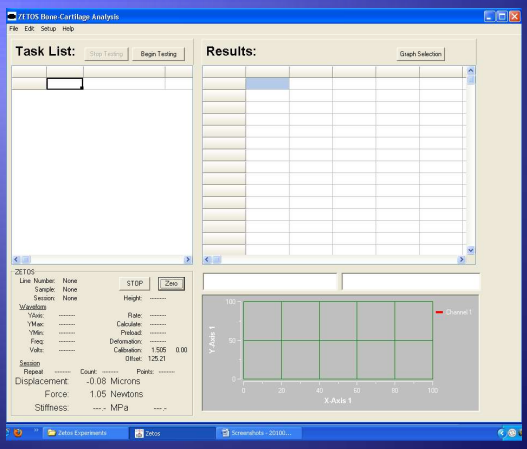

Click Setup → Calibrate Force

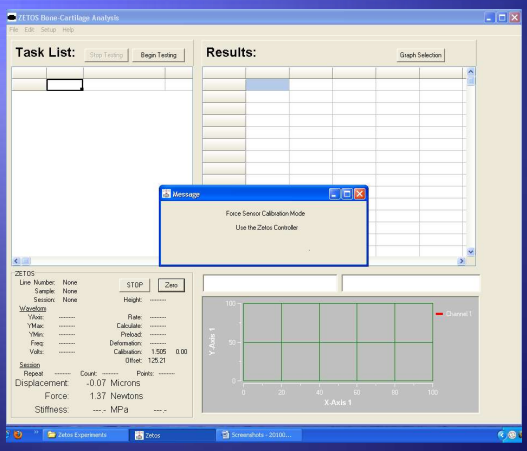

- Message box as shown will pop up, further tasks is via remote controller

Press Enter button on remote controller

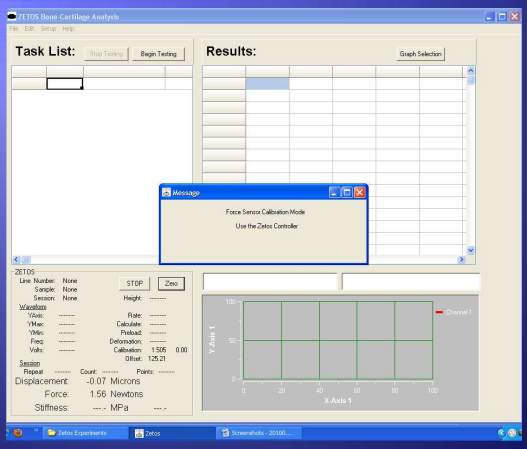

Add calibration weight

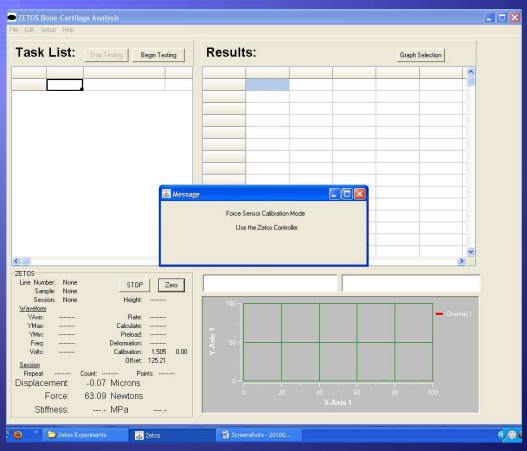

Press Calibrate button on remote monitor

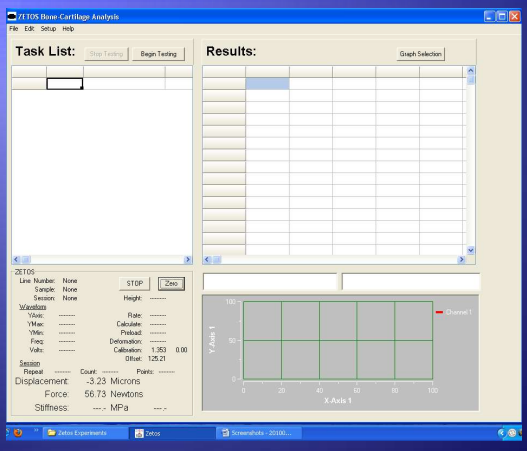

Remove calibration weight

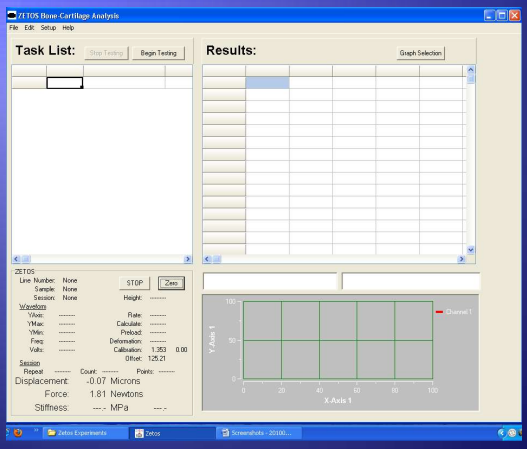

Click File ⟶ Open Experiment

- Choose appropriate experiment in pop-up window (*.zxp file)
- List of samples (REF01 to REF10) will come up on Task List and Results panes on Zetos™ software
- Column with current date will also be added in Results pane
- Then choose appropriate session (*.zsf file) to be run on each sample from drop-down list in Session 1, Session 2,…etc as required

Click Zero (on software)

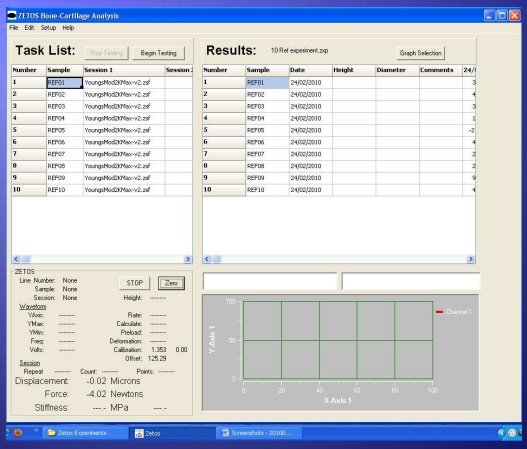

Click Begin Testing in Task List pane

- Software will automatically start with REF01
- Microscanner will turn on automatically - align barcode of reference body to be read
- Follow instructions on remote controller LCD panel
- If it says "WRONG SAMPLE" recheck reference body number and rescan the barcode again

Scan REF01, insert and pre-load to 20 Newtons

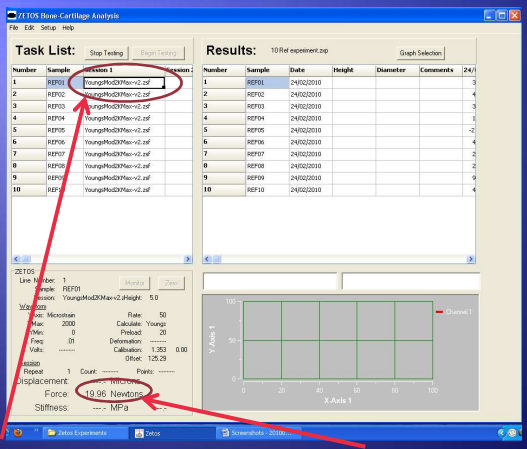

1. Indicates that the Zetos™ is currently working on REF01
2. Pre-load value

Software performs survey scan

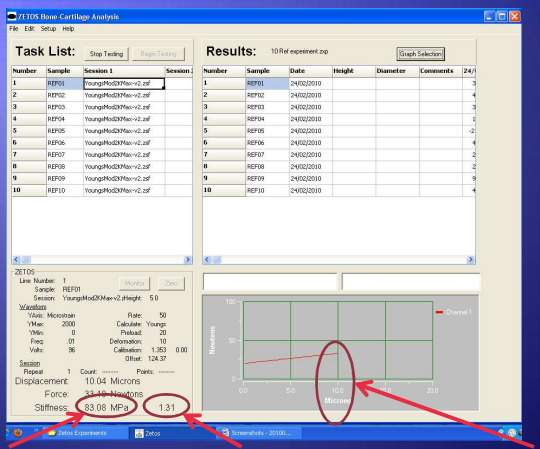

3. Estimated stiffness in Megapascal
2. Estimated K (Kest pre) value for REF01
1. Survey scan will perform until displacement of 10 microns reached

Zetos™ applies force (stress) and measures displacement (strain)

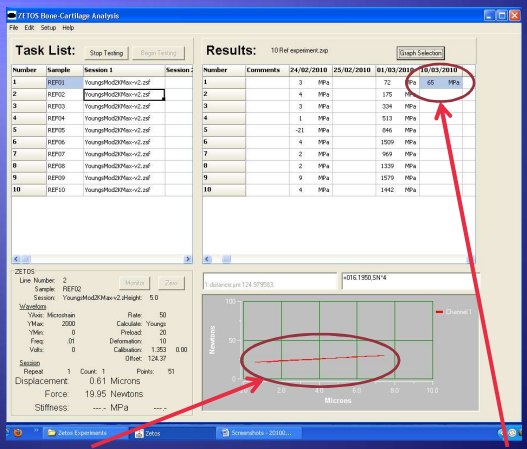

1. Real-time stress-strain curve plotted during testing
2. Measured stiffness in Megapascal is shown in Results pane at end of session

Scan REF02, insert and pre-load to 20 Newtons

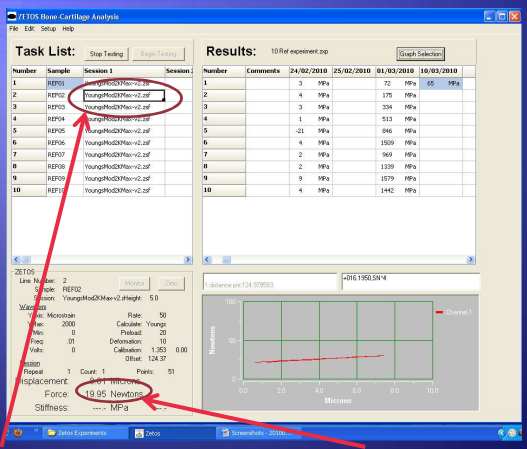

1. Indicates that the Zetos™ is currently working on REF02
2. Pre-load value

Software performs survey scan

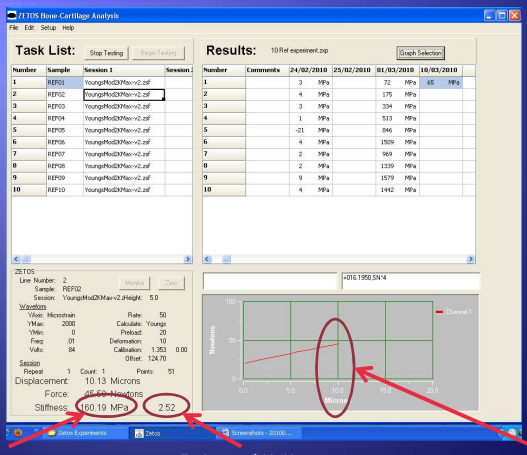

3. Estimated stiffness in Megapascal
2. Estimated K (Kest pre) value for REF02
1. Survey scan will perform until displacement of 10 microns reached

Zetos™ applies force (stress) and measures displacement (strain)

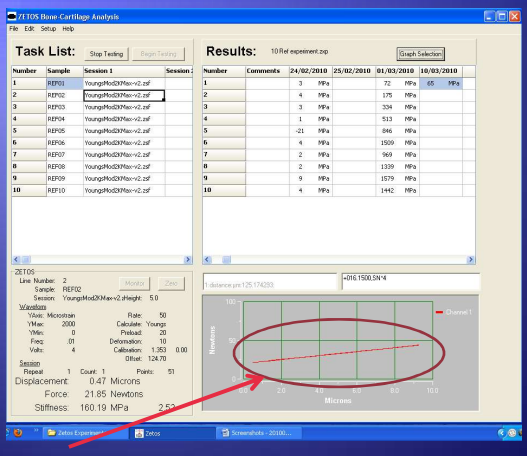

1. Real-time stress-strain curve plotted during testing

Scan REF03, insert and pre-load to 20 Newtons

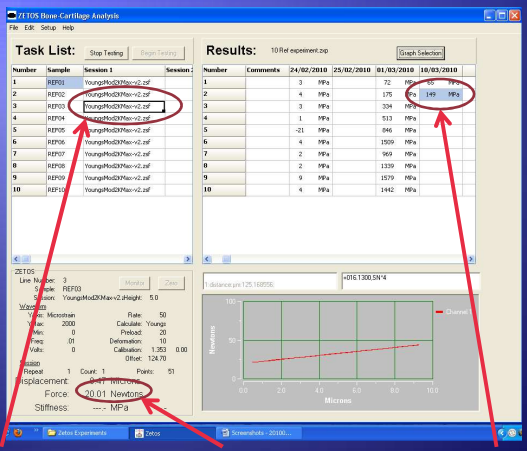

2. Indicates that the Zetos™ is currently working on REF03
3. Pre-load value
2. Measured stiffness in Megapascal for REF02 is shown in Results pane

Software performs survey scan

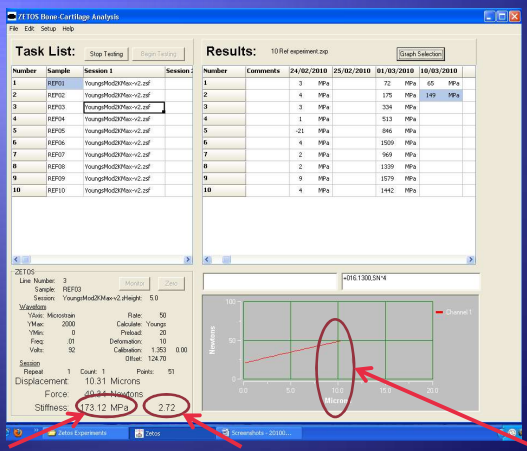

3. Estimated stiffness in Megapascal
2. Estimated K (Kest pre) value for REF03
1. Survey scan will perform until displacement of 10 microns reached

Zetos™ applies force (stress) and measures displacement (strain)

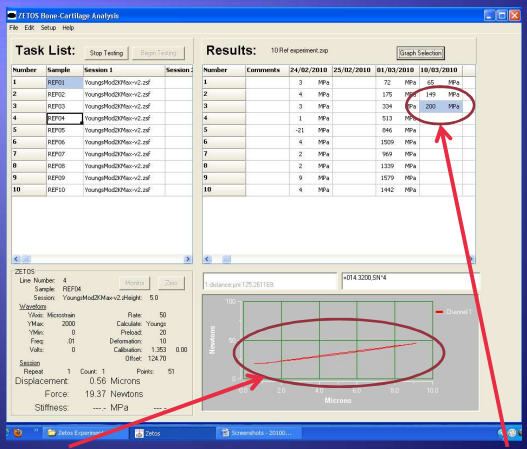

1. Real-time stress-strain curve plotted during testing
2. Measured stiffness in Megapascal is shown in Results pane at end of session

Scan REF04, insert and pre-load to 20 Newtons

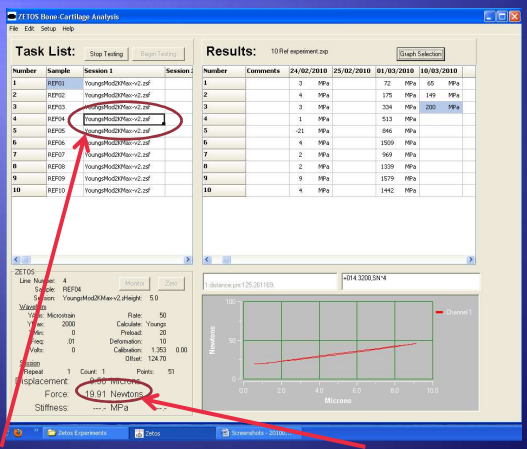

1. Indicates that the Zetos™ is currently working on REF04
2. Pre-load value

Software performs survey scan

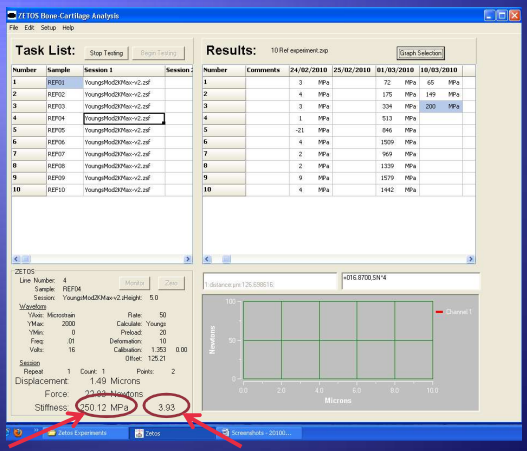

1. Estimated stiffness in Megapascal
2. Estimated K (Kest pre) value for REF04

Zetos™ applies force (stress) and measures displacement (strain)

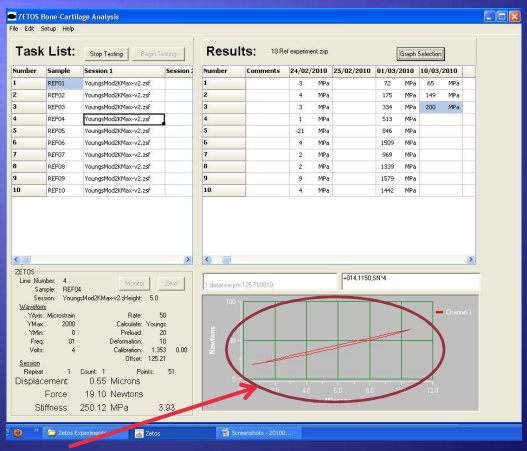

1. Real-time stress-strain curve plotted during testing, values for x- and y-axis will adjust automatically

Scan REF05, insert and pre-load to 20 Newtons

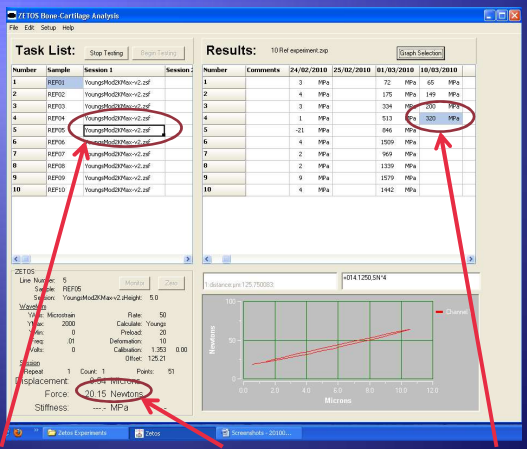

2. Indicates that the Zetos™ is currently working on REF05
3. Pre-load value
2. Measured stiffness in Megapascal for REF04 is shown in Results pane

Software performs survey scan

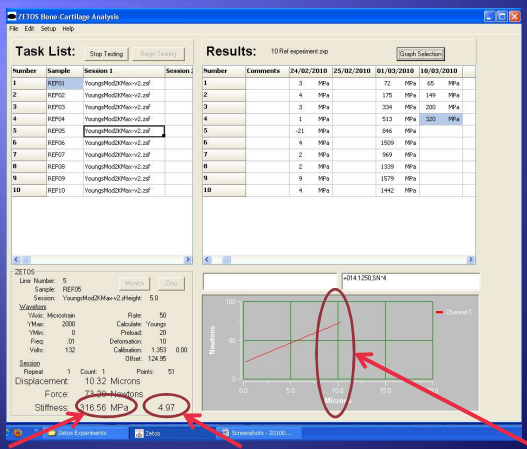

3. Estimated stiffness in Megapascal
2. Estimated K (Kest pre) value for REF05
1. Survey scan will perform until displacement of 10 microns reached

Zetos™ applies force (stress) and measures displacement (strain)

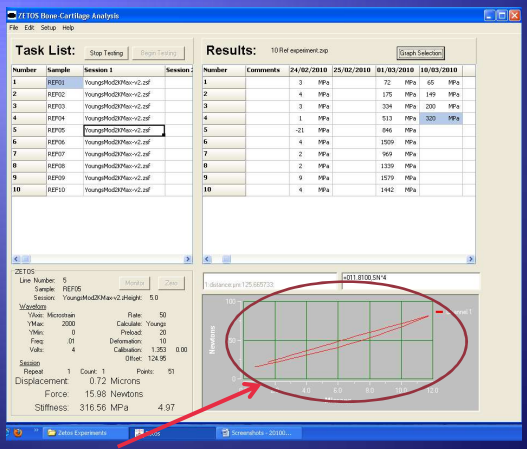

1. Real-time stress-strain curve plotted during testing, values for x- and y-axis will adjust automatically

Scan REF06, insert and pre-load to 20 Newtons

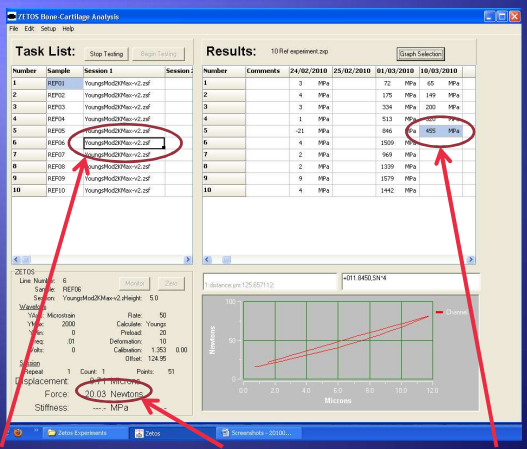

2. Indicates that the Zetos™ is currently working on REF06
3. Pre-load value
2. Measured stiffness in Megapascal for REF05 is shown in Results pane

Software performs survey scan

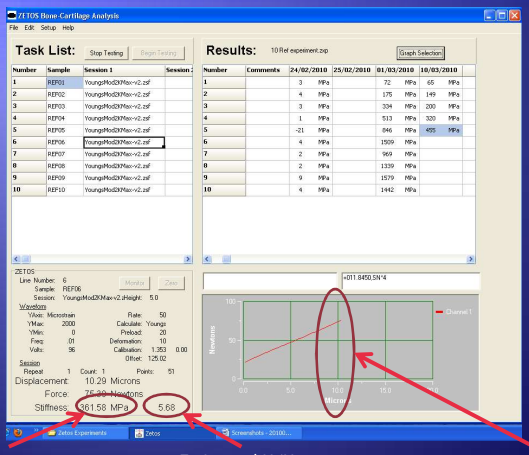

3. Estimated stiffness in Megapascal
2. Estimated K (Kest pre) value for REF06
1. Survey scan will perform until displacement of 10 microns reached

Zetos™ applies force (stress) and measures displacement (strain)

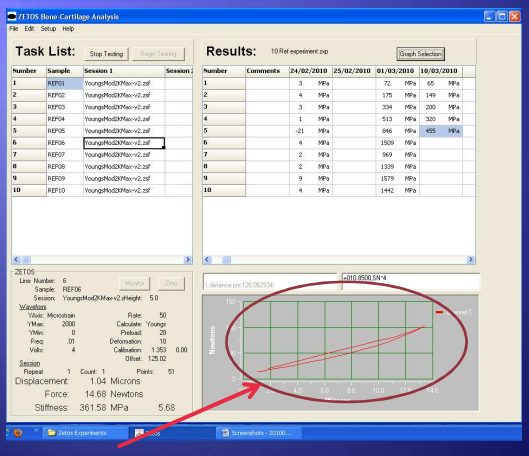

1. Real-time stress-strain curve plotted during testing, values for x- and y-axis will adjust automatically

Scan REF07, insert and pre-load to 20 Newtons

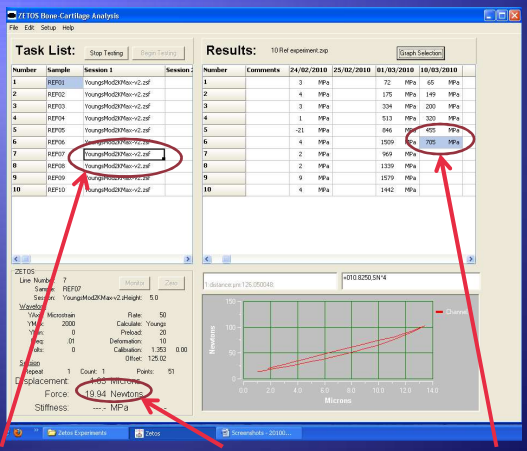

2. Indicates that the Zetos™ is currently working on REF07
3. Pre-load value
2. Measured stiffness in Megapascal for REF06 is shown in Results pane

Software performs survey scan

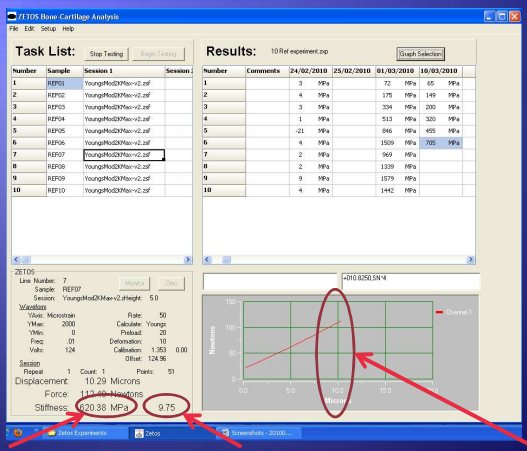

3. Estimated stiffness in Megapascal
2. Estimated K (Kest pre) value for REF07
1. Survey scan will perform until displacement of 10 microns reached

Zetos™ applies force (stress) and measures displacement (strain)

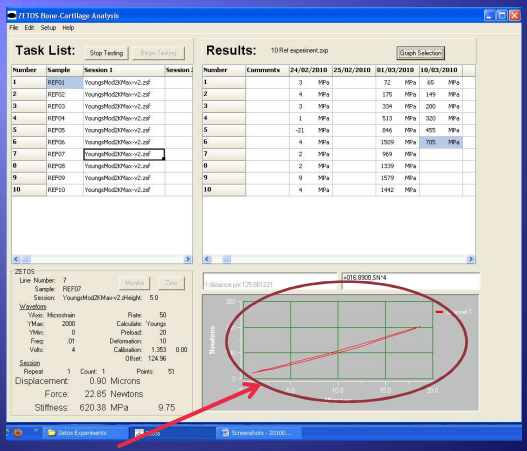

1. Real-time stress-strain curve plotted during testing, values for x- and y-axis will adjust automatically

Scan REF08, insert and pre-load to 20 Newtons

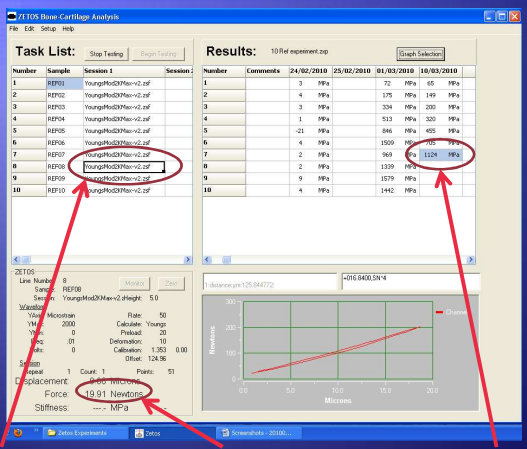

2. Indicates that the Zetos™ is currently working on REF08
3. Pre-load value
2. Measured stiffness in Megapascal for REF07 is shown in Results pane

Software performs survey scan

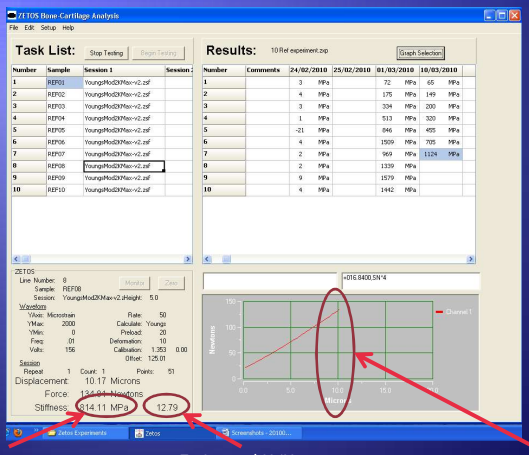

3. Estimated stiffness in Megapascal
2. Estimated K (Kest pre) value for REF08
1. Survey scan will perform until displacement of 10 microns reached

Zetos™ applies force (stress) and measures displacement (strain)

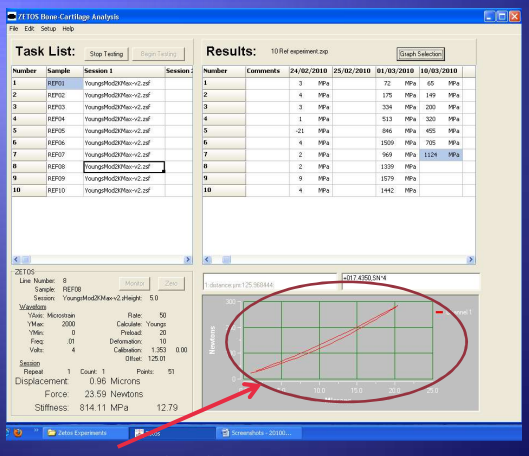

1. Real-time stress-strain curve plotted during testing, values for x- and y-axis will adjust automatically

Scan REF09, insert and pre-load to 20 Newtons

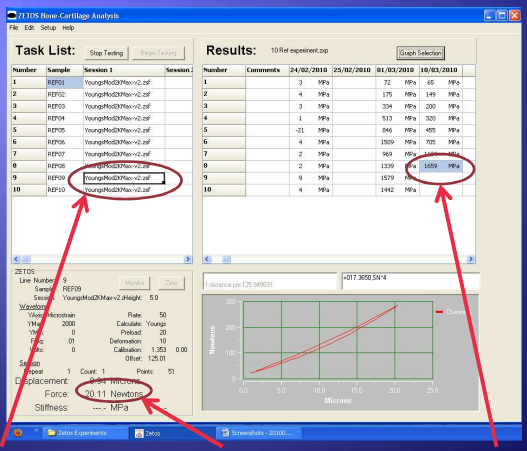

2. Indicates that the Zetos™ is currently working on REF09
3. Pre-load value
2. Measured stiffness in Megapascal for REF08 is shown in Results pane

Software performs survey scan

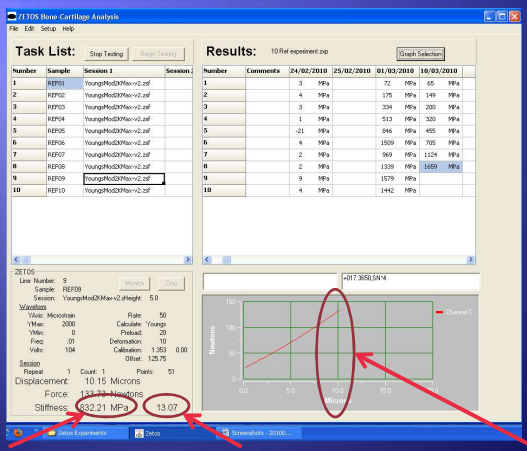

3. Estimated stiffness in Megapascal
2. Estimated K (Kest pre) value for REF09
1. Survey scan will perform until displacement of 10 microns reached

Zetos™ applies force (stress) and measures displacement (strain)

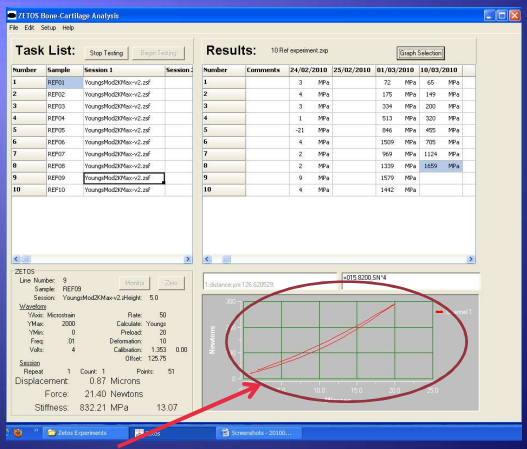

1. Real-time stress-strain curve plotted during testing, values for x- and y-axis will adjust automatically

Scan REF10, insert and pre-load to 20 Newtons

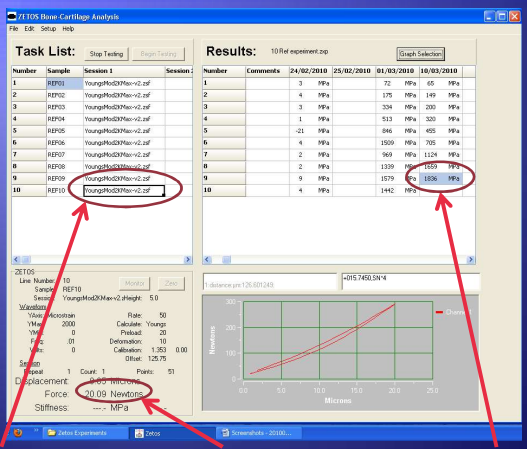

2. Indicates that the Zetos™ is currently working on REF10
3. Pre-load value
1. Measured stiffness in Megapascal for REF09 is shown in Results pane

Software performs survey scan

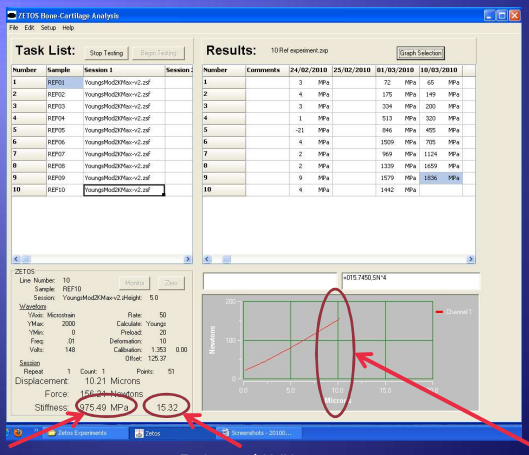

3. Estimated stiffness in Megapascal
2. Estimated K (Kest pre) value for REF10
1. Survey scan will perform until displacement of 10 microns reached

Zetos™ applies force (stress) and measures displacement (strain)

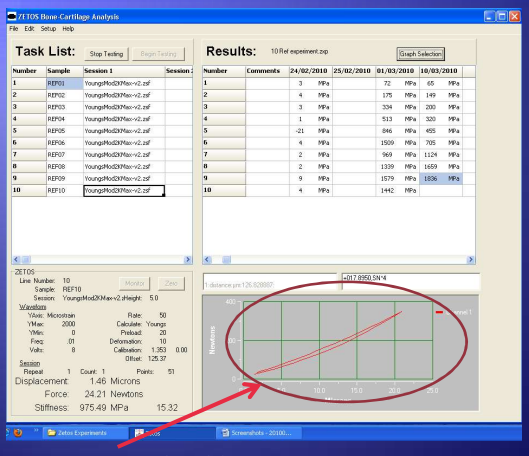

1. Real-time stress-strain curve plotted during testing, values for x- and y-axis will adjust automatically

Task List Completed

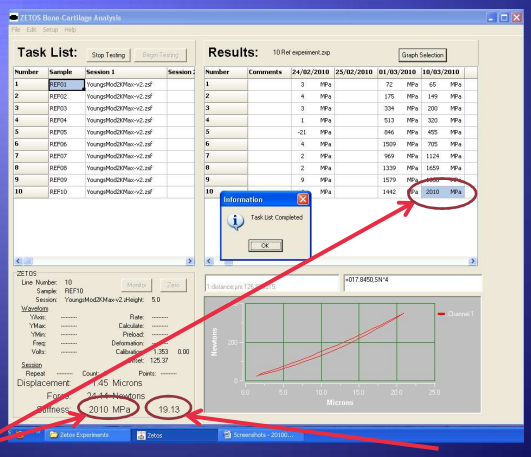

1. Measured stiffness for REF10 (in Megapascal)
2. Kest main value for REF10

Click File ⟶ Export To Excel

- Look up data values for REF01 to REF10 for the appropriate date (from row 133 onwards)
- Note down the measured value for the Kest Main (column J) for each reference body
- Transfer these Kest Main values into column B of the 'ZETOS Calibration worksheet.xlsx' file to get the calculated polynomial factors from the trendline in the graph

Calculated polynomial factors

K Values	Standards
1.35	0.88
2.56	1.91
3.18	3.42
4.44	5.24
5.68	8.65
7.73	12.15
10.89	16.75
15.16	20.90
16.88	24.32
19.13	27.81

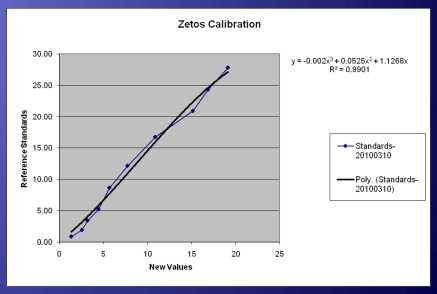

Term Values

- The values for the trendline of the graph are for TermA, TermB and TermC
- In this case
  - TermA= -0.002
  - TermB= 0.0525
  - TermC= 1.1268
- Change these values in the Zetos.ini file to get the correct Estimated k values

6.4 Appendix IV – Setting new experiment and sessions files for the Zetos™

Kamarul

SETTING NEW EXPERIMENT AND SESSIONS FILES FOR THE ZETOS™

Startup

- Power on laptop and connect USB cable to laptop
- Start Zetos™ software

Change values for TermA, TermB and TermC in the Zetos.ini file

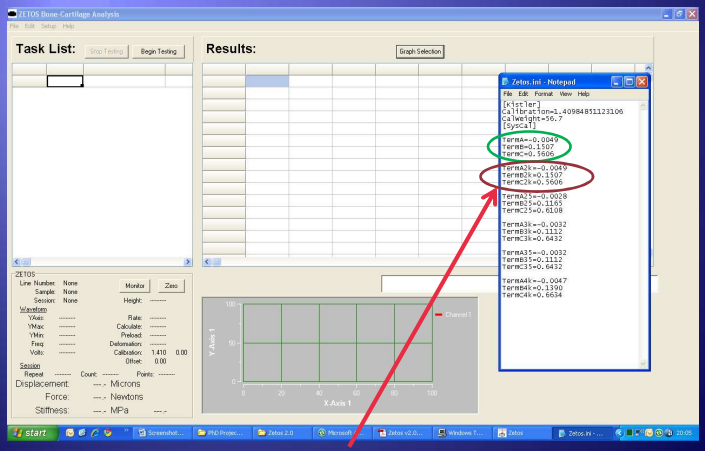

- I surmised that these are the standard values for TermA, TermB and TermC that you have worked out for loading at a maximum of 2,000 µstrain and changed the values above (green circle) accordingly

Create new Zetos experiment file (.zxp) by clicking on File → New Experiment

1. Name the new experiment file accordingly

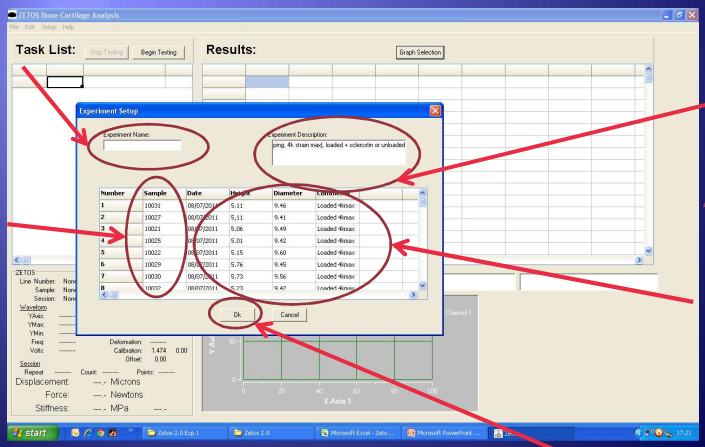

2. Add in some details as required

3. Insert the barcode of the chambers in the order that they are in on the perfusion pump.

4. Add the height, diameter and comment for each sample as appropriate

NB: Computer must be attached to the Zetos machine, which must also be switched on to create ne experiment file

5. Click on 'Ok' once finished

Create new Zetos session file (.zsf) by clicking on File → New Session

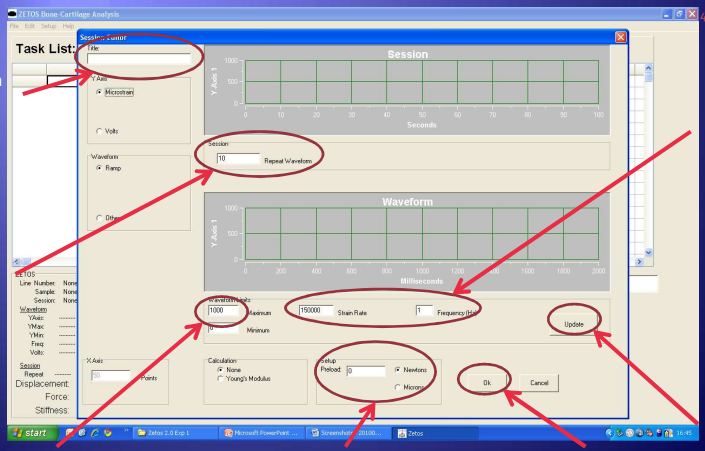

1. Name the new session file accordingly
2. Put in the number of cycles that the samples will be exercised for each session
3. Change to determine the maximum load the samples will be subjected to
4. Change these values to simulate the appropriate type of 'exercise' that will be applied to the samples
5. Click on 'Update' to see the resultant graphs
6. Change preload value to 20 Newtons
7. Click on 'Ok' once done

Zetos 2.0 Exp 1-100x 150K per sec 2K Max 1Hz.zsf

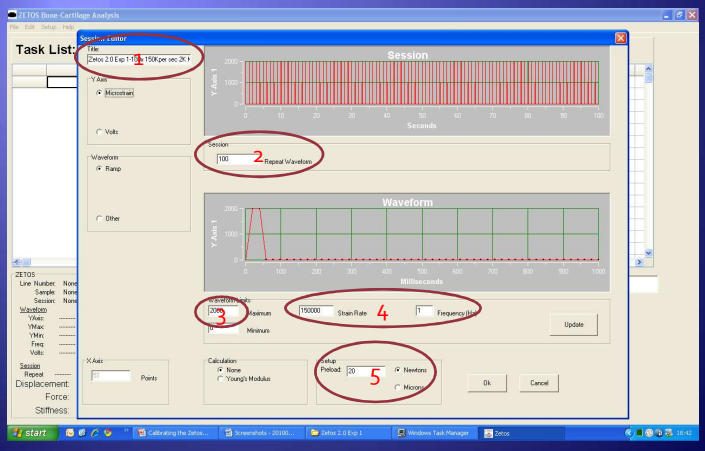

Zetos 2.0 Exp 1-300x 150Kper sec 2K Max 1Hz.zsf

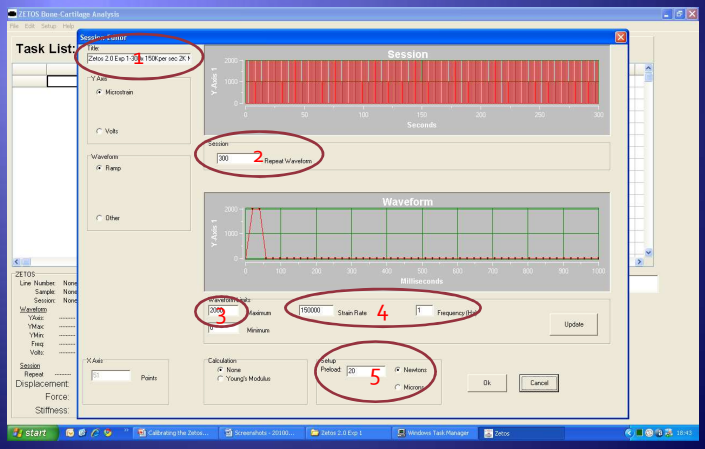

Zetos 2.0 Exp 1 Youngs Mod 2K Max.zsf

- Choose 'Young's Modulus' to set the software to do the necessary for measuring and calculating it for the sample when this session is chosen